VOLUME 81 JUNE 16, 1977 NUMBER 12

JPCHAx

THE JOURNAL OF PHYSICAL CHEMISTRY

PUBLISHED BIWEEKLY BY THE AMERICAN CHEMICAL SOCIETY

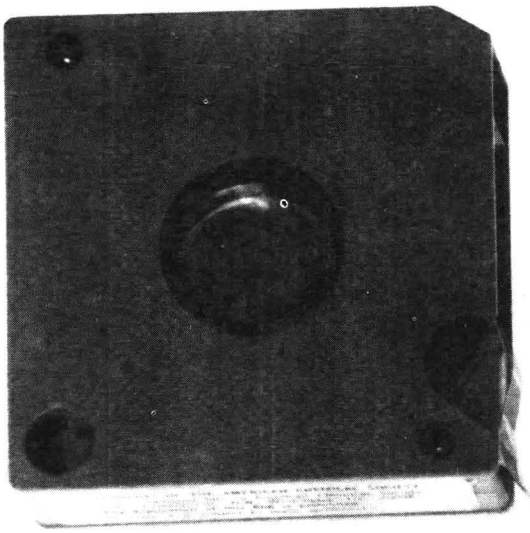

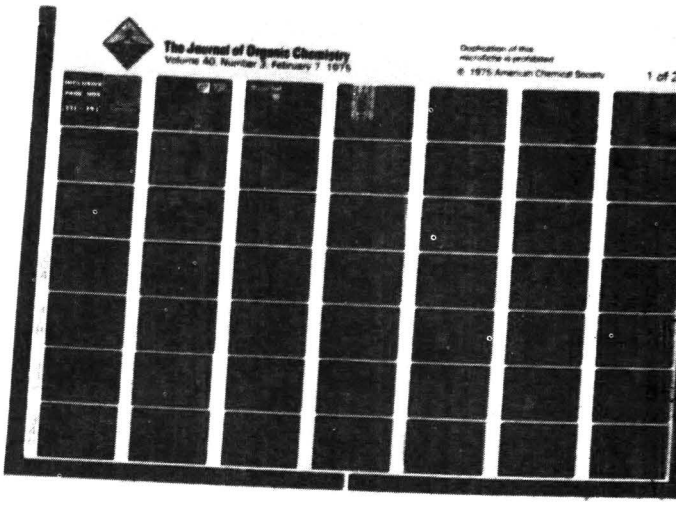

MICROFORMS

American Chemical Society publications in microform

MICROFILM OR MICROFICHE?

With the ACS microform program you can receive either, or both

Microfilm

All periodical publications back to volume one

Copying privileges included with current subscriptions

All non-print supplementary materials provided free on microfiche

Archival quality silver halide film supplied as you request; positive or negative; 16 or 35mm; cartridge, reel, or cassette.

Microfiche

Current issues of primary journals, beginning with January 1975

Individual issues or full volumes available

Supplementary materials also available on microfiche

Fiche supplied are archival quality silver halide, negative, 105 x 148mm (4" x 6"); 24x, with eye legible headers, start and end targets, and page numbers

For information about our microfilm/microfiche write:

Microform Program
Special Issues Sales
American Chemical Society
1155 16th Street, N.W.
Washington, D.C. 20036
(202) 872-4363

Derivative unit to any Perkin-Elmer Beam Spectrophotometer and background interference...

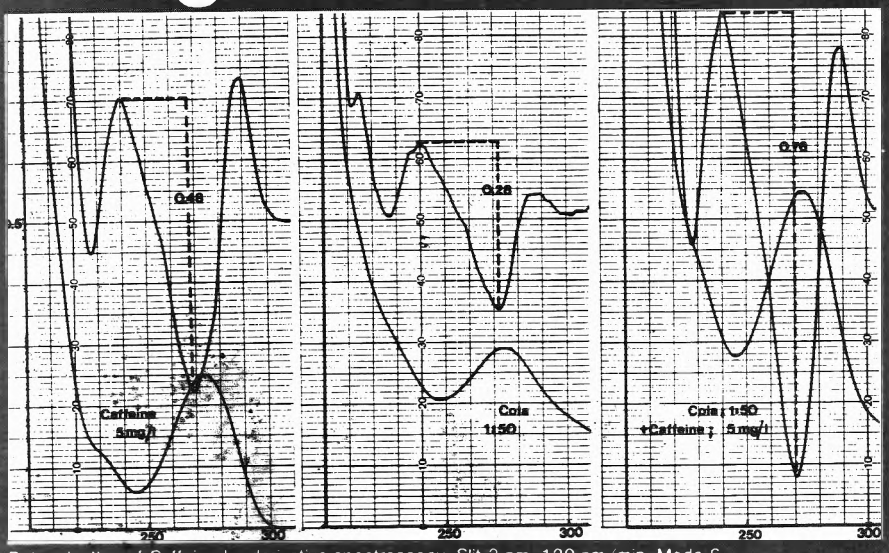

Determination of Caffeine by derivative spectroscopy. Slit 2 nm, 120 nm/min. Mode 6.

background cancellation and produces a flatter baseline for subsequent scale expansion. Second derivative spectra retain the inherent quantitative nature of UV-Visible spectroscopy, after speeding analysis by eliminating time-consuming sample pretreatment.

Why Perkin-Elmer ? Our second derivative accessory actually differentiates with respect to time and the faster you scan the larger will be the derivative peaks. The spectrophotometer should scan at up to 240 nm/min with a response of approximately 0.5 sec (98% full scale deflection) for maximum sensitivity. All of Perkin-Elmer's current line of double-beam UV-Vis instruments from the low-cost 550 series, thru the versatile 200, to the high performance 57 series, can satisfy these requirements. If the tear-off card has been used, for further information contact: Instrument Division, Norwalk, CT 06856 USA Bodenseewerk Perkin-Elmer & Co., GmbH, 7770 Ueberlingen, West Germany

...for better Quantitative Analysis!

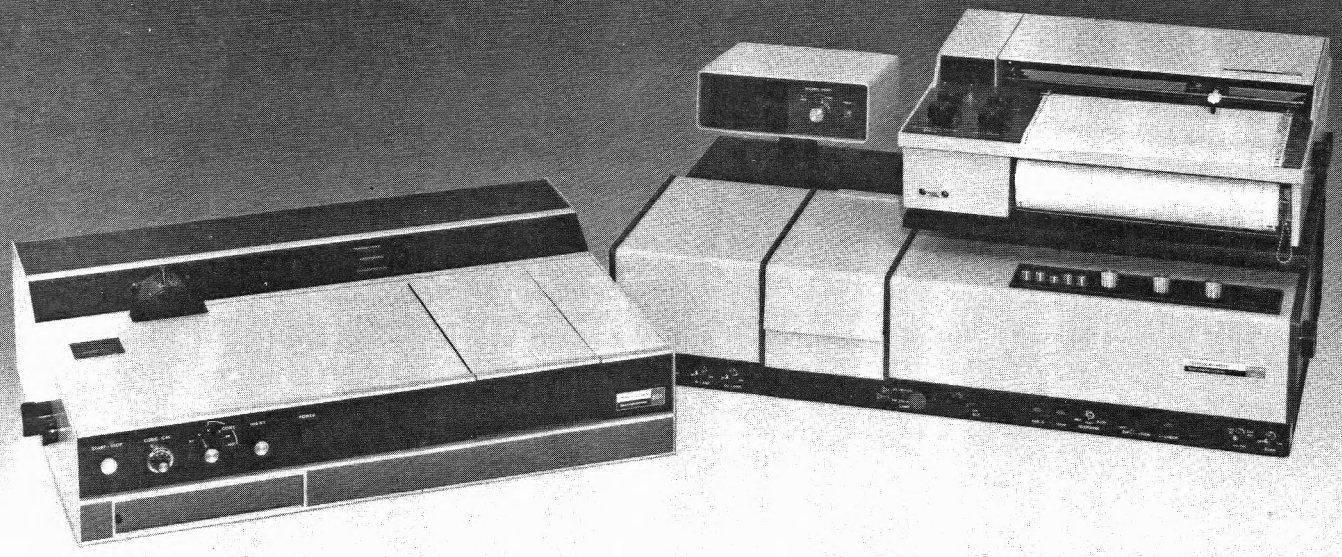

PERKIN-ELMER

THE JOURNAL OF

PHYSICAL CHEMISTRY

Published by the
AMERICAN CHEMICAL SOCIETY
BOOKS AND JOURNALS DIVISION

D. H. Michael Bowen, Director

Marjorie Laflin, Assistant to the Director

Editorial Department: Charles R. Bertsch, Head; Marianne C. Brogan, Associate Head; Celia B. McFarland, Joseph E. Yurvati, Assistant Editors

Magazine and Production Department: Bacil Guiley, Head

Research and Development Department: Seldon W. Terrant, Head

Advertising Office: Centcom, Ltd., 25 Sylvan Road South, Westport, Conn. 06880.

Published biweekly by the American Chemical Society at 20th and Northampton Sts., Easton, Pennsylvania 18042. Second class postage paid at Washington, D.C. and at additional mailing offices.

Editorial Information

Instructions for authors are printed in the first issue of each volume. Please conform to these instructions when submitting manuscripts.

Manuscripts for publication should be submitted to *The Journal of Physical Chemistry*, Department of Chemistry, University of Minnesota, Minneapolis, Minn. 55455. Correspondence regarding **accepted papers and proofs** should be directed to the Editorial Department at the ACS Easton address.

Page charges of $60.00 per page may be paid for papers published in this journal. Ability to pay does not affect acceptance or scheduling of papers.

Bulk reprints or photocopies of individual articles are available. For information write to Business Operations, Books and Journals Division at the ACS Washington address.

Requests for **permission to reprint** should be directed to Permissions, Books and Journals Division at the ACS Washington address. The American Chemical Society and its Editors assume no responsibility for the statements and opinions advanced by contributors.

Subscription and Business Information

1977 Subscription rates—including surface postage

	U.S.	PUAS	Canada, Foreign
Member	$24.00	$33.00	$34.00
Nonmember	96.00	105.00	106.00
Supplementary material	15.00	19.00	20.00

Air mail and air freight rates are available from Membership & Subscription Services, at the ACS Columbus address.

New and renewal subscriptions should be sent with payment to the Office of the Controller at the ACS Washington address. **Changes of address** must include both old and new addresses with ZIP code and a recent mailing label. Send all address changes to the ACS Columbus address. Please allow six weeks for change to become effective. **Claims for missing numbers** will not be allowed if loss was due to failure of notice of change of address to be received in the time specified: if claim is dated (a) North America—more than 90 days beyond issue date, (b) all other foreign—more than 1 year beyond issue date; or if the reason given is "missing from files". Hard copy claims are handled at the ACS Columbus address.

Microfiche subscriptions are available at the same rates but are mailed first class to U.S. subscribers, air mail to the rest of the world. Direct all inquiries to Special Issues Sales, at the ACS Washington address or call (202) 872-4554. **Single issues** in hard copy and/or microfiche are available from Special Issues Sales at the ACS Washington address. Current year $4.75. Back issue rates available from Special Issues Sales. **Back volumes** are available in hard copy and/or microform. Write to Special Issues Sales at the ACS Washington address for further information. **Microfilm** editions of ACS periodical publications are available from volume 1 to the present. For further information, contact Special Issues Sales at the ACS Washington address. **Supplementary material** mentioned in the journal appears in the microfilm edition. Single copies may be ordered directly from Business Operations, Books and Journals Division, at the ACS Washington address.

	U.S.	PUAS, Canada	Other Foreign
Microfiche	$2.50	$3.00	$3.50
Photocopy			
1–7 pages	4.00	5.50	7.00
8–20 pages	5.00	6.50	8.00

Orders over 20 pages are available only on microfiche, 4 × 6 in., 24X, negative, silver halide. Orders must state photocopy or microfiche if both are available. Full bibliographic citation including names of all authors and prepayment are required. Prices are subject to change.

American Chemical Society
1155 16th Street, N.W.
Washington, D.C. 20036
(202) 872-4600

Member & Subscription Services
American Chemical Society
P.O. Box 3337
Columbus, Ohio 43210
(614) 421-7230

Editorial Department
American Chemical Society
20th and Northampton Sts.
Easton, Pennsylvania 18042
(215) 258-9111

Notice to Authors last printed in the issue of January 13, 1977

THE JOURNAL OF

PHYSICAL CHEMISTRY

Volume 81, Number 12 June 16, 1977

JPCHAx 81(12) 1125–1216 (1977)

ISSN 0022-3654

COMMUNICATIONS TO THE EDITOR

■ Supplementary and/or miniprint material for this paper is available separately (consult the masthead page for ordering information); it will also appear following the paper in the microfilm edition of this journal.

* In papers with more than one author, the asterisk indicates the name of the author to whom inquiries about the paper should be addressed.

AUTHOR INDEX

THE JOURNAL OF
PHYSICAL CHEMISTRY

VOLUME 81, NUMBER 12 JUNE 16, 1977

Ion–Molecule Reactions in Thiols and Alkyl Sulfides. Photoionization of Methyl, Ethyl, Propyl, and *tert*-Butyl Mercaptan, and Methyl and Ethyl Sulfide

J. M. Brupbacher,[1a] C. J. Eagle,[1b] J. A. Koprio,[1b] and E. Tschulkow-Roux*

Department of Chemistry, The University of Calgary, Calgary, Alberta, Canada T2N 1N4 *(Received September 19, 1975; Revised Manuscript Received February 25, 1977)*

Photoinduced ion–molecule reactions of the primary ions occurring in a number of thiols and alkyl sulfides have been investigated over the pressure range 1–20 mTorr using a Kr resonance lamp (10.03 and 10.6 eV) as the excitation source. Rate coefficients at 298 K have been determined for the reaction $R_{2-n}{}^+SH_n + R_{2-n}SH_n \rightarrow R_{2-n}{}^+SH_{n+1} + R_{2-n}SH_n(-H)$ (k_1), $n = 0, 1$. For the mercaptans values of k_1 were found to be 14.1, 12.5, 11.3, and 5.7×10^{-10} cm^3 s^{-1} for R = CH_3, C_2H_5, C_3H_7, and $(CH_3)_3C$. These values agree with the general trend established for the analogous reactions in amines. In the case of $(CH_3)_2S$ and $(C_2H_5)_2S$, no hydrogen transfer was observed. Photoionization of C_2H_5SH in CH_3OH could indicate that mercaptans behave as hydrogen atom acceptors rather than as proton donors. However, for *tert*-butyl mercaptan, the proton transfer reaction $(CH_3)_3C^+ + (CH_3)_3CSH \rightarrow (CH_3)_2CCH_2 + (CH_3)_3CS^+H_2$ (k_2) was also observed.

Introduction

Previous studies of ion–molecule reactions occurring in the gas phase have yielded rate constants for hydrogen atom and proton transfer reactions. Comparison of experimental results with theoretical predictions have shown that most unambiguous H^+ transfer processes[2,3] are adequately described by the average-dipole-orientation (ADO) model[4] if they are not sterically hindered. In a previous study from this laboratory[5] it has been suggested that the unit mass transfer reactions in alkylamines (methyl, ethyl, and propyl) can be adequately described by a reaction model which assumes a collision complex in which the polar molecule is aligned with the ion similar to that invoked by Solka and Harrison,[6] and the actual transfer rate is determined by the number and type of hydrogen atoms in the molecule.

In the present study, the hydrogen transfer reactions[7] occurring in a number of simple thiols and alkyl sulfides have been investigated with the aim of determining the rate coefficients for the reactions:

$$\dot{R}SH + RSH \xrightarrow{k_1} R\dot{S}H_2 + RSH(-H) \qquad (1)$$

for R = CH_2, C_2H_5, C_3H_7, $(CH_3)_3C$, and

$$R_2\dot{S} + R_2S \xrightarrow{k_2} R_2\dot{S}H + R_2S(-H) \qquad (2)$$

for R = CH_3 and C_2H_5. With the exception of H_2S[8–11] and CH_3SH[8–12] there appear to be no previous reports on the determination of rate coefficients of these systems. Furthermore, all of the above studies were carried out using electron beams as sources of ionization in contrast to the photoionization technique reported in this work.

In their investigation of the ion–molecule reactions of H_2S, Huntress and Pinizzotto[11] found that the unit mass transfer process occurred with almost equal probability via the H-atom and H^+-transfer pathways. This is in contrast to the NH_3, CH_4, and H_2O systems which proceed primarily via proton transfer. This difference in chemical behavior was attributed to the fact that H abstraction by the parent ion from the neutral reactant would leave the MH^+ ion (M = NH_3, CH_4, H_2O) in an unfavorable geometrical configuration. This is not the case for H_2S.

Experimental Section

All experiments were carried out using a high pressure (up to 20 mTorr) quadrupole mass spectrometer with a Kr resonance lamp (10.03 and 10.6 eV) as the photoionization source. The energy of the 10.03-eV line, which accounts

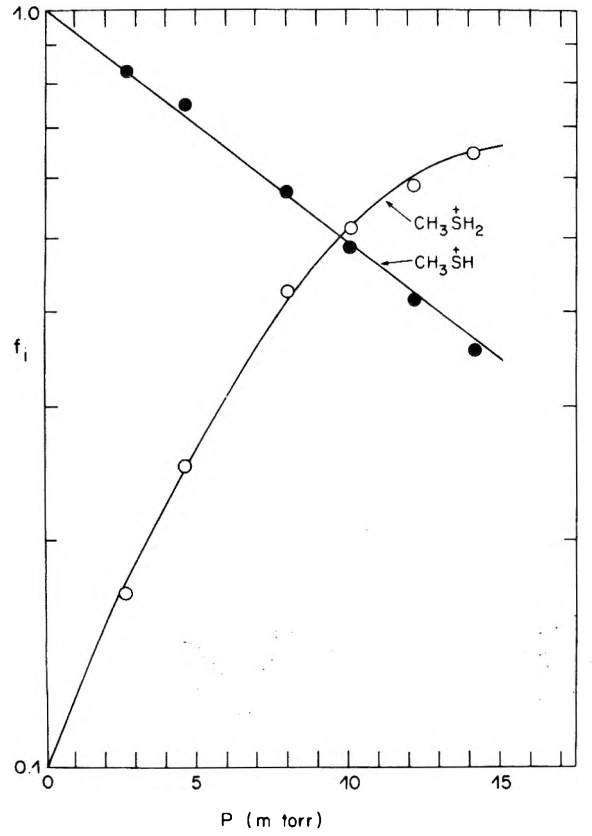

Figure 1. Plot of log f_i vs. pressure for methyl mercaptan: solid circles, decay of CH_3S^+H; open circles, formation of product ion $CH_3S^+H_2$. Each experimental point represents the average of three determinations of f_i at each pressure.

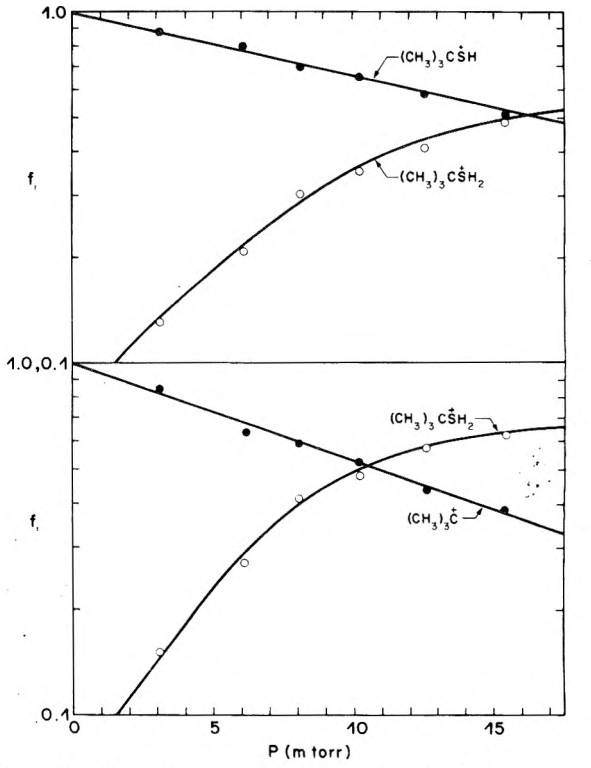

Figure 2. Plots of log f_i vs. pressure for t-C_4H_9SH: upper plot corresponds to the reaction t-$C_4H_9S^+H$ + t-C_4H_9SH → t-$C_4H_9S^+H_2$ + t-$C_4H_9SH(-H)$; lower plot corresponds to reaction 3. Solid circles and open circles correspond to loss of the primary ion and formation of secondary ions, respectively. Each experimental point represents the average of three determinations of f_i at each pressure.

for about 90% of the total lamp intensity, was 13.6, 17.2, 19.4, and 20.5 kcal mol^{-1} in excess of the ionization potential (IP) for methyl, ethyl, propyl, and *tert*-butyl mercaptan,[13] and 31.1 and 36.9 kcal mol^{-1} in excess for methyl and ethyl sulfide, respectively, using thermochemical data from the literature.[14-17] The experimental apparatus, as well as the procedure for data reduction, have been discussed previously.[5] All compounds were reagent grade materials which were outgassed and fractionally distilled in vacuo. Electron impact mass spectral analysis of the purified compounds showed only trace amounts (<0.05%) of contaminants. Also, the photoionization mass spectra taken at the time of kinetic measurements gave no indication of any impurities in the reaction cell.

Results

Photoionization of methyl, ethyl, and propyl mercaptan was performed over the pressure range 1-15 mTorr and 298 K. The two ions, corresponding to the parent ion at mass m and the secondary ion at mass $m + 1$ resulting from reaction 1, were monitored in each case. In the case of CH_3SH the $m - 1$ ion (CSH_3^+) was also observed as were ions at m/e 63 ($C_2H_7S^+$) and m/e 96 ($C_2H_8S_2^+$), the latter two only appearing at the upper end of the pressure range. After determination of the mole fraction of the parent ion, $f_i = I_m/(I_m + I_{m+1})$ at each pressure from the observed ion intensities (I_i), plots of ln f_i vs. pressure were constructed. One such plot for CH_3SH is shown in Figure 1. The plots for C_2H_5SH and C_3H_7SH are similar in appearance and are not included. From the slopes of these plots the rate constants for the unit mass transfer reactions were then determined relative to the standard reaction

$$NH_3^+ + NH_3 \xrightarrow{k_0} NH_4^+ + NH_2$$

using $k_0 = 2.1 \times 10^{-9}$ cm^3 s^{-1} which was reported by Sieck et al.,[18] for ammonium ions produced by photoionization of NH_3 at 10.6 eV.

For *tert*-butyl mercaptan, a fragment ion at m/e 57 corresponding to the species $(CH_3)_3C^+$ was also observed. This ion was found to undergo the proton-transfer reaction

$$(CH_3)_3\dot{C} + (CH_3)_3CSH \xrightarrow{k_3} (CH_3)_2CCH_2 + (CH_3)_3C\dot{S}H_2 \quad (3)$$

The ion intensity for $(CH_3)_3CS^+H_2$ (m/e 91) at each pressure was separated into the contributions from reactions 1 and 3 by consideration of the charge balance. If $I_{m+1}^{(3)}$ denotes the contribution to the $m + 1$ ion from reaction 3 we can write the charge balance as

$$I_m^0 = I_m + I_{m+1} - I_{m+1}^{(3)}$$

$$I_{m-33}^0 = I_{m-33} + I_{m+1}^{(3)}$$

where I_i^0 refers to the primary ion current in the absence of secondary reactions. We now define the ratio $\beta = I_{m-33}^0/I_m^0$ and hence obtain

$$I_{m+1}^{(3)} = [\beta(I_m + I_{m+1}) - I_{m-33}]/(1 + \beta)$$

The resulting fractional ion currents for primary ions in terms of observed or calculable ion intensities are therefore

$$f_m = I_m/(I_m + I_{m+1} - I_{m+1}^{(3)})$$

for the parent ion of m/e 90, and

$$f_{m-33} = I_{m-33}/(I_{m-33} + I_{m+1}^{(3)})$$

for the fragment ion of mass m/e 57. The value of β is obtained as a first approximation by extrapolation to zero pressure a plot of $I_{m-33}/(I_m + I_{m+1})$ as a function of pressure. Plots of log f_i vs. pressure for reactions 1 and 3 in *tert*-butyl mercaptan are shown in Figure 2. A value of $k_3 = 1.1 \times 10^{-9}$ cm^3 s^{-1} was found for the proton transfer reaction 3.

With the aim to determine whether the mercaptans behave as H^+ donors or H acceptors, a mixture of 50%

TABLE I: Results and Comparison of Rate Constants[a]

$R_{3-n}NH_n$	k_1	Ref	$R_{2-n}SH_n$	k_1	k_{ADO}[b]	k_1/k_{ADO}
NH_3	21.3	18	HSH	7.5[c]	14.5	0.52
CH_3NH_2	12.2	d	CH_3SH	14.1	16.4	0.86
$C_2H_5NH_2$	12.6	5	C_2H_5SH	12.5	15.8	0.79
$C_3H_7NH_2$	11.6	5	C_3H_7SH	11.3	15.3	0.74
			$(CH_3)_3CSH$	5.7	14.9	0.38
$(CH_3)_2NH$	10.2	5, *d*	$(CH_3)_2S$	*e*	15.5	$\ll 1$
$(C_2H_5)_2NH$	8.3	5	$(C_2H_5)_2S$	*e*	14.9	$\ll 1$
$(CH_3)_3N$	5.5	5				
	6.8	d				
$(C_2H_5)_3N$	4.7	5				

[a] In units of 10^{-10} cm^3 s^{-1}. Estimated reproducibility in k_1 is ±5%. [b] Calculated ion-molecule collision number based on average-dipole-orientation theory, ref 4. Molecular polarizabilities were calculated using bond polarizabilities in ref 24, and dipole moments were taken from ref 25. [c] Average of values tabulated in ref 11. [d] L. Hellner and L. W. Sieck, *Int. J. Chem. Kinet.*, 5, 177 (1973). [e] Estimated upper limit in $k_1 < 10^{-11}$ cm^3 s^{-1}.

C_2H_5SH in CH_3OH was photolyzed. The IP of CH_3OH is 0.25 eV above the 10.6 eV Kr resonance line and hence any observed $CH_3O^+H_2$ ions must result from the H^+-transfer reaction

$$C_2H_5\dot{S}H + CH_3OH \rightarrow C_2H_5SH(-H) + CH_3\dot{O}H_2 \quad (4)$$
$$\Delta H = 8.5 \text{ kcal mol}^{-1}$$

Photoionization of this mixture showed only ions at m/e 62 and 63 corresponding to $C_2H_5S^+H$ and $C_2H_5S^+H_2$ which clearly demonstrates that proton transfer from $C_2H_5S^+H$ to CH_3OH does not take place. However, the analysis of this data showed an enhanced production of $C_2H_5S^+H_2$ which suggests the reaction

$$C_2H_5\dot{S}H + CH_3OH \rightarrow C_2H_5\dot{S}H_2 + CH_3OH(-H) \quad (5)$$
$$\Delta H = 7 \pm 2 \text{ kcal mol}^{-1}$$

with a rate constant of $k_5 = 4.4 \pm 0.3 \times 10^{-10}$ cm^3 s^{-1}.

The photoionization mass spectra of methyl and ethyl sulfide, when corrected for isotope effects, show only one ion in each case. To ensure that this ion was the primary ion of mass m for methyl sulfide and not a fragment ion, e.g., $m - 1$, a mixture of 50% $(CH_3)_2S$ in $(CH_3)_3N$ was prepared. Photoionization of this mixture showed peaks at m/e 58 through 63. The peaks corresponding to m/e 58–61 result from the normal photoionization mass spectra of $(CH_3)_3N$ where m/e 58 identifies the $m - 1$ cracking ion, m/e 59 the trimethylamine parent ion, m/e 60 results from the hydrogen or proton transfer reaction between $(CH_3)_3N^+$ and $(CH_3)_3N$, and m/e 61 is the isotopic contribution to the $m + 1$ peak. Of the remaining two peaks, the major one at m/e 62 was unambiguously identified as the primary ion $(CH_3)_2S^+$, while that at m/e 63 could be accounted for as its isotopic contribution. From this experiment it was deduced that neither the H-transfer nor the H^+-transfer reactions

$$(CH_3)_2S^+ + (CH_3)_2S \rightarrow (CH_3)_2\dot{S}H + CH_2SCH_3 \quad (6)$$
$$\Delta H \simeq 8 \text{ kcal mol}^{-1}$$

occurred. The absence of the m/e 63 peak above the normal isotopic abundance indicates also that the reaction

$$(CH_3)_3N^+ + (CH_3)_2S \rightarrow (CH_3)_2NCH_2 + (CH_3)_2\dot{S}H \quad (7)$$
$$\Delta H \simeq 29 \text{ kcal mol}^{-1}$$

did not occur to any significant degree. By analogy, for ethyl sulfide reactions 6 and 7 must also be very slow. However, analysis of the trimethylamine data in the reaction mixture $(CH_3)_3N/(CH_3)_2S$ again revealed that the production of $(CH_3)_3NH^+$ was enhanced, which can be accounted for by the reaction

$$(CH_3)_3N^+ + (CH_3)_2S \rightarrow (CH_3)_3\dot{N}H + CH_2SCH_3 \quad (8)$$
$$\Delta H = -1 \text{ to } +5 \text{ kcal mol}^{-1}$$

The rate constant for this reaction was estimated to be $k_8 = 9.2 \pm 0.6 \times 10^{-11}$ cm^3 s^{-1} based on the assumption that $(CH_3)_2S^+$ is not a proton donor (cf. reaction 6).

The experimental rate constants, k_1, for the sulfur containing compounds and the analogous amines are summarized in Table I and compared with the collision numbers predicted by the ADO theory.[4]

Discussion

With reference to Table I the rate constants for the mercaptans are found to decrease with increasing alkyl substitution. The collision efficiencies (k_1/k_{ADO}) are somewhat less than unity in each case, which can be attributed to structural factors in the reactant ion.[19] These observations agree with the trends previously established for the alkylamines.[5] The rate constant for CH_3SH is comparable to the value of $11.9 \pm 0.6 \times 10^{-10}$ cm^3 s^{-1} reported to Nagy et al.[20] in a study using the electron impact pressure variation technique. The agreement is considered satisfactory if one takes into account their ion exit energy of 3.4 eV compared to the field free reaction chamber used in the present work. In a more recent study using the ion-trapping technique Solka and Harrison[6] report for methyl mercaptan an overall disappearance rate coefficient of $7.7 \pm 0.2 \times 10^{-10}$ cm^3 s^{-1} at low (unspecified) ionizing electron energy but do not discuss the difference with the earlier work.

A survey of the thermochemistry for the sulfur compounds[6,14-17] indicates that reaction 9 is thermoneutral or slightly exothermic

$$CH_3\dot{S}H + CH_3SH \rightarrow CH_3\dot{S}H_2 + CH_3S \quad (9)$$
$$\Delta H \sim -1 \text{ kcal mol}^{-1}$$

The enthalpy change for unit mass transfer in ethyl and propyl mercaptan is expected to be similar. Solka and Harrison[12] and Hemsworth et al.[21] have shown that for proton transfer reactions the collision efficiency k_1/k_{ADO} is essentially unity for reactions which are exothermic by more than 10 kcal mol^{-1} and the collision coefficiency decreases with decreasing exothermicity. The situation with respect to endothermic reactions where the ion has some excess energy as a result of photoionization could show a similar trend. The observation of H transfer from CH_3OH to $C_2H_5SH^+$ where the excess ion energy is up to 10 kcal mol^{-1} above the endothermicity of the reaction ($\Delta H \approx 7$ kcal mol^{-1}) would support this view. Furthermore the observed H transfer from CH_3OH to $C_2H_5SH^+$ rather than H^+ transfer from $C_2H_5S^+H$ to CH_3OH strongly suggests that mercaptans behave entirely as H-atom acceptors and not as proton donors although both reactions are endothermic.

According to the model proposed to account for hydrogen transfer in alkylamines,[5] the rate constant, k_1, for

$(CH_3)_3CSH$ should be approximately one-half that of H_2S since *tert*-butyl mercaptan has only one "transferable" hydrogen atom.[22] Inspection of Table I shows that this is at least qualitatively the case. Also, it would be anticipated that k_1 for CH_3SH, which has four transferable hydrogen atoms, would be significantly larger than that for $(CH_3)_3CSH$, an expectation which is also roughly borne out. These observations suggest that the parameters controling the rate of hydrogen transfer in amines are probably also operative in the analogous mercaptans. The low rate constants for hydrogen or proton transfer reactions in methyl and ethyl sulfides stand in sharp contrast to those observed for dimethyl- and diethylamines. The thermochemical data for $(CH_3)_2S$ suggests that reaction 6 is endothermic by ca. 8–15 kcal mol^{-1}.[23] Despite an ion energy between 23 and 16 kcal mol^{-1} in excess of this endothermicity no hydrogen transfer occurs. It is not clear how this possible excess energy is dissipated and it must be assumed that either only a fraction of the excess ion energy is accessible during the lifetime of the collision complex or factors other than energy content, such as structure, are paramount in limiting the transfer rate for this reaction. The very low values of k_1/k_{ADO} (Table I) for sulfides may be a direct consequence of this situation.

References and Notes

(1) (a) Postdoctoral Fellow (1972–1974); (b) Postgraduate Fellow.
(2) T. Su and M. T. Bowers, *J. Am. Chem. Soc.*, **95**, 7609 (1973).
(3) T. Su and M. T. Bowers, *Int. J. Mass Spectrom. Ion. Phys.*, **12**, 347 (1973).
(4) T. Su and M. T. Bowers, *J. Chem. Phys.*, **58**, 3207 (1973).
(5) J. M. Brupbacher, C. J. Eagle, and E. Tschuikow-Roux, *J. Phys. Chem.*, **79**, 671 (1975).
(6) B. H. Solka and A. G. Harrison, *Int. J. Mass Spectrom. Ion. Phys.*, **14**, 295 (1974).
(7) The term hydrogen transfer is used here synonymously to denote unit mass transfer since, in the case of reactions of type (1) or (2), it is not possible, in general, to distinguish between hydrogen and proton transfer with the experimental setup used.
(8) S. K. Gupta, E. G. Jones, A. G. Harrison, and J. J. Myher, *Can. J. Chem.*, **45**, 3107 (1967).
(9) A. G. Harrison, *Int. J. Mass Spectrom. Ion Phys.*, **6**, 297 (1971).
(10) W. E. W. Ruska and J. L. Franklin, *Int. J. Mass Spectrom. Ion Phys.*, **3**, 221 (1969).
(11) W. T. Huntress, Jr., and R. F. Pinizzotto, Jr., *J. Chem. Phys.*, **59**, 4742 (1973).
(12) B. H. Solka and A. G. Harrison, *Int. J. Mass Spectrom. Ion Phys.*, **17**, 379 (1975).
(13) The ionization potential of t-C_4H_9SH was not available and that of n-C_4H_9SH was used in its place based upon the observation that the ionization potentials of t-C_4H_9Cl (10.61) and n-C_4H_9Cl (10.67) are essentially equivalent.
(14) J. L. Franklin, J. G. Dillard, H. M. Rosenstock, J. T. Herron, K. Draxl, and F. W. Field, *Natl. Stand. Ref. Data Ser., Natl. Bur. Stand.*, **No. 26** (1969).
(15) J. L. Beauchamp, *Annu. Rev. Phys. Chem.*, **22**, 527 (1971).
(16) S. W. Benson, "Thermochemical Kinetics", Wiley, New York, N.Y., 1968.
(17) S. W. Benson, *J. Chem. Educ.*, **42**, 502 (1965).
(18) L. W. Sieck, L. Hellner, and R. Gordon, Jr., *Chem. Phys. Lett.*, **10**, 502 (1971).
(19) T. Su and M. T. Bowers, *J. Am. Chem. Soc.*, **95**, 1370 (1973).
(20) G. P. Nagy, T. C. T. Thynne, and A. G. Harrison, *Can. J. Chem.*, **46**, 3609 (1968).
(21) R. S. Hemsworth, J. D. Payzant, H. I. Schiff, and D. K. Bohme, *Chem. Phys. Lett.*, **26**, 417 (1974).
(22) As defined here for hydrogen transfer in amines, only hydrogen atoms on the nitrogen or on the carbon atom α to the nitrogen are in a geometrically favorable position for hydrogen transfer in an aligned ion-polar molecule collision complex. Such hydrogen atoms are designated "transferable".
(23) Estimated value of CH_3SCH_2–H bond dissociation energy 94–99 kcal mol^{-1}.
(24) R. J. W. Le Fèvre, "Advances in Physical Organic Chemistry II", Academic Press, New York, N.Y., 1965.
(25) R. D. Nelson, Jr., D. R. Lide, Jr., and A. A. Maryott, *Natl. Stand. Ref. Data Ser., Natl. Bur. Stand.*, **No. 10** (1967).

The Reaction of Cyanogen Chloride and Hydrogen Behind Reflected Shock Waves[1a,b]

J. M. Brupbacher, C. P. Esneault, R. D. Kern,* T. Niki, and D. E. Wilbanks

Department of Chemistry, University of New Orleans, New Orleans, Louisiana 70122

(Received December 14, 1976)

Publication costs assisted by the National Science Foundation

The rate law for the production of HCN over the temperature range 1850–2900 K was established by recording the time-dependent infrared emission from this species at 3.0 μm in the reflected shock zone. Four mixtures of ClCN and H_2 dilute in argon, differing in the ratio of initial reactant concentrations and initial shock pressures, were studied in order to determine the various order dependencies. The formation of the product was in all experiments observed to be nonlinear with respect to reaction time. The data were fit to the equation $1 - f_{HCN}/f_{HCN,max} = \exp(-k[ClCN]_0^{0.5}[H_2]_0^{0.1}[Ar]^{0.4}t^2)$, where $k = 10^{21.8\pm0.06}\exp(-70.3 \pm 0.6/RT)$ cm^3 mol^{-1} s^{-2}. The units for the activation energy are kcal mol^{-1}. Experiments in which the reflected shock zone was analyzed with a time-of-flight mass spectrometer revealed the products to be HCN, HCl, and C_2N_2. Computer calculated profiles of HCN using a 14 step atomic mechanism with available literature rate constants failed to reproduce the experimental profiles.

Introduction

Previous reports from this laboratory have concerned the nonlinear time dependence of product formation and the importance of this observation with regard to the existence of complex mechanisms in exchange systems involving simple molecules: $H_2 + D_2$,[2] $HCl + D_2$,[3] $HCN + D_2$,[4] and $HBr + D_2$.[5] The nature of the multistep sequence for the first three reactions is not known in detail but it has been suggested that excitation to the higher vibration and/or rotational levels of the ground electronic state is a prerequisite to product formation.[6] Evidence has been presented for the exchange of $HBr + D_2$ to proceed via atomic pathways.[5]

Two metathetical reactions of limited complexity have also been studied, $C_2N_2 + H_2 \rightarrow 2HCN$[7] and $H_2 + CO_2 \rightarrow H_2O + CO$.[8] In both of these systems, the time dependence for product formation was shown to be quadratic and arguments were made to demonstrate that their respective

mechanisms were not atomic and that the rate laws could be explained in terms similar to the three exchange systems previously mentioned.[2-4] However, both of the investigations were performed with limited objectives (testing of symmetry predictions for $C_2N_2 + H_2$ and formation of known amounts of water from a practically thermoneutral reaction) and as a consequence the individual reactant concentrations and total mixture pressures were not varied extensively.

The reaction of cyanogen chloride and hydrogen is an appealing prospect for a more complete rate law determination for several reasons: it is a relatively clean reaction at high temperatures; the infrared emission from one of the major products HCN is free from interference of other emitting species; the products and possible intermediates appear in a conveniently observed portion of the time-of-flight mass spectrum; and lastly, most of the elementary rate constants necessary for computer calculation of the product formation profiles (assuming an atomic mechanism) are available in the literature.

Although the metathesis has received surprisingly little attention, the pyrolysis of ClCN has been studied with the single pulse shock tube technique[9] and the dissociation of hydrogen has been reported by many shock tube workers employing a variety of analytical methods.[10]

Experimental Section

The source of the kinetic data reported herein was taken from a shock tube which was equipped to record simultaneously the infrared emissions from HCN and ClCN in the reflected shock zone. Experimental details pertaining to the apparatus and procedure have been described.[5] An interference filter centered at 3.0 μm (0.10-μm bandpass at half-peak height) was used for HCN emission while a 4.45-μm narrow band filter served for ClCN.

The following mixtures were tested for interference at the 3.0-μm filter observation port: 2% ClCN; 2% HCl; and 3% C_2N_2. The balance of the three mixtures was argon. Interference was observed only at the 4.45-μm station. Therefore, only the initial signal from that detector was used and solely for the purpose of establishing time zero for product formation.

Four reacting mixtures, labeled A–D, respectively, were prepared by the method of partial pressures: 1.5% ClCN–1.5% H_2, P_1 = 5 Torr; 1.5% ClCN–1.5% H_2, P_1 = 10 Torr; 3% ClCN–3% H_2, P_1 = 5 Torr; 3% ClCN–9% H_2, P_1 = 5 Torr. The diluent for all four mixtures was Linde argon (99.95%). Cyanogen chloride was purchased from Matheson and further purified by three consecutive liquid nitrogen bulb-to-bulb distillations in which only the middle fraction was retained in each step. Mass spectrometric analysis revealed impurity levels of 0.6% HCN and 1.1% HCl. No other foreign species were detected. Linde H_2 (99.95%) was treated by trapping the gas onto a previously purged Linde type 4A molecular sieve at 77 K. After slight warming, the middle fraction of the desorbing vapor was employed for mixture blending.

Three calibration mixtures were shocked to test the relation of detector signal amplitude and HCN concentration: 1.5% HCN–1.5% H_2; 3% HCN–3% H_2; 3% HCN–9% H_2. The diluent was argon. Hydrogen was added to suppress the formation of cyanogen from the reaction $2HCN \rightarrow C_2N_2 + H_2$ and to simulate a collision partner environment more similar to reaction conditions. Hydrogen cyanide evolved from KCN upon addition of concentrated sulfuric acid was collected and purified by bulb-to-bulb distillation.

Two Biomation 610 B transient recorders were connected in parallel to monitor the emission signal from the 3.0-μm filter station. One recorder was set to digitize the signal at selected sampling intervals of 0.5–2.0 μs in order to maximize data collection during the initial stages of the reaction. These settings were chosen to minimize any heating effects due to reaction exothermicity (–25 kcal mol^{-1}). The second recorder was set at a 5-μs sampling rate in order to determine the maximum signal intensity achieved by HCN production. Some 255 data points were generated by each Biomation. Polaroid pictures of oscilloscope traces of the emissions passing through the 3.0- and 4.45-μm filters were taken at sweep speeds of 50 and 10 μs/cm, respectively. The faster speed picture was used to determine time zero for the reaction from an analysis of the initial ClCN emission at 4.45 μm. The other picture provided a check on the Biomation recorders.

A time-of-flight (TOF) mass spectrometer was utilized to sample the reflected shock zone which contained mixture A in a diluent of neon–1% Ar. The primary purpose was to detect the presence of minor products and intermediates. Peaks corresponding to HCN, HCl, ClCN, and C_2N_2 were measured at 20-μs intervals during a total observation time of 440 μs. A mixture of 1.5% HCN, 1.5% ClCN, 1.5% C_2N_2, balance Ne–1% Ar, was prepared for static analysis in order to measure the relative ionization sensitivities of those species containing CN.

Hydrogen was used as the driver gas for all experiments performed in either the TOF or IR emission shock tube.

Results

Dynamic sampling of reaction mixture A by the TOF at 20-μs intervals revealed that the major products were indeed HCN and HCl and that, at high temperatures, minor amounts of C_2N_2 were formed. Cl_2 was not observed nor was any other readily identifiable intermediate. The temperature range covered was 1784–2455 K. The peak heights corresponding to m/e 27 (HCN), 52 (C_2N_2), and 61 (CNCl) were measured as a function of reaction time.

An expression for the mole fraction of HCN for an equimolar mixture of reactants was used:

$$f_{HCN} = [HCN]/([ClCN]_0 + [H_2]_0) \quad (1)$$

$$= [HCN]/2[ClCN]_0 \quad (2)$$

Mass balance for CN is given by the following equation:

$$[ClCN]_0 = [HCN] + 2[C_2N_2] + [ClCN] \quad (3)$$

Substitution of eq 3 into eq 1 along with the relative ionization sensitivities as determined from static analysis of a mixture of known concentrations of the various species yielded the working equation

$$f_{HCN} = \frac{1.5P_{27}}{2(1.5P_{27} + 2.0P_{52} + P_{61})} \quad (4)$$

where P represents the respective peak heights. Other mole fraction equations were likewise constructed and plots of f_{HCN}, f_{ClCN}, and f_{HCl} are displayed in Figure 1.

In addition to identifying the species present during the course of the reaction, the TOF data showed clearly the near disappearance of ClCN and the nonlinear time dependence of product formation. The long time mole fraction levels recorded by the TOF runs were in accord with equilibrium calculations on this particular mixture. The calculated mole fractions are listed in Table I. The chlorine amounts predicted were below the detectability threshold in our experiments.

The instrumentation which processed the infrared emission signals produced a 10- to 40-fold increase in the number of data points during the initial stages of HCN

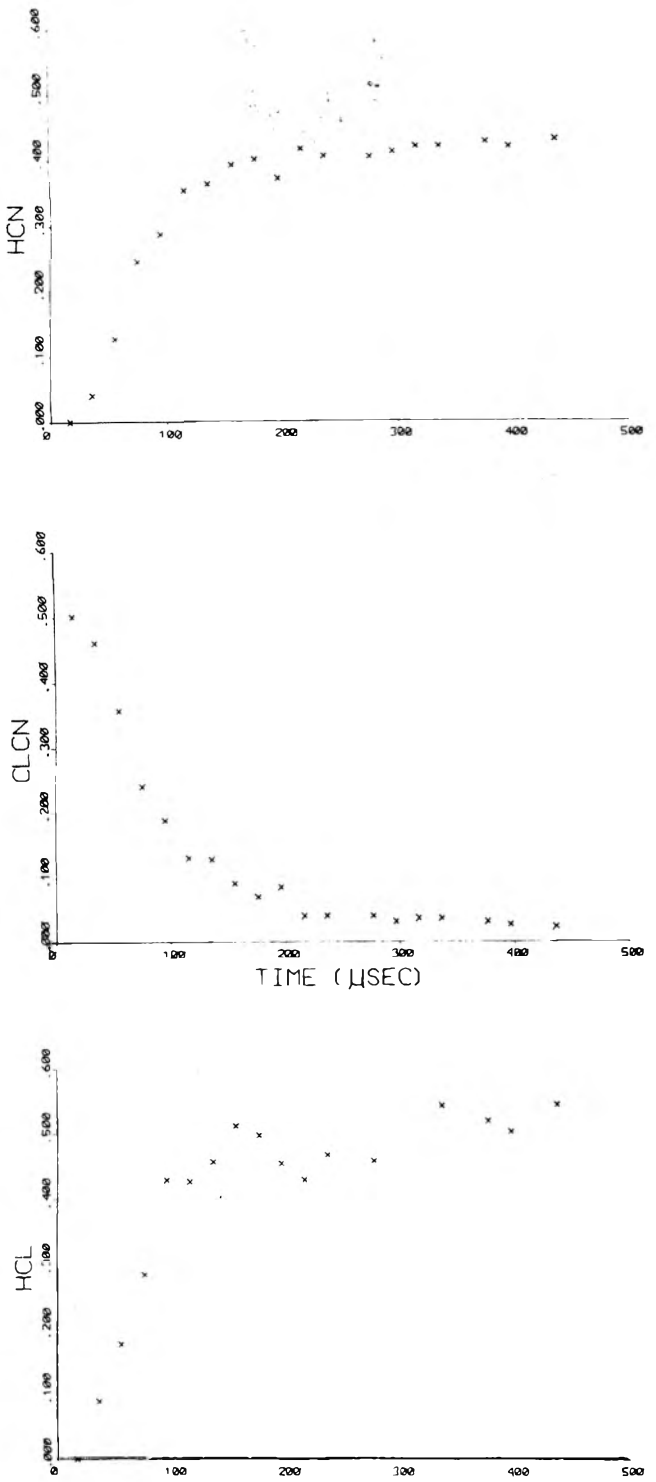

Figure 1. Mole fraction profiles of HCN, ClCN, and HCl for TOF experiment at 2339 K.

TABLE I: Mole Fractions in ClCN-H_2 Reaction at Equilibrium (Initial Mixture Equimolar)

T, K	HCN	HCl	ClCN	H_2	C_2N_2	Cl_2
1700	0.441	0.498	0.002	0.030	0.028	3×10^{-6}
2000	0.427	0.496	0.004	0.038	0.035	1.7×10^{-5}
2300	0.414	0.493	0.007	0.046	0.040	6.2×10^{-5}
2500	0.406	0.491	0.009	0.052	0.042	1.2×10^{-4}
2800	0.396	0.486	0.013	0.059	0.046	2.8×10^{-4}

formation. Thus, the product profile could be determined at early reaction times thereby reducing the effects of heat release. Shocked mixtures of 2% ClCN, 2% HCl, and 3% C_2N_2 (each diluted with argon) revealed an absence of signal at the 3.0-μm filter detector station. Calibration

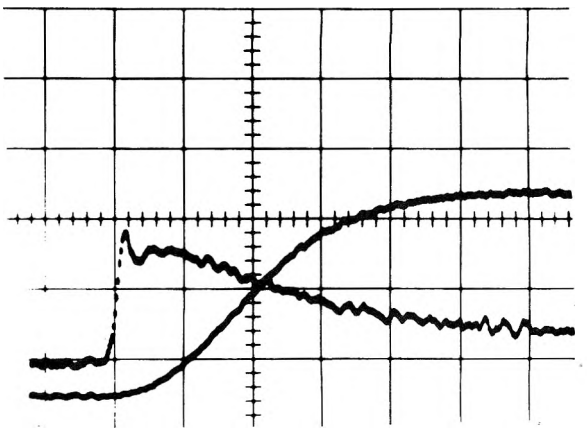

Figure 2. Infrared emission record from mixture B reacting at 2104 K. HCN emission is lowest trace on left-hand side. The sweep speed is 50 μs/cm.

experiments conducted with the 1.5% HCN and 3% HCN in argon mixtures demonstrated that, within experimental error, the signal intensity doubled with a twofold increase of HCN concentration over the temperature range spanned for the reaction mixtures. These facts, coupled with the circumstance that time zero is more accurately determined in the IR shock tube than in the TOF shock tube, indicated that analysis of the HCN emission signal was the best source of kinetic data for this system.

A typical oscilloscope record for a reacting mixture is displayed in Figure 2. The abruptly increasing signal on the left-hand side of the figure is due to ClCN emission and was used primarily to determine time zero for the reaction. It is interesting to note that the ClCN emission signal does not diminish to a level consistent with that shown in Figure 1 or Table I. This observation is easily explained by the emission at 4.45 μm of other species formed during the reaction, thus rendering the signal unsuitable for kinetic analysis.

The signal at 3.0 μm was due entirely to HCN emission and was treated according to the following equation:

$$Q = I/I_{max} = f_{HCN}/f_{HCN,max} \tag{5}$$

where I is the signal intensity at known reaction intervals and I_{max} is the maximum signal intensity plateau observed during a given run. The further equation of intensities to mole fractions is derived from the results of the calibration experiments.

The data were fit successfully to the following equation

$$1 - Q = \exp(-k't^z) \tag{6}$$

where z is the time dependence for product formation. The value of z was determined by a plot of the ln ln of the left-hand side of eq 6 vs. ln t. The slopes in all cases were linear and fell into the range 1.7–2.1 with no apparent pattern emerging with regard to temperature or mixture composition. A typical plot is shown in Figure 3. Since a constant time power is helpful in comparing rates, the value of 2.0 was chosen for z in all rate calculations.

After selection of the quadratic time dependence, the value of k' for each experiment was calculated. In order to minimize the effect of temperature change in the reflected shock zone due to reaction exothermicity, only those points with Q less than 0.5 were utilized. The best fit profile along with the experimental data were plotted for all runs. A typical example is displayed in Figure 4. An Arrhenius plot of the four mixtures studied (A–D) is shown in Figure 5.

TABLE II: Rate Constants for ClCN-H_2 Reaction

T, K	$10^6\rho_5$ mol cm^{-3}	$10^{-14}k$ cm^3 mol^{-1} s^{-2}	T, K	$10^6\rho_5$ mol cm^{-3}	$10^{-14}k$ cm^3 mol^{-1} s^{-2}
A. 1.5% ClCN-1.5% H_2, P_1 = 5 Torr					
1877	1.82	0.526	2368	2.01	18.8
1899	1.83	0.558	2423	2.02	29.3
1942	1.85	0.689	2538	2.06	50.3
2003	1.88	1.29	2617	2.08	80.7
2005	1.88	1.13	2659	2.09	90.1
2032	1.89	1.45	2761	2.12	184
2045	1.89	2.03	2819	2.13	193
2130	1.93	2.78	2829	2.14	260
2198	1.95	6.07	2843	2.14	163
2330	2.00	13.6	2897	2.15	273
2331	2.00	17.5			
B. 1.5% ClCN-1.5% H_2, P_1 = 10 Torr					
1968	3.73	0.848	2298	3.96	15.0
1989	3.73	1.48	2319	3.98	11.3
2068	3.80	2.25	2363	4.01	22.9
2104	3.83	2.91	2375	4.01	18.6
2229	3.91	7.91	2401	4.03	24.8
2257	3.94	11.2	2620	4.16	90.1
2263	3.94	13.5			
C. 3% ClCN-3% H_2, P_1 = 5 Torr					
1972	2.00	0.785	2333	2.14	18.9
2018	2.02	1.26	2373	2.16	19.7
2040	2.03	1.71	2390	2.16	22.3
2092	2.05	2.61	2526	2.22	51.2
2109	2.06	2.55	2544	2.22	64.5
2129	2.06	3.95	2564	2.22	78.3
2178	2.08	3.99	2566	2.22	56.5
2183	2.09	5.53	2648	2.25	88.3
2236	2.11	8.10	2654	2.25	102
2258	2.12	8.56	2656	2.25	98.2
2276	2.12	10.8	2691	2.26	133
2289	2.13	11.3			
D. 3% ClCN-9% H_2, P_1 = 5 Torr					
1855	2.08	0.373	2228	2.26	7.30
1867	2.09	0.319	2236	2.26	7.29
1869	2.09	0.393	2313	2.27	13.4
1946	2.13	0.705	2331	2.30	15.9
1950	2.13	0.905	2377	2.32	23.3
1952	2.13	0.821	2410	2.33	29.5
1992	2.15	1.21	2441	2.35	27.5
1998	2.15	1.09	2445	2.35	29.8
2011	2.16	1.52	2474	2.36	35.0
2016	2.16	1.43	2533	2.38	53.6
2075	2.19	2.65	2547	2.38	48.8
2091	2.20	2.12	2561	2.39	62.5
2150	2.23	4.03	2668	2.43	106

The order of the reaction with respect to ClCN, H_2, and Ar was found from the following equation

$$k' = k(\mathrm{ClCN})_0^a(\mathrm{H_2})_0^b(\mathrm{Ar})^c \quad (7)$$

where a, b, and c are the respective individual orders. A computer program, into which the reflected shock zone gas density for each experiment was input, employed an iterative routine to calculate the set of orders which gave the least statistical variance. The best fit values were a = 0.5, b = 0.1, and c = 0.4. The concentration independent rate constant k was calculated for all IR experiments and is represented by the following Arrhenius equation:

$$k = 10^{21.78\pm0.06}\exp(-70.3 \pm 0.6/RT)\ \mathrm{cm^3\ mol^{-1}\ s^{-2}} \quad (8)$$

The units for the activation energy are kcal mol^{-1}. The rate constants and the best fit line are presented in Figure 6 and listed in Table II. The reflected shock pressures varied from 0.28 to 0.89 atm.

TABLE III: Arrhenius Parameters for Computer Simulation Program[a]

Reaction	log A	E^*	Ref
a	16.53	91.5	9
b	13.97	88.9	16
c	14.00	34.0	9
d	13.05	6.0	9
e	13.78	5.0	Est
f	13.78	5.0	Est
g	13.92	5.5	17
h	13.53	7.0	18
i	13.78	10.0	Est
j	14.52	2.9	Est
k	16.79	117.1	19
l	9.82	70.0	20
m	16.81	98.6	21
n	10.94	48.0	22

[a] Units: A = cm^3 mol^{-1} s^{-1}; E^* = kcal mol^{-1}.

Discussion

The inert gas dependence and the nonlinear production of HCN argue persuasively against a direct bimolecular mechanism involving the reactants and suggest that the reaction is proceeding via a series of elementary steps.

Of prime consideration is an atomic mechanism consisting of the following steps:

$$\mathrm{ClCN + Ar \rightleftharpoons CN + Cl + Ar} \quad (a)$$

$$\mathrm{H_2 + Ar \rightleftharpoons 2H + Ar} \quad (b)$$

$$\mathrm{Cl + ClCN \rightleftharpoons Cl_2 + CN} \quad (c)$$

$$\mathrm{CN + ClCN \rightleftharpoons C_2N_2 + Cl} \quad (d)$$

$$\mathrm{H + ClCN \rightleftharpoons HCN + Cl} \quad (e)$$

$$\mathrm{H + ClCN \rightleftharpoons HCl + CN} \quad (f)$$

$$\mathrm{Cl + H_2 \rightleftharpoons HCl + H} \quad (g)$$

$$\mathrm{CN + H_2 \rightleftharpoons HCN + H} \quad (h)$$

$$\mathrm{H + C_2N_2 \rightleftharpoons HCN + CN} \quad (i)$$

$$\mathrm{H + Cl_2 \rightleftharpoons HCl + Cl} \quad (j)$$

$$\mathrm{HCN + Ar \rightleftharpoons H + CN + Ar} \quad (k)$$

$$\mathrm{HCl + Ar \rightleftharpoons H + Cl + Ar} \quad (l)$$

$$\mathrm{C_2N_2 + Ar \rightleftharpoons 2CN + Ar} \quad (m)$$

$$\mathrm{Cl_2 + Ar \rightleftharpoons 2Cl + Ar} \quad (n)$$

All but four of the forward direction rate constants have values in the literature. Reasonable estimates for those not measured were made[11-13] and the values used in a computer calculated profile of HCN are listed in Table III. The appropriate thermodynamic data necessary for the reverse reaction rate constants were taken from the JANAF tables.[14] Calculations were performed at 1900, 2300, 2600, and 2800 K for each of the four mixtures studied, A–D, at their respective initial shock pressures.[15]

The resulting profiles were observed to have nonlinear shapes similar to those recorded experimentally. In fact, the resulting profiles could be fit for each of the mixtures by eq 5 and 6. Values of the time dependence z were found to be in the range 2.08–2.11. The respective values of k' for each mixture were used to calculate the individual Arrhenius lines. Lastly, the reaction orders a, b, and c were determined, which yielded the following result:

$$k' = k(\mathrm{ClCN})_0^{0.50}(\mathrm{H_2})_0^{0.62}(\mathrm{Ar})^{0.77} \quad (9)$$

A grand Arrhenius line for the computer generated profiles was obtained

$$k = 10^{29.5}\exp(-94.5/RT) \quad (10)$$

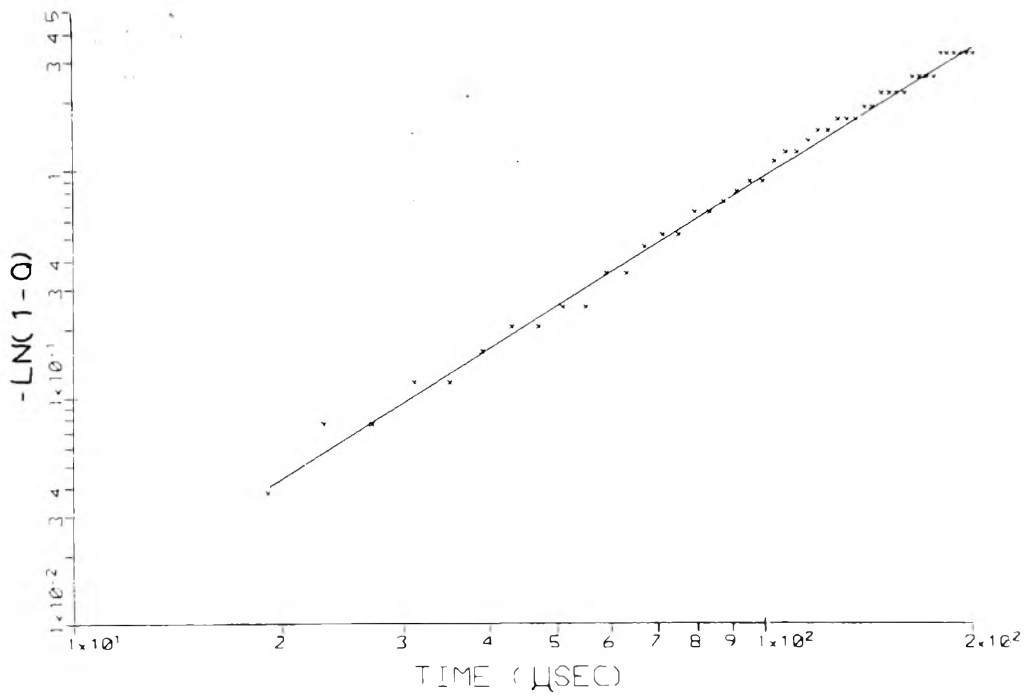

Figure 3. Time power plot for an IR experiment at 2178 K, $z = 1.93$.

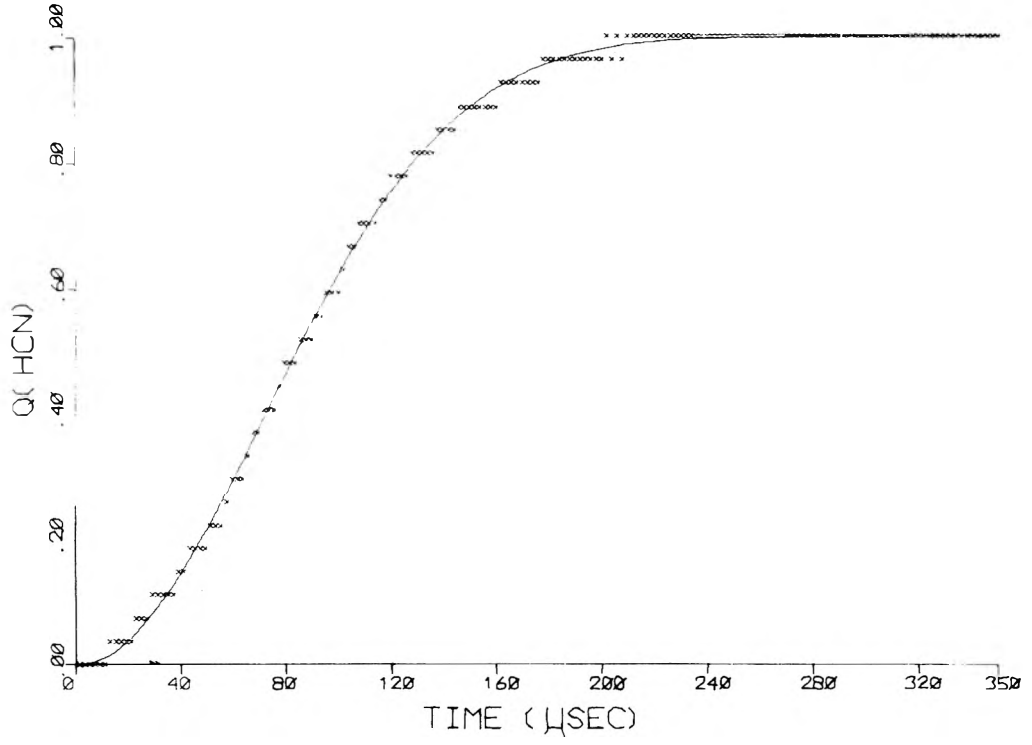

Figure 4. Reaction profile for HCN from an IR experiment at 2178 K.

The units for the preexponential factor are $(cm^3\ mol^{-1})^{-1.89}\ s^{-2}$.

Comparison between an experimental HCN profile and a computed profile is shown in Figure 7. The Arrhenius line for eq 10 appears in Figure 8.

The fractional orders, inert gas dependence, and nonlinear time dependence are all predicted by an atomic mechanism. The most serious discrepancy with regard to experimental results is the magnitude of the activation energy: 70.3 vs. 94.5 kcal mol^{-1}. Variation of the rate constants of the three center reactions did not produce "agreement". The most significant steps are the dissociations of the reactants and the computed magnitude of the apparent activation energy for the metathesis reflects this fact.

One possible reconciliation involves the proposal of a reactant catalyzed dissociation occurring with an activation energy some 19–21 kcal less than that measured with an inert gas.

$$ClCN + H_2 \rightarrow Cl + CN + H_2 \quad (o)$$

$$H_2 + ClCN \rightarrow H + H + ClCN \quad (p)$$

There exists no evidence to support this proposal and there is indirect evidence that decompositions occur with an activation energy not much different from that recorded with an inert gas. The dissociation of H_2 have been

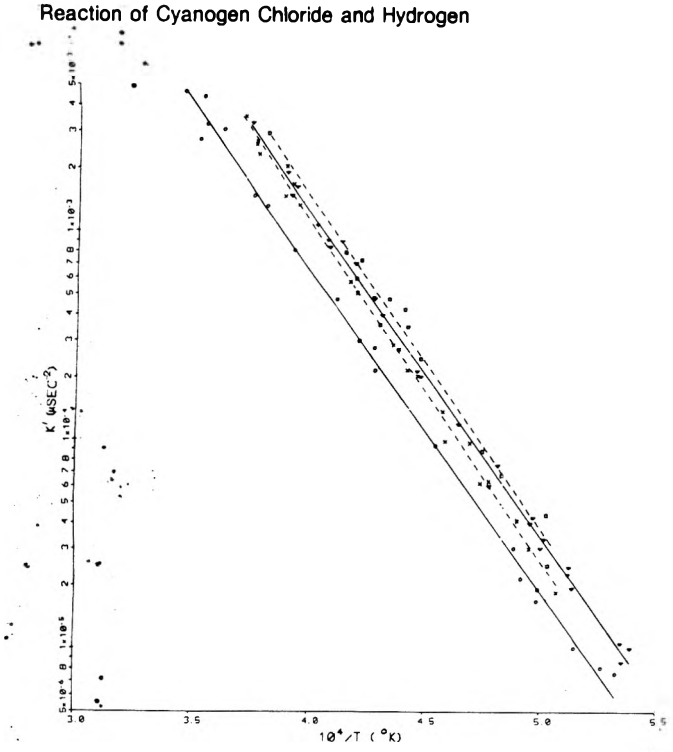

Figure 5. Arrhenius plot of k' rate constants for mixtures A–D: (O) A; (□) B; (×) C; (▽) D.

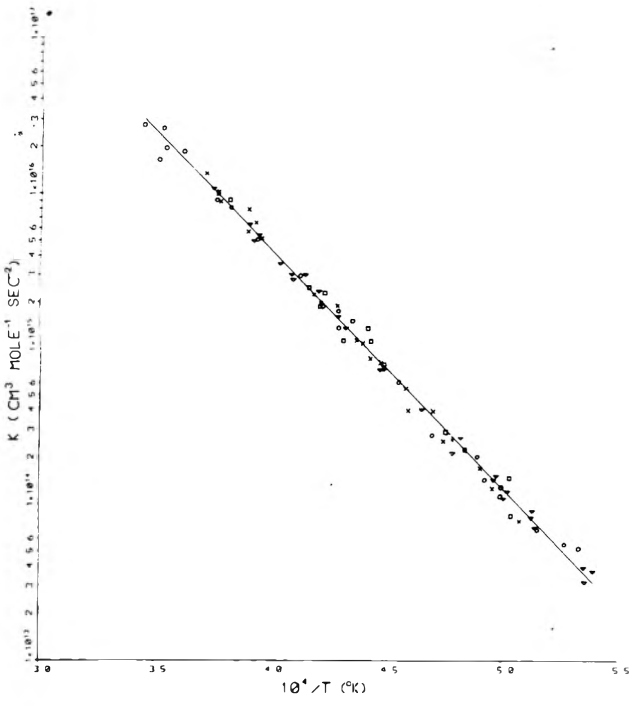

Figure 6. Arrhenius plot for data in Table II. Symbols identical with those used in Figure 5.

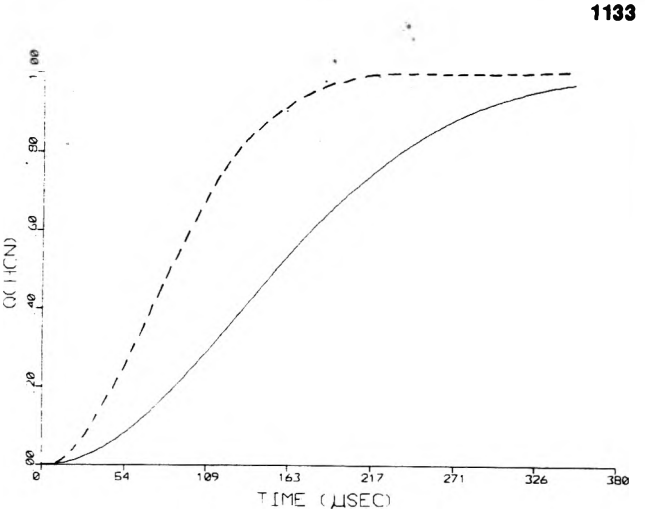

Figure 7. Comparison of experimental (dashed line) and atomic mechanism (solid line) profiles for HCN at 2178 K.

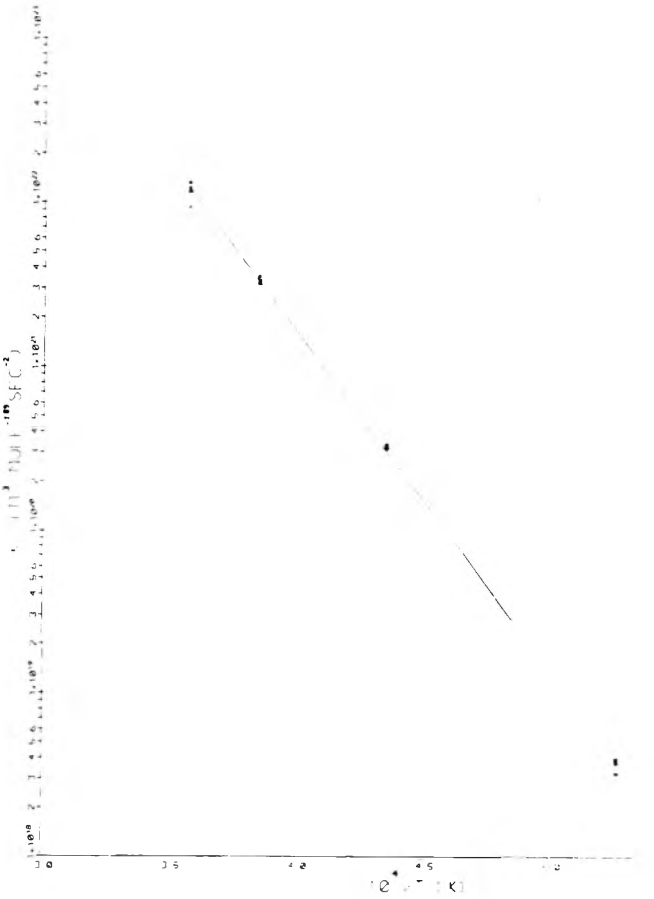

Figure 8. Combined Arrhenius plot for rate constants derived from atomic mechanism. Symbols are the same as those in Figure 5.

measured with Ar, H_2, and H as collision partners.[16] The respective rate constants differ but the difference is not of the magnitude required to explain the results herein.

$$k_{H_2\text{-Ar}} = 9.35 \times 10^{13} \exp(-88900/RT) \quad (11)$$

$$k_{H_2\text{-}H_2} = 3.30 \times 10^{15} \exp(-105300/RT) \quad (12)$$

$$k_{H_2\text{-H}} = 2.12 \times 10^{15} \exp(-87200/RT) \quad (13)$$

The reactions represented by eq 12 and 13 may be considered in the same category as (o) and (p), since it is well known that the respective exchange reactions take place with activation energies of 40[2,6] and 7[23] kcal mol^{-1}. The corresponding dissociations occur at rates closer to the noncatalyzed H_2–Ar decomposition.

The remaining possible mechanism involves the excitation of the reactants to certain rotational–vibrational states prior to the collision events which lead to products. This idea has been advanced previously[6] and its application to ClCN + H_2 is similar to the CO_2 + H_2 system.[8] Unfortunately, the tabulation of relevant rate constants for a computer simulation is not yet available. However, results from laser photochemistry experiments indicate that vibrational excitation of reactants can have a dramatic effect upon product formation. For instance, vibrational excitation of HCl by radiation from a HCl laser increases the rate 5000-fold of the reaction

$$O + HCl \rightarrow OH + Cl \quad (q)$$

compared to the ground state reaction rate.[24]

References and Notes

(1) (a) Paper presented at the 32nd Southwest Regional Meeting of the American Chemical Society, Fort Worth, Tex., Dec, 1976. (b) Support of this work by the National Science Foundation, Grant CHE 76-08529, is gratefully acknowledged.
(2) R. D. Kern and G. G. Nika, *J. Phys. Chem.*, **75**, 1615 (1971).
(3) R. D. Kern and G. G. Nika, *J. Phys. Chem.*, **75**, 171 (1971).
(4) R. D. Kern and J. M. Brupbacher, *J. Phys. Chem.*, **76**, 285 (1972).
(5) R. D. Kern and G. G. Nika, *J. Phys. Chem.*, **78**, 2549 (1974).
(6) S. H. Bauer and E. Ossa, *J. Chem. Phys.*, **45**, 434 (1966).
(7) J. M. Brupbacher and R. D. Kern, *J. Phys. Chem.*, **77**, 1329 (1973).
(8) J. M. Brupbacher, R. D. Kern, and B. V. O'Grady, *J. Phys. Chem.*, **80**, 1031 (1976).
(9) D. Schofield, W. Tsang, and S. H. Bauer, *J. Chem. Phys.*, **42**, 2132 (1965).
(10) R. D. Kern, *Compr. Chem. Kinet.*, **18**, 1 (1976).
(11) S. W. Benson, "Thermochemical Kinetics", Wiley, New York, N.Y., 1968.
(12) M. R. Dunn, C. G. Freeman, M. J. McEwan, and L. F. Phillips, *J. Phys. Chem.*, **75**, 2662 (1971).
(13) K. Tabayashi, O. Kajimoto, and T. Fueno, *J. Phys. Chem.*, **79**, 204 (1975).
(14) "JANAF Thermochemical Tables", 2nd ed, U.S. Department of Commerce, Washington, D.C., 1971.
(15) Dr. A. M. Dean kindly provided us with a copy of his computer program.
(16) W. D. Breshears and P. F. Bird, *Symp. (Int.) Combust., [Proc.], 14th*, (1972).
(17) P. G. Ashmore and J. Chanmugam, *Trans. Faraday Soc.*, **49**, 254 (1953).
(18) P. Hartel and M. Polanyi, *Z. Phys. Chem. B*, **11**, 97 (1930).
(19) T. Just and P. Roth, *Ber. Bunsenges. Phys. Chem.*, **80**, 171 (1976).
(20) T. A. Jacobs, N. Cohen, and R. R. Giedt, *J. Chem. Phys.*, **46**, 1958 (1967).
(21) T. Fueno, K. Tabayashi, and O. Kajimoto, *J. Phys. Chem.*, **77**, 575 (1973).
(22) A. C. Lloyd, *Int. J. Chem. Kinet.*, **3**, 39 (1971).
(23) A. A. Westenberg and N. de Haas, *J. Chem. Phys.*, **47**, 1393 (1967).
(24) E. Stark, *Ind. Res.*, **18**, 78 (1976).

Rate Constants for the Reactions of Hydrogen Atoms with Some Silanes and Germanes†

E. R. Austin and F. W. Lampe*

Davey Laboratory, Department of Chemistry, The Pennsylvania State University, University Park, Pennsylvania 16802

(Received November 5, 1976)

Publication costs assisted by the U. S. Energy Research and Development Administration

Rate constants for the reactions of H atoms, formed by mercury photosensitization of H_2–substrate mixtures at 32 °C, with $(CH_3)_nSiH_{4-n}$ and $(C_2H_5)_nSiH_{4-n}$ for n = 0, 1, 2, 3; with $(CH_3)_nSiD_{4-n}$ for n = 0, 1; and with Si_2H_6, Si_2D_6, GeH_4, and Ge_2H_6 have been determined in experiments involving the competitive reaction of H atoms with C_2H_4 and i-C_4H_8. Activation energies, estimated from these rate constants, have been combined with thermochemical data by means of a bond-energy–bond-order (BEBO) method of calculation to yield a consistent set of dissociation energies for Si–H bonds in the R_nSiH_{4-n} series of silanes for n = 0, 1, 2, 3.

Introduction

During the past decade there has developed a considerable body of consistent kinetic data pertaining to the gas-phase reactions of methyl,[1-9] ethyl,[3,10] propyl,[10] and fluoromethyl[3,11-17] radicals with various silanes and methylsilanes. The predominant reaction that occurs is the abstraction of a hydrogen atom bound to silicon and this process is followed by the combination and disproportionation of the silyl radicals.[18-23] The rate constants for the abstraction reaction exhibit strikingly little variation in the preexponential factors and in the activation energies for attack by different alkyl radicals on the same silicon–hydrogen bond.[24] Comparatively little kinetic data are available for the reactions of hydrogen atoms with silanes[20,25-31] and practically no such information exists for germanes.[30] Moreover, serious disagreements exist among the rate constants at room temperature reported for the reaction of hydrogen atoms with monosilane, the ratio of the highest[30] to the lowest[31] value being of the order of 20.

We have conducted mass-spectrometric studies of the rates of hydrogen-atom induced decomposition of a number of silanes and germanes relative to the rate of hydrogen-atom addition to ethylene at 32 °C. From these studies, we have determined the specific reaction rates for hydrogen-atom attack on the substrate molecules and this paper is a report of our results.

† U.S. Energy Research and Development Administration Document No. EY-76-S-02-3416-1.

Experimental Section

Hydrogen atoms were generated by $Hg(^3P_1)$ photosensitization of hydrogen–substrate mixtures which in all cases contained about 98% hydrogen. Under these conditions more than 95% of the $Hg(^3P_1)$ atoms that undergo collisional quenching react with hydrogen, thereby forming hydrogen atoms. Most of our experiments were conducted in the pressure range of 35–60 Torr although in a few instances pressures as low as 20 Torr were used. At these pressures gas-phase recombination of hydrogen atoms and diffusion of hydrogen atoms to the walls is negligible compared with the reported rates of reaction with substrate molecules.[20,25-38]

The reactions were carried out in a photolysis cell containing a pin-hole leak leading into the ionization region of a Bendix Model 14-101 time-of-flight mass spectrometer. The photolysis cell is connected via 0.25-in. stainless steel and 6-mm pyrex tubing to large reservoirs (5–12 L) containing the reactants. Premixed reactant gases thus flow continuously through the pin-hole leak into the mass spectrometer. The reaction cell is uniformly illuminated and the average times required for diffusion of reactive transients (i.e., H atoms, >Si radicals, and >C radicals) from the center to the most remote regions of the cell are shorter by at least a factor of 30 than the mean residence time of a molecule in the cell (i.e., ~500 s). Before turning on the light the reactant concentration in the cell attains a steady state determined solely by the flow rates into and out of the cell as indicated by the constancy of the per-

tinent ion-current with time. When the shutter is opened and the cell is irradiated a chemical reaction loss channel is suddenly opened. It can be shown by straightforward kinetic analysis that the derivative of the ion current with respect to time, evaluated at the instant the shutter is opened, is equal to the rate of the chemical loss channel provided by the illumination. The flow rates are such that during the course of a single experiment (typically 2–3 min) the pressure decrease in the reservoir is of the order of 0.5% or less. The apparatus has been previously described in detail.[23]

The source of 2537-Å radiation for generation of $Hg(^3P_1)$ atoms was a General Electric 4-W G4T4/1 germicidal lamp. Measurements of the initial rate of formation of n-C_4H_{10} in H_2–C_2H_4 mixtures, assuming a disproportionation-to-combination ratio[39] of 0.1, indicate that hydrogen atoms are formed in our experiments at a rate of 6.7×10^{13} atoms/cm^3 s. This number, which is presented only to orient the reader, is actually a lower limit, since we have neglected formation of HgH in the interaction of $Hg(^3P_1)$ with H_2.[40] Although HgH will not react with C_2H_4,[40,41] its possible reaction with C_2H_5 radicals to form C_2H_6 and Hg (and therefore not C_4H_{10}) will tend to make our estimate of the formation rate of H atoms too low. In the competitive experiments the presence of NO prevents the reaction of HgH and C_2H_5 with each other,[42] and in any event the concentration of H atoms does not play a role since it cancels out in the initial-rate ratio expression (cf. eq 11). The temperature of the photolysis cell was measured using a chromel–alumel thermocouple and was found to be 32 ± 2 °C.

Monosilane, hydrogen, nitric oxide, and isobutylene were obtained from Matheson Gas Products; methylsilane, dimethylsilane, diethylsilane, trimethylsilane, and triethylsilane were obtained from Peninsular Chemresearch; and disilane-d_6 was obtained from Merck and Co. Ethylene was obtained from Phillips Petroleum Co. Monosilane-d_4 and methylsilane-d_3 were obtained by the reduction of tetrachlorosilane and trichloromethylsilane, respectively, with lithium aluminum deuteride. Similarly, disilane and ethylsilane were prepared by the reduction of hexachlorodisilane and trichloroethylsilane, respectively, with lithium aluminum hydride. Monogermane was prepared by reacting an aqueous solution of potassium hydroxide, germanium dioxide, and potassium tetrahydroborate with glacial acetic acid. Digermane is also produced in the monogermane synthesis, to the extent of about 10%, and these latter two compounds were always run simultaneously. All compounds were purified on a high-vacuum line prior to use.

Results and Discussion

1. *Basis of the Relative Rate Measurements.* Consider a gaseous system containing C_2H_4, some other substrate X, Hg vapor, and an excess of H_2. If it is supposed that H_2 is in such great excess that electronically excited $Hg(^3P_1)$ atoms are collisionally deactivated only by H_2, irradiation of this gaseous mixture by 2537-Å radiation initiates the following reaction sequence:

$$Hg(^1S_0) + h\nu(2537\ \text{Å}) \rightarrow Hg(^3P_1) \quad (1)$$

$$Hg(^3P_1) + H_2 \rightarrow Hg(^1S_0) + 2H \quad (2a)$$

$$Hg(^3P_1) + H_2 \rightarrow HgH + H \quad (2b)$$

$$H + X \rightarrow \text{free radical product} \quad (3)$$

$$H + C_2H_4 \underset{b}{\overset{a}{\rightleftarrows}} C_2H_5^* \xrightarrow[c]{(M)} C_2H_5 \quad (4)$$

The rates of reactions 3 and 4 can be determined from the time dependencies of the concentrations of X and C_2H_4 provided the free-radical products of these reactions are intercepted and thereby prevented from reacting with X, C_2H_4, and each other. On the basis of previous studies in this[43,44] and other laboratories,[18] NO at a level of 1–2% of the total substrate concentration, i.e., [X] + [C_2H_4], would appear to be an excellent interceptor. With NO present we must add to the above reaction sequence the following:

$$Pr\cdot + NO \rightarrow PrON \quad (5)$$

$$C_2H_5 + NO \rightarrow C_2H_5NO \quad (6)$$

in which Pr· represents the radical product of (3). In reaction 5 addition of this radical to the oxygen atom is indicated because in most of our studies Pr· is a silyl radical and silyl radicals have been shown[18,43] to add to NO in this manner. We think it is likely that germyl radicals will add the same way. It has been shown that PrON· radicals react further with NO and produce intermediates that attack silanes,[18,43] and presumably germanes. However, such reactions will be observed in our experiments[43] as secondary processes and will not affect our results, provided we measure *initial* rates of depletion of X and C_2H_4.

Assuming that H atoms are at a steady-state concentration, the initial rates of disappearance of reactants are

$$-(d[X]/dt)_0 = k_3[H][X]_0 \quad (7)$$

$$-(d[C_2H_4]/dt)_0 = k_4[H][C_2H_4]_0 \quad (8)$$

where the subscript zero indicates initial values. If s is an ion of m/e that is unique to the mass spectrum of the standard, C_2H_4, and x is an ion of m/e that is unique to the mass spectrum of X, then the relationships between initial ion currents and those at some later time are

$$i_s/i_s^0 = [C_2H_4]/[C_2H_4]_0 \quad (9)$$

$$i_x/i_x^0 = [X]/[X]_0 \quad (10)$$

Substitution of these latter expressions into (7) and (8) followed by division of (7) by (8) yields the expression

$$\frac{i_s^0}{i_x^0}\frac{(di_x/dt)_0}{(di_s/dt)_0} = \frac{k_3}{k_4} \quad (11)$$

Therefore, according to (11) we may determine the ratio k_3/k_4 simply from measurements of the initial ion currents of s and x and their initial rates of decrease during irradiation. Absolute calibrations relating observed ion currents to ion-source concentrations are not required. Typical recorder tracings of such experiments are shown in Figure 1. It is clear that reliable initial slopes can be obtained and k_3/k_4 calculated.

The simple expression in (11) was derived with the assumption that $Hg(^3P_1)$ atoms are collisionally deactivated only in collisions with H_2. This is only approximately true because, as pointed out in the Experimental Section, the gases C_2H_4 and X can contribute up to about 5% of the total collisional deactivation of $Hg(^3P_1)$.[45] It is easy to show that inclusion of collisional quenching by X and C_2H_4, with rate constants of k_2^x and k_2^s, respectively, transforms (11) to (12), for our conditions of $[H_2]/[X] = [H_2]/[S] = 98$.

$$\frac{i_s^0}{i_x^0}\frac{(di_x/dt)_0}{(di_s/dt)_0} = \frac{k_3}{k_4}\left\{\frac{196 + \frac{k_2^x}{k_2}\left(2 + \frac{k_4}{k_3}\right)}{196 + \frac{k_2^s}{k_2}\left(1 + \frac{k_3}{k_4}\right) - \frac{k_2^x}{k_2}}\right\} \quad (12)$$

Comparison of values of k_3/k_4 calculated from (11) with those calculated from (12) using available quenching cross sections[18,45] shows that the maximum error introduced in the ratio by use of the simple expression is 2% and is

TABLE I: Rate Constants for H-Atom Induced Decomposition at 32 °C[a]

Substrate	m/e	No. of runs	k_3/k_4	k_3(cm³/s) × 10^{12} (this work)	k_3(cm³/s) × 10^{12} (lit.)
$(CH_3)_2C{=}CH_2$	56	10	5.6 ± 0.5	4.7 ± 0.8[b]	5.3 ± 1.5,[c] 3.8 ± 0.6[d] 3.4 ± 1.0,[e] 4.6 ± 1.2[f] 4.8 ± 1.3[g]
SiH_4	31	12	0.51 ± 0.07	0.43 ± 0.09	0.45 ± 0.03,[h] 2.6 ± 0.3,[i] 8.5 ± 0.7[j]
SiD_4	32	10	0.18 ± 0.01	0.15 ± 0.02	0.27 ± 0.05,[k] 0.18[h]
Si_2H_6	62	9	4.40 ± 0.06	3.7 ± 0.6	3.6[l]
Si_2D_6	68	10	1.80 ± 0.05	1.5 ± 0.2	2.3[l]
CH_3SiH_3	43	11	0.73 ± 0.03	0.62 ± 0.10	1.2 ± 0.2[i]
CH_3SiD_3	48	10	0.27 ± 0.02	0.23 ± 0.04	
$(CH_3)_2SiH_2$	59	13	0.78 ± 0.07	0.66 ± 0.12	0.41 ± 0.09[i]
$(CH_3)_3SiH$	59	11	0.67 ± 0.06	0.56 ± 0.10	0.37 ± 0.10[i]
$(CH_3)_4Si$	88	1	<0.01	<0.01	
$C_2H_5SiH_3$	60	10	0.89 ± 0.06	0.75 ± 0.13	
$(C_2H_5)_2SiH_2$	88	9	1.5 ± 0.2	1.3 ± 0.3	
$(C_2H_5)_3SiH$	87	9	1.2 ± 0.1	1.0 ± 0.2	
GeH_4	70,72	17	2.4 ± 0.2	2.0 ± 0.4	430 ± 30[j]
Ge_2H_6	148	16	19 ± 2	16 ± 3	

[a] All experiments were carried out using an ionizing energy of 50 eV except for the isobutylene experiments which were done at 15 eV. [b] This value is taken as the average of the results of ref 47 and 48. [c] Reference 32. [d] Reference 33. [e] Reference 46. [f] Reference 47. [g] Reference 48. [h] Reference 31. [i] Reference 29. [j] Reference 30. [k] Reference 28. [l] Reference 20.

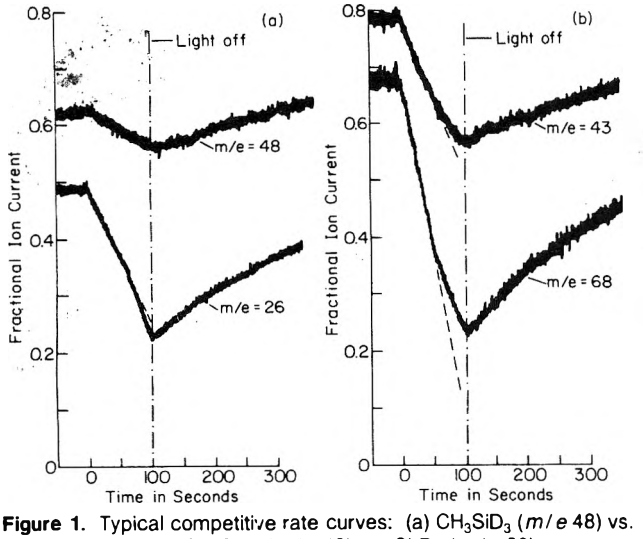

Figure 1. Typical competitive rate curves: (a) CH_3SiD_3 (m/e 48) vs. C_2H_4 (m/e 26); (b) CH_3SiH_3 (m/e 43) vs. Si_2D_6 (m/e 68).

usually less than 1%. Since this lies within our precision of measurement of initial slopes we have calculated the rate constant ratios by the simpler expression in (11).

Although the reaction mechanism and kinetic treatment have been written with C_2H_4 as the standard, mass interferences from products of the C_2H_5 + NO reaction forced us in some cases to use secondary standards. For example, as shown in Figure 1b, the depletion rate of CH_3SiH_3 (m/e 43) was measured relative to that of Si_2D_6 (m/e 68). It was not possible to use C_2H_4 as a standard for CH_3SiH_3 because of mass interferences from products of the C_2H_5 + NO reaction in the m/e range of 43–45. The rate constant of the H + Si_2D_6 reaction relative to that of the H + C_2H_4 reaction had been determined previously (cf. Table I).

2. *Rate Constants and Activation Energies.* The values of the rate constant ratios k_3/k_4 determined as the average of many replicate experiments are shown in Table I. Also shown in Table I are the numbers of replicate experiments involved, the m/e values of the ions used in the mass-spectrometric monitoring of the substrate X concentrations, the absolute values of the rate constants, and corresponding literature values for these latter quantities. The ion of m/e 26 was used to monitor C_2H_4 concentration.

Conversion of the relative rate constants in the fourth column of Table I to absolute values of k_3 in the fifth column of this table requires knowledge of k_4, the rate constant for addition of H atoms to C_2H_4. Since the internally excited ethyl radicals, C_2H_5*,[61] formed by (4a) may decompose back to the reactants by (4b) before being collisionally stabilized by (4c), the rate constant for H-atom removal by C_2H_4 is actually pressure dependent. It may be written as

$$k_4 = k_{4a}\Big/\left(1 + \frac{k_{4b}}{k_{4c}[M]}\right) \qquad (13)$$

The high-pressure limiting value of k_4, for which $k_{4c}[M] \gg k_{4b}$, is known to be 1.21 ± 0.19 × 10^{-12} cm³/s.[32-38] Within our experimental error and limited pressure range we were unable to detect a pressure dependence of the relative rate constants. However, evidence[46] does exist which indicates that the effective rate constant for H atom removal by C_2H_4 will be somewhat below the high-pressure limit. On the other hand, it has been shown that H-atom removal by C_3H_6 and C_4H_8 is in the high-pressure limit over our entire pressure range.[46] Cvetanovic and coworkers[32,47,48] have carried out a number of studies of the competitive addition of H atoms to C_2H_4 and i-C_4H_8 under conditions such that both reactions are in the high-pressure limit. As stated in the two latter papers,[47,48] their most reliable value for the ratio $k(i\text{-}C_4H_8)/k(C_2H_4)$ is 3.90 ± 0.08. This value is in excellent agreement with the same ratio calculated from the absolute values of the rate constants reported by Braun and Lenzi,[33] namely, 3.80. Comparison with the corresponding ratio in Table I of 5.6 ± 0.5 indicates that the absolute rate constant for removal of H atoms by C_2H_4 in our experiments is (70 ± 6)% of the high-pressure limit, or 0.85 ± 0.05 × 10^{-12} cm³/s. This latter value is in reasonable accord with experimental studies of the pressure dependence of k_4.[34,37,46,49] Accordingly we have used this latter value of k_4 to convert the rate constant ratios k_3/k_4 to absolute values of k_3. These absolute values are shown in the fifth column of Table I.

Inspection of Table I reveals that our values for the rate constants for H-atom attack on SiH_4, SiD_4, Si_2H_6, and Si_2D_6 are in satisfactory agreement with those reported by Potzinger,[31] Potzinger, Glasgow, and Reimann,[28] and Pollock, Sandhu, Jodhan, and Strausz.[20] There is also

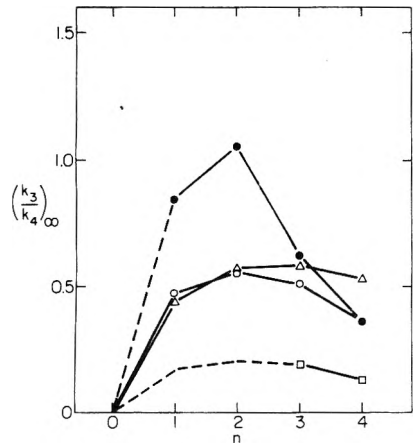

Figure 2. Reactivity of alkylsilanes expressed in terms of $(k_3/k_4)_\infty$ as a function of the number of Si–H bonds: (●) H + $(C_2H_5)_{4-n}SiH_n$; (○) H + $(CH_3)_{4-n}SiH_n$; (△) D + $(CH_3)_{4-n}SiH_n$ (ref 26); (□) H + $(CH_3)_{4-n}SiD_4$.

TABLE II: Arrhenius Parameters for H-Atom Induced Decomposition of Silanes

Substrate	$10^{11}A$, cm^3/s	E, kcal/mol
SiH_4	2.7	2.5
CH_3SiH_3	2.0	2.1
$(CH_3)_2SiH_2$	1.3	1.8
$(CH_3)_3SiH$	0.67	1.5
$C_2H_5SiH_3$	2.0	2.0
$(C_2H_5)_2SiH_2$	1.3	1.4
$(C_2H_5)_3SiH$	0.67	1.1
SiD_4	2.9	3.2
CH_3SiD_3	2.2	2.8

approximate agreement of our values for the reaction of H atoms with $(CH_3)_2SiH_2$ and $(CH_3)_3SiH$ with those reported by Cowfer, Lynch, and Michael,[29] although the latter authors' value for the rate constant for H + SiH_4 is higher than ours by a factor of about 6 and their value for the H + CH_3SiH_3 is higher by a factor of about 2. The recent values reported by Choo, Gaspar, and Wolf[30] for the rate constants of the reactions of H atoms with SiH_4 and GeH_4 appear to be much too high.

As mentioned earlier, and shown in Figure 2, the rate constants measured in this work for the reactions of H atoms with $(CH_3)_{4-n}SiH_n$ (n = 1, 2, 3, 4) follow the same trend as the analogous values for the reactions of D atoms with methylsilanes.[26] Moreover, the general trend in the rate constants with number of Si–H bonds is not changed when CH_3 is replaced by C_2H_5 and, although we have only two points, the same behavior appears to obtain in the methylsilanes when Si–D bonds are present rather than Si–H bonds. The observed magnitude of the variation of k_3/k_4 with n in Figure 2 is many times smaller than the analogous variation that exists for H-atom attack on $(CH_3)_3CH$, $(CH_3)_2CH_2$, CH_3CH_3, and CH_4. The principal reason for this contrast in reactivity is difference in activation energy.[26] Unfortunately, it was not possible to vary the temperature in our experiments and so, from our data alone, it is not possible to calculate Arrhenius rate parameters for these reactions. However, Potzinger, Glasgow, and Reimann[28] have carried out a study of the temperature dependence of the H + SiD_4 reaction from which they report an activation energy of 3.2 kcal/mol. In addition, Mihelcic, Potzinger, and Schindler[27] have studied the D + SiH_4 reaction as a function of temperature and find an activation energy of 2.5 kcal/mol. Using these two activation energies and our rate constants from Table I, we have estimated the Arrhenius parameters by making use of the following assumptions:

TABLE III: Dissociation Energies[a] of Silicon–Hydrogen Bonds and Standard Enthalpies of Formation[a] of Silyl Radicals

Molecule	$D(\geq Si-H)$, kcal/mol	$\Delta H_f^\circ(\geq Si\cdot)$, kcal/mol
SiH_4	93	49
CH_3SiH_3	90	34
$(CH_3)_2SiH_2$	88	19
$(CH_3)_3SiH$	85	3
$C_2H_5SiH_3$	90	30
$(C_2H_5)_2SiH_2$	84	8
$(C_2H_5)_3SiH$	80	−12

[a] On the basis of comparisons with the literature and of consideration of approximations involved we estimate the uncertainty in these values to be ± 3 kcal/mol.

(1) It is assumed that the preexponential factors per Si–H bond and per Si–D bonds, obtained from the above activation energies[27,28] and the specific reaction rates in Table I, are constant over the series $(CH_3)_{4-n}SiH_n$ and $(C_2H_5)_{4-n}SiH_n$ with n = 1, 2, 3, 4 and $(CH_3)_{4-n}SiD_n$ with n = 3, 4. This assumption is supported by the observation that for the reactions of CH_3 radicals with $(CH_3)_{4-n}SiH_n$ (n = 1, 2, 3, 4) the preexponential factors per Si–H bond are remarkably constant at 9.0 ± 1.1 × 10^{-13} cm^3/s.[4,9]

(2) It is assumed that the activation energy for the reaction of H atoms with SiH_4 is the same as that for D atoms with SiH_4. Since the same bond is being broken in both cases and the energies of the bonds being formed differ by only 0.8 kcal/mol,[50] this is surely valid well within the approximation involved in assumption 1.

The Arrhenius parameters A and E ($k = Ae^{-E/RT}$) that are obtained for the silanes by this admittedly crude approximation are tabulated in Table II. It is to be noted from Table II that the activation energies fall off slowly as the Si–H bonds in SiH_4 are successively replaced by Si–CH_3 and Si–C_2H_5 bonds. The same effect appears when an Si–D bond in SiD_4 is replaced by an Si–CH_3 bond. The molecules Si_2H_6 and Si_2D_6 are not included in the estimates shown in Table II because the total H atom induced decomposition of these substances appears to involve two parallel reactions, one being attack on the Si–H bonds and the other being attack at the Si–Si bond.[20]

3. *Dissociation Energies of Si–H Bonds.* The continuous lowering of the activation energy by successive replacement of the first three H atoms in SiH_4 with alkyl groups is observed also in the paraffin series. Thus for the reaction of H atoms with the molecules R_nC-H_{4-n}, where R is an alkyl radical, it is well known that the activation energy parallels smoothly the dissociation energy of the ≡C–H bond as n changes from 0 to 3. The same trend in activation energies for the reactions of H atoms with R_nSi-H_{4-n}, seen in Table II, suggests that there should exist an analogous decrease in dissociation energy of the ≡Si–H bond in the series R_nSi-H_{4-n} as n changes from 0 to 3. Confirmation of this suggestion by comparison with known dissociation energies of Si–H bonds is not possible, however, because of the present imprecise knowledge of these quantities. The most recent, and probably most reliable, determination[51] reports a value of 89 ± 4 kcal/mol for all of the ≡Si–H bonds in the series $(CH_3)_nSiH_{4-n}$ with n = 0, 1, 2, 3.

The most successful semiempirical technique of relating activation energies for H-atom abstraction to bond dissociation energies is that known as the bond-energy–bond-order (BEBO) method.[52] We have used this method to calculate Si–H bond dissociation energies in the series R_nSi-H_{4-n} that are consistent simultaneously with the error spread reported in these values[51] and with the activation

energies shown in Table II. For the calculation we used the same input data, with the exception of the Si–H bond energies, as other authors.[26,53] A dissociation energy of the H_3Si–H bond, within the range reported, was chosen and the Sato parameter of the BEBO method[52] adjusted such that the calculated activation energy agreed with the measured value of 2.5 kcal/mol. The dissociation energies of the Si–H bonds in R_nSi–H_{4-n} (n = 1, 2, 3) that brought the calculated activation energies into agreement with those of Table II were then determined. The process was repeated until a set of bond dissociation energies were obtained which fell within the experimental range of 85–93 kcal/mol (i.e., 89 ± 4)[51] and simultaneously were in agreement with the activation energies of Table II.

The results are shown in Table III. It may be seen there that the bond dissociation energy changes by 2–3 kcal/mol with each successive replacement of an Si–H bond in SiH_4 by an Si–CH_3 bond. This is in agreement with the conclusion of Hosaka and Rowland[54] from their studies of the reactions of hot tritium atoms with silanes. Also, the dissociation energies of the H_3Si–H and $(CH_3)_3Si$–H bonds are in accord with values derived from other kinetic evidence.[55-59] Successive ethylation of the Si–H bonds in SiH_4 appears to have a somewhat greater effect of lowering the dissociation energy of the Si–H bond. We are unaware of thermochemical data with which to compare our estimates of the dissociation energies of the ethylsilane series.

Combination of the Si–H bond dissociation energies with the standard enthalpies of formation of the parent molecules[51,60] yields the standard enthalpies of formation of the corresponding silyl radicals which are also given in Table III.

Acknowledgment. This work was supported by the U.S. Energy Research and Development Administration under Contract No. EY-76-S-02-3416.

References and Notes

(1) J. A. Kerr, D. H. Slater, and J. C. Young, *J. Chem. Soc. A*, 104 (1966).
(2) J. A. Kerr, D. H. Slater, and J. C. Young, *J. Chem. Soc. A*, 134 (1967).
(3) J. A. Kerr, A. Stephens, and J. C. Young, *Int. J. Chem. Kinet.*, **1**, 339, 371 (1969).
(4) O. P. Strausz, E. Jakubowski, H. S. Sandhu, and H. E. Gunning, *J. Chem. Phys.*, **51**, 552 (1969).
(5) E. R. Morris and J. C. J. Thynne, *J. Phys. Chem.*, **73**, 3294 (1969).
(6) A. U. Chaudhry and B. G. Gowenloch, *J. Organometal. Chem.*, **16**, 221 (1969).
(7) T. N. Bell and A. E. Platt, *J. Phys. Chem.*, **25**, 603 (1971).
(8) H. E. O'Neal, S. Pavlou, T. Lubin, M. A. Ring, and L. Batt, *J. Phys. Chem.*, **75**, 3945 (1971).
(9) R. E. Berkley, I. Safarik, H. E. Gunning, and O. P. Strausz, *J. Phys. Chem.*, **77**, 1734 (1973).
(10) R. E. Berkley, I. Safarik, O. P. Strausz, and H. E. Gunning, *J. Phys. Chem.*, **77**, 1741 (1973).
(11) T. N. Bell and B. B. Johnson, *Aust. J. Chem.*, **20**, 1545 (1967).
(12) W. J. Cheng and M. Szwarc, *J. Phys. Chem.*, **72**, 494 (1968).
(13) E. Jakubowski, H. S. Sandhu, H. E. Gunning, and O. P. Strausz, *J. Chem. Phys.*, **52**, 4242 (1970).
(14) T. N. Bell and U. F. Zucker, *J. Phys. Chem.*, **74**, 979 (1970).
(15) T. N. Bell and U. F. Zucker, *Can. J. Chem.*, **48**, 1209 (1970).
(16) E. R. Morris and J. C. J. Thynne, *Trans. Faraday Soc.*, **66**, 183 (1970).
(17) J. A. Kerr and D. M. Timlin, *Int. J. Chem. Kinet.*, **3**, 1, **69** (1971).
(18) M. A. Nay, G. N. C. Woodall, O. P. Strausz, and H. E. Gunning, *J. Am. Chem. Soc.*, **87**, 179 (1965).
(19) P. Cadman, G. M. Tilsley, and A. F. Trotman-Dickenson, *J. Chem. Soc., Faraday Trans. 1*, **68**, 1849 (1972).
(20) T. L. Pollock, H. S. Sandhu, A. Jodhan, and O. P. Strausz, *J. Am. Chem. Soc.*, **95**, 1017 (1973).
(21) B. Reimann, R. Laupert, and P. Potzinger, *Ber. Bunsenges. Phys. Chem.*, **79**, 1160 (1975).
(22) E. R. Austin and F. W. Lampe, *J. Photochem.*, **5**, 155 (1976).
(23) E. R. Austin and F. W. Lampe, *J. Phys. Chem.*, **80**, 2811 (1976).
(24) I. M. T. Davidson, *Spec. Period. Rep., Chem. Soc.*, **1** 214 *ff* (1975).
(25) M. A. Contineanu, D. Mihelcic, R. N. Schindler, and P. Potzinger, *Ber. Bunsenges. Phys. Chem.*, **75**, 426 (1971).
(26) K. Obi, H. S. Sandhu, H. E. Gunning, and O. P. Strausz, *J. Phys. Chem.*, **76**, 3911 (1972).
(27) D. Mihelcic, P. Potzinger, and R. N. Schindler, *Ber. Bunsenges. Phys. Chem.*, **78**, 82 (1974).
(28) P. Potzinger, L. C. Glasgow, and B. Reimann, *Z. Naturforsch. A*, **29**, 493 (1974).
(29) J. A. Cowfer, K. P. Lynch, and J. V. Michael, *J. Phys. Chem.*, **79**, 1139 (1975).
(30) K. Y. Choo, P. P. Gaspar, and A. P. Wolf, *J. Phys. Chem.*, **79**, 1752 (1975).
(31) P. Potzinger, private communication.
(32) K. R. Jennings and R. J. Cvetanovic, *J. Chem. Phys.*, **35**, 1233 (1961).
(33) W. Braun and M. Lenzi, *Discuss. Faraday Soc.*, **No. 44**, 252 (1967).
(34) M. C. Kurglo, N. C. Peterson, and W. Braun, *J. Chem. Phys.*, **53**, 2776 (1970).
(35) J. A. Eyre, T. Hikida, and L. M. Dorfman, *J. Chem. Phys.*, **53**, 1281 (1970).
(36) R. D. Penzhorn and B. deB. Darwent, *J. Chem. Phys.*, **55**, 1508 (1971).
(37) J. V. Michael, D. T. Osborne, and G. N. Suess, *J. Chem. Phys.*, **58**, 2800 (1973).
(38) D. Mihelcic, V. Schubert, F. Höfler, and P. Potzinger, *Ber. Bunsenges. Phys. Chem.*, **79**, 1230 (1975).
(39) P. J. Boddy and J. C. Robb, *Proc. R. Soc. London, Ser. A*, **249**, 518 (1959), and references contained therein.
(40) A. B. Callear and R. E. M. Hedges, *Trans. Faraday Soc.*, **66**, 615 (1970).
(41) A. B. Callear and W. P. D. Pereira, *Trans. Faraday Soc.*, **59**, 2758 (1963).
(42) A. B. Callear and P. M. Wood, *J. Chem. Soc., Faraday Trans. 2*, **68**, 302 (1972).
(43) E. Kamaratos and F. W. Lampe, *J. Phys. Chem.*, **74**, 2267 (1970).
(44) H. S. Tan and F. W. Lampe, *J. Phys. Chem.*, **76**, 3303 (1972).
(45) J. V. Michael and G. N. Suess, *J. Phys. Chem.*, **78**, 482 (1974).
(46) J. A. Cowfer, D. G. Keil, J. V. Michael, and C. Yeh, *J. Phys. Chem.*, **75**, 1584 (1971).
(47) G. R. Woolley and R. J. Cvetanovic, *J. Chem. Phys.*, **50**, 4697 (1969).
(48) R. J. Cvetanovic and L. C. Doyle, *J. Chem. Phys.*, **50**, 4705 (1969).
(49) J. A. Cowfer and J. V. Michael, *J. Chem. Phys.*, **62**, 3504 (1975).
(50) *Natl. Bur. Stand. (U.S.), Tech. Note*, **No. 270-3** (1968).
(51) P. Potzinger, A. Ritter, and J. R. Krause, *Z. Naturforsch. A*, **30**, 347 (1975).
(52) H. S. Johnston, "Gas-Phase Reaction Rate Theory", Ronald Press, New York, N.Y., 1966, pp 339 *ff*.
(53) L. C. Glasgow, G. Olbrich, and P. Potzinger, *Chem. Phys. Lett.*, **14**, 466 (1972).
(54) A. Hosaka and F. S. Rowland, *J. Phys. Chem.*, **77**, 705 (1973).
(55) R. Walsh and J. M. Wells, *J. Chem. Soc., Chem. Commun.*, 513 (1973).
(56) I. M. T. Davidson and A. V. Howard, *J. Chem. Soc., Faraday Trans. 1*, **71**, 69 (1975).
(57) R. Walsh and J. M. Wells, *J. Chem. Soc., Faraday Trans. 1*, **72**, 100 (1976).
(58) W. H. Duewer and D. W. Setser, *J. Chem. Phys*, **58**, 2310 (1973).
(59) K. J. Reed and J. I. Brauman, *J. Chem. Phys.*, **61**, 4830 (1974).
(60) P. Potzinger and F. W. Lampe, *J. Phys. Chem.*, **74**, 719 (1970).
(61) We wish to thank one of the referees of this paper for bringing this point to our attention.

Flame Structure Studies of CF_3Br-Inhibited Methane Flames. 3. The Effect of 1% CF_3Br on Composition, Rate Constants, and Net Reaction Rates

Joan C. Biordi,* Charles P. Lazzara, and John F. Papp

U.S. Bureau of Mines, Pittsburgh Mining and Safety Research Center, 4800 Forbes Avenue, Pittsburgh, Pennsylvania 15213 *(Received January 5, 1977)*

Publication costs assisted by the U.S. Bureau of Mines

Molecular beam-mass spectrometry has been used to determine the complete microstructure of a 10.1% CH_4–21.2% O_2–67.6% Ar–1.1% CF_3Br flame and its uninhibited analogue, both stabilized at 32 Torr on a cooled flat flame burner. Composition and temperature profiles for the inhibited flame are shown. Kinetic analyses of the profiles yield values for the rate coefficients for the reactions $H + CH_4 \rightarrow H_2 + CH_3$, $H + O_2 \rightarrow OH + O$, $CO + OH \rightarrow CO_2 + H$, and $CH_3 + O \rightarrow H_2CO + H$ over the temperature ranges 1500–1600 and 1725–1825 K. Comparison of clean and inhibited flames shows more pronounced "inhibition" effects with 1.1% CF_3Br than previously observed. These effects include, for the flame containing 1.1% CF_3Br, a shift of the primary reaction zone to high temperature, a higher final flame temperature (quenched flames), a reduction in maximum H_2CO concentration, and a reduction in the concentrations of H, O, and OH at low temperature. Comparison of flames containing 1.1 and 0.3% CF_3Br initially shows the net reaction rate of the inhibitor also shifted to higher temperature in the former. CF_3Br is judged to decay by thermal decomposition as well as by abstraction reactions.

Introduction

In the preceding papers[1,2] of this series we have reported on the general character of the microstructure of low pressure methane flames containing a small amount of CF_3Br and on the detailed kinetics and mechanisms for flames containing 0.3% CF_3Br in comparison with its uninhibited analogue. It was clear from examination of these flames that the fluorine part of the inhibitor molecule reacts rapidly in the flame, but it was not possible to detect the CF_3 radical despite the ability to detect and measure other flame radicals with mole fractions of the order of 10^{-4}–10^{-5}. It was found that although the H atom concentration was reduced at low temperatures in the inhibited relative to the clean flame, some manifestations of inhibition observed for other chemical inhibitors, e.g., HBr,[3] were only marginally evident. We therefore chose to examine the detailed microstructure of a flame containing significantly more CF_3Br in order to improve our chances of observing the CF_3 radical, to look for more pronounced effects of the inhibitor, and to obtain more data for clarifying mechanisms in this complex reaction system.

A large amount of information is generated in flame microstructure studies where both radical and stable species profiles are measured. We choose to emphasize here observations on the rate coefficients determined for "well-known" reactions, comparisons between clean and inhibited flames, and the reactions related to the decay of the inhibitor. Part IV will examine the behavior of inhibitor related species in the flame. Other papers have emphasized different aspects of this study which, however, are useful for the present discussion, and the results of those considerations are summarized here.

An examination[4] of the effect of CF_3Br on the concentrations of the principal radical species, H, O, and OH, reveals that, for flames containing 0.3% CF_3Br initially, only H atoms are reduced at equivalent temperatures below ~1600 K relative to the clean flame. At higher inhibitor concentration, 1.1% CF_3Br, all three radicals are reduced in the low temperature region of the flame. The maximum radical concentrations are those expected assuming the characteristic H_2/O_2 reactions balanced at the final flame temperature. These maximum concentrations may increase or decrease, and both were observed, with inhibitor in quenched flames. The methyl radical concentration is also reduced in inhibited relative to clean flames below 1500 K, but the peak methyl radical concentration occurs at a higher temperature and is actually larger in the 1.1% CF_3Br flame than its clean analogue.

Experimental Section

Two flames were examined at 0.042 atm, an uninhibited, slightly lean CH_4–O_2–Ar flame and one of similar stoichiometry containing 1.1% CF_3Br initially. These quenched, flat flames differ from those studied previously in initial mass flow rate and, therefore, in burning velocity. A burning velocity of about 48 cm s^{-1} for the clean flame was found to give satisfactorily stable (for quantitative microstructure determinations) inhibited flames when the CF_3Br was added.

The molecular beam sampling-mass spectrometric detection system was the same as described previously, as were the techniques for radical detection and measurement.[1,2] Only departures from previously described procedures will be given here.

The formaldehyde profiles, determined at 30 amu, were corrected for $C^{18}O$; this correction was not made in previously reported profiles for H_2CO.[2,5] The effect of this correction to flames I and II, the clean and 0.3% CF_3Br flames, respectively, was to reduce the maximum X_{H_2CO} by 15% in flame I and 25% in flame II and to eliminate the apparent residual H_2CO in the secondary reaction zone.

The change in burning velocity for the clean flames from that previously used resulted in a different final flame temperature. The area expansion ratio profile was also different at the lower linear flow velocity. The two flames studied may be described as follows: Flame III, initial composition 10.1% CH_4–21.5% O_2–68.4% Ar, v_0 = 47.6 cm s^{-1}, T_{max} = 1781 K; Flame IV, initial composition 10.1% CH_4–21.2% O_2–67.6% Ar–1.1% CF_3Br, v_0 = 48 cm s^{-1}, T_{max} = 1966 K; Area ratio, $A(z) = 1.0 + 0.35z$ (cm) for $0 \leq z \leq 1$ cm. The temperature maxima cited are those

determined in the absence of the sampling probe.

Mass spectral sensitivities for CH_3Br, CH_2CF_2, F_2CO, HF, and Br in the 1.1% CF_3Br flame were determined by direct comparison with the flame containing initially 0.3% CF_3Br. That is, the 0.3% CF_3Br flame served as the calibration standard for the named species in the 1.1% CF_3Br flame. For CH_3Br (±10%), CH_2CF_2 (±2%), and F_2CO (±18%), the relative ionization cross section calculations were also performed in the manner previously described[5] and the agreement between the two approaches is given in the parentheses. This agreement gives an indication of the precision of the cross section calculations from one set of ionizer conditions to another. For HBr (±8%), Br (<1%), and HF (±6%) conservation of mass calculations showed good agreement, as noted parenthetically, with the 0.3% CF_3Br flame calibration procedure and this is an indication of the precision with which these flames can be reproduced on the burner over extended periods of time.

For CF_3Br, the initial points of the profile were set equal to the known, initial CF_3Br concentration. This is a more reliable procedure for CF_3Br than calibration with the initial, cold gas mixture because of possibly different temperature dependencies in the scattering function for CF_3Br and Ar, and the possible temperature effects on the CF_3Br fragmentation pattern. Both of these effects are, quantitatively, unknown but, since the temperature over the initial portion of the profile reaches 900 K, the procedure adopted essentially corrects for them up to that temperature.

In addition to the CF_2 radical,[6] two other previously unobserved species were observed and measured. They are CF_3H and Br_2. CF_3H was monitored as CHF_2^+ at mass 51, corrected for ^{13}C contributions from mass CF_2^+ at mass 50. The latter ion is formed from several other inhibited flame species. At the position in the flame for which CF_3H is a maximum, these corrections amounted to 10% of the observed intensity at 51 amu. An ionization efficiency curve for 51 amu determined at the maximum yielded an appearance potential of 15.4 ± 0.5 eV. The lowest reported appearance potential for CHF_2^+ from CF_3H is 15.75 eV.[7] Other compounds[8] for which CHF_2^+ appearance potentials have been reported can be eliminated either on the basis of their appearance potentials, or, in the case of some unlikely molecules because of lack of supporting mass spectral evidence for their existence in this flame. Lifshitz and Long[9] calculated a value of 15.7 eV for CHF_2^+ from CH_2CF_2, which is present in the flame, but consider that the rearrangement required to give this ion has a very low probability of occurrence. The profiles of mass 64 and mass 51, determined simultaneously in order to test this conclusion, are sufficiently different to ensure that they derive from different species. The cross section technique[6] was used to estimate the CF_3H concentration. Two calculations were made, with the comparison ion CF_2^+ at 50 amu from CF_3Br and with FCO^+ at 47 amu from F_2CO. The results were the same to ±10%.

Br_2 was identified by its characteristic triplet at 158–160–162 amu, a feature not observed in the mass spectrum of CF_3Br or HBr. The uncertainty in the absolute concentration of Br_2 is great on account of the need to estimate a partial ionization cross section for CF_3Br^+, the only possible comparison ion to minimize discrimination in the mass filter. The value for $X_{Br_2}(max)$ that we calculate, $\sim 3 \times 10^{-5}$, is probably good only as an order of magnitude.

The physical model and computational techniques used to analyze the profile data as well as a program listing and

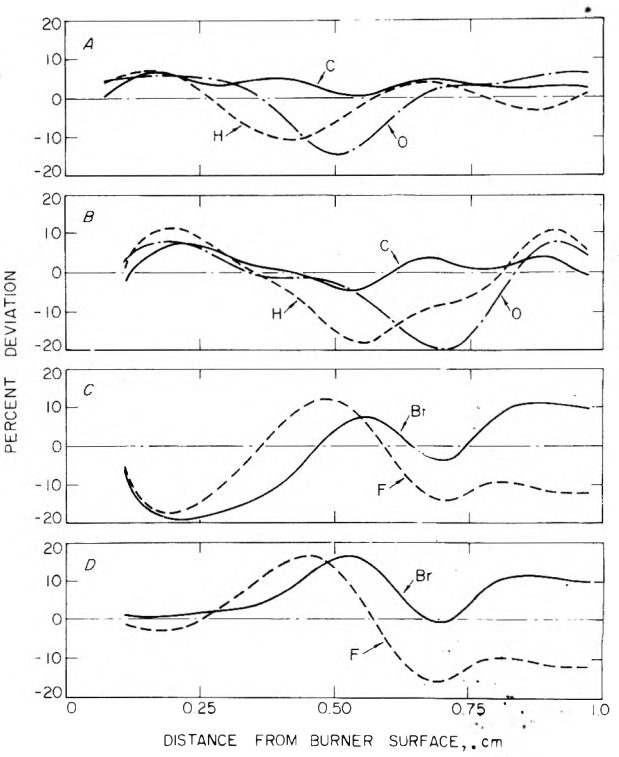

Figure 1. Element conservation for clean and inhibited flames: (A) carbon, hydrogen, oxygen in flame III; (B) carbon, hydrogen, oxygen in flame IV; (C) bromine and fluorine in flame IV; (D) same as in C except that thermal diffusion is ignored in the flux calculation.

output for one flame have been published.[10] From the concentration profiles, profiles of fractional mass flux, G_i, for each species are calculated according to the equation

$$G_i = \left[\frac{M_i}{\Sigma X_i M_i}\right]\left\{X_i - \left(\frac{D_{i\text{-Ar}}}{v}\right)\left[\frac{dX_i}{dz} + k_{T_i}\right]\frac{d \ln T}{dz}\right\}$$

where z is the normal to the burner surface, X_i denotes mole fraction, M_i molecular weight, $D_{i\text{-Ar}}$ the binary diffusion coefficient in argon, k_{T_i} the thermal diffusion ratio, and v the average bulk flow velocity. Individual species net reaction rates, the difference between the sum of the rates of all the reactions forming and the sum of the rates of all the reactions consuming a given species, are calculated as

$$K_i = \frac{\rho_0 v_0}{A(z) M_i}\left(\frac{dG_i}{dz}\right)$$

where ρ_0 and v_0 are the cold gas density and bulk velocity, respectively.

Application of the requirements of conservation of matter at the atomic level provides a test of the internal consistency and accuracy of the concentration profiles and their reduction to fluxes.[11] At each point in the flame the deviation of the net flux of any atomic species from its known inlet flux should be zero. Figure 1 shows the results of these calculations for C, H, and O in flames III and IV, and for F and Br in flame IV. Figure 1D is a calculation for flame IV in which k_T was set equal to zero. This calculation suggests that part of the reason for the low F and Br flux at low z, where the CF_3Br profile is nearly flat, is an error in evaluation of the thermal diffusion flux for the inhibitor. Whether this is due primarily to the use of unrealistic molecular parameters[10] in calculating k_T for CF_3Br or in probe perturbation to the temperature gradient close to the burner is not known. In the region of the flame where the net reaction rate for CF_3Br is near its

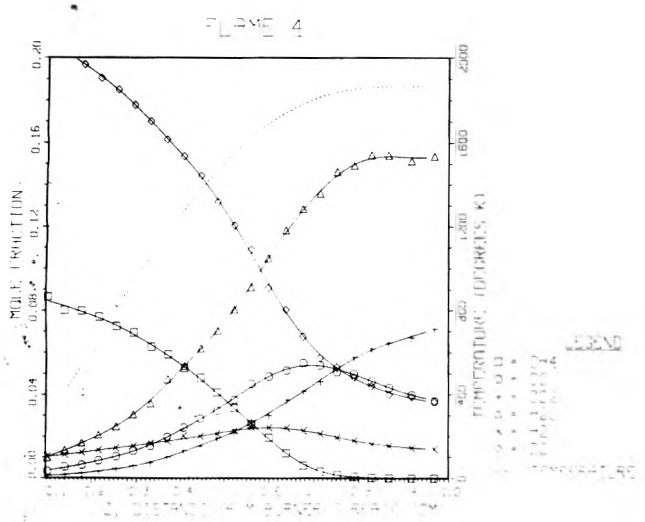

Figure 2. Composition profiles for the major stable species unrelated to the inhibitor flame IV.

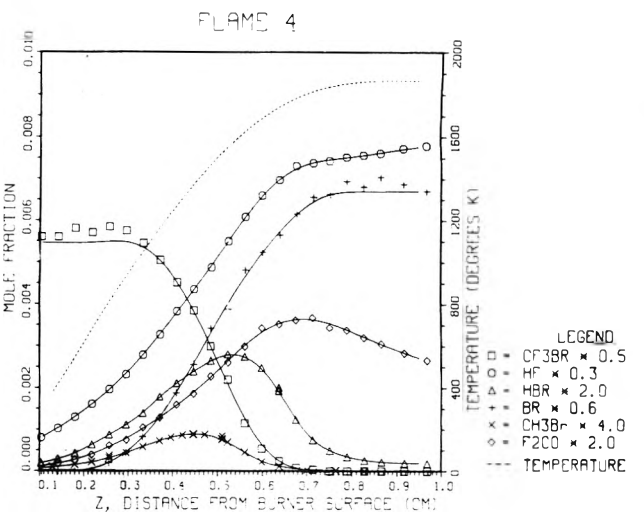

Figure 4. Composition profiles for major stable species related to the inhibitor in flame IV.

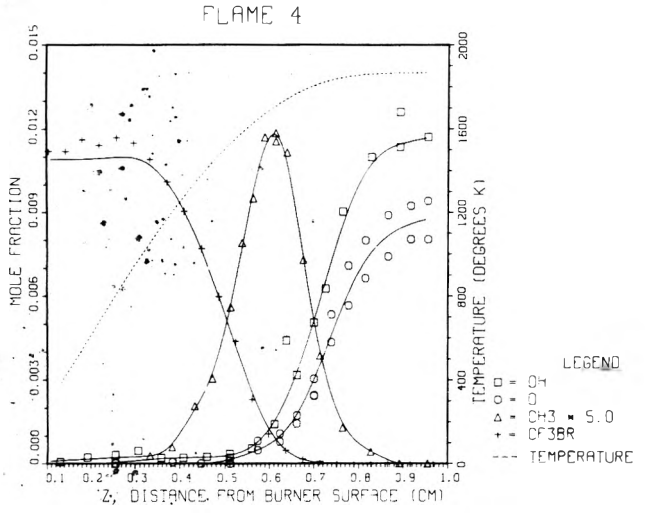

Figure 3. Composition profiles of principal unstable species (except H) and the inhibitor, flame IV.

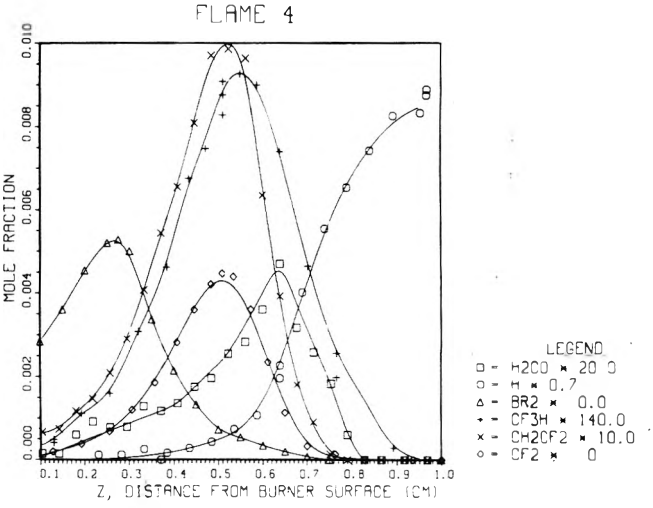

Figure 5. Composition profiles for minor intermediate species, both stable and unstable, and for H atom, flame IV.

maximum, $z \sim 0.6$, and at higher temperatures, the thermal diffusion term is very small and errors in the term make negligible differences in K_{CF_3Br}. Thus, calculation of reaction rate constants involving CF_3Br in this part of the flame are not strongly affected by errors in the modeling of thermal diffusion. At lower temperature, e.g., 1400 K where $K_{CF_3Br} \sim 0.1K_{CF_3Br}(\max)$, the net reaction rate is about 50% higher with $k_T = 0$.

Results and Interpretation

Composition. As before, the complete microstructure of a clean flame and its inhibited analogue were determined. We emphasize here the inhibited flame. Figures 2–5 show the mole fraction profiles determined for the inhibited flame for $z \leq 1$ cm. In these figures, the symbols are the data points and the lines through them are the results of application of smoothing techniques[10] to the data points for the purpose of calculating smooth first and second derivatives. Profiles were actually measured, though with a smaller density of data points, as far as z = 13 cm; and the smoothing was carried out using data points to 1.7 cm, and the ostensibly too low, flat portion of the Br curve reflects the average of all these data points. The H, O, and OH profiles shown here appear to be inconveniently truncated at z = 1 cm. Extended profiles of these species are given in ref 4. No attempt was made to measure the radicals HCO and HO_2 in either flame, although both had been observed in earlier studies.

A comparison of the maximum concentrations of species related to the inhibitor in flames containing 0.3 and 1.1% CF_3Br initially shows them to be 3–4 times greater in the latter flame. This corresponds roughly to the ratio of initial CF_3Br concentrations and implies no marked changes in the mechanism of formation and decay of these species between the two inhibited flames. In detail, of course, this must depend upon the relative temperature dependencies of the reactions involved. CF_3H and Br_2 have maximum mole fractions of 6.6×10^{-5} and 2.6×10^{-5}, respectively, in flame IV. They were not observed in the 0.3% CF_3Br, probably because ($^1/_3$–$^1/_4$) of these maxima is near the limit of detection for our apparatus as presently used. For the same reason, we could not unambiguously detect the CF_3 radical in either flame. The observation of CF_3H provides a route for calculating the concentration profile for CF_3.[6] This calculation gives a maximum mole fraction of CF_3 of about 3×10^{-5} occurring at z = 0.52 cm in flame IV. Because the appearance potential for CF_3^+ from CF_3 is only 2 eV less than that from CF_3Br, and because of the relatively broad electron energy spread of the ionizer, it is not surprising that such a small contribution to the 69 amu intensity could not be identified in the "tail" of the relatively very strong signal from CF_3Br.

Rate Coefficients. From the appropriate species net reaction rates, rate coefficients for the following four

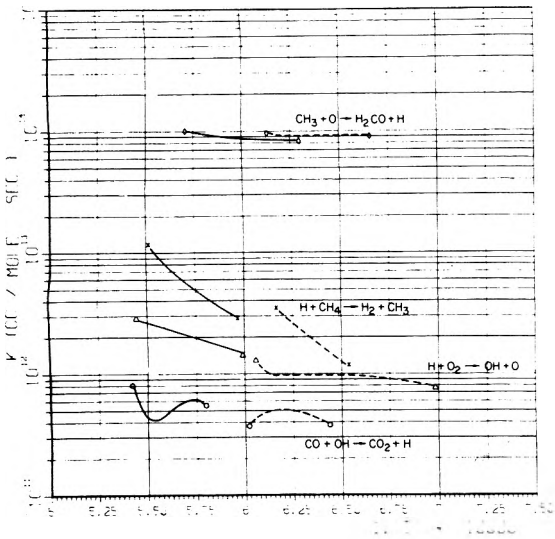

Figure 6. Rate coefficients determined for elementary reactions occurring in methane flames: dashed lines, results from flame III; solid lines, results from flame IV.

reactions were calculated over a 100 K range in each flame

$$H + CH_4 \rightarrow H_2 + CH_3 \quad (1)$$

$$H + O_2 \rightarrow OH + O \quad (2)$$

$$CO + OH \rightarrow CO_2 + H \quad (3)$$

$$CH_3 + O \rightarrow H_2CO + H \quad (4)$$

The details of these calculations have been discussed elsewhere.[2,12] The results are shown in Figure 6 where ln k is plotted vs. $1/T$ K, for each reaction. The broken lines are from flame III, 1500–1600 K, and the solid lines from flame IV, 1725–1825 K. Individual data points are shown only at the beginning and end of the range.

The rate constants shown in Figure 6 are similar in absolute value and temperature dependence to those obtained for the same reactions in earlier flame structure studies in our laboratory. There are several points to be made regarding these results. The first is in regard to observed temperature dependencies for H + CH_4 and CO + OH. It is the case that the rate coefficient for H + CH_4 exhibits curvature above about 1000 K.[13-15] Thus, straight line extrapolation of the rate coefficients in Figure 6 to lower temperature will lead to erroneously low values for k for this reaction. A smooth extrapolation is not possible even over the 100° gap that separates temperature ranges covered in these two flames. This reflects upon the precision with which the temperature dependence of a rate coefficient can be determined for a flame reaction when the calculation relies upon the net reaction rate for a species (CH_4) being consumed by other significant reactions (CH_4 + OH → H_2O + CH_3). For reaction 3, we cannot discern any temperature dependence for the rate coefficient over the temperature range available in a single flame. However, the difference between the average values for k_3 in each flame gives an activation energy consistent with recent results for this reaction in this temperature range.[16]

For flame IV, k_1 is calculated without consideration of the possible interfering reaction

$$Br + CH_4 \rightarrow HBr + CH_3 \quad (5)$$

This reaction has been proposed in some mechanisms of halocarbon inhibition as the source of regeneration of HBr, which is considered to be the principal radical scavenger. At the maximum rate of methane disappearance in flame IV, the temperature is 1790 K and reaction 5 can be

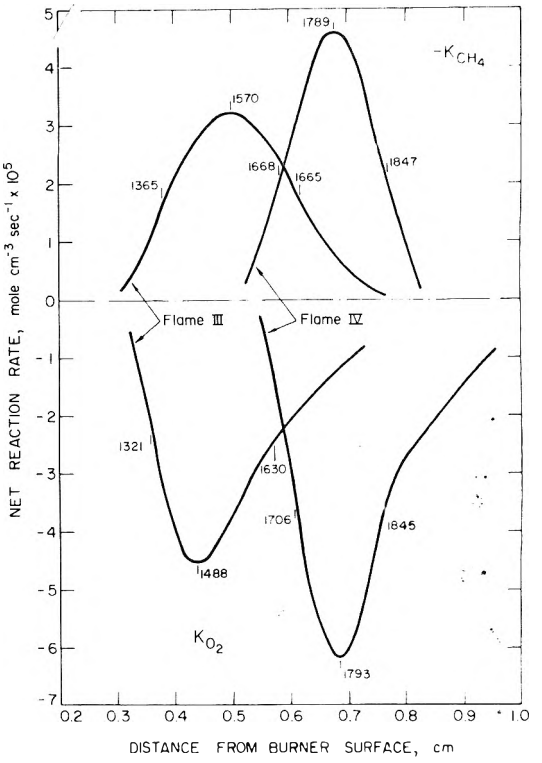

Figure 7. Net reaction rate as a function of distance from the burner surface for methane and oxygen in flames III and IV. The temperature is given at several values of z.

calculated to account for about 6% of the observed net reaction rate for methane, using a rate constant for k_1, determined in clean flames[14] and for k_5 extrapolated from low temperature studies.[17] To the extent that this extrapolation is correct, reaction 5 is not important over the range of temperature for which k_1 is calculated in flame IV. Similar considerations apply to the calculation of k_4 in flame IV. If in the inhibited flame there are significant new routes for methyl radical disappearance, then k_4 will be lower than calculated here. One possible reaction is

$$CF_2 + CH_3 \rightarrow CH_2CF_2 + H \quad (6)$$

and consideration of this reaction would reduce k_4 by $\{k_6(X_{CF_2}/X_O)\}$ at every point in flame IV. The ratio X_{CF_2}/X_O is 1 at 1600 K and ~0.02 at 1800 K. A reasonable estimate for k_6 is 10^{13} cm^3 mol^{-1} s^{-1}, by analogy with a similar reaction involving methylene,[18,19] so that k_4 might be lower than shown in Figure 6 by as much as 12% at the low temperature end of its range in the inhibited flame.

The relatively good temperature overlap of the rate constants shown in Figure 6, reaction 1 notwithstanding, between clean and inhibited flames suggests that no significant changes in mechanism are occurring for the reaction of the species in question (CH_4, O_2, CO_2, CH_3) in the regions of the flame where they are reacting most rapidly. These reactions are simply delayed to higher temperatures when the inhibition is present.

Comparisons Among Clean and Inhibited Flames. As with the flame containing 0.3% CF_3Br, the profiles shown in Figures 2–5 are all shifted downstream relative to those of the clean flame. The shift is greater here, about 2 mm. The net reaction rate profiles for methane and oxygen, Figure 7, are also shifted to higher temperatures and are narrower in the inhibited flame. This effect was not pronounced with the lower inhibitor concentration.[2,5] These results are similar to those obtained by Wilson and co-workers[3] for very lean CH_4–O_2 flames at 0.05 atm containing initially 1.88% HBr. Radicals could not be observed in that study, but a recent molecular beam in-

vestigation of a clean flame of similar composition and pressure[20] shows that OH and O are the dominant chain carriers and are first detected at about the same value of z. The concentration of hydrogen atom is at least 4–5 times smaller than [OH] and [O] in the lean flame.[28] In the nearly stoichiometric clean flames studied here, H is the chain carrier in greatest concentration everywhere in the flame and it is observed earliest in the flame. The onset of OH and O is downstream of that for H, but the concentration differences among the three radicals are not as great in the stoichiometric as in the lean flame. Thus, even though different radical species predominate in the early part of these flames, the inhibitor has the same effect on the rates of disappearance of fuel and oxidant in each case. There are no data available that show directly the effect of CF_3Br or HBr on the radical species concentration in lean flames.

The shifting of the primary reaction zone to higher temperature with the addition of inhibitor is responsible for the observed increase in peak methyl radical concentration in flame IV and also provides some insight into the nature of the reactions responsible for the decay of formaldehyde. The reactions forming methyl radical are reaction 1 and the analogous reaction with OH and, less important, with O. The rate coefficients for these reactions are temperature dependent. In the inhibited flame they occur at a higher temperature and therefore CH_3 is formed at a faster rate than in the clean flames. The principal reaction removing CH_3, reaction 4, is not temperature dependent so its rate of decay is about the same in both flames (at the peak X_{CH_3} in each flame, the concentration of O atoms is about the same). The net effect is a higher peak concentration for CH_3 in the inhibited flame.

On the other hand, the product of reaction 4, formaldehyde, is reduced by nearly a factor of 4 in the 1.1% CF_3Br flame. A reduction of formaldehyde peak concentration was observed for the flame containing 0.3% CF_3Br[2] and in methane flames containing HBr.[3] Since its formation rate is not substantially different between flames III and IV, the decrease in maximum [H_2CO] must be caused by a greatly increased rate of decay in the inhibited flame. This implies a strongly temperature dependent rate coefficient for the reactions responsible for that decay. It is possible to estimate that temperature dependence. At any given z, the net reaction rate for H_2CO is the difference between the overall rate of formation, K_f, and the overall rate of decay, K_d, of formaldehyde at that point in the flame

$$K_{H_2CO} = K_f - K_d$$

If it is assumed that reaction 4 is the only significant process forming H_2CO then

$$K_f = k_4[CH_3][O]$$

$$K_d = k_4[CH_3][O] - K_{H_2CO} \quad (I)$$

The decay processes are usually[11,21] thought to be abstraction reactions

$$H(O,OH) + H_2CO \rightarrow H_2(OH,H_2O) + HCO \quad (7)$$

and there is evidence[22] that thermal decomposition reactions may be particularly important, e.g.

$$H_2CO + M \rightarrow H_2 + CO + M \quad (8)$$

We can write

$$K_d = k_7[H_2CO]\Sigma[i] \quad i = H, O, OH$$

or

$$K_d = k_8[H_2CO][M] \quad (II)$$

TABLE I: Temperature for Maximum Rate of Decay of Fuel and Inhibitor in 0.042 atm, Stoichiometric CH_4-O_2-Ar Flames[a]

Flame	Initial [CF_3Br], %	T_{final}	T at $\lvert K_{CH_4}\rvert_{max}$	T at $\lvert K_{CF_3Br}\rvert_{max}$
I	0	1858	1640	
III	0	1781	1570	
II	0.3	1911	1660	1310
IV	1.1	1966	1790	1675

[a] All temperatures are in Kelvin.

where approximation is made that all of the abstraction reactions represented by (7) have the same magnitude and temperature dependence. Substituting one of the equations (eq II) into eq I, it is possible to solve for k_7 or k_8 at any point in either flame. These calculations were carried out for both flames and spanned a temperature range of over 500 K.

The activation energy calculated for reactions 7 was 26 kcal mol^{-1} and for reaction 8, 44 kcal mol^{-1}. Such high activation energies suggest that reaction 8 or a similar thermal decomposition reaction is responsible for a significant part of the decay of formaldehyde, since the abstraction reactions have, characteristically, $E_a \sim 2$–4 kcal mol^{-1}.[23,24] This is not to say that abstraction reactions do not occur. Indeed, the fact that the activation energy calculated for (8) is rather higher than previously measured suggests that attributing *all* the H_2CO decay to (8), as is done in the calculation described here, overestimates k_8. Our observations are consistent with a distribution between abstraction and thermal decomposition reactions first suggested by Mahnen and Peeters in their studies of lean CH_4-O_2 flames.[20]

One model of flame inhibition proposes a zone of inhibition between the transport zone and the primary reaction zone of the flame.[20] In this region of the flame, the inhibitor and/or its products of decomposition are thought to scavenge radicals efficiently and to compete with the normal chain propagating or branching reactions, delaying those reactions until the temperature has increased to a point where the inhibiting reactions can no longer compete. Much of the data we have obtained is consistent with this model. The directly observed reduction of chain carrier concentrations in the low temperature region of inhibited relative to clean flames, the early reaction of the inhibitor molecule relative to fuel, and the shifting to higher temperatures of the net reaction rate of fuel and oxidant in the presence of inhibitor are examples. However, the behavior of the inhibitor in the 1.1% CF_3Br flame relative to the 0.3% flame is not similarly consistent. In each case, the inhibitor does begin to react and achieves its maximum rate of decay earlier (i.e., at lower z and T) than methane, but the CF_3Br reacts rapidly at significantly higher temperature in the 1.1% flame than in the 0.3% flame. Figure 8 shows K_{CF_3Br} as a function of temperature in flames II and IV. Table I lists the temperatures at which the maximum rates of decay occur for methane and CF_3Br in all four flames examined. Flames I and III differ initially in mass flow rate only and hence the difference in final flame temperature.[25] The temperature at which CH_4 disappears most rapidly reflects the difference. Flames II and IV differ similarly in initial mass flow rate as well as in initial inhibitor concentration. The final flame temperature is 50 K higher for IV, but the maximum net reaction rate for CF_3Br occurs at a temperature 365 K higher in IV than II. The appearance of K_{CF_3Br} in flame IV relative to flame II, Figure 8, is not unlike that of methane in the inhibited relative to the clean

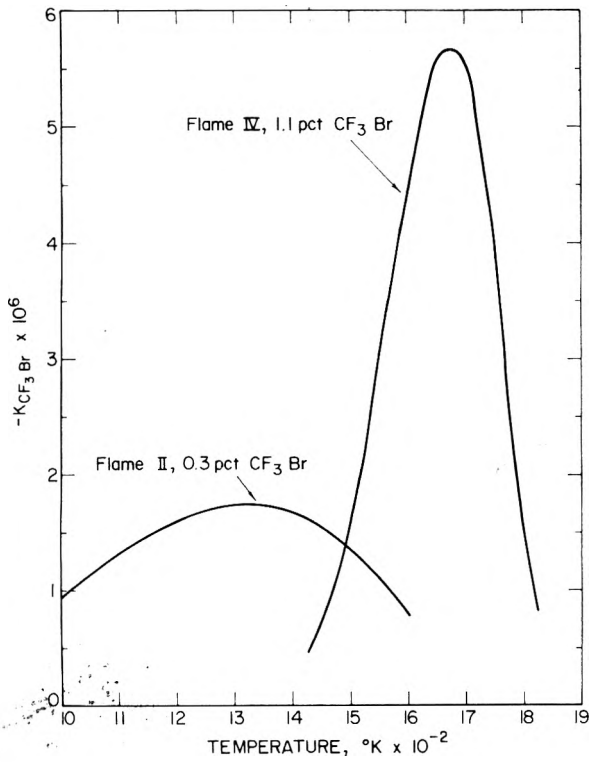

Figure 8. Net reaction rate for the inhibitor as a function of temperature for two nearly stoichiometric methane flames containing initially different amounts of CF_3Br.

flames. The maximum rate of decay of CF_3Br in IV is greater than that in II and this is due to the greater initial CF_3Br concentration in the former.

With increasing inhibitor concentration, the zone of inhibition, if that idea is at all applicable, is also shifted to higher temperature, and the reaction of the inhibitor itself is also delayed. At equivalent temperatures the concentrations of H, O, and OH are smaller than in flame II,[4] and the observed delay in inhibitor decay seems to be a consequence of this reduction in radical concentration. The implication is that of the several possible reactions that can be written to account for the observed reduction of radical concentration in the low temperature region of the flame, those between CF_3Br and radicals, e.g.

$$H + CF_3Br \rightarrow HBr + CF_3 \quad (9)$$

are not the most important. Reaction 9 does occur and is still a significant reaction destroying CF_3Br in the flame, as will be discussed presently, but it is delayed to higher temperatures, just as reaction 1.

The Disappearance of CF_3Br. In the 0.3% CF_3Br flame it was found that at the maximum rate of disappearance of CF_3Br, thermal decomposition could account for, at most, 8% of the decay rate. The rate constant, k_{td}, given by Benson and O'Neal[26] was used. Reaction with H atom to give HBr and CF_3 was responsible for the disappearance of CF_3Br and a rate constant could be calculated. The result was given by $2.2 \times 10^{14} \exp(-9460/RT)$ for $700 < T < 1550$ K. In the flame containing 1.1% CF_3Br initially, at the maximum disappearance rate for CF_3Br, the predicted rate of thermal decomposition (again using Benson and O'Neal's rate constant) is nearly 10 times greater than the observed decay rate.

The value for the thermal decomposition rate coefficient recommended by Benson and O'Neal is from an RRK calculation and represents an attempt to calculate the limit high pressure value. The only experimental value for k_{td}, reported by Sehon and Szwarc[27] is more than a factor of

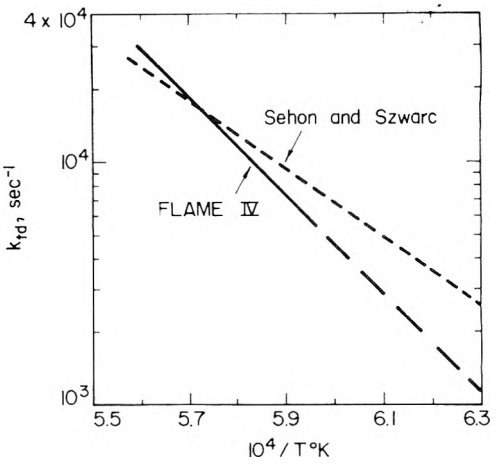

Figure 9. The rate constant for thermal decomposition of CF_3Br, expressed as first order, calculated assuming Br atom abstraction occurs with the rate constant previously determined:[2] solid line, flame IV; dashed line from ref 27.

10 lower than Benson and O'Neal's. Thus, at the temperature of interest, using Sehon and Szwarc's number, we might conclude that CF_3Br disappears by thermal decomposition.

Hydrogen atoms are present in the region of the flame over the temperature range in which CF_3Br disappears. Although H atom concentration at any given temperature below the maximum temperature is lower than in flame III, these concentrations are not negligible. At the point of maximum CF_3Br decay, if we assume the abstraction reaction alone is responsible for the decay we calculate a value of $k_9 = 1.6 \times 10^{13}$ cm^3 mol^{-1} s^{-1}, $T = 1666$ K. The number agrees well with value (1.3×10^{13}) extrapolated using the expression given earlier.

Thus assigning the decay of CF_3Br to either thermal decomposition or to H atom abstraction would yield values for the rate constant for these reactions which are not inconsistent with what is known about either reaction. This holds over the range of CF_3Br decay for which $1600 \leq T < 1800$ K.

It is not reasonable to suppose that, in this flame, CF_3Br is consumed solely by one or the other of these two reactions. It is more likely that both types of decay occur. If we assume that the abstraction reaction occurs with the rate coefficient measured in flame II, we can estimate a CF_3Br decay rate due to abstraction. Where the observed CF_3Br decay rate is greater than this calculated rate, we assign the difference to thermal decomposition. For $T \geq 1670$ K the difference is positive and the thermal decomposition rate constant, expressed as a first-order coefficient, is the solid line shown in Figure 9. At temperatures lower than 1670 K, the abstraction reaction predicts a greater rate of CF_3Br decay than observed, and so a meaningful k_{td} cannot be calculated. At 1600 K, e.g., the observed K_{CF_3Br} is 75% of that required if the abstraction and thermal decomposition were occurring, the latter proceeding at a rate required by extrapolating the solid line in Figure 9 to 1600 K. On the basis of this analysis, thermal decomposition accounts for about 50% of the CF_3Br disappearance rate at its maximum in flame IV and at higher temperature.

We expect[12] to be able to use net reaction rate curves, Figure 8, to about $\pm{}^1/_2 K_i(\max)$, $1550 \leq T \leq 1780$ K. The fact that we cannot utilize the low temperature portion of the K_{CF_3Br} is an inconsistancy that is ultimately due to experimental limitations of this flame data: the errors in modeling thermal diffusion noted earlier; error in determining the absolute value of H atom concentration,

particularly at low z; and possibly inadequacies in the new curve smoothing operation which give somewhat different second derivatives for reactant type profiles at low z than previous techniques. All of these possible sources of error diminish in magnitude with increasing z and T.

The dashed line in Figure 9 is the expression for k_{td} of Sehon and Szwarc; extrapolated to flame temperature. The conditions of Sehon and Szwarc's experiment were 5–20 Torr and 1020–1090 K. From Benson and O'Neal's calculations, it is likely that these conditions are well into the pressure falloff region for CF_3Br decomposition. The pressure here is higher, 32 Torr, but so is the temperature, and our conditions are also probably well in the pressure falloff region. In absolute value, our calculated rate constant for thermal decomposition is not very different from expectations from Sehon and Szwarc's measurements, and both are at least an order of magnitude lower than the computated high pressure limiting value.

As before,[5] reactions of CF_3Br with O and Br atoms were found to be negligibly important. Abstraction by methyl radial to give CH_3Br accounted for 10–30% of the decay rate of CF_3Br below 1700 K. The reaction was considered, quantitatively, in making the calculations for the contribution of thermal decomposition. The reverse reactions, forming CF_3Br, are also unimportant in the flame.

Summary

The microstructure, including radical species, of nearly stoichiometric CH_4–O_2–Ar flames containing initially 1.1% CF_3Br has been determined. These data are analyzed in light of previous microstructure studies of flames containing 0.3% CF_3Br initially and of the analogous clean flame.

Comparison of the maximum concentration of inhibitor-related species in flames containing 1.1 and 0.3% CF_3Br initially suggest similar mechanisms for formation and decay of these species are operating in both flames. These reactions, as well as those responsible for the disappearance of the major reactants and production of the major products, are shifted to higher temperatures in the presence of 1.1% CF_3Br. The effect of this inhibitor on the net reaction curves for methane and oxygen, and on the maximum concentration of formaldehyde, are similar to effects observed with HBr in very lean flames where different chain carriers predominate in the preheat zone of the flame.

The different temperature regions for the primary reaction zones in the inhibited vs. the analogous clean flame account for the greater maximum CH_3 concentration in the former. The difference in formaldehyde maxima between the inhibited and clean flames is consistent with a mechanism of decay for that species that includes a large contribution from thermal decomposition reactions.

The behavior of CF_3Br in the 1.1% flame is different from its behavior in the 0.3% flame. Its net reaction rate is shifted to higher temperature and is narrower in the flame containing more inhibitor. By analogy to the major reactants, we conclude that the decay of CF_3Br is also delayed on account of the reduction of radicals at low temperature in the inhibited relative to the clean flame. This observation is inconsistent with the idea of a zone of inhibition just prior to the primary reaction zone in which the inhibitor and/or its decomposition products scavenge radicals in direct competition with chain branching reactions.

Analysis of the decay of CF_3Br suggests that, in contrast to the earlier study, the inhibitor is consumed not only by reaction with H, but also by thermal decomposition. Each pathway is equally important at the maximum rate of decay of CF_3Br.

References and Notes

(1) J. C. Biordi, C. P. Lazzara, and J. F. Papp, *Symp. (Int.) Combust., [Proc.], 14th*, 367 (1974).
(2) J. C. Biordi, C. P. Lazzara, and J. F. Papp, *Symp. (Int.) Combust., [Proc.], 15th*, 917 (1975).
(3) W. E. Wilson, J. T. O'Donovan, and R. M. Fristrom, *Symp. (Int.) Combust., [Proc.]*, 929 (1972).
(4) J. C. Biordi, C. P. Lazzara, and J. F. Papp, *ACS Symp. Ser.*, **No. 16**, 256 (1975).
(5) J. C. Biordi, C. P. Lazzara, and J. F. Papp, Bureau of Mines Report of Investigation No. 8029, 1975.
(6) J. C. Biordi, C. P. Lazzara, and J. F. Papp, *J. Phys. Chem.*, **80**, 1042 (1976).
(7) C. Lifshitz and F. A. Long, *J. Phys. Chem.*, **69**, 3731 (1965).
(8) F. H. Field and J. F. Franklin, "Electron Impact and Ionization Phenomena", revised edition, Academic Press, New York, N.Y., 1970, pp 239–493.
(9) C. Lifshitz and F. A. Long, *J. Phys. Chem.*, **67**, 2463 (1963).
(10) J. F. Papp, C. P. Lazzara, and J. C. Biordi, Bureau of Mine Report of Investigation No. 8019, 1975.
(11) R. M. Fristrom and A. A. Westenberg, "Flame Structure", McGraw-Hill, New York, N.Y., 1965.
(12) J. C. Biordi, C. P. Lazzara, and J. F. Papp, *Combust. Flame*, **26**, 57 (1975).
(13) T. C. Clark and J. E. Dove, *Can. J. Chem.*, **51**, 2147 (1973).
(14) J. C. Biordi, C. P. Lazzara, and J. F. Papp, *J. Chem. Phys.*, **61**, 741 (1974).
(15) P. Roth and Th. Just, *Ber. Bunsenges. Phys. Chem.*, **79**, 682 (1975).
(16) J. Vandooren, J. Peeters, and P. J. Van Tiggelen, *Symp. (Int.) Combust., [Proc.], 15th*, 745 (1975).
(17) V. N. Kondratiev, "Rate Constants of Gas Phase Reactions", Translated by L. J. Holtschlag, R. M. Fristrom, Ed., National Bureau of Standard, Washington, D.C., COM-72-10014, 1972.
(18) M. J. Pilling and Robertson, *Chem. Phys. Lett.*, **33**, 336 (1975).
(19) A. H. Laufer and A. M. Bass, *J. Phys. Chem.*, **79**, 1635 (1975).
(20) J. Peeters and G. Mahnen, *Symp. (Int.) Combust., [Proc.], 14th*, 133 (1974).
(21) H. Wise and W. A. Rosser, *Symp. (Int.) Combust., [Proc.], 9th*, 733 (1963).
(22) J. Reuther and W. Kaskan, Paper presented at the 16th Combustion Symposium, Boston, Mass., Aug. 21–25, 1976.
(23) A. A. Westenberg and N. deHaas, *J. Phys. Chem.*, **76**, 2213 (1972).
(24) A. A. Cordiero, P. M. Becker, and R. J. Heinsohn, "Computer Simulations of Two Lean Premixed Methane-Oxygen Flames", Pennsylvania State University, University Park, Pa., 1972.
(25) W. E. Kaskan, *Symp. (Int.) Combust., [Proc.], 6th*, 134 (1957).
(26) S. W. Benson and H. E. O'Neal, *Natl. Stand. Ref. Data Ser., Natl. Bur. Stand.*, **No. 21** (1970).
(27) A. H. Sehon and M. Szwarc, *Proc. R. Soc. London, Ser. A*, **209**, 110 (1951).
(28) "Flame" in the context of this discussion refers to the preheat and primary reaction zones, to $0 < z \sim < 1$ cm in the low pressure studies.

Mass Spectrometric and Spectroscopic Study of the Reaction of H_3BCO and B_2H_6 with Oxygen and Nitrogen Atoms

G. K. Anderson and S. H. Bauer*

Department of Chemistry, Cornell University, Ithaca, New York 14853 *(Received July 12, 1976; Revised Manuscript Received March 21, 1977)*

A low pressure flow reactor was set up to measure the extent of destruction of H_3BCO and of B_2H_6 when injected into an excess of either oxygen or nitrogen atoms. High concentrations of these atoms were generated by microwave discharges. The atom densities were measured by titration with NO. Losses of the H_3BCO or of B_2H_6 as a function of flow time were determined with a TOF mass spectrometer coupled to the reactor through a supersonic molecular beam sampling system. A detailed analysis was made of the fidelity of sample transfer from the reactor, at several Torr, into the mass spectrometer ion source at $\approx 10^{-5}$ Torr. The bimolecular rate constants, measured under pseudo-first-order conditions, were, at 295 K, $k\{O + H_3BCO\} = 3.9 \times 10^{11}$ mol^{-1} cm^3 s^{-1}; $k\{N + H_3BCO\} \approx 4 \times 10^{11}$; $k\{O + B_2H_6\} = 2.7 \times 10^9$ mol^{-1} cm^3 s^{-1}; $k\{N + B_2H_6\}$ not observable. Upper limits were estimated for the rate constants of the attack of these boranes by N_2O, NO, NO_2, and O_2; these were all less than 10^6 mol^{-1} cm^3 s^{-1}. Emission spectra for mixed flows of $H_3BCO + O$ (in the absence of O_2) showed only $A^2\Pi \rightarrow X^2\Sigma$ for BO, up to $v' = 11$ for the upper state (103 kcal above the ground level). To account for the mass spectra, the chemiluminescence and the observed stoichiometry one must assume that the borane carbonyl is destroyed by oxygen atoms via two initiation steps, one in which O atoms abstract H's from H_3BCO, and another wherein the O atoms attach the B atom ejecting the CO.

Introduction

The oxidation reactions of boron hydrides and related compounds are characterized by rapid rates, large exothermicities, and, frequently, strong visible and ultraviolet chemiluminescence. These observations led to the speculation that the reactions may generate products in nonthermal distributions, and consequently could be used to construct chemical lasers at visible wavelengths. Despite this interest few data are available on the mechanisms and elementary rates of attack of oxidizing agents on borane adducts; also there is no concensus on the mechanism for the attack on B_2H_6 by O atoms. We report here the investigation of the reaction of borane carbonyl and of diborane with ground state oxygen and nitrogen atoms. The rates of primary atom attack were measured in a fast flow reactor coupled to a mass spectrometer. Some reaction products and intermediates were identified in this way. Also, emission spectra were taken to identify the source of chemiluminescence from $H_3BCO + O$ mixtures and these facilitated the elucidation of the reaction mechanism.

Experimental Section

Apparatus. The flow reactor, shown schematically in Figure 1, was a pyrex tube 2.0 cm i.d., with a 30 cm long reaction zone. Accurately known flow rates of the various gases were established by metering valves which were calibrated by observing the rates of pressure decrease in a known volume. Various atomic species were generated in a microwave discharge, and introduced into the reaction zone through a side arm. Borane carbonyl was injected by means of a multiholed teflon mixer (detail, Figure 1) on the end of a 0.25-in. o.d. pyrex tube, which slid along the axis of the reactor. The vacuum seal for the injector tube was far enough behind the side arm so that atomic species would not come in contact with the vacuum grease on the tube. The reactor was pumped by a 55 cfm Stokes mechanical pump, which was usually baffled to control its effective pumping speed, and minimize oil contaminations.

The interface between the reactor and mass spectrometer, shown schematically in Figure 2, consisted of a differentially pumped orifice–skimmer combination. The reacting gases at 1–4 Torr total pressure, expanded in near-continuum flow through a 0.076-cm orifice, into a region where the background pressure was maintained at less than 10^{-3} Torr by a 4-in. oil diffusion pump. The orifice was placed on the end of a short cone in order to ensure that sampling took place outside of the end wall boundary layer. The centerline portion of the expanded jet passed through the 0.041-cm skimmer aperture and into the ion source of the mass spectrometer, which was maintained at less than 10^{-5} Torr by a 2-in. mercury diffusion pump. The drift section is evacuated by a trapped 6-in. mercury diffusion pump.

The following comments briefly summarize the extensive analysis we made of the design parameters for a "beam" source, to maximize the intensity of the sample in the ionization region and to retain fidelity of composition in transfering the sample from the reactor to the mass spectrometer. For ideal gas dynamic behavior Parker[1] derived an expression for the flux through the skimmer. Early attempts to test his equation showed large discrepancies between the theoretical and observed intensities, the latter generally being low. There are many factors which introduce nonideal behavior; these are as follows: (1) viscous effects in the vicinity of the sampling orifice may cause depletion of reactive species; (2) viscous dissipation in the core of the free jet retards the growth of M (Mach number) and hence decreases the beam intensity; (3) scattering of jet molecules by the background gas can decrease the beam intensity; so can (4) shock formation upstream of the skimmer, and (5) interaction of beam molecules with the gas inside the skimmer cone; (6) mass separation in the jet may alter the sample composition.

In the sampling process, only a small portion of the gas from the reactor passes through the orifice, while the remainder of the flow is diverted radially. Thus the flow pattern between the end of the flow tube and the end wall may be treated approximately as axisymmetric stagnation flow, as shown in Figure 3, where U and W are the axial and radial velocity components, respectively. In frictionless (potential) flow, the axial and radial velocity components have the form (Schlichting[2]) $U = -2az$; $W =$

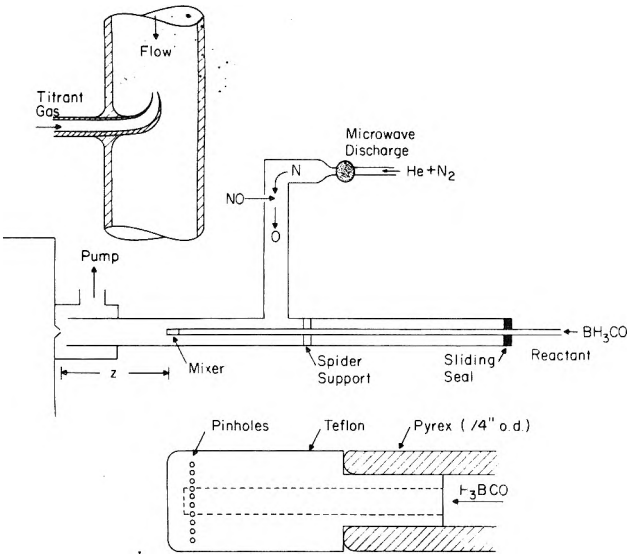

Figure 1. Schematic of reactor, showing movable mixer for injecting H_3BCO or B_2H_6 into the discharged gas flow.

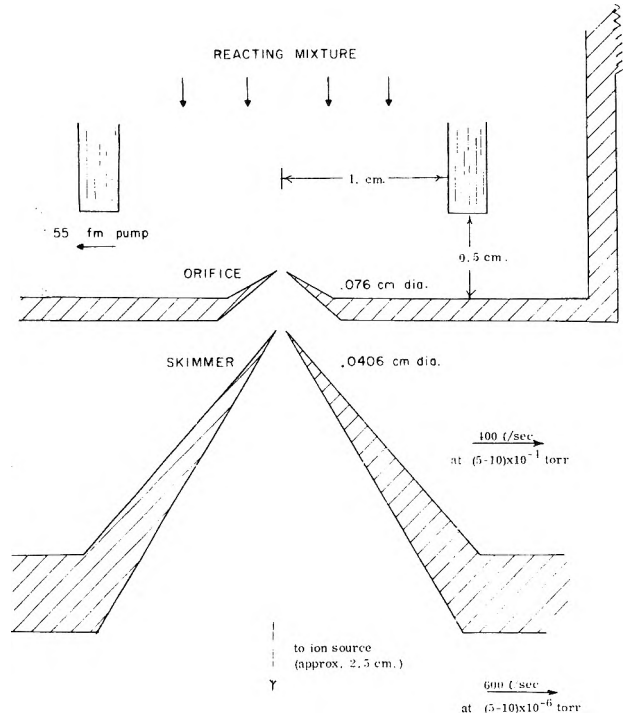

Figure 2. Scale drawing of the sampling orifices. The position of the 0.076-cm opening can be varied under operating conditions relative to the fixed location of the skimmer, by means of an external gear.

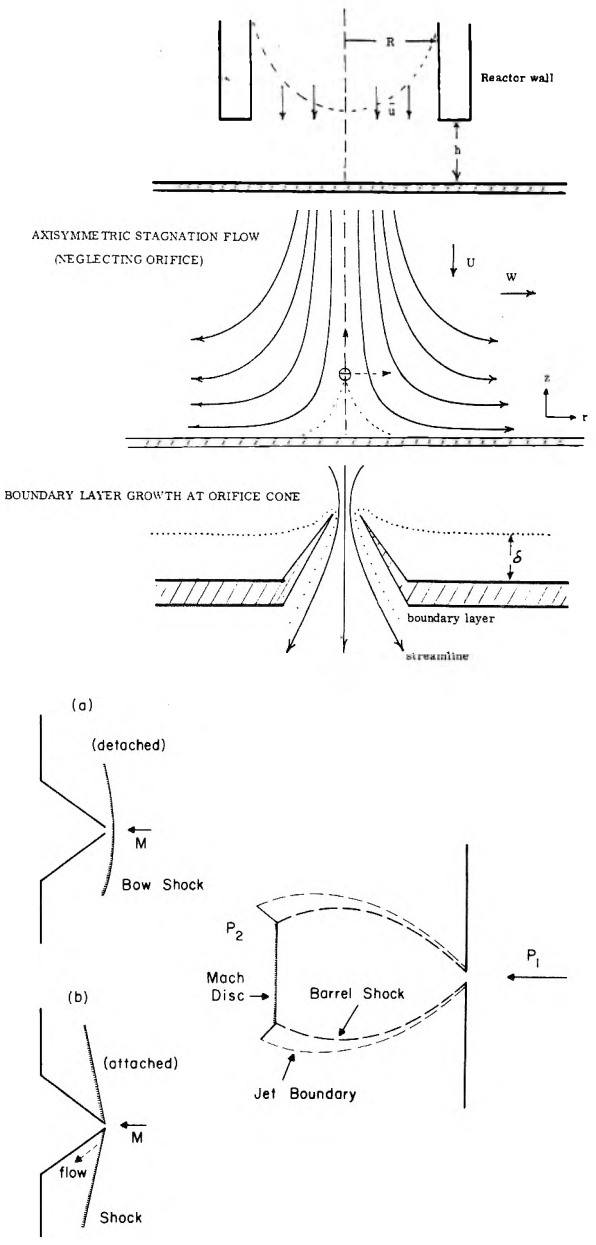

Figure 3. (a,b) Schematics which illustrate stream lines for axisymmetric flow, boundary layer growth, and shock locations for various experimental conditions.

ar; where a is a constant determined by the boundary conditions. The actual flow pattern is modified by viscous effects which require that $W = 0$ at the end wall. Schlichting solved for the actual velocity components near the end wall, u and w, and defined a boundary layer thickness δ as the height at which $w/W = 0.99$. For laminar flow, $\delta = 2.8(\nu h/\bar{u})^{1/2}$, where ν is the kinematic viscosity, h is the distance between the reactor terminus and the end wall (0.5 cm), and $\bar{u}$ is the mean flow velocity in the reactor.

If the sampling orifice consists of a small hole drilled in the end wall, it will sample gas from the boundary layer, which does not, in general, have the same composition as the gas in the reactor. Therefore it is imperative that the sampling orifice be placed on the end of a small cone which protrudes well beyond the end wall boundary layer of thickness δ, as shown in Figure 3. It is also imperative that the sample have a nonzero flow component toward the orifice ($\bar{u}$).

When the flow *through* the sampling orifice is considered, another viscous effect is noted, boundary layer growth around the tip and on the inside of the orifice cone, which reduces its effective cross-sectional area. However, as long as the boundary layer does not grow too rapidly, the centerline flow remains unaffected. According to Chang,[3] Knudsen numbers (ratio of local mean free path to orifice diameter) less than 2×10^{-3} are sufficient to ensure that the centerline flow is not perturbed by this factor.

Low pressure sources lead to low orifice Reynolds numbers, and under these conditions viscous dissipation due to velocity and temperature gradients in the core of the free jet may be important. Ashkenas and Sherman[4] used a perturbation approach to treat this factor. Calculations showed that some viscous dissipation was to be expected in our configuration, but it was difficult to estimate how much, since the rapid transition to free molecular flow would be expected to occur in the same region

of the jet where the viscous effects were becoming significant.

In the derivation of Parker's equation one assumes that the free jet expands into a perfect vacuum, so that all the molecules on the axis of the jet pass through the skimmer. However, with finite background pressures, collisions between jet molecules and background gas may cause considerable intensity loss due to scattering. This is especially true for low pressure sources, where the flow changes from continuum to free molecular very close to the orifice. Weakening of the barrel shock in such a case makes the jet "porous". Fenn and Anderson[5] experimentally determined the orifice–skimmer distance at which the background gas reached its ambient concentration in the free jet, for a wide range of pressure ratios, orifice diameters, and for gases with different heat capacity ratios. On this basis, jet permeation in our unit was expected to occur at very short axial distances, requiring short orifice–skimmer distances to prevent excessive beam degradation.

Two types of shocks may exist upstream of the skimmer: (i) the Mach disk of the free jet, and (ii) shocks due to disturbance of the flow by the skimmer. We set the orifice–skimmer distance such that the skimmer tip was located well upstream of the position of the Mach disk, as calculated via the Ashkenas–Sherman equation.[4]

The shock at the skimmer will interfere with sampling if it is detached; however, when it is attached to the skimmer cone, the centerline flow is unaffected. For a given minimum Mach number, there exists an external angle for the skimmer such that the shock will be attached for all Mach numbers greater than the specified minimum. Standard gas tables are available for determining the shock attachment angle for cones in supersonic flow.[6]

A third type of shock is formed when the flow outside the skimmer impinges on the end wall. If its standoff distance is large enough to engulf the skimmer lip serious depletion of beam intensity may occur, as shown by Bossel.[7] For the low density jets in the present study, this type of shock is so weak and diffuse as to have a negligible effect on the beam intensity.

In a mixture of gases of different molecular weights, the beam composition may differ from that of the source gas, for a variety of reasons, some of which are related to the nonideal effects discussed above. For example, background scattering may be more effective in removing lighter molecules leading to an enrichment of the heavier species. If curved shock fronts exist between the orifice and skimmer, they will affect heavy and light molecules differently, giving rise to a velocity separation. Radial diffusion and flow due to radial pressure gradients in the jet also will enrich the beam in heavy molecules. In general, the conditions required to minimize mass separation in the jet are the same as those required to eliminate background and viscous effects, namely, high orifice Reynolds numbers, low orifice Knudsen numbers, and low background pressures. Mass separation also occurs in the free molecular flow regime, where the higher transverse velocities of the lighter molecules lead to beam enrichment of the heavier species. Since not all causes of mass separation can be eliminated, careful calibration of the entire system is required if absolute concentration measurements are desired.

In the early work, skimmer interactions were found to contribute most to the discrepancy between the predicted and measured beam intensities. Although the exact nature of these interactions is still uncertain, a good correlation exists which allows one to predict the magnitude of the effect. Fenn and Deckers[8] showed that reasonable fractions of the theoretical beam intensity may be obtained only if the skimmer Knudsen number is approximately equal to (or greater than) the Mach number at the skimmer. The quantitative application of the quoted relations led to an optimum design, compatible with the available pump speeds. Details are given in Anderson's dissertation.[9] Similar design aspects were considered by Petrel,[10] and comparable features were incorporated in his sampling system. Additional references to previous studies are cited therein.

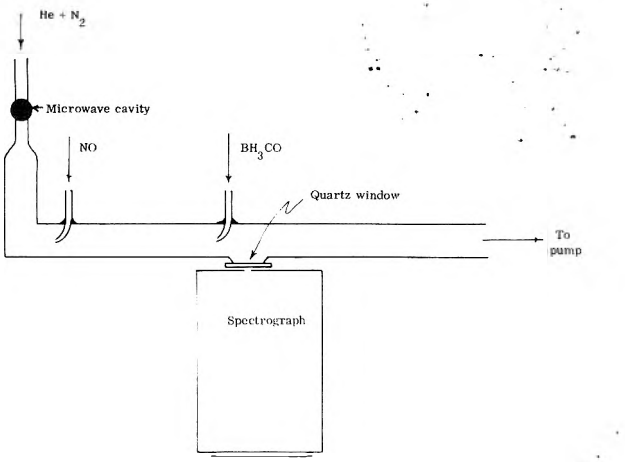

Figure 4. Schematic of the experimental configuration for recording the chemiluminescence spectra for H_3BCO + O mixtures (in the absence of O_2).

The mass spectrometer was a Bendix 1009 SP, TOF operated in the pulsed mode, at 30 kHz. The electrostatic lens in the ion source was modified to permit large ionizing currents at low electron energies (15–25 V).

The spectroscopic data were obtained with the configuration shown schematically in Figure 4. A quartz observation window was placed immediately downstream of the fixed H_3BCO injector. The chemiluminescence was recorded with an Engis (0.75 m, Czerny-Turner) spectrograph, at a linear dispersion of 10 Å/mm in the first order, on Royal-X sheet film, and developed in D-76.

Reagents. Helium, Airco (99.996%), was passed through an activated carbon trap at 77 K, 10 psig, to remove air and hydrocarbon impurities. Oxygen, Airco (99+%), was used as supplied. The nitrogen was Airco "prepurified" (99.995%) N_2. Nitric oxide, Matheson (98.5%), was passed through a silica gel trap at 195 K to remove NO_2, the major impurity. Borane carbonyl, H_3BCO, was synthesized by the method of Burg and Schlesinger,[11] by equilibrating B_2H_6 and CO. The adduct was isolated by freezing at 113 K (isopentane slush) and pumping off the volatile CO and B_2H_6. It was stored at 77 K, and used at its vapor pressure above the liquid at 195 K (about 320 Torr). Diborane, for some experiments, was obtained as a byproduct from a borazine preparation. Mass spectral analysis showed it to be 99+% pure. For later experiments, B_2H_6 was obtained from an old cylinder (Callery Chemical Co.). Extensive conversion to B_4 and B_5 hydrides, plus H_2, had taken place. The higher hydrides were removed by trapping at 195 K, and the H_2 was removed by freezing out the B_2H_6 at 77 K and pumping.

Procedure. To illustrate the procedure we used to measure atom–molecule rate constants, we described in this section the sequence of operations for measurement of the rate of disappearance of H_3BCO in an excess of oxygen atoms. Pseudo-first-order kinetics were applicable. Oxygen atoms were generated (and measured) by the standard visual titration procedure:

$$N + N + M \rightarrow N_2^* + M \xrightarrow[\text{(yellow)}]{h\nu} N_2 + M \quad \text{(R1)}$$

$$N(^4S) + NO(^2\Pi) \rightarrow N_2(^1\Sigma) + O(^3P) \quad \text{(R2)}$$

$$NO + O + M \rightarrow NO_2^* + M \xrightarrow[\text{(green)}]{h\nu} NO_2 + M \quad \text{(R3)}$$

The nitrogen atoms were generated in a microwave discharge through a He–N_2 mixture. Nitric oxide was added, thus producing $O(^3P)$ by the rapid reaction R2. When the NO flow rate was less than the initial flow rate of nitrogen atoms, the yellow afterglow was seen. When the flow rate of NO exceeded that of N, the green air afterglow was seen. When the N and NO flow rates were equal, no emission was observed downstream of the NO injection port since at the total pressures employed in this work (R2) is much faster than (R1) or (R3). The titration procedure had two desirable features: (i) the oxygen atom concentration was measured directly by the known NO flow rate, and (ii) molecular oxygen was absent from the system (except for the O_2 produced by atom recombination, a negligible amount under the flow conditions employed). The presence of O_2 would have seriously complicated the analysis of the reaction mechanism.

Borane carbonyl was metered into the stream of atoms such that the initial concentration was less than 10% of the oxygen atom concentration. The mass spectrometer was tuned to the H_3BCO fragment at m/e 41, and the signal intensity was recorded as a function of the distance between the movable mixer and the sampling orifice.

Determination of the Rate Constants. To determine a pseudo-first-order rate constant from the measured spatial concentration profiles, it is necessary to determine how the effective reaction time is related to the distance flowed in the reactor. This is most often done by introducing the "plug-flow" assumption

$$\frac{dc}{dz} = \frac{1}{\bar{u}} \frac{dc}{dt} \quad (1)$$

where $\bar{u}$ is the bulk, or average velocity of flow. This procedure is not necessarily valid for laminar flow, which always obtains for low pressure flow reactors. Equation 1 rests on the following two assumption: (1) axial diffusion is too slow to affect significantly the concentration profile, and (2) radial diffusion is fast enough to average out the distribution of residence times over the radius of the reactor [due to the parabolic velocity profile for laminar flow, $u(r) = 2\bar{u}(1 - r^2/R^2)$, where R is the radius of the reactor]. The first of these assumptions can be shown[9] to valid when

$$D_{ab}k/\bar{u}^2 << 1 \quad (2)$$

where D_{ab} is the binary diffusion coefficent of the reactant a (H_3BCO) in the diluent b (mostly helium), and k is the pseudo-first-order rate constant for the disappearance of a. The second assumption is valid[12] (for 10% accuracy in k) when

$$D_{ab}/(kR^2) > 0.3 \quad (3)$$

Hence, it is necessary that

$$0.3kR^2 < D_{ab} << \bar{u}^2/k \quad (4)$$

Since D_{ab} is inversely proportional to the pressure, the above relationship can only be valid in a limited range of pressures and flow speeds, for a given rate constant.[13] In this study, the above inequality held, and the required correction factors for deviations from plug flow amounted to less than 10%. For the reaction

$$H_3BCO + O \rightarrow \text{products} \quad \text{(R4)}$$

where $[O] = [O]^0 \gg [H_3BCO]^0$, the following rate law holds:

$$d[H_3BCO]/dt = -k[H_3BCO]$$

where $k = k_4[O]$. On introducing the plug-flow assumption and integrating

$$\ln \{[H_3BCO]/[H_3BCO]^0\} = -kz/\bar{u} \quad (5)$$

The raw data were plotted in the form of $\ln (S - S_b)$ vs. z, where S is the H_3BCO signal from the mass spectrometer (arbitrary units), and S_b is the background m/e 41 signal. The slope gave the pseudo-first-order rate constant, from which the bimolecular rate constant was derived.

To check on the accuracy and internal consistency of the apparatus, the metering of flows, and the absence of severe viscous interaction effects, the rate of the well-studied reaction between atomic oxygen and ethylene was measured. The rate constant at 295 K for the disappearance of C_2H_4 was determined from the decrease of the m/e 27 signal in the present of excess of O atoms. These were produced by means of a microwave discharge of He–O_2 mixtures or He–N_2 mixtures, followed by titration with NO. In a representative run the slope of the $\ln (S - S_b)$ line was found by least squares to be -227 s^{-1}. Dividing by the measured O atom concentration (7.87×10^{-10} mol cm^{-3}) gives the bimolecular rate constant, 2.89×10^{11} cm^3 mol^{-1} s^{-1}. The results for several runs averaged to $2.87^{+1.00}_{-0.46} \times 10^{11}$, in acceptable agreement with the literature values.[14]

TABLE I: Apparent Rate Constants at 295 K for the Reaction $H_3BCO + O \rightarrow$ Products

Run	$\bar{u} \times 10^{-3}$ cm/s	P_t, Torr	$[O] \times 10^{10}$ mol/cm^3	(First set) $k_4 \times 10^{-11}$ cm^3 mol^{-1} s^{-1}
1	1.73	2.22	0.865	8.10
2	1.39	3.82	2.32	4.76
3	1.39	3.82	2.32	7.80
4	1.52	3.87	2.04	4.66
5	1.53	4.50	1.94	5.69
6	1.48	3.33	1.41	5.87
7	1.47	4.04	7.16	4.43
8	1.71	3.13	2.84	6.71
9	1.42	2.84	3.33	3.95
10	1.30	3.01	3.61	2.44
11	1.30	3.01	3.61	2.44
12	1.31	2.98	4.09	2.68
13	1.25	3.11	5.03	4.20
14	1.31	2.99	5.45	4.42

Results

Mass Spectrometric Data. $H_3BCO + O$. The apparent rate constants derived from the first series of measurements for (R4) are listed in Table I. The initial concentration of H_3BCO was not measured in each case, but generally it was less than 10% of the oxygen atom concentration. The large variation in the apparent rate constant showed no systematic trends with reactor pressure, flow speed, or oxygen atom concentration. In addition, the decay plots showed considerable curvature in some cases, indicating a breakdown of pseudo-first-order conditions. The only variable that seemed to have a systematic effect on these rate constants was the condition of the reactor walls. Large values were always obtained

TABLE II: Measured Rate Constants at 295 K for the Reaction $H_3BCO + O \rightarrow$ Products with Varying Wall Conditions

Run	Wall condition	Apparent k_4 $cm^3\ mol^{-1}\ s^{-1}$
15	Coated with $Si(CH_3)_2(Cl)_2$	3.87×10^{11}
16	Clean	6.06×10^{11}
17	Products from run 16	5.32×10^{11}
18	Products from runs 16-17	4.80×10^{11}
19	Products from runs 16-18	4.11×10^{11}
20	Coated with $Si(CH_3)_2(Cl)_2$	3.50×10^{11}

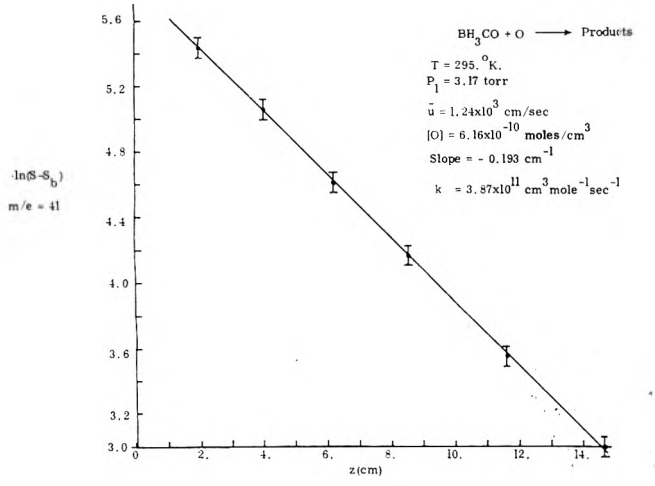

Figure 5. First-order decay curve for H_3BCO in excess O atoms.

when the reactor walls were freshly cleaned with hydrofluoric acid. The observed rate decreased as a white powdery reaction product (probably B_2O_3) built up on the walls. We surmise that the tube walls were catalytic, probably by adsorption of H_3BCO on the OH sites of the glass. To test this possibility, a rate was measured after coating the walls with dichlorodimethylsilane, which covers the reactive sites and generates a surface of methyl groups. The coating was found to be inert to oxygen atoms. The result of this run (run 15) is given in Table II, and the decay plot is shown in Figure 5. Next the walls were cleaned with hydrofluoric acid and dried with hot air. A series of rate measurements were made (runs 16–19) in which the reaction products were allowed to build up on the walls from run to run. Finally, in run 20, the walls were cleaned and again coated with $Si(CH_3)_2Cl_2$. Runs 15 → 20 were made under identical conditions with the following initial partial pressures: He, 2.87 Torr; N_2, 0.21 Torr; O, 0.011 Torr; H_3BCO, 0.000 55 Torr. Table II shows that the reaction is strongly catalyzed by a clean glass surface. The results of runs 15 and 20 are probably closest to the unperturbed homogeneous rate constant. After correcting for diffusion effects, the average of runs 15 and 20 gives $k_4 = 3.92^{+1.40}_{-0.63} \times 10^{11}$ $cm^3\ mol^{-1}\ s^{-1}$ (T = 295 K).

Under flow conditions similar to those for run 15, except for a larger flow rate of H_3BCO, the absolute change in concentration of both O and H_3BCO was measured for a fixed reaction distance, giving the following stoichiometry:

$$\Delta[O]/\Delta[H_3BCO] = 2.0 \pm 0.5$$

Mass spectrometer scans were made in an attempt to observe the reaction products and reactive intermediates. A strong signal was detected for H_2, which increased at approximately the same rate as the H_3BCO decreased. Measurement of other products and reactive intermediates was beset with many difficulties. Most of the possible intermediates are expected to be more reactive toward O atoms than the parent compound. Since O atoms were present in excess, the residual concentrations of these species would be very low. Second, the products and/or intermediates reacted rapidly with the walls, as evidenced by the deposits which accumulated. There was also the possibility of loss of reactive species in the end-wall boundary layer. Finally, of those molecules which were sampled, the presence of some species may have been masked by interference with others in the background of the mass spectrometer ion source. For example, BH, BH_2, and BH_3 would have been masked by the corresponding peaks produced in the fragmentation of H_3BCO, which could not be avoided even at electron energies as low as 20 V. Peaks due to $HB^{11}O$ and CO would have been overwhelmed by the N_2 peak. The species $B^{11}O$ and $B^{10}O$, while known to be present, could not be observed because of interference from the fragmentation of B_2H_6, which could not be completely eliminated from the H_3BCO preparation. Finally, the production of OH and H_2O could not be demonstrated because of the very large background signals due to H_2O in the ion source.

TABLE III: Transient Species Observed from (H_3BCO + O) Mixtures

m/e	Probable parent species	Emission spectra
2 (s)	H_2	$BO(A^2\Pi)$ is produced with v' up to 11; 103 kcal above ground level
26 (vw)	($B^{10}O$)	Strongest emission from $v' = 4$
27 (vw)	($B^{11}O$)	
28 (vw)	($HB^{11}O$)	OH emission (weak) at 3064 and 3077 Å
29 (w)	(HBOH)	
30 (w)	H_2BOH, (H_3BO)	No BO_2 emission observed unless O_2 is present in system
32 (m)	O_2	No $BO(B^2\Sigma^+ \rightarrow X^2\Sigma^+)$ emission
43 (m)	BO_2	
44 (m)	OBOH	

To increase the sensitivity of detection of reactive intermediates, and to discriminate between beam and background molecules in the ion source, a "chemical modulation" technique was installed. The power delivered to the microwave discharge cavity (from which the O atoms were derived) was square-wave modulated at 17 Hz. The electrometer output of the mass spectrometer was fed to a lock-in amplifier while the spectrometer was slowly scanned from 10 to 50 mass units. Although the background signals were minimized, the results were rather disappointing. Large signals were seen for O and H_3BCO, of opposite polarity (as atoms are produced, H_3BCO is destroyed), but the only evidence for other species were several weak and quantitatively nonreproducible peaks in the range m/e 26–28. The failure of this technique may have been due to the loss of reactive intermediates on the reactor walls, or simply to their high mutual reactivity and consequent low steady state concentration. A listing of our observations of reactive intermediates (including spectroscopic data) is given in Table III. Most of the assignments are tentative; only H_2, BO, and BO_2 were observed with certainty; the latter two are based on spectroscopic data.

Emission Spectra. H_3BCO + O. In the absence of O_2, the injection of H_3BCO into a stream of O atoms gave a deep blue reaction zone. The recorded spectra covered the range 2700–3900 Å; virtually all the emission was due to the $A^2\Pi \rightarrow X^2\Sigma$ transition in BO. The photographed band system was identical with that observed by Mulliken,[15] except that bands extended to significantly higher vibrational quantum numbers (in the $A^2\Pi$ state) than

previously reported. The strongest emission came from the $v' = 4$ and $v' = 5$ levels, but levels up to $v' = 11$ were observed. Very weak A → X emission from OH was also recorded at 3064 and 3077 Å. Otherwise, no other species (including BO_2) could be positively identified in emission, although there were several very weak, diffuse bands below 3000 Å which defied identification. In the presence of molecular oxygen, when the oxygen atoms were generated by discharging He–O_2 mixtures, the "flame" had a bright green appearance. A spectrum of the 5250–5850-Å region showed the diffuse, undulating bands characteristic of BO_2. A photograph of the 3250–3850-Å region showed that BO bands were also present, with intensities similar to those observed in the absence of O_2.

Mass Spectrometric Data. H_3BCO + N and B_2H_6 + O. The reaction between H_3BCO and N atoms was studied under very nearly the same conditions as was the [H_3BCO + O] pair. Here also the apparent rate constant showed large variations from run to run, due to wall catalysis and atom depletion. The results for four runs averaged to 1.54×10^{11} mol^{-1} cm^3 s^{-1} (295 K). However, the conditions under which these runs were made were later found to have up to 80% depletion of the original atom concentration. Since most of the depletion took place at very short reaction times, the curvature of the ln ($S - S_b$) vs. z plots would have been apparent only at very short reaction lengths, where no data were taken. Subsequent runs were made in an attempt to minimize atom depletion by using very small flow rates for the H_3BCO. This gave a value 5 times larger. In turn, we suspect that strong wall catalysis was occurring in this run (clean walls), since measurement of the [H_3BCO + O] rate immediately after this run gave a large values (8.1×10^{11}) for attack by oxygen. We conclude that the bimolecular homogeneous rate constant for the reaction between H_3BCO with N is about the same as with O atoms.

Two measurements of the stoichiometry of the (H_3BCO + N) system gave the following results:

$$\Delta[N]/\Delta[H_3BCO] = 3.6; 3.8$$

On mixing H_3BCO with N atoms an intense blue-green chemiluminescence was produced. Unfortunately, time did not permit a detailed spectroscopic analysis.

The reaction between diborane and oxygen atoms was slow compared to that of H_3BCO. The reactor conditions had to be altered to permit its measurement. A smaller flow velocity was employed, and a He–O_2 mixture was discharged to give the highest possible atom concentrations. Even so, the B_2H_6 signal decreased by only about 10% over the length of the reaction zone. The derived rate constant is 2.68×10^9 cm^3 mol^{-1} s^{-1} (295 K). A mass spectral scan showed weak evidence for H_2, BO, and BO_2.

The system (B_2H_6 + N) was unlike the previous three in that an induction time appeared in which the B_2H_6 concentration did not change significantly, followed by a rapid decay of B_2H_6. The blue-green chemiluminescence (similar to that from H_3BCO + N) reached its maximum intensity at about the same time that the B_2H_6 signal started to change rapidly. No quantitative data were obtained.

It has been stated that B_2H_6 and H_3BCO react spontaneously (sometimes explosively) at room temperature with air and other oxygen-containing molecular species. We attempted to measure the rate of reaction of these boron hydrides with O_2, N_2O, NO, and NO_2. Flow conditions had to be suitably adjusted, since these rates were expected to be much lower than the rates with the atomic species. Very low flow speeds were used (approximately 300 cm/s), no helium diluent was added, so that the small reactant flow was introduced into a vast excess of oxidant. Despite these efforts, no decrease in reactant signal could be observed for any of the above combinations. The signal-to-noise ratio of a particular experiment determined what extent of reaction would be barely detectable; this in turn set an upper limit to the rate constant for the reaction in question. They ranged from 2.5 to 9.7×10^5 mol^{-1} cm^3 s^{-1}.

Discussion

For (H_3BCO + O) the magnitude of the rate constant provides the clue for the initial step of the reaction. It is known[16] that at room temperature and above H_3BCO rapidly attains equilibrium with borane and CO

$$H_3BCO \rightleftarrows BH_3 + CO \qquad (R5)$$

If the dissociation of H_3BCO were the rate limiting step in the oxidation, followed by the rapid reaction of BH_3 with O atoms, our observed first-order rate constant for the decay of H_3BCO would have to be less than (or nearly equal to) the rate constant for the forward step of (R5). On the basis of Burg's data[17] for the thermal decomposition of H_3BCO, one finds for the unimolecular rate constant (R5) at room temperature 2.0×10^{-3} s^{-1}. Since our observed first-order rate constant for the decay was on the order of 2.0×10^2 s^{-1} (a factor of 10^5 larger) clearly reaction R5 plays no important role in the O atom attack on borane carbonyl; the *initial step must be a direct reaction between O and H_3BCO.*

It seems unlikely that the CO group is directly involved in the reaction. This leaves two plausible reaction paths: (a) abstraction of one or two hydrogens, followed by the breaking of the B:CO bond, and (b) formation of a B–O bond (eliminating CO), followed by rearrangement and/or fragmentation of the excited complex. The available evidence suggests that both mechanisms operate concurrently. The initiation steps, and subsequent reactions needed to account for our observations, are given in Table IV. The corresponding heats of reaction were calculated in most cases from the heats of formation listed in the JANAF Thermochemical Tables.[18]

Initiation mechanism 2 accounts for many of the observed products and intermediates, but fails to account for the emission spectra. BO was produced in the $A^2\Pi$ state with up to 11 quanta of vibrational energy. This state lies 103 kcal/mol above the ground state of BO ($X^2\Sigma$, $v'' = 0$). The ($A^2\Pi$, $v' = 4$) state, which appeared to give the strongest emission, lies more than 81 kcal/mol above the ground state. Thus, the reaction(s) producing BO must be highly exoergic. Although the intermediates from mechanism 2 may react further to produce BO (R12, R13, etc.), none of these is sufficiently exoergic to account for these emissions. However, the intermediates from mechanism 1 (BH and BH_2) can produce BO at the observed levels of excitation via (R14) and (R15). Indeed, Hand and Derr[14] proposed that reaction R14 is the source of BO chemiluminescence in the B_2H_6 + O system.

The observation of O_2 as a minor product can be most easily accounted for by reaction R19, which has a room temperature rate constant[19] of 2.52×10^{13} cm^3 mol^{-1} s^{-1}. This very high rate indicates that OH could not play an important role in the initiation mechanism, since the steady state concentration of OH would always be much lower than the concentration of O atoms, which were initially in excess. The very weak OH UV emission could have arisen from collisional excitation of OH by BO*.

The direct and indirect evidence for the presence of OH seems to favor (R6) over (R7) for the initiation step, if only mechanism 1 were considered. If the reaction sequence

TABLE IV: Postulated Mechanism for the $H_3BCO + O$ System

	Reaction	Estimated ΔH°_{298}, kcal/mol	
Initiation (mechanism 1)	$O + H_3BCO \rightarrow OH + [H_2BCO]^* \rightarrow OH + BH_2 + CO$	−4	R6
	$\rightarrow H_2O + [HBCO]^* \rightarrow H_2O + BH + CO$	−12	R7
Initiation (mechanism 2)	$O + H_3BCO \rightarrow [H_3BO]^* + CO \rightarrow BO + H_2 + H + CO$	−9	R8
	$\rightarrow HBO + H_2 + CO$	−80	R9
	$\rightarrow HBOH + H + CO$	−26	R10
	$\rightarrow H_2BOH + CO$	−131	R11
BO formation	$HBO + O \rightarrow BO + OH$	−31	R12
	$HBO + OH \rightarrow BO + H_2O$	−47	R13
	$BH_2 + O \rightarrow BO + H_2$	−108	R14
	$BH + O \rightarrow BO + H$	−113	R15
	$BH_2 + O \rightarrow BH + OH$	+7	R16
BO_2 formation	$BO + O + M \rightarrow BO_2 + M$	−169	R17
	$BO + O_2 \rightarrow BO_2 + O$	−50	R18
O_2 formation	$OH + O \rightarrow O_2 + H$	−17	R19

proceeded *entirely* through (R6), however, the observed stoichiometry would have been at least *three* oxygen atoms consumed per H_3BCO consumed, via

$O + H_3BCO \rightarrow OH + BH_2 + CO$ (rate limiting) (R6)

$OH + O \rightarrow O_2 + H$ (fast) (R19)

$BH_2 + O \rightarrow BO + H_2$ (fast) (R14)

A stoichiometry of 2 would be expected if the only initiation step were (R7), via

$O + H_3BCO \rightarrow H_2O + BH + CO$ (rate limiting) (R7)

$BH + O \rightarrow BO + H$ (fast) (R15)

The stoichiometry anticipated for any of the initiation steps in mechanism 2 is less than 2, since the products of reactions R8 through R11 are more stable than BH and BH_2, and are expected to react more slowly with O atoms. The observed stoichiometry of 2.0 ± 0.5 suggests that (R7) may be the dominant initiation step, but (R6), and to a lesser extent the reactions in mechanism 2 [(R8)–(R11)], also contribute.

The observations regarding BO_2 emission may be rationalized by considering reactions R17 and R18. The former requires a termolecular collision to remove excess energy, which may explain why no BO_2 emission was observed when molecular oxygen was not present in the initial reactants, i.e., three-body processes would have been very slow at the low pressures involved. The small amount of BO_2 observed in the mass spectrometer was probably due to the reaction of BO and O on the reactor walls. The green BO_2 emission observed when O_2 was present in the initial reactants was probably generated by reaction R18.

In summary, there is evidence that the ($H_3BCO + O$) reaction proceeds via two mechanisms, one in which the O atom abstracts hydrogen(s) from the BH_3 group, and the other in which the O atom directly attacks the boron atom. In the first case, the remaining fragment reacts rapidly with O atoms to produce highly excited BO, which gives rise to chemiluminescence in the visible and near UV.

Superficially the ($H_3BCO + N$) system resembles ($H_3BCO + O$); the rate of attack on the adduct is the same, and strong chemiluminescence is observed in both cases. However, the origin of the blue-green emission from this system is in doubt, since no spectroscopic measurements were made.

Two band systems for electronically excited BN have been reported in the literature. The Douglas–Herzberg[20] transition ($^3\Pi \rightarrow X^3\Pi$) appears at 3400–4000 Å, when BCl_3 is injected into a stream of active nitrogen. Under similar conditions, Anderson[21] observed an additional band system in the spectral range 5900–10 000 Å, which he tentatively identified as the $A^3\Sigma \rightarrow X^3\Pi$ transition. The blue-green emission from the ($H_3BCO + N$) system does not seem to correspond to either of these unless one assumes that the emission is from high vibrational levels ($v' > 7$) of the state which Anderson designated as $A^3\Sigma$. It is not likely that blue-green emission was due to an oxygen impurity which would generate BO* and BO_2*. This was demonstrated by titrating the N atoms with NO, in which case the familiar blue BO* emission was seen, but green BO_2* emission was absent. The ($H_3BCO + N$) pair deserves further study, since the emission may belong to a new band system of BN, or to some polyatomic species that has not been observed previously.

The stoichiometry (3.6) for the ($H_3BCO + N$) reaction is greater than that for ($H_3BCO + O$), suggesting a more complicated mechanism. Perhaps one of the intermediates catalyzes the recombination of N atoms. Without spectroscopic data or observations of intermediates and products, no definite conclusions can be made regarding this mechanism.

The observed rate constant for the disappearance of B_2H_6 when mixed with O atom, 2.68×10^9 cm^3 mol^{-1} s^{-1}, agrees very well with the value reported by Hand and Derr,[13] $(2.5 \pm 1.6) \times 10^9$. They also observed BO (α) emission bands, down to wavelengths corresponding to the transmission limit of their pyrex reactor, but report that this emission was visible only when B_2H_6 was in excess, in contrast to the present study. In our experiments, emission was seen under all conditions. In addition, they observed a stoichiometry of about 10 oxygen atoms consumed per B_2H_6 consumed. We cannot explain these differences; we have no stoichiometric data and we have no evidence for reactive intermediates other than BO.

In two older investigations of the $B_2H_6/O/O_2$ system alternate mechanisms were suggested, based on qualitative observations of product distributions. Fehlner and Strong[22] proposed an initiation step analogous to the left half of R8: $B_2H_6 + O \rightarrow H_3B + H_3BO$. The nascent borane oxide is presumed to decompose into H_2 and a solid. Their major gaseous products were characteristic of the borane pyrolysis, as anticipated, since they investigated fuel rich compositions in a reactor which incorporated a closed loop for recirculating the mixture through a quartz photolysis cell. The mechanism cited by Carabine and Norrish[23] is difficult for us to rationalize. They observed high levels of OH in absorption. Clearly this radical plays a major role in near stoichiometric mixtures of $B_2H_6 + O_2$,

while our data indicate that it is relatively unimportant in fuel lean mixtures. However, they proposed not a single step which includes O atoms, they include three four-center reactions of O_2 with several borane species, and some of their key steps are substantially endoergic.

Conclusion

Concurrent data collection via mass spectrometry and emission spectroscopy can yield information on reaction mechanisms which neither technique by itself can pinpoint. Heterogeneous effects, however, can give rise to misleading rate measurements as well as difficulties in observing reactive intermediates.

Acknowledgment. This investigation was supported in part by ARPA-ONR N00014-671A-0077-0006. The authors sincerely thank Professor W. J. McLean for many helpful discussions regarding the complex gas dynamic problems limiting fidelity of sampling of reactor compositions via beam-mass spectrometry.

References and Notes

(1) H. Parker et al. in "Rarefied Gas Dynamics", F. M. Devienne, Ed., Pergamon Press, New York, N.Y., 1960, p 69.
(2) H. Schlichting, "Boundary Layer Theory", 6th ed, McGraw-Hill, New York, N.Y., 1968, p 90.
(3) J. Chang, AERL Research Report 326, 1969.
(4) H. Ashkenas and F. Sherman in "Rarefied Gas Dynamics", Vol. II, J. H. deLeeuw, Ed., Academic Press, New York, N.Y., 1966, p 84.
(5) J. Anderson and J. Fenn, *Phys. Fluids*, **8**, 780 (1965).
(6) Ames Research Staff, NACA Report 1135, U.S. Government Printing Office, Washington, D.C., 1953.
(7) U. Bossel, Ph.D. Thesis, Berkeley, 1968.
(8) J. Fenn and J. Deckers in "Rarefied Gas Dynamics", Vol. I, J. A. Laurman, Ed., Academic Press, New York, N.Y., 1963, p 497.
(9) G. K. Anderson, Ph.D. Thesis, Cornell University, August, 1975.
(10) R. Petrel, *Int. J. Mass Spectrum Ion Phys.*, **16**, 39 (1975).
(11) A. Burg and H. Schlesinger, *J. Am. Chem. Soc.*, **59**, 780 (1937).
(12) R. Poirier and R. Carr, *J. Phys. Chem.*, **75**, 1593 (1971).
(13) See also P. J. Ogren, *J. Phys. Chem.*, **79**, 1749 (1975).
(14) C. Hand and L. Derr, *Inorg. Chem.*, **13**, 2, 339 (1974).
(15) R. S. Mulliken, *Phys. Rev.*, **25**, 259 (1925).
(16) M. Garabedian and S. W. Benson, *J. Am. Chem. Soc.*, **86**, 176 (1964).
(17) A. B. Burg, *J. Am. Chem. Soc.*, **74**, 3482 (1952).
(18) JANAF Thermochemical Tables, *Natl. Stand. Ref. Data Ser., Natl. Bur. Stand.*, **No. 37** (1971).
(19) M. Clyne and B. Thrush, *Proc. R. Soc. London, Ser. A*, **275**, 544 (1963).
(20) A. Douglas and G. Herzberg, *Can. J. Res.*, **18A**, 179 (1940).
(21) R. Anderson, Ph.D. Thesis, Cornell University, 1972.
(22) F. P. Fehlner and R. L. Strong, *J. Phys. Chem.*, **64**, 1522 (1960).
(23) M. D. Carabine and R. G. W. Norrish, *Proc. R. Soc. London, Ser. A*, **296**, 1 (1966).

Primary Processes in the 147- and 123.6-nm Photolyses of 1,1,1-Trifluoro-2-chloroethane

T. Ichimura, A. W. Kirk, and E. Tschuikow-Roux*

Department of Chemistry, The University of Calgary, Calgary, Alberta, Canada T2N 1N4 *(Received February 17, 1977)*

Trifluorochloroethane (CF_3CH_2Cl) was photolyzed at 147 and 123.6 nm in the presence and absence of nitric oxide. The effects of added CF_4 were also studied. The quantum yields of molecular processes increase with decreasing wavelength. The quantum yield for FCl elimination is small at 147 nm ($\Phi \leq 0.07$) but becomes the major mode of photodecomposition at 123.6 nm ($\Phi = 0.38$). Substantial hydrogen chloride elimination occurs at both wavelengths ($\Phi = 0.15$–0.19) and hydrogen fluoride elimination is also observed. The results are interpreted in terms of the preferential formation of a Rydberg state as the photon energy increases.

Introduction

Previous investigations of the photolyses of haloethanes in this laboratory have been restricted to 147 nm.[1-4] At this wavelength molecular eliminations are the dominant primary processes. However, some parallel carbon–halogen and carbon–carbon bond rupture is generally observed and we have previously concluded that more than one excited state may initially be formed upon absorption of the monochromatic radiation. We have also suggested that carbon–halogen bond fission is probably associated with the first ($n \rightarrow \sigma^*$) absorption band of the species in question,[5-7] while the molecular elimination processes are more clearly associated with the higher "Rydberg type" transitions, for example, $n \rightarrow 4s$. We believe it is the broad overlapping nature of the ultraviolet absorption spectra[5] that allows this simultaneous formation of distinctly different states and it is therefore reasonable to suppose that small changes in the wavelength of the incident radiation might well result in modifications of the relative populations and lifetimes of the excited states so formed. Some experimental evidence already supports these ideas. Cremieux and Herman[8] photolyzed ethyl chloride at 123.6 nm and found a higher proportion of molecular HCl elimination than that observed at 147 nm.[1] There was also evidence that the excited state precursor formed at 147 nm was sufficiently long-lived to undergo collisional modification. This was not the case at 123.6 nm. The photolysis of 1,1-$C_2H_4Cl_2$ at 147 nm is characterized by competitive molecular eliminations.[2] However, at wavelengths longer than 190 nm, no elimination of HCl is observed and the molecule decomposes mainly by carbon–chlorine bond fission.[9] The photolysis of CF_3CH_2Cl is a continuation of our work with haloethanes to establish the nature and extent of molecular elimination processes occurring in the vacuum ultraviolet. In these experiments we were particularly interested in the wavelength dependence of the quantum yields of these processes.

Experimental Section

Photolyses were carried out at room temperature in the same conventional apparatus used in previous work.[1-4] The xenon and krypton resonance lamps were powered by a microwave generator (KIVA Instruments Inc., Model MPG 4M). The lamps were operated at intensities of $3.5 \pm 0.3 \times 10^{13}$ and $8.5 \pm 1 \times 10^{12}$ photons s^{-1}, respectively, and for periods such that overall conversions were less than 0.1%. The chromatic purity of the lamps was checked using a McPherson (218-0.3 m) vacuum ultraviolet

TABLE I: Photolysis of CF_3CH_2Cl at 147 and 123.6 nm[a]

Run no.	P-(CF_3CH_2Cl), Torr	P-(additive), Torr	Quantum yields (ϕ)						
			CF_2CH_2	CF_2CHF	CF_2CHCl	CF_3H	CH_3Cl	($C_4H_4F_6$)	C_4[b]
1	5.6		0.22	0.13	0.04	0.07		0.13	0.20
2	6.4		0.20	0.14	0.05	0.07	0.01	0.11	0.22
3	9.7		0.16	0.15	0.04	0.06	0.02	0.10	
4	10.9		0.16	0.16	0.04	0.06			0.22
5	12.7		0.15	0.15	0.04	0.06	0.01	0.09	
6	20.0		0.13	0.16	0.03	0.06	0.01	0.10	0.24
7	282		0.06	0.17	0.04	0.05			
8	7.7	NO 0.4	0.070	0.15	0.02	0.0	0.0	0.0	0.0
9	11.9	NO 0.7	0.070	0.15	0.02	0.0	0.0	0.0	0.0
10	12.5	H_2S 0.2	0.12	0.15	0.03	0.08	0.06		
11	10.0	CF_4 210	0.057	0.15	0.03	0.06	0.01		
12	10.5	CF_4 380	0.050	0.15	0.04	0.07	0.01		
13	10.2	NO 0.5 CF_4 122	0.060	0.16	0.02	0.0	0.0	0.0	0.0
14	13.8	NO 1.2 CF_4 292	0.055	0.17	0.02	0.0	0.0	0.0	0.0
15	11.0	NO 0.7 CF_4 410	0.050	0.18	0.01	0.0	0.0	0.0	0.0
16	11.5	NO 0.7 CF_4 538	0.047	0.19		0.0	0.0	0.0	0.0
17	7.9		0.43	0.18	0.09	0.06		~0	0.10
18	10.7		0.44	0.20	0.10	0.07	0.01	~0	
19	14.0		0.43	0.19	0.11	0.07	0.01	~0	0.09
20	10.5	NO 0.4	0.38	0.20	0.10	0.0	0.0	0.0	0.0
21	11.9	NO 0.2	0.38	0.19	0.09	0.0	0.0	0.0	0.0
22	13.2	H_2S 0.3	0.43	0.20	0.11	0.08	0.06		
23	11.9	NO 0.4 CF_4 204	0.36	0.19	0.11	0	0	0	0
24	11.7	NO 0.3 CF_4 356	0.38	0.19	0.10	0	0	0	0

[a] Runs 1-16, 147 nm. Runs 17-24, 123.6 nm. [b] Sum of the two products thought to be chlorinated fluorobutanes.

monochromator. For the liquid oxygen cooled xenon lamp,[4] contributions from the 129.5-nm line were minimal. The titanium filament gettered krypton lamp was similar in design to that described by Gordon et al.[10] The only undesirable emission observed between 110 and 200 nm was at 165 nm. However, the intensity relative to the 123.6-nm line was very small (<1%). The 0.5-mm thickness lithium fluoride window of the krypton lamp was opaque to wavelengths shorter than 110 nm.

Actinometry was based upon the production of acetylene from the photolysis of ethylene (Φ = 1.0 at 147 and 123.6 nm).[11] The extinction coefficient of 1,1,1-trifluoro-2-chloroethane at 147 nm was determined by measurement of the photoionization currents of mixtures of CF_3CH_2Cl and $(CH_3)_3N$.[12]

Product analysis was by flame ionization gas chromatography (Varian Aerograph 1740). Low molecular weight products (C_1 and C_2) were separated on a 3-m Porapak N column at 125 °C and a helium flow rate of ~30 cm^3 min^{-1}. The three higher molecular weight products were separated at 60 °C on a 1.5-m SE30 column at a helium flow rate of 40 cm^3 min^{-1}. Identification of the products CF_2CH_2, CF_2CHF, CF_2CHCl, CF_3H, and CH_3Cl was by comparison with the retention times of authentic samples. The first product peak eluting after CF_3CH_2Cl was thought to be 1,1,1,4,4,4-$C_4H_4F_6$ though this could not be confirmed. The two remaining high molecular weight products were tentatively identified as chlorofluorobutanes. All three products were arbitarily assigned detector sensitivities of twice that of ethylene. Authentic samples of the appropriate isomeric butanes could not be obtained.

The 1,1,1-trifluoro-2-chloroethane was obtained from Peninsular Chemresearch Inc. Prior to its use, low boiling impurities were removed by trap to trap distillations. The final purity was better than 99%. The H_2S and CF_4 from Matheson, of stated purities 99.5 and 99.7%, respectively, were used without further purification. The NO, also from Matheson, contained traces of NO_2 which were removed by distillation at -78 °C.

Results

The extinction coefficient of CF_3CH_2Cl at 147 nm and 296 K was found to be 332 ± 33 atm^{-1} cm^{-1}. The corresponding value at 123.6 nm was not measured but is known to be an order of magnitude larger than at 147 nm for this class of compounds.[13]

Table I shows the quantum yields of the products as a function of the pressure of CF_3CH_2Cl and of the added gases NO and CF_4. The quantum yields of the major olefinic products were also found to be independent of photolysis time in the ranges 30–85 min (147 nm) and 50–90 min (123.6 nm).

At 147 nm and low pressures (~10 Torr), CF_2CH_2 is a major product. The yield, however, decreases with increasing pressure both in the presence and absence of NO. Runs 8 and 9 indicate clearly that much of the CF_2CH_2 formed at low pressures is of free radical origin. At 123.6 nm the yield of CF_2CH_2 is even larger and much less dependent upon total pressure and the pressure of NO. Trifluoroethylene (CF_2CHF) is a major product at both wavelengths. At 123.6 nm the yield is constant. At 147 nm there is an indication that the yield of CF_2CHF in-

creases slightly with increasing pressure. Runs 8 and 13–16 suggest that this increase might well be related to the decreases in the yields of CF_2CH_2 and CF_2CHCl with increasing pressure. The yields of CF_2CHF obtained in runs 11 and 12 are somewhat inconsistent with the trends established by the remaining data. One might expect them to be a little larger. As is the case with CF_2CH_2, the yield of CF_2CHCl is also fairly constant at 123.6 nm ($\Phi = 0.1$). At the longer wavelength, the yield is again lower and dependent upon the presence of NO.

Corresponding to the large radical yield of CF_2CH_2 at 147 nm at lower pressures there is a significant yield of the product tentatively identified as hexafluorobutane. In the presence of NO this product is not observed. Not too surprisingly, at 123.6 nm the yield of hexafluorobutane is close or equal to zero at low pressures even in the absence of NO, since there is obviously little CF_2CH_2 of radical origin. There is also a corresponding decrease with decreasing wavelength of the total yield of the remaining C_4 products. While the yield of C_4 products is substantial at 147 nm, subsequent discussion will indicate that the yield is still somewhat lower than one might expect.

The maximum yield of CF_3H is the same at both wavelengths ($\Phi = 0.08$, runs 10 and 22) and virtually independent of pressure in the absence of H_2S. Its formation is suppressed completely by the addition of NO and it is, therefore, presumably entirely of free radical (CF_3) origin. Similarly it is likely that CH_3Cl is formed from CH_2Cl radicals. The maximum yield of CH_3Cl ($\Phi = 0.06$) obtained in the presence of H_2S is similar to that for CF_3H. However, unlike CF_3H in the absence of H_2S, the yield is considerably lower.

Discussion

Since the quantum yield of CF_2CH_2 at 123.6 nm is hardly affected by the presence of NO and there is no evidence of a large yield of free radicals, most, if not all, of the CF_2CH_2 produced at 123.6 nm would appear to be formed by a molecular elimination of FCl in a primary process represented by reactions 1 and 2. The numbered

$$CF_3CH_2Cl + h\nu \rightarrow CF_3CH_2Cl^{\dagger(1)} \quad (1)$$

$$CF_3CH_2Cl^{\dagger(1)} \rightarrow CF_2CH_2 + FCl \quad (\phi_{123.6} = 0.38) \quad (2)$$

dagger identifies one of two or more initially formed electronically excited states. The experiments performed at 147 nm in the presence of NO show that the quantum yield for the same process at the longer wavelength is much lower and there is in addition a discernable decrease in the quantum yield with increasing pressure ($\Phi_{147} = 0.07 \rightarrow 0.04_7$). The data are similar for CF_2CHCl. The quantum yield at 123.6 nm is constant and unaffected by the addition of NO. At 147 nm it is again much lower and a decrease with increasing pressure is just discernable in the presence of NO. Therefore, it is reasonable to suppose that the molecular elimination of HF is a process analgous to reaction 2:

$$CF_3CH_2Cl^{\dagger(1)} \rightarrow CF_2CHCl + HF \quad (\phi_{123.6} = 0.09) \quad (3)$$

The quantum yield at 147 nm has a maximum value of 0.02. The fact that at ~12 Torr (cf. runs 9 and 21) the yields of CF_2CH_2 and CF_2CHCl both rise by a factor of approximately 5, as the wavelength decreases, lends support to this view, as does the fact that both processes are α,β in nature.

At 123.6 nm the quantum yields of CF_2CH_2 and CF_2CHCl are quite large and yet the yields of radical products (e.g., combination products) are small. Thus it would seem that the FCl and HF undergo very little subsequent dissociation at this wavelength despite the very large excess energies available to the products. Furthermore, no substituted acetylenes are formed and it is therefore difficult to assign the major fraction of the excess energy to the olefins unless one postulates that the olefins are formed in electronically excited states which cannot further decompose. In view of the above, at 147 nm, there is even less reason to suppose FCl and HF dissociate and the free radicals which are produced at this wavelength must presumably have another origin. The imposition of constraints upon energy distributions among the products of primary molecular eliminations as a result of a lack of appropriate secondary products is not uncommon in the ultraviolet photolysis of haloethanes at 147 nm (see ref 2, 3, and 4, for example). It is, however, difficult to accept the more severe constraints that the observed lack of radical products and/or appropriately substituted acetylenes at 123.6 nm demand. Nevertheless we have no alternative explanation.

The yield of CF_2CHF at 123.6 nm is also constant and unaffected by the addition of NO. However, the yield at 147 nm, unlike those of CF_2CH_2 and CF_2CHCl, is similar in magnitude. If we allow CF_2CHF to be formed by the α,α molecular elimination of HCl from a second initially formed excited state, $CF_3CH_2Cl^{\dagger(2)}$, and in addition propose, as previously,[1] that the decreases in the yields of CF_2CH_2 and CF_2CHCl at 147 nm with increasing pressure are the result of a collisionaly induced cross over of the longer-lived $CF_3CH_2Cl^{\dagger(1)}$ to the second state, then we are also able to account for the corresponding increase in CF_2CHF with increasing pressure at 147 nm:

$$CF_3CH_2Cl + h\nu \rightarrow CF_3CH_2Cl^{\dagger(2)} \quad (4)$$

$$CF_3CH_2Cl^{\dagger(2)} \rightarrow CF_3CH^* + HCl \quad (5)$$

$$\hookrightarrow CF_2CHF \quad (\phi_{147} \geq 0.15)$$

$$CF_3CH_2Cl^{\dagger(1)} + M \rightarrow CF_3CH_2Cl^{\dagger(2)} \quad (\phi_{147} \leq 0.04_3) \quad (6)$$

At 123.6 nm, the quantum yield of reaction 5 is approximately 0.20 and constant. That is, reaction 6 is not observed. The increases in the quantum yields of reactions 2, 3, and 5 with decreasing wavelength then simply reflect the decrease in lifetimes of $CF_3CH_2Cl^{\dagger(1)}$ and $CF_3CH_2Cl^{\dagger(2)}$, particularly the former, as a function of their vibrational energy contents. Again there is little evidence that the products of reaction 5 undergo any further decomposition.

Reactions 2, 3, 5, and 6 are simple competitive processes. If at 147 nm reaction 6 occurs upon every collision and there are no sources of CF_2CH_2 other than secondary radical disproportionations, then a plot of $1/\Phi_{CF_2CH_2}$ vs. total pressure, from data obtained in the presence of NO, should be linear with a positive slope equal to k_6/k_2. Figure 1 shows that this is indeed the case at 147 nm. If the collision frequency at 1 Torr is $\sim 10^7$ s^{-1}, then k_2 (147 nm) = $1.0 \pm 0.5 \times 10^9$ s^{-1}. The lack of a pressure dependence of the quantum yield of CF_2CH_2 at 123.6 nm enables us to estimate a minimum value of k_2 (123.6 nm) of 1.6×10^{10} s^{-1}. The lifetime ($1/k_2 = 1 \times 10^{-9}$ s) of $CF_3CH_2Cl^{\dagger(1)}$ at 147 nm is similar to those of $C_2H_5Cl^{\dagger(1)}$ (3.6×10^{-10} s) and 1,2-$C_2H_4FCl^{\dagger(1)}$ (3×10^{-10} s), previously reported.[1,3]

The formation of CF_3H and CH_3Cl particularly in the presence of H_2S indicates carbon–carbon bond cleavage is also a primary process, reaction 7. There is little or no

$$CF_3CH_2Cl^{\dagger} \rightarrow CF_3 + CH_2Cl \quad (\phi \simeq 0.08) \quad (7)$$

apparent increase in the quantum yield with decreasing wavelength (cf. runs 10 and 12). Therefore, the state undergoing decomposition is unlikely to be $CF_3CH_2Cl^{\dagger(1)}$.

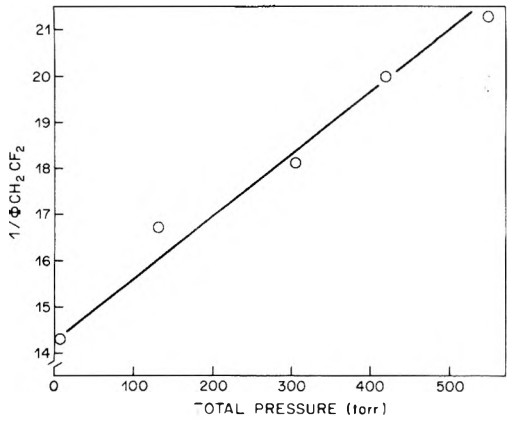

Figure 1. $1/\Phi_{(CF_2CH_2)}$ vs. total pressure in the presence of NO.

A third state which is antibonding with respect to the carbon–carbon bond is a possibility. The lower yield of CH_3Cl produced in the absence of H_2S is a reflection, no doubt, of the lower predicted reactivity of CH_2Cl radicals compared with CF_3.[14]

The sum of the quantum yields of molecular processes and carbon–carbon bond cleavage at 147 nm is 0.32 and at 123.6 nm it rises to a value of 0.75. The formation of "scavengeable" CH_2CF_2 and C_4 compounds means that carbon–halogen bond cleavage occurs, particularly at 147 nm. The preferential formation of one olefin particularly at low pressures is again characteristic of ultraviolet haloethane photolyses.[1,3] The fact that disproportionation products such as CF_3CH_2F are not seen leads us to conclude that the major disproportionation reaction is a chlorine atom transfer between CF_3CH_2 and CF_2CH_2Cl radicals and that both carbon–chlorine and carbon–fluorine bond fission, therefore, occur.

We have indicated earlier in the introduction that we believe that the ultraviolet photolysis of haloethanes is characterized by the simultaneous formation of two or more states corresponding to the overlap of the n–σ^* and "Rydberg type" absorption bands and that a small decrease in the wavelength should favor the formation of shorter-lived Rydberg states. The increases here in the quantum yields of molecular processes and the corresponding decrease in carbon–halogen bond fission with increasing photon energy are certainly further evidence for this viewpoint, as is the "disappearance" at 123.6 nm of the pressure dependence of the quantum yields of CF_2CH_2, CF_2CHF, and CF_2CHCl in the presence of NO. The quantum yield of carbon–halogen bond fission, however, cannot be 0.68 at 147 nm or 0.25 at 123.6 nm. There are insufficient disproportionation/combination products. Thus one or more of the initially formed states may also undergo some photophysical decay processes leading to the regeneration of the ground state of CF_3CH_2Cl.

Acknowledgment. The support of the National Research Council of Canada is gratefully acknowledged.

References and Notes

(1) T. Ichimura, A. W. Kirk, G. Kramer, and E. Tschuikow-Roux, *J. Photochem.*, **6**, 77 (1976).
(2) D. Salomon, A. W. Kirk, and E. Tschuikow-Roux, *Int. J. Chem. Kinet.*, in press.
(3) T. Ichimura, A. W. Kirk, and E. Tschuikow-Roux, *Int. J. Chem. Kinet.*, in press.
(4) T. Ichimura, A. W. Kirk, and E. Tschuikow-Roux, *Int. J. Chem. Kinet.*, in press.
(5) M. B. Robin, "Higher Excited States of Polyatomic Molecules", Vol. 1, Academic Press, New York, N.Y., 1974, p 157.
(6) B. R. Russel, L. O. Edwards, and J. W. Raymonda, *J. Am. Chem. Soc.*, **95**, 2129 (1973).
(7) H. Tsubomura, K. Kimura, K. Koyo, J. Tanaka, and S. Nagakura, *Bull. Chem. Soc. Jpn.*, **37**, 417 (1964).
(8) L. Cremieux and J. A. Herman, *Can. J. Chem.*, **52**, 3098 (1974).
(9) T. Fujimoto and M. H. J. Wijnen, *J. Chem. Phys.*, **56**, 4032 (1972).
(10) R. Gordon, R. E. Rebbert, and P. Ausloos, *Natl. Bur. Stand. Tech. Note*, **No. 494** (1969).
(11) P. Potzinger, L. C. Glasgow, and G. von Bünau, *Z. Naturforsch. A*, **27**, 628 (1972).
(12) D. Salomon and A. A. Scala, *J. Chem. Phys.*, **62**, 1469 (1975).
(13) J. Doucet, P. Sauvageau, and C. Sandorfy, *J. Chem. Phys.*, **62**, 355 (1975).
(14) A. F. Trotman-Dickenson and G. S. Milne, *Natl. Stand. Ref. Data Ser., Natl. Bur. Stand.*, **No. 9** (1967).

Search for Selectivity between Optical Isomers in the Interactions of Positrons with Chiral Molecules

Yan-ching Jean and Hans J. Ache*[1]

Department of Chemistry, Virginia Polytechnic Institute and State University, Blacksburg, Virginia 24061 *(Received January 24, 1977) Publication costs assisted by the Petroleum Research Fund*

Positron lifetime measurements were performed in the optical isomers of six organic chiral molecules, such as 2-methylbutanol, 2-aminobutanol, octanol-2, α-methylbenzylamine, carvone, and diethyltartrate over a temperature range from −196 to 100 °C. No significant differences in the lifetimes of τ_1 and τ_2, and the intensities, I_1 and I_2, associated with the short- and long-lived components in the positron lifetime spectra could be observed between the D and L enantiomers of these chiral molecules if the experiments were carried out in the liquid state. Since I_2 is directly related to the (relative) number of orthopositronium atoms formed, the experimental results provide no evidence for the assumption that optical isomers display different cross sections for orthopositronium formation. The failure to observe such differences appears to be inconsistent with the predictions of previously proposed models for the interaction of longitudinally polarized positrons with spin polarized electrons in chiral molecules. Possible reasons for these discrepancies such as the invalidity of (1) the "helical electron gas model" and the general assumption that electrons in chiral molecules possess a certain helicity when they form Ps with positrons, and (2) the assumption that positrons retain their longitudinal polarization until they form Ps are discussed. Differences observed in the I_2 values if the above experiments were carried out in the solid state are most likely due to variations in phase and crystalline structure and not related to the different helical structures of the enantiomers.

Introduction

One of the most intriguing problems in chemical evolution is the origin of optical asymmetry in biomolecules.

It is a well established fact that amino acids occurring in natural proteins belong overwhelmingly to the L series whereas natural sugars are made up almost exclusively of D optical isomers. However, very little is known about the origin of this asymmetry.

Several theories which do not consider the predominance of the L-amino acids in natural proteins as a matter of chance have been suggested.

One "nonchance" explanation is based on the unequal decomposition of optical isomers and the subsequent generation of optical activity in light mediated reactions.[2-5]

In 1959 Ulbricht[6] discussed a possible connection between the asymmetry at the level of elementary particles and at the molecular level. He proposed a novel mechanism which would relate the phenomenon of asymmetry found in biological systems with parity nonconservation in weak interaction. This mechanism is essentially based on the discovery by Lee and Yang[7] who showed that electrons emitted in β decays are polarized.

Ulbricht and Vester[8] suggested several possible mechanisms by which polarized β radiation may induce optical activity in matter. They postulate, for example, that longitudinally polarized β-decay electrons are interacting in matter to generate circularly polarized bremsstrahlung[9] which in turn may undergo reaction with organic matter leading to asymmetric syntheses or degradation. Attempts by Ulbricht and Vester[9] to induce optical activity with polarized β radiation, however, failed to confirm this hypothesis. Most of the subsequent experiments carried out by several authors[10-12] to generate optical activity by irradiating racemic mixtures with polarized β radiation proved to be inconclusive.

Garay[11] reported that D-tyrosine in dilute aqueous alkaline solution was more decomposed than L-tyrosine after 18 months exposure to 0.36 mCi of $^{90}SrCl_2$. Bonner[12] repeated these experiments using DL-tyrosine in alkaline solution, looking for optical rotation after exposing the sample to a dose of 4.1×10^8 rads of β-ray bremsstrahlung in a 61 700 Ci ^{90}Sr–^{90}Y source at ORNL for 1.34 years. This latter study included also other racemic amino acids, both in the solid state and in neutral, acidic, or alkaline solution. In no case, however, did he observe the development of optical activity.

More recently Bonner et al.[13] irradiated samples of solid DL-leucine with longitudinally polarized 120-keV electrons. The authors claim to have observed preferential decomposition of one of the optical isomers. The experimental conditions under which these studies were performed led to 50–75% degradation of the leucine samples (after 331–860 nA h total irradiation dose).

The inherent difficulties of such long term β-radiolysis experiments or experiments which involve significant destruction of the substrate and which in turn depend on an extremely accurate analysis of the radiolysis products formed are obvious, e.g., the presence of small amounts of impurities introduced as a result of the degassing process occurring under radiation in the walls of the irradiation vessels may in a noncontrollable way affect the radiolysis process.

Furthermore since β particles each create several orders of magnitude more secondary electrons during their energy degradation, the direct chemical consequences of the primary particle itself should be trivial and any correlation between the properties of the primary particle (e.g., polarization) and the end products of their interaction with matter would be largely obscured by the reactions of the secondary electrons with the same matter.

Thus it appeared much more advantageous to investigate the potential correlation between the asymmetry found in living material and the asymmetry of weak interaction directly by obtaining information about the interaction process itself carried out by the primary particle rather than relying on the analysis of the end products of this interaction, whose yields as pointed out above may be affected by a variety of parameters not related to the primary interaction.

One approach in this direction was made by Lemmon et al.[14] who studied the interaction of epithermal muonium atoms with solid L- or D-alanine and liquid L- and D-oc-

TABLE I: Values of τ_1 (ns), τ_2 (ns), and I_2 (%) for 2-Methylbutanol at Different Temperatures

Temp, °C	State	No. of runs	D form $[\alpha]_D^{22} = 5.90°$			DL form $[\alpha]_D^{22} = 0.0$		
			τ_1	τ_2	I_2	τ_1	τ_2	I_2
100	L	2	0.498 ± 0.021	3.02 ± 0.22	21.97 ± 0.48	0.483 ± 0.012	2.92 ± 0.14	22.41 ± 0.78
60	L	2	0.473 ± 0.023	2.93 ± 0.05	21.87 ± 0.20	0.485 ± 0.024	2.79 ± 0.09	22.02 ± 0.04
22	L	7	0.443 ± 0.034	3.04 ± 0.08	22.18 ± 0.33	0.429 ± 0.076	3.20 ± 0.11	22.65 ± 0.23
−78	L	2	0.391 ± 0.066	2.86 ± 0.04	22.31 ± 0.70	0.386 ± 0.012	2.70 ± 0.06	24.30 ± 0.47
−196	S	4	0.367 ± 0.012	1.50 ± 0.07	23.90 ± 0.84	0.363 ± 0.061	1.47 ± 0.02	26.42 ± 0.34

tanol-2. However, they could not observe any changes in the residual muon polarization, which would be indicative of differences in the reactivity of these polarized epithermal muonium atoms toward the two optical isomers.

Garay et al.[15] reported on the results of a similar process which could provide such direct information, namely, the formation of the positronium in optical isomers. Positronium (Ps), which is the bound state of a positron and an electron,[16] can be formed in two ground states, as singlet or para Ps, with antiparallel spin orientation, and as triplet or ortho Ps, with parallel spin orientation.

Garay et al.[15] suggested that longitudinally polarized positrons, i.e., positrons which have a parallel orientation of spin and direction of motion, as emitted in the radioactive decay of certain nuclides, may interact differently with the D and L isomers of a chiral compound, resulting in slight variances in the Ps formation probability and also in a change of the ratio of *o*- to *p*-Ps formation. Initial experiments carried out by these authors with optical active isomers of amino acids in the solid state seem to confirm this assumption. Hrasko[17,18] et al. and Garay[19] et al. subsequently rationalized these findings, i.e., the interactions of positrons with electrons in optical active compounds, in terms of the "helical electron gas model" and "neutral currents" (see also Discussion section).

Dezsi et al.[20a] and Brandt and Chiba[20b] who repeated these experiments, however, related the differences observed in o-Ps formation in the two optical isomers to differences in the crystalline structure of the two isomers, and thus to differences in the Ps trapping in the crystalline lattice by defects etc.

Most recently Rich[21] questioned Hrasko and Garay's theoretical explanation of their results by arguing that the positrons have lost their helicity before they can form Ps. Thus, in view of the importance of the problem of the origin of molecular chirality and the continuing controversy about the conclusiveness and interpretation of the experimental data in the positron annihilation experiments, we systematically measured the relative *p*- to o-Ps formation probabilities in a series of optically active stereoisomers such as 2-methylbutanol, 2-aminobutanol, α-methylbenzylamine, carvone, octanol-2, and diethyltartrate by positron annihilation techniques in order to provide an unambiguous answer to the question of the possible connection between asymmetry at the level of elementary particles and at the molecular level, as this might relate the intrinsic asymmetry of matter with the asymmetry found in biological systems on this planet.

By carrying out the experiments with optical isomers in the liquid (and solid) state we were able to exclude the contribution made by Ps trapping in defects, etc., so that the observed results directly reflect any possible effect of the optical activity of the substrates on the Ps formation process.

Experimental Section

A. *Materials.* All compounds were of highest available purity, they were purified by distillation and preparative gas chromatography until subsequent tests showed a purity of better than 99.5%. The sources of these compounds were as follows: DL- and D-2-methylbutanol (Pfaltz and Bauer Inc.); D- and L-2-aminobutanol (ICN Life Science, K and K); D- and L-octanol-2, α-methylbenzylamine, and carvone (Aldrich Chemical Co.). D- and L-diethyltartrates were prepared by the reaction of D- and L-tartaric acid (obtained from Aldrich Chemical Co.) with absolute ethanol. The reaction products as well as the other substrates listed above were purified by distillation, crystallization, and finally by gas chromatography until the physical constants, melting points, refractive index, optical activity, and NMR spectrum agreed with the literature data and no impurities could be detected by any of these techniques.

B. *Preparation of Sample.* Specially designed sample vials (cylindrical glass tubes 100 mm long and 10 mm i.d.) were filled with 1 mL of sample. The positron sources were 3–5 μCi ^{22}Na, prepared by evaporating carrier free neutral solutions of either $^{22}NaHCO_3$ or ^{22}NaCl (obtained from Amersham/Searle Co.) onto a thin aluminum foil. The sources were placed inside the vials and completely immersed in the liquid sample. The vials were subsequently sealed off and transferred into a specially designed thermostat which controlled the temperature within ±1.0 °C. For the low temperature work the sample vial was immersed into suitable cooling mixtures contained in a specially designed dewar vessel. In the solid state work special attention was given to the solidification process so that the D or L isomers crystallized under the same conditions.

C. *Positron Lifetime Measurements.* Positron lifetime measurements were carried out by the usual delayed coincidence method.[22] The resolution of the system, as measured by the prompt time distribution of ^{60}Co source and without changing the 1.27- and 0.511-MeV bias, was found to be 0.390 ns fwhm. Corrections for the source component, which had an intensity of less than 4%, were made in the usual way by using conventional computational methods.

D. *Data Analysis.* The resulting positron-lifetime spectra were analyzed into two or three components by using the PAL,[23] POSITRONFIT, and POSITRONFIT EXTENDED[24] computer programs. No significant differences were observed between the results obtained by each of these programs. Thus, the PAL program was consistently used to separate the spectra into two components. In agreement with previous work, the intensity of the long-lived component, I_2, was considered to be directly related to the number of thermal *o*-Ps atoms formed in the substance.

Results and Discussion

The results of the positron lifetime measurements are shown in Tables I–VI, where the lifetimes of both the short- and long-lived component, and I_2, the intensity of the long-lived component, are listed as a function of temperature for the various enantiomers under study: D- and DL-2-methylbutanol, D- and L-2-aminobutanol, D- and L-α-methylbenzylamine, D- and L-octanol-2, D- and L-carvone, and D- and L-diethyltartrate.

The values obtained for the lifetimes, τ_1 and τ_2, as well as I_2, which represents the thermal o-Ps formation

TABLE II: Values of τ_1 (ns), τ_2 (ns), and I_2 (%) for 2-Aminobutanol at Different Temperatures

Temp, °C	State	No. of runs	D form $[\alpha]_D^{22} = 15°$			L form $[\alpha]_D^{22} = -15°$		
			τ_1	τ_2	I_2	τ_1	τ_2	I_2
60	L	3	0.385 ± 0.032	2.71 ± 0.04	23.79 ± 0.42	0.384 ± 0.010	2.75 ± 0.01	22.07 ± 1.04
22	L	4	0.382 ± 0.038	2.71 ± 0.04	23.41 ± 0.20	0.381 ± 0.032	2.73 ± 0.08	23.15 ± 0.33
−78	S	4	0.344 ± 0.031	1.51 ± 0.03	29.38 ± 1.02	0.345 ± 0.024	1.58 ± 0.02	27.72 ± 0.93
−196	S	6	0.338 ± 0.054	1.28 ± 0.06	26.74 ± 0.45	0.342 ± 0.049	1.29 ± 0.14	23.91 ± 0.78

TABLE III: Values of τ_1 (ns), τ_2 (ns), and I_2 (%) for α-Methylbenzylamine at Different Temperatures

Temp, °C	State	No. of runs	D form $[\alpha]_D^{22} = 39.7°$			L form $[\alpha]_D^{22} = -39.0°$		
			τ_1	τ_2	I_2	τ_1	τ_2	I_2
100	L	2	0.413 ± 0.024	2.65 ± 0.01	31.89 ± 1.46	0.400 ± 0.021	2.62 ± 0.04	31.21 ± 2.50
60	L	2	0.415 ± 0.049	2.55 ± 0.02	29.79 ± 1.19	0.401 ± 0.053	2.55 ± 0.03	29.78 ± 1.02
22	L	2	0.403 ± 0.051	2.55 ± 0.04	28.34 ± 0.23	0.405 ± 0.043	2.46 ± 0.04	26.96 ± 1.53
−78	L	2	0.365 ± 0.041	2.05 ± 0.04	25.21 ± 0.54	0.376 ± 0.052	2.15 ± 0.06	23.58 ± 0.45
−196	S	3	0.368 ± 0.066	1.40 ± 0.05	20.86 ± 1.26	0.351 ± 0.048	1.39 ± 0.02	21.54 ± 0.20

probability, show no significant difference between the D and L isomer (or D and DL form as in 2-methylbutanol) in any of these various pairs of enantiomers if the experiment is carried out in the liquid phase. They all fall within the experimental error, which is listed as one standard deviation in the tables. Typical results are, e.g., for the D and L isomers of 2-aminobutanol, I_2 (in %): 23.41 ± 0.20 and 23.15 ± 0.33, respectively; τ_2 (ns): 2.71 ± 0.04 and 2.73 ± 0.8, respectively (at 22 °C). Obvious differences in I_2, however, can be observed in most systems when the experiments are carried out in the solid state at low temperature (−196 °C). The I_2 values measured at this temperature in all the systems under study, with the exception of α-methylbenzylamine, vary significantly when one replaces one optical isomer by the other. However, no consistent trend can be observed between the relative magnitude of the I_2 values in the D or L form in a pair of enantiomers. For example, while in the case of 2-aminobutanol or carvone the D form (26.74 or 15.64%) shows a greater I_2 than the corresponding L form (23.91 or 13.41%), in the octanol-2 system the opposite is true (D, 21.84% vs. L, 24.01%); nor is there any correlation between the direction in which the plane of the polarized light is rotated in the enantiomers (+ or −) and the relative magnitude of I_2, e.g., in the 2-aminobutanol I_2 in the D(+) enantiomer is 26.74% and in the L(−) form 23.91% whereas the D(+) enantiomer of octanol-2 is 21.84% and the corresponding L(−) isomer has a higher I_2 value of 24.01%.

The experiments further show a pronounced dependence of I_2 on the solidification conditions; e.g., differences can be observed if the sample is measured in its crystalline or glassy state at −196 °C; while in the former case I_2 in DL-octanol-2 is 23.70%, the glassy state displays a substantially smaller I_2 of 20.61%.

An interesting effect of the orientation of the molecules and the composition of the crystalline phase can be observed in the DL-octanol-2 systems. The I_2 values of this compound as shown in Figure 1 display a sudden increase from about 24 to 36% at 226 K, where crystallization begins. A further decrease in the temperature of the sample is associated with a gradual decrease in I_2, which levels off at 25% at 178 K and remains constant down to 80 K. For comparison, a similar study was carried out with the pure D enantiomer of octanol-2 (see Figure 1) where only a slight effect could be observed. Since the crystallization of DL-octanol-2 may involve a temperature dependent equilibrium between pure D and L crystals, as well as the mixed DL phase, the changes observed in I_2 may reflect these conditions. On the other hand, in the pure D form no such equilibria exist and I_2 remains essentially constant in this temperature range. As shown in Figure 1, the corresponding changes of the lifetime, τ_2, are less dramatic except at the melting point where τ_2 suddenly drops.

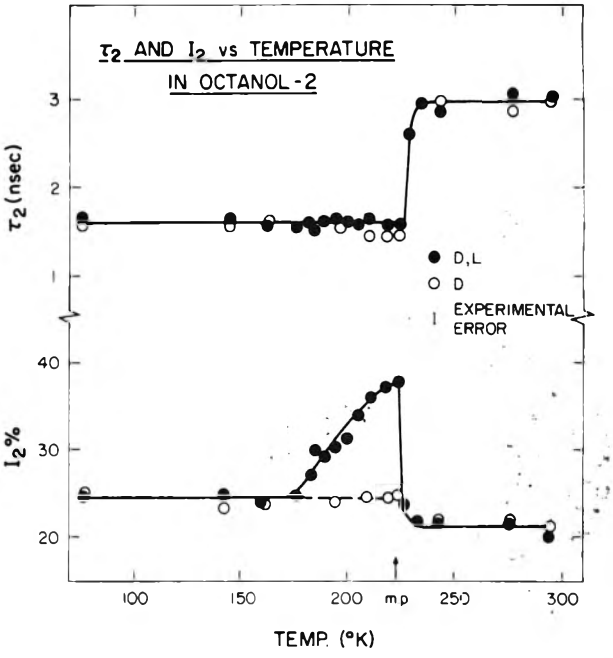

Figure 1. I_2 and τ_2 plotted as a function of temperature in D- and D,L-octanol-2.

In view of these results which clearly point to a dependence of I_2 on the crystalline structure and the corresponding free volume in the crystals, we agree with the assumptions made by Dezsi et al.[20a] and Brandt and Chiba[20b] that the differences in the I_2 values observed by Garay et al.[15] in solid amino acids cannot necessarily be related to differences of the o-Ps formation in optical isomers and reliable results can only be expected from liquid phase experiments, where these complications are excluded.

As pointed out above on the basis of results observed in this study with optical isomers in the liquid state, which showed no significant differences in I_2 between the two isomers in each pair of enantiomers, we would have to reach the conclusion that the relative ortho to para formation probability does not change between optical isomers.

It seems therefore important to consider the possible reasons for this discrepancy between Garay and Hrasko's hypothesis[17-19] and our experimental results, apart from the possibility that the effect may be too small to be observed.

TABLE IV: Values of τ_1 (ns), τ_2 (ns), and I_2 (%) for Carvone at Different Temperatures

Temp, °C	State	No. of runs	D form $[\alpha]_D^{22} = +58.0°$			DL form $[\alpha]_D^{22} = 0.0°$			L form $[\alpha]_D^{22} = -58.0°$		
			τ_1	τ_2	I_2	τ_1	τ_2	I_2	τ_1	τ_2	I_2
100	L	4	0.444 ± 0.014	2.30 ± 0.08	18.07 ± 0.41				0.466 ± 0.001	2.33 ± 0.03	17.96 ± 0.24
60	L	4	0.455 ± 0.019	2.14 ± 0.03	18.55 ± 0.25				0.466 ± 0.021	2.16 ± 0.04	18.14 ± 0.49
22	L	4	0.451 ± 0.032	2.15 ± 0.04	17.59 ± 0.52				0.441 ± 0.028	2.12 ± 0.06	17.35 ± 0.30
−78	S	4	0.369 ± 0.021	1.37 ± 0.03	20.32 ± 0.54	0.367 ± 0.032	1.42 ± 0.03	20.81 ± 0.60	0.389 ± 0.007	1.38 ± 0.05	20.49 ± 0.20
−196	S	4	0.371 ± 0.018	1.33 ± 0.05	15.64 ± 0.12	0.364 ± 0.040	1.41 ± 0.02	12.92 ± 0.54	0.379 ± 0.003	1.37 ± 0.03	13.41 ± 0.21

TABLE V: Values of τ_1 (ns), τ_2 (ns), and I_2 (%) for Octanol-2 at Different Temperatures

Temp, °C	State	No. of runs	D, $[\alpha]_D^{22} = +9.0°$			75% D 25% L, $[\alpha]_D^{22} = 4.5°$			DL $[\alpha]_D^{22} = 0°$			75% L 25% D, $[\alpha]_D^{22} = -4.5°$			L, $[\alpha]_D^{22} = -9.0°$		
			τ_1	τ_2	I_2	τ_1	τ_2	I_2	τ_1	τ_2	I_2	τ_1	τ_2	I_2	τ_1	τ_2	I_2
100	L	4	0.450	3.17	24.62				0.453	3.03	23.83				0.460	2.88	23.64
			±0.021	±0.03	±0.83				±0.008	±0.12	±0.22				±0.022	±0.13	±0.46
60	L	4	0.420	3.15	22.16				0.452	2.90	22.73				0.415	2.94	22.50
			±0.006	±0.08	±0.95				±0.020	±0.11	±0.65				±0.039	±0.08	±0.30
22	L	4	0.412	3.14	21.91				0.428	2.97	21.72				0.442	2.85	21.28
			±0.021	±0.14	±0.40				±0.011	±0.14	±0.97				±0.011	±0.30	±0.32
−78	S	5	0.385	1.70	18.84	0.387	1.60	24.78	0.376	1.55	31.40	0.355	1.59	27.18	0.370	1.57	20.89
			±0.007	±0.08	±0.79	±0.018	±0.05	±0.21	±0.021	±0.06	±0.28	±0.009	±0.02	±0.64	±0.02	±0.05	±0.10
−196	S	6	0.370	1.49	21.84				0.371	1.43	25.24				0.369	1.44	24.01
			±0.009	±0.07	±0.71				±0.015	±0.10	±1.17				±0.012	±0.03	±0.50

TABLE VI: Values of τ_1 (ns), τ_2 (ns), and I_2 (%) and Optical Activity for Diethyltartrate at Different Temperatures

Temp, °C	State	No of runs	D form				L form			
			$[\alpha]_D^{22}$	τ_1	τ_2	I_2	$[\alpha]_D^{22}$	τ_1	τ_2	I_2
22	L	2	10.30	0.386 ± 0.023	2.78 ± 0.08	17.81 ± 0.078	−9.2	0.401 ± 0.013	2.79 ± 0.03	17.61 ± 0.35
33	L	2	10.88	0.385 ± 0.022	2.77 ± 0.07	17.71 ± 0.52	−9.8	0.407 ± 0.004	2.76 ± 0.03	17.41 ± 0.085
47	L	2	12.06	0.390 ± 0.009	2.75 ± 0.01	17.43 ± 0.3	−10.9	0.411 ± 0.005	2.73 ± 0.03	16.21 ± 0.59
63	L	2	13.7	0.396 ± 0.024	2.71 ± 0.01	17.27 ± 0.23	−12.6	0.419 ± 0.003	2.61 ± 0.08	16.59 ± 1.24
73	L	2	13.9	0.400 ± 0.027	2.68 ± 0.01	16.93 ± 0.29	−13.5	0.421 ± 0.007	2.56 ± 0.11	16.59 ± 0.85
89	L	2	15.7	0.404 ± 0.018	2.64 ± 0.02	17.07 ± 0.29	−13.7	0.426 ± 0.008	2.50 ± 0.11	16.98 ± 0.099
100	L	2	16.0	0.407 ± 0.017	2.62 ± 0.08	16.33 ± 1.17	−14.4	0.432 ± 0.004	2.54 ± 0.01	15.39 ± 1.30

Basic to the model of interaction between positron and electrons in helical molecules is that the orbital electrons in the two optical isomers are differently spin polarized with respect to their direction of motion (helical electron gas model),[17-19] i.e., the electron spins are aligned predominantly to the motion of the electron in one and antiparallel in the other enantiomer. The authors further postulate that the positron possesses helicity when it undergoes Ps formation with these electrons. They also assume that the probability of Ps formation depends on the relative velocity of electron and positron. Thus, the probability for *o*- to *p*-Ps formation will switch when one replaces one optical isomer by the other.

Experimental evidence for the validity of the helical electron gas model in excited chiral molecules has been obtained by Garay et al.[25] and Laczko et al.[26] by determining the magnetic transition dipole moment of molecules such as *o*-, *m*- and *p*-tyrosine. The authors found that the population of the molecules in the triplet state is increased if the magnetic transition dipole is greater, a fact which they interpret in terms of spin polarization with respect to the motion of the electrons during excitation. However, so far no independent evidence (except Garay's positron annihilation experiments) has been derived for such spin polarization in the ground state of chiral molecules.

Furthermore, there exists some controversy regarding the question whether the positron has some helicity left when it forms the Ps. While experimental evidence by Hanna and Preston,[27] Dick et al.,[28] and Bisi et al.[29] seems to indicate that positrons emitted in the radioactive decay partly retain their polarization during slowing down and Ps formation, Bouchiat and Levy-Lebland[30] approach this problem theoretically and postulate that in collisions at lower energies the spin is quenched and no longer follows the momentum in a collision, so that the positrons will lose their helicity before Ps formation is possible, as recently pointed out by Rich.[21]

Although the results obtained in this study cannot prove the validity or invalidity of the helical electrons gas model,[17-19] or any of the other arguments they certainly do not provide any positive evidence for Garay's and Hrasko's theories. Especially, one would have to conclude from the failure of the experiments that so far no experimental evidence for the validity of the helical electron gas model for the ground state chiral molecules has been presented.

On the other hand, the negative results of these experiments could also indicate that one basic assumption of the mechanism of Ps formation may be in error. According to the accepted Ore mechanism of Ps formation positrons with a few eV of kinetic energy abstract electrons from the substrate molecules to form Ps.[16] More recently this mechanism has been questioned by Mogensen,[31] who postulated that at least partial Ps formation occurs via the combination of thermal positrons with dry or solvated electrons in a radiation spur created by the positron. In this case the electrons are ejected prior to the combination process and an open question would be whether these electrons retain their helicity, which they might have otherwise possessed when residing in the chiral molecules as postulated by the helical electron gas model.

If it can be shown that a majority of the electrons had lost their helicity prior to the Ps formation in the liquid phase the applicability of this process for this kind of investigation would be severely restricted.

Experiments to determine the helicity of positrons at the time of Ps formation as well as the detailed mechanism

of the latter process are presently being carried out in this laboratory.

Acknowledgment. This work was partially supported by the U.S. Energy Research and Development Administration and the donors of the Petroleum Research Fund, administered by the American Chemical Society.

References and Notes

(1) Author to whom correspondence should be addressed.
(2) W. Kuhn and E. Braun. *Naturwissenschaften*, **17**, 227 (1929).
(3) S. Mitchell, *J. Chem. Soc.*, 452 (1930).
(4) W. J. Berstein, M. Calvin, and O. Burchardt, *J. Am. Chem. Soc.*, **94**, 494 (1972); *Tetrahedron Lett.*, **No. 22**, 2195 (1972).
(5) W. A. Bonner in "Exobiology", C. Ponnamperuma, Ed., North Holland Publishing Co., Amsterdam, 1972, p 209.
(6) T. L. V. Ulbricht, *Q. Rev. Chem. Soc.*, **13**, 48 (1959).
(7) T. D. Lee and C. N. Yang, *Phys. Rev.*, **104**, 254 (1956).
(8) F. Vester, T. L. V. Ulbr cht, and H. Krauch, *Naturwissenschaften*, **46**, 68 (1959).
(9) K. W. McVoy, *Phys. Rev.*, **106**, 828 (1957); **111**, 1484 (1958); M. Goldhaber, L. Grodzins, and A. W. Sunyar, *ibid.*, **106**, 826 (1957); S. Galster and H. Schopper, *Nucl. Phys.*, **6**, 125 (1958).
(10) T. L. V. Ulbricht and F. Vester, *Tetrahedron*, **18**, 629 (1962).
(11) A. S. Garay, *Nature (London)*, **219**, 338 (1968).
(12) W. A. Bonner, *J. Mol. Evol.*, **4**, 23 (1974).
(13) W. A. Bonner, M. A. vanDorf, and M. R. Yearian, *Nature (London)*, **258**, 419 (1975).
(14) R. M. Lemmon, K. M. Crowe, F. N. Gygax, R. F. Johnson, B. D. Patterson, J. H. Brewer, and D. G. Fleming, *Nature (London)*, **252**, 692 (1974).
(15) A. S. Garay, L. Keszthelyi, I. Demeter, and P. Hrasko, *Chem. Phys. Lett.*, **23**, 549 (1973).
(16) For general reviews on positron annihilation and positronium formation see, e.g., (a) J. Green and J. Lee, "Positronium Chemistry", Academic Press, New York, N.Y., 1964; (b) V. I. Goldanskii, *At. Energy Rev.*, **6**, 3 (1968); (c) J. D. McGervey in "Positron Annihilation", A. T. Steward and L. O. Roellig, Ed., Academic Press, New York, N.Y., 1967, p 143; (d) J. A. Merrigan, S. J. Tao, and J. H. Green, "Physical Methods of Chemistry", Vol. 1, A. Weissberger and B. W. Rossiter, Ed., Wiley, New York, N.Y., 1972, Part III D; (e) H. J. Ache, *Angew. Chem., Int. Ed. Engl.*, **11**, 179 (1972); (f) J. H. Green, *MTP Int. Rev. Sci.* 8, 251 (1972); (g) V. I. Goldanskii and V. G. Virsov, *Annu. Rev. Phys. Chem.*, **22**, 209 (1971).
(17) P. Hrasko, KFKI-73-40, Report, Central Research Institute Hungarian Academy of Sciences, Budapest.
(18) P. Hrasko, A. Garay, and L. Keszthelyi, *ATOMKI Közl., Suppl.*, **1612**, 195–198 (1974).
(19) A. S. Garay and P. Hrasko, *J. Mol. Evol.*, **6**, 77 (1974).
(20) (a) I. Dezsi, D. Horvath, and Zs. Kajcsos, *Chem. Phys. Lett.*, **24**, 514 (1974); (b) W. Brandt and T. Chiba, *Phys. Lett.*, **57A**, 395 (1976).
(21) A. Rich, *Nature (London)*, **264**, 482 (1976).
(22) See, e.g., T. L. Williams and H. J. Ache, *J. Chem. Phys.*, **50**, 4493 (1969).
(23) PAL is a version of the CLSQ nuclear decay analysis program (J. B. Cummings, BNL report 6470) modified for positron lifetime analysis by A. L. Nichols at the Chemistry Department, Virginia Polytechnic Institute and State University.
(24) P. Kirkegaard and M. Eldrup, *Computer Phys. Commun.*, **3**, 240 (1972); **7**, 401 (1974).
(25) A. S. Garay, I. Laczko, J. Czegé, K. Kovacss, L. Tolvay, M. Toth, and M. Szabo, *Acta Biol. Acad. Sci. Hung.*, **24**, 137 (1973).
(26) I. Laczko, L. Gaspar, and A. S. Garay, *J. Lumin.*, **8**, 131 (1973).
(27) S. S. Hanna and R. S. Preston, *Phys. Rev.*, **109**, 79 (1958).
(28) L. Dick, L. Feuvais, L. Madansky, and V. L. Tegledy, *Phys. Lett.*, **3**, 26 (1963).
(29) A. Bisi, A. Fiorentini, E. Gatti, and L. Zappa, *Phys. Rev.*, **128**, 2195 (1962).
(30) C. Bouchiat and J. M. Lévy-Lebland, *Nuovo Cim.*, **XXXIII**, 193 (1964).
(31) O. E. Mogensen, *J. Chem. Phys.*, **60**, 998 (1974).

Pressure Neutralization of Substrate Inhibition in the Alcohol Dehydrogenase Reaction

Eddie Morild

Department of Chemistry, University of Bergen, N-5014 Bergen, Norway *(Received June 28, 1976; Revised Manuscript Received March 14, 1977)*

The substrate inhibition of horse liver alcohol dehydrogenase (LADH) is neutralized at high pressures. By variation of substrate concentrations the kinetic constants are evaluated at pressures of 1, 500, 1000, and 1500 bar. In this way the activation and dissociation volumes of the different steps have been found. The method has been used for determination of the E·alc complex as the one responsible for the inhibition. At high pressures this complex dissociates, releases bound enzyme, and thereby compensates for a rate reduction due to the effect of k_1 as a function of pressure. Maxima occurring in the rates at high pressures are explained by the increase of k_3 dominating at lower pressures and the decrease of k_2 dominating at higher pressures. Correlations of the volume changes with known structural properties of liver and yeast ADH are discussed.

Introduction

From the early studies of Theorell et al.[1] it has been known that ethanol has an inhibitory effect on the horse liver alcohol dehydrogenase reaction. The original Theorell–Chance mechanism[2] assumes only binary complexes but, although it accounts satisfactorily for the steady state kinetics, it does not imply an inhibition mechanism. Later investigations[3–5] have established the existence of ternary complexes, but the maximum velocity is little influenced by their presence. Due to their rapid dissociations and interconversions, they require special techniques of investigation. The nature of the complex responsible for the inhibition has therefore not yet been definitely established.[6,7]

In a preliminary pressure study of LADH[8] it was discovered that the reaction rate at saturating conditions was considerably increased at high pressures. At low ethanol concentrations, however, the effect of pressure on the reaction rate was negligible or inhibitory. It was noted that the intermediate concentration between pressure activation and pressure inhibition was about 10 mM, just the lower inhibitory ethanol concentration at atmospheric pressure. This suggested the use of pressure as a means to clarify the role of the complex participating in the substrate inhibition mechanism.

Experimental Section

Pressure Equipment. The measuring cell was an improved version of the optical pressure cell described by Andersen and Broe.[9] Some minor changes ensured better tightening and faster connection to the pressure reservoir. The cell was also surrounded by a thermostated oil jacket, where the temperature was controlled to within 0.1 °C. The pressure was generated by an Enerpac handpump. A large pressure vessel served as a reservoir from which a predetermined pressure could be reached in the cell within

1 s. Usually the pressure increased for about 5 s so that the heat generated could be dissipated gently. The interval from the moment of mixing enzyme with substrate to the recording of the rate was 20–30 s. As the enzyme concentrations generally were kept low, and the substrate concentrations high, the recorder tracings obtained were linear for at least 4 min in most cases. Measurements were carried out at 1, 500, 1000, and 1500 bar, with an accuracy better than 10 bar.

Materials and Methods. Horse liver alcohol dehydrogenase [alcohol–NAD^+ oxidoreductase, EC 1.1:1.1], (E) came from Boehringer, and NAD^+ (S_1) from Sigma. The substrate (S_2) was absolute ethanol from A/S Vinmonopolet, Norway. For stabilizing purpose, 20 μM cys–HCl (Sigma), 20 μM EDTA (Merck), and 1 g of bovine serum albumin (Sigma) were added per litre of buffer. All rate studies were carried out in pH 7.0 Tris–HCl buffer (Sigma), μ = 0.1, at 25.0 °C. All chemicals were used without further purification. The concentrations of enzyme used were within the range 10^{-6}–10^{-10} M. The concentration of NAD^+ ranged from 0.02 to 1 mM, the concentration of ethanol ranged from 1 to 200 mM. (Table I, see paragraph at end of text regarding supplementary material.) For each combination of concentrations and pressure there were four–five or more parallel runs. The wavelength used was 340 nm, and the spectrophotometric equipment was a combination of Zeiss M4 QIII and PM QII.

Treatment of Data. All rate and equilibrium constants in the equations must be considered to be pressure dependent, and this leaves five constants to be determined at each pressure. The pressure dependence of a rate constant is determined by the molal volume difference between the activated state and the reactants in the actual step

$$\Delta\bar{V}^{\ddagger} = \bar{V}^{\ddagger} - \bar{V}_R \tag{1}$$

where $\bar{V}^{\ddagger}$ is the molal volume of activated complex and $\bar{V}_R$ is the molal volume of reactants. Then

$$(\partial \ln k/\partial p)_T = -\Delta\bar{V}^{\ddagger}/RT \tag{2}$$

At equilibrium, the dissociation volume is given by

$$\Delta\bar{V} = \bar{V}\ (\text{dissoc species}) - \bar{V}\ (\text{complex}) \tag{3}$$

and analogously for the dissociation constant

$$(\partial \ln K/\partial p)_T = -\Delta\bar{V}/RT \tag{4}$$

It was necessary to vary the enzyme concentration at the various pressures to obtain the most accurate data. Assuming the proportionality relation between rates and enzyme concentration to hold at all pressures, all observations were brought to a common reference concentration. By means of cross adjustments over concentrations and pressures, it was assured that the data were in accordance with literature data at 1 atm.[10,12] Because of this procedure, there are no uncertainties associated with the 1-atm data. Based on the adjusted v_{obsd} values, the constants in the kinetic equations were evaluated simultaneously at each pressure by a computer program executing an iterative nonlinear least-squares procedure. The constants were fitted to the v_{obsd} values in the v–$[S_1]$–$[S_2]$ space by minimizing

$$\sum_i \left[\left(\frac{e}{v_{obsd}}\right)_i - f_i\right]^2 \tag{5}$$

where f_i is either eq 10 or 11, calculated with the ith substrate concentration combination. The uncertainties given are those resulting from both the uncertainties of the v_{obsd} values themselves (±0.1), and from the scattering of the e/v_{obsd} values around those calculated from the resulting constants.

Theory

Kinetic Model. The basic model is that of the Theorell–Chance mechanism,[2] neglecting intermediary ternary complexes:

$$E + S_1 \underset{k_{-1}}{\overset{k_1}{\rightleftarrows}} ES_1$$

$$ES_1 + S_2 \underset{k_{-2}}{\overset{k_2}{\rightleftarrows}} EP_1 + P_2 \tag{6}$$

$$EP_1 \underset{k_{-3}}{\overset{k_3}{\rightleftarrows}} E + P_1$$

It seems safe, at ordinary pressure at least, to assume that the rate constant of breakdown of the intermediary ternary complex ES_1S_2 is much greater than the rate-determining constant k_3. The rate equation resulting from this model is

$$\frac{e}{v} = \frac{1}{k_3} + \frac{1}{k_1[S_1]} + \frac{1}{k_2[S_2]} + \frac{k_{-1}}{k_1k_2[S_1][S_2]} \tag{7}$$

Two alternative steps may now be considered important for inhibition to occur: (a) The formation of a binary, abortive ES_2 complex which prevents the formation of an ES_1 complex.

$$E + S_2 \rightleftarrows ES_2 \qquad K_a \tag{8}$$

(b) The formation of an abortive ternary complex EP_1S_2 which does not break down to ES_2 and P_1.

$$EP_1 + S_2 \rightleftarrows EP_1S_2 \qquad K_b \tag{9}$$

Dalziel[11] has shown that the inclusion of these steps in the mechanism changes rate eq 7 to either

$$\frac{e}{v} = \frac{1}{k_3} + \frac{1}{k_1[S_1]}\left(1 + \frac{[S_2]}{K_a}\right) + \frac{1}{k_2[S_2]} + \frac{k_{-1}}{k_1k_2[S_1][S_2]} \tag{10}$$

or

$$\frac{e}{v} = \frac{1}{k_3}\left(1 + \frac{[S_2]}{K_b}\right) + \frac{1}{k_1[S_1]} + \frac{1}{k_2[S_2]} + \frac{k_{-1}}{k_1k_2[S_1][S_2]} \tag{11}$$

with step a and b, respectively. Since pressure has been found to increase the reaction rate considerably at high ethanol concentrations, it seems obvious that one of the equilibria (8) and (9) is displaced to the left at high pressure. The concentrations of available E or EP_1 is thus increased relative to the inhibited situation, and the reaction proceeds according to the basic model (6) at an increased rate.

Results and Discussion

Dissociation and Activation Volumes. Several attempts to evaluate the constants by eq 11 failed, although several rearrangements of the equation were made to avoid diverging constants during the iteration process. The constants, especially K_b, k_2, and k_3, varied in a non-monotonous manner with pressure, and tended to diverge or take negative values. Some attempts were also made to evaluate both K_a and K_b simultaneously, but the increase from five to six constants also decreased the accuracy and

TABLE II: The Kinetic Constants Fitted to Eq 10 by Means of a Least-Squares Procedure at Four Different Pressures

Pressure, bar	1[a]	500	1000	1500
k_1, mM^{-1} s^{-1}	520	145 ± 20	250 ± 90	65 ± 15
k_{-1}, s^{-1}	70	2.5 ± 2.0	3 ± 4	1.5 ± 1.0
k_2, mM^{-1} s^{-1}	12.2	0.9 ± 0.2	0.6 ± 0.2	0.4 ± 0.1
k_3, s^{-1}	3.12	8.0 ± 0.5	13 ± 2	12 ± 6
K_a, mM	20	120 ± 15	85 ± 25	600 ± 100

[a] Literature data.[10,12]

resulted in ambiguous solutions.

The evaluation according to eq 10, however, gave a successful result and yielded constants being largely monotonous functions of pressure. These constants are tabulated in Table II and their logaritmic variations with pressure are shown in Figure 1. The last term in eq 10 and 11 contributes relatively little to e/v and due to the mutual coupling between k_1, k_2, and k_{-1} they are somewhat inaccurate, especially the later.

From the slopes of the curves in Figure 1 the volume changes associated with the respective steps are readily obtained by means of eq 2 and 4. These volume changes are given in Table III.

The evaluation of k_1 and k_{-1} is equivalent to the evaluation of the dissociation constant K_1 of the ES_1 complex. Once $\Delta\bar{V}_1^{\ddagger}$ and $\Delta\bar{V}_{-1}^{\ddagger}$ have been found as the volumes of activation of the ES_1 association and dissociation, the dissociation volume $\Delta\bar{V}$ of ES_1 can therefore be calculated.

If we assume that the activated complex $ES_1^{\ddagger}$ has the same volume $\bar{V}^{\ddagger}$ both during association and dissociation, the activation volumes of the forward and reverse reaction are

$$\Delta\bar{V}_1^{\ddagger} = \bar{V}^{\ddagger} - \bar{V}(E + S_1) \quad (12)$$

$$\Delta\bar{V}_{-1}^{\ddagger} = \bar{V}^{\ddagger} - \bar{V}(ES_1) \quad (13)$$

Here, $\bar{V}(E + S_1)$ and $\bar{V}(ES_1)$ are the molal volumes of $E + S_1$ and ES_1, respectively. The dissociation volume may be defined by

$$\Delta\bar{V} = \bar{V}(E + S_1) - \bar{V}(ES_1) = -RT\left(\frac{\partial \ln K_1}{\partial p}\right)_T \quad (14)$$

Equations 12 and 13 inserted into eq 14, with the values found from Table III, give

$$\Delta\bar{V} = (\bar{V}^{\ddagger} - \Delta\bar{V}_1^{\ddagger}) - (\bar{V}^{\ddagger} - \bar{V}_{-1}^{\ddagger})$$
$$= \Delta\bar{V}_{-1}^{\ddagger} - \Delta\bar{V}_1^{\ddagger} = 46\ cm^3/mol \quad (15)$$

It is now possible to make a diagram of the volume changes as a function of the reaction coordinate. This can be seen in Figure 2. The dotted lines indicate that only the relative vertical distances are known, whereas the absolute position of the states along the volume coordinate are largely unknown.

The volume of $E + S_2$ is used as a reference state for the volume of ES_2, the volume $E + S_1$ is used as a reference state for the volumes of $ES_1^{\ddagger}$ and ES_1, and the initial volume of $E + S_1 + S_2$ is used as a reference state for the final volume of $E + P_1 + P_2$. The last volume difference ($-7\ cm^3/mol$) has been found from pressure studies of the equilibrium of the overall reaction. (E. Morild and I. Tvedt, unpublished results). Finally, the volume of ES_1

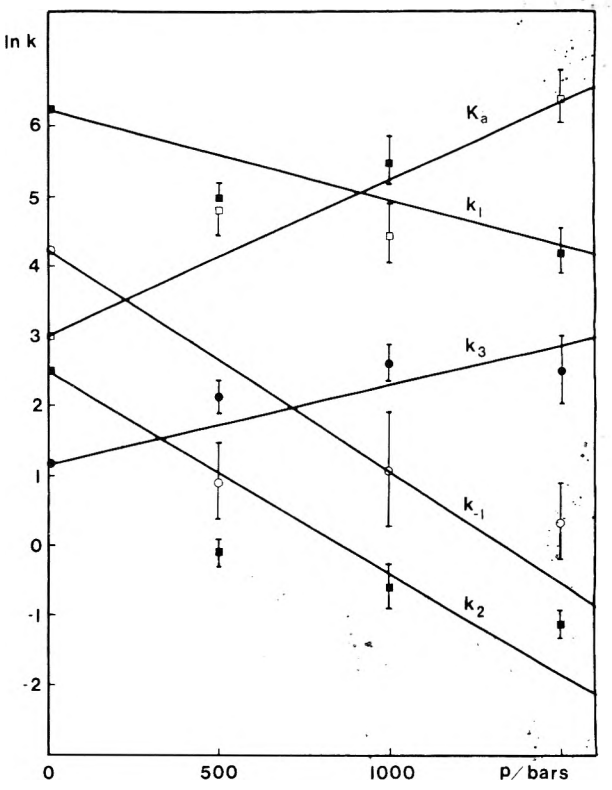

Figure 1. Logarithm of the kinetic constants appearing in eq 10 as a function of pressure.

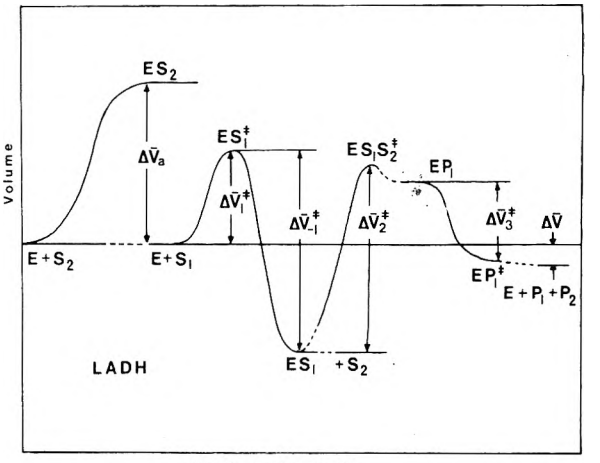

Figure 2. Volume changes in the LADH reaction as function of the reaction coordinate. Dotted lines indicate that the reference states is not identical for all changes.

+ S_2 is used as a reference state for the volume of the activated state $ES_1S_2^{\ddagger}$ and the volume of EP_1 is used as a reference state for the volume of $EP_1^{\ddagger}$.

This diagram gives an approximate representation of this reaction as far as activation volumes are concerned. It is seen that these results are consistent with the results from the equilibrium study. Two interesting features now appear from this diagram: First, the formation of the activated complex $ES_1^{\ddagger}$ is accompanied by a volume increase of about 30 cm^3/mol, while the "opposite" process of splitting the EP_1 complex is followed by a volume decrease of nearly the same size. This indicates a characteristic volume change of the contact between the en-

TABLE III: The Four Activation Volumes and the Dissociation Volume of Importance to the Kinetics at High Pressures According to Eq 10

	$\Delta\bar{V}_1^{\ddagger}$	$\Delta\bar{V}_{-1}^{\ddagger}$	$\Delta\bar{V}_2^{\ddagger}$	$\Delta\bar{V}_3^{\ddagger}$	$\Delta\bar{V}_a$
Volume changes, cm^3/mol	31 ± 5	77 ± 20	71 ± 20	−28 ± 5	−55 ± 10

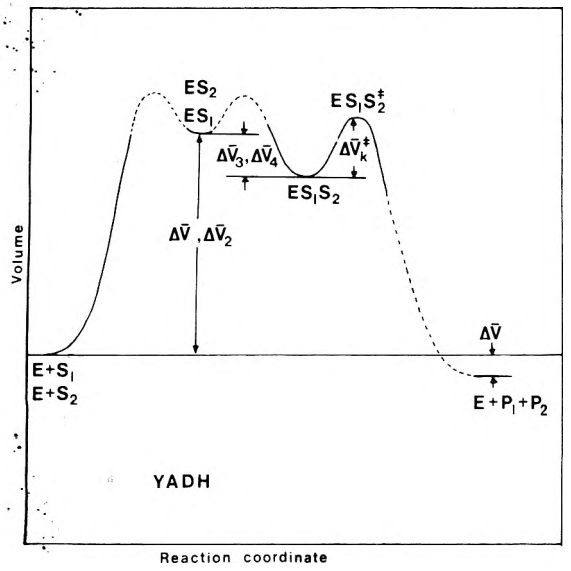

Figure 3. Volume changes in the YADH reaction as function of the reaction coordinate. Dotted lines indicate that the height of the curve for activated states are not known, and that the reference states for intermediates and end products are not identical.

zyme and coenzyme in the activated complex. Second, the formation of both activated complexes $ES_1^‡$ and $ES_1S_2^‡$ from ES_1 is accompanied by a volume increase of about 70 cm^3/mol.

These findings may be compared to those of the yeast enzyme, YADH,[8] the analogous diagram of which is shown in Figure 3. Due to the difference in mechanism and kinetic constants in the rate equation, most of the volume changes found for this enzyme were dissociation volumes. The formation of both complexes ES_1 and ES_2 from E + S_1 and E + S_2, respectively, was followed by a volume increase of about 70 cm^3/mol, while the formation of ES_1S_2 from either binary complex resulted in a volume decrease of about 10 cm^3/mol.

Thus there seems to be intrinsically different modes of action involved in the operation of these enzymes. This will be further discussed below.

The Inhibitor Complex. The result showing the ES_2 complex as being responsible for the inhibition was somewhat unexpected, as Shore and Theorell[7] concluded that the inhibitor complex most probably was ternary EP_1S_2. Their conclusion was based on a greater variation of K_a than of K_i with S_1 concentration, the uncertainty in both cases being about 25%.

An interesting observation is that the molal volume of the ES_2 complex is 50 cm^3 greater than the volume of E + S_2, while the molal volume of the ES_1 complex is 50 cm^3 lower than that of E + S_1. Considering the random mechanism exhibited by YADH as reflected in the symmetrical nature both of binary and of ternary complex formation, the present asymmetrical volume properties might suggest an explanation of the ordered LADH mechanism: The addition of S_1 to the enzyme introduces a conformational change which is favorable for the formation of a ternary ES_1S_2 complex. The opposite volume change appearing by formation of the ES_2 complex indicate that a change of an entirely different character is taking place, one which is unfavorable for ternary complex formation. Of the two resulting complexes, only ES_1 is capable of further reaction and the mechanism is ordered.

The Reason for a Maximum Rate at High Pressures. It was observed[8] that the reaction rates at high ethanol concentrations passed through maxima at certain pressures. These maxima were dependent on substrate concentrations and had to be the results of two opposing tendencies, each dominating a certain part of the pressure range. Such maxima have been observed earlier for simple reactions, but then as a result of viscosity and diffusion controlling the rate and at very high pressures.

For a complex mechanism such as the present one, the cause of the maxima lies in the relative magnitude of increasing and decreasing rate constants as functions of pressure. At low ethanol concentrations (<10 mM) the step associated with k_2 is rate determining at high pressures. At such concentrations, therefore, the rate is pressure inhibited. At higher concentrations of ethanol, this step is no longer rate determining in the lower pressure range (<1000 bar), but still dominates at higher pressures. The usual rate-determining step associated with k_3 is responsible for the increased rate at higher ethanol concentrations, due to its negative activation volume. This explains the maximum; between 1000 and 1500 bar the effect of the increase of k_3 is opposed by the decrease of k_2.

Another interesting observation when the NAD concentration is not too low (>0.1) is a compensatory effect between the step associated with k_1 and equilibrium 8. As the factor $k_1[S_1]$ decreases with pressure, the factor $1 + [S_2]/K_A$ also decreases in nearly the same proportion, so that the ratio $(1 + [S_2]/K_a)/(k_1[S_1])$ is maintained nearly constant. For this reason only the two last steps involving k_2 and k_3 determine the high pressure behavior of the LADH enzyme.

When $[S_1]$ = 1 mM and $[S_2]$ = 100 mM the maximum rate occurred at about 1250 bar. Now, the explicit pressure dependence of all constants used is of the form

$$k^p = k^0 e^{-p\Delta V/RT} \tag{16}$$

where k^p is a constant at pressure p, and k^0 the same constant at atmospheric pressure. If all constants are written in the form of (16) in eq 10, this equation may be differentiated with respect to p and the $\Delta\bar{V}$ values inserted. Then the theoretical maximum is found from $d(v/e)/dp = 0$. For the given choice of $[S_1]$ and $[S_2]$ this procedure yields a maximum at the pressure p = 1280 bar. This is in very good agreement with the observation. Other tests and comparisons with observations show that the volume changes found are quite able to describe the behavior of this enzyme system according to the chosen model.

Correlations with Structural Properties. The three-dimensional structure of LADH at 2.4-Å resolution has recently been reported.[13] From the crystallization properties of the enzyme some important inferences can be drawn. The presence of ethanol during crystallization have not been found to induce any major conformational change, whereas the complexes containing coenzyme result in different crystal forms. It is interesting that the ES_2 complex formation with a volume increase of about 50 cm^3/mol is not accompanied by any conformational change. The association of alcohols to this enzyme has earlier been found to be of a hydrophobic nature.[7] The inhibitory effect of alcohols and other aliphatic derivatives is increased with increasing carbon chain length. This has been confirmed by Eklund et al.,[13] who have identified a deep pocket between the coenzyme binding domain and the catalytic domain as the substrate binding pocket. This pocket is lined with hydrophobic residues, creating a hydrophobic environment for the nicotinamide moiety and the substrate.

The observed volume change of association of ethanol to the enzyme (or at least the positive sign) may be a general feature of hydrophobic interactions between enzymes and substrates. If this is so, this kind of volume

change should also be found in YADH, and indeed it is (+70 cm^3/mol).[8]

Eklund and Brändén[14] have found some interesting differences among the residues lining the active site pockets of the liver and yeast enzymes, which seem to narrow the pocket of the yeast enzyme. This is consistent with the narrower substrate specificity of YADH and may also explain the greater volume change observed there.

The different crystal forms resulting from coenzyme-containing enzyme suggest that a conformational change followed by a volume reduction occurs, and this may be necessary for the reaction to proceed. Although the coenzyme-binding domains exhibit fundamental similarities both in their structure and mode of coenzyme binding within the family of dehydrogenases, minor differences in primary structure may be enough to alter the volume properties considerably. The conformational differences found between the substructures of the yeast and liver enzyme therefore suggest that the conformational changes upon coenzyme association may be quite different. Such a difference is perhaps reflected in the volume changes following formation of the ES_1 complex, being about +70 and −50 cm^3/mol, respectively.

At the moment it is impossible to relate such volume changes to specific rearrangements, due to the complexity of positive and negative contributions to the volume changes. Perhaps something more can be said when details of the interactions between enzyme, substrate, and coenzyme have been further studied.[13]

It is most interesting, however, that detectable changes of conformation can take place at very small volume changes, considering that the total molar volume of LADH is about 65 L.

Some obvious error sources of importance to investigations of the present type have been discussed earlier.[8] The author is quite aware of problems such as subunit dissociation, isoenzymes, and the change of the rate-determining step with pressure, and these will be discussed elsewhere.

Acknowledgment. This work has been supported by the Norwegian Research Council for Science and the Humanities. The author is grateful to Professor T. Brun for his interest in this work and for reading the manuscript.

Supplementary Material Available: Table I containing the observed reaction rates at all combinations of reactant concentrations and pressures (2 pages). Ordering information is available on any current masthead page.

References and Notes

(1) H. Teorell, A. P. Nygaard, and R. Bonnichsen, *Acta Chem. Scand.*, **9**, 1148 (1955).
(2) H. Theorell and B. Chance, *Acta Chem. Scand.*, **5**, 1127 (1951).
(3) H. Theorell and T. Yonetani, *Arch. Biochem. Biophys. Suppl.*, **1**, 209 (1962).
(4) C. C. Wratten and W. W. Cleland, *Biochemistry*, **2**, 935 (1963).
(5) C. C. Wratten and W. W. Cleland, *Biochemistry*, **4**, 2442 (1965).
(6) H. Theorell and J. S. McKinley-McKee, *Acta Chem. Scand.*, **15**, 1811, 1834 (1961).
(7) J. D. Shore and H. Theorell, *Arch. Biochem. Biophys.*, **117**, 375 (1966).
(8) E. Morild, *Biophys. Chem.*, in press.
(9) B. Andersen and E. Broe, *Acta Chem. Scand.*, **26**, 3691 (1972).
(10) J. D. Shore and H. Theorell, *Arch. Biochem. Biophys.*, **116**, 255 (1966).
(11) K. Dalziel, *Acta Chem. Scand.*, **11**, 1706 (1957).
(12) H. Sund and H. Theorell in "The Enzymes", P. D. Boyer, H. Lardy, and K. Myrback, Ed., 2nd ed, Vol. 7, Academic Press, New York, N.Y., 1963, pp 25–83.
(13) H. Eklund, B. Nordström, E. Zeppezauer, G. Söderlund, I. Ohlsson, T. Boiwe, B.-O. Söderberg, O. Tapia, C. I. Brändén, and Å. Åkeson *J. Mol. Biol.*, **102**, 27 (1976).
(14) H. Eklund and C. I. Brändén, *J. Mol. Biol.*, **102**, 61 (1976).

Heats of Mixing of Polyelectrolyte Solutions Having a Common Polyion. 2. Polystyrenesulfonic Acid and Its Tetramethylammonium Salt with Alkali Polystyrenesulfonates

J. Škerjanc* and M. Pavlin

Department of Chemistry, University of Ljubljana, 61000 Ljubljana, Yugoslavia *(Received January 25, 1977)*

The heats of mixing of aqueous solutions containing polystyrenesulfonic acid or its tetramethylammonium salt with solutions of alkali polystyrenesulfonates of the same concentration (0.0600 monoM) have been measured at 25 °C. Mixing of HPSS with LiPSS, KPSS, CsPSS, or TMAPSS, and mixing of TMAPSS with LiPSS or NaPSS gives exothermic heat effects, while mixing of HPSS with NaPSS, and TMAPSS with KPSS or CsPSS gives endothermic effects. The heats of mixing are approximately quadratic functions of the solute mole fraction.

Introduction

During the course of the past 15 years the enthalpy of mixing of solutions of simple electrolytes has been extensively investigated and dependence of this thermodynamic property on various parameters has been demonstrated. On the contrary, heat of mixing data on solutions of synthetic polyelectrolytes are, in spite of the increasing interest for calorimetric measurements with these systems, scarce for the present. As far as we could ascertain there are only two articles on this subject. In the article by Boyd et al.[1] the enthalpy changes on mixing aqueous solutions of simple electrolyte (sodium chloride) with solutions of polyelectrolyte (sodium polystyrenesulfonate) are presented. The other article,[2] the first paper of this series, treats pure polyelectrolyte solutions and reports on heat effects accompanying the mixing of two polystyrenesulfonate solutions, one containing monovalent (hydrogen) and the other divalent (magnesium) counterions. It has been found that the enthalpy of mixing is positive and that it increases with decreasing concentration. Some previous calorimetric studies[3,4] from this laboratory have disclosed, however, that the heat of dilution of solutions of polystyrenesulfonates is strongly affected not only by the valency of the counterions but also

by the ionic radius of the counterions. Therefore, one could expect that the heat of mixing of like-charged ions should display a definite specificity too.

In this paper we shall present the calorimetric results obtained with solutions containing monovalent counterions. As in the preceding paper of this series, the polystyrenesulfonate anion has been chosen for the common ion and measurements have been made of the enthalpy change ensuing from mixing an aqueous solution of this polyelectrolyte containing hydrogen or tetramethylammonium ion with a solution containing an alkali metal ion.

Experimental Section

Sodium polystyrenesulfonate, NaPSS, purchased from Polysciences Inc. (Rydal, Pa.) was used as starting material. According to the manufacturer's specification the NaPSS had a molecular weight of 100 000 and a degree of sulfonation of 1.00. The method of purification has been described previously.[2] A dialyzed solution of NaPSS was converted to the acid, HPSS, by ion exchange and its concentration was determined by potentiometric titration to within 0.2%. The lithium and potassium salts, LiPSS and KPSS, respectively, were prepared from the acid solution by adding the corresponding metal carbonate until the pH was between 4 and 5. During the operation nitrogen was blown through the solution. The cesium and tetramethylammonium salts, CsPSS and TMAPSS, were prepared by dialysis of the NaPSS solution against several changes of CsCl and TMACl solutions, respectively, and finally against water. The solutions were adjusted by adding the corresponding hydroxide to give pH values ranging from 4 to 5. Preliminary experiments showed that a slight excess of free acid (less than 0.2%) had no influence on the results, whereas solutions with pH values higher than 6 gave unreproducible and unreliable results. All solutions were passed through 0.15-μm pore size SM 11308 filters (Sartorius-Membranfilter GmbH, Göttingen) to eliminate eventual impurities and biological growth and stored in polyethylene bottles.

The concentration of the salts was determined from the optical density at 261.5 nm of solutions prepared by diluting the sample solutions with a known excess of a 5% KCl solution. The monomolar extinction coefficient in 5% KCl, obtained from calibrations with the HPSS solution of known concentration, was found to be 420 L cm^{-1} mol^{-1}. Stock solutions of the acid and salts (about 0.1 monoM) were diluted with water to obtain solutions of the same concentration (0.0600 monoM), used in calorimetric experiments.

All the inorganic chemicals used were of reagent grade.

Calorimetric measurements were performed at 25 °C in an LKB 10700-2 batch microcalorimeter with golden reaction cells. Into one compartment of the reaction cell one polyelectrolyte solution was pipetted, and into the other an appropriate volume of another solution, so that the total volume of both solutions was 5.00 mL. The solutions were pipetted by means of Hamilton syringes and no weighing was judged necessary. The detailed description of the calorimeter and experimental procedure have been given by the designer of the instrument, Wadsö.[5]

Results and Discussion

The heats of mixing, ΔH_m, in the present study were obtained in experiments in which two polystyrenesulfonate solutions, A and B, of the same concentration were mixed. Solution A contained n_A monomoles of polystyrenesulfonic acid or its tetramethylammonium salt, and solution B contained n_B monomoles of an alkali polystyrenesulfonate.

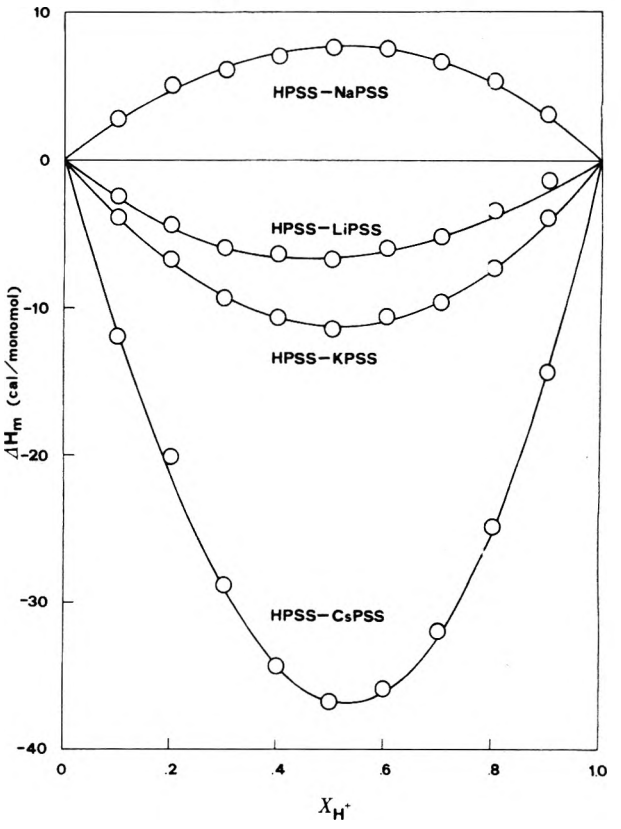

Figure 1. Heats of mixing of polystyrenesulfonic acid with alkali polystyrenesulfonates in water at 25 °C as a function of the mole fraction of the acid. Polymer concentration: 0.0600 monomol/L.

By mixing appropriate amounts of solutions A and B the dependence of ΔH_m on the mole fraction of the acid or TMA salt, X_A, was obtained. It is convenient to express the results of mixing processes in terms of the change in the enthalpy divided by $(n_A + n_B)$, the total amount of polyelectrolyte in the mixed solution. Then ΔH_m is related to the enthalpies of the mixed and both single solutions, containing 1 monomole of polyelectrolyte, by

$$\Delta H_m = H_{\text{mixed soln}} - X_A H_A - (1 - X_A) H_B \qquad (1)$$

The calorimetric results are shown in Figures 1 and 2. It is seen that the curves, having either maximum or minimum, are approximately symmetrical with respect to mole fraction. Heats of mixing of HPSS with alkali polystyrenesulfonates are in general exothermic, decreasing in the order CsPSS, KPSS, LiPSS, which is also the order of hydration of the counterions. The sodium salt is an exception, giving endothermic heat effects when mixed with HPSS. The anomalous behavior of the sodium salt has also been noticed in some previous papers dealing with heat of dilution[3] and osmotic coefficient measurements[6] of polystyrenesulfonates. The above, at first sight unusual behavior of polystyrenesulfonates, however, is not restricted to polyelectrolytes. A similar situation can be found for simple electrolytes. So, for the systems hydrochloric acid with alkali metal chlorides,[7] exothermic heat effects have been observed when mixing HCl with KCl, RbCl, or CsCl, and endothermic when mixing HCl with LiCl or NaCl. The values of ΔH_m at $X_A = 0.5$ at total molality of $m = 1$ mol/kg are 13.01, 32.52, −3.74, −20.55, and −34.01 cal/mol in the order beginning with LiCl and ending with CsCl. We see that for all, for polystyrenesulfonates as well as for chlorides, there is a tendency from relatively small, positive (HCl–LiCl) or negative (HPSS–LiPSS) values to numerically large and negative values as the molecular weight of the salt increases, and in both

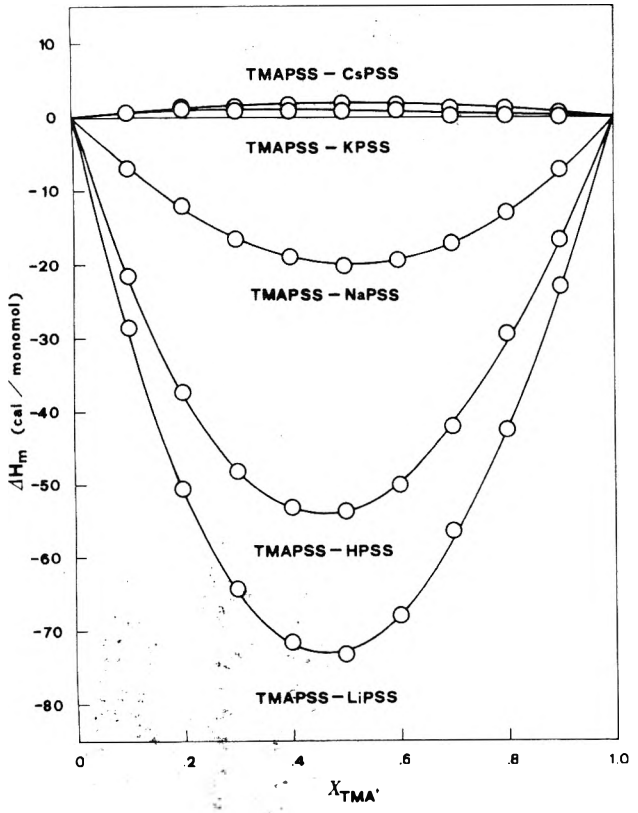

Figure 2. Heats of mixing of tetramethylammonium polystyrenesulfonate with alkali polystyrenesulfonates and with polystyrenesulfonic acid in water at 25 °C as a function of the mole fraction of the tetramethylammonium salt. Polymer concentration: 0.0600 monomol/L.

cases the heat of mixing for the sodium salt is positive and seems to be irregularly high.

If the small and highly hydrated hydrogen ion is replaced by the large tetramethylammonium ion which is considered anhydrous, or only slightly hydrated, just the reverse may be observed. Figure 2 shows the calorimetric results obtained when a 0.0600 monoM solution of TMAPSS is mixed with solutions of the alkali polystyrenesulfonates of the same concentration. We see that the mixing of TMAPSS with LiPSS and NaPSS is accompanied by the evolution of heat while the mixing with KPSS and CsPSS is accompanied by the absorption of heat. Again, we can find a close analogy in the field of simple electrolytes. For instance, mixing of TMACl with LiCl, KCl, and CsCl at 0.5 total ionic strength has given the following values of ΔH_m at $X_A = 0.5$: −20.0, 14.8, and 10.2 cal/mol, respectively.[8] Although a direct comparison of this values with those obtained with polystyrenesulfonates is difficult owing to the different experimental conditions and specific behavior of the polyion, we see again that in both cases the enthalpy of mixing changes in the same order. However in contrast to the results obtained with the acids, in this case the maximum value of ΔH_m passes from negative values to positive as the molecular weight of the alkali salts increases.

Comparison of the values of ΔH_m at $X_A = 0.5$ for chlorides and polystyrenesulfonates is given in Figure 3.

Two features of the results obtained with solutions of simple electrolytes are significant. One is that they seem to be little dependent on the nature of the common ion; so, for instance, the mixing of HBr with alkali bromides has given results similar to those obtained with chlorides.[7] The other feature is that these measurements support the idea of classifying ions into two groups, into those which enhance the structure of water and those which break it. The mixing of two structure makers (such as H^+, Li^+, Na^+)

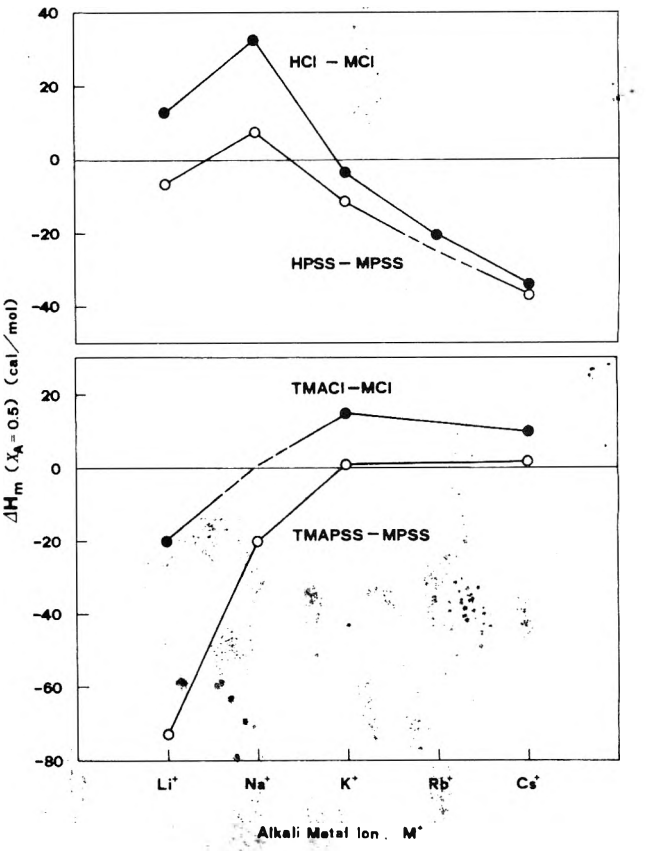

Figure 3. Heats of mixing of some chlorides[7,8] and polystyrenesulfonates at $X_A = 0.5$ at constant concentration ($t = 25$ °C): solid circles, heats of mixing of HCl ($m = 1$ mol/kg) and TMACl ($m = 0.5$ mol/kg) with alkali chlorides; empty circles, heats of mixing of HPSS and TMAPSS with alkali polystyrenesulfonates at 0.06 monomol/L.

or two structure breakers (K^+, Rb^+, Cs^+, TMA^+) gives endothermic heats of mixing, while the mixing of a structure maker with a structure breaker gives an exothermic heat effect. We can see that these two features are preserved even if solutions contain instead of the small chloride ion the huge polystyrenesulfonate ion as the common ion. Among the pairs studied in the present work the only pair which displays some polyelectrolytic character of the polystyrenesulfonate anion is the HPSS–LiPSS pair, giving the exothermic heat of mixing and thus indicating that hydrogen and lithium ions act as opposites when mixed with each other in the presence of the polystyrenesulfonate ion.

Experimental results ensuing from mixing of simple electrolytes at constant ionic strength have originally been represented by empirical equations of the type:

$$\Delta H_m = X_A X_B [a + b(X_B - X_A)] \quad (2)$$

where X_A and X_B are the solute mole fractions. This equation has some advantages: the first empirical constant a is four times the ordinate at $X_A = 0.5$, and if b, the measure of skew, is zero the plot of ΔH_m against X_A is symmetrical with a maximum or minimum at $X_A = 0.5$. The physical meaning of both constants has been given by Friedman[9] who applied Mayer's ionic solution theory[10] to a primitive electrolyte model consisting of hard spheres in a continuous dielectric. Since measurements are made at constant ionic strength and with a common ion, effects of the ionic atmosphere and oppositely charged ion pairs cancel for charge-symmetrical mixtures. Therefore, the pairwise and triplet interaction of like-charged ions are reflected in the constants a and b.

If the present experimental data are fitted to eq 2 by the method of least squares, the values of constants a and

TABLE I: Results of Least-Squares Fit to Eq 2

Polyelectrolyte pair[a]	a	b	ΔH_m at X_A = 0.5
HPSS-LiPSS	−26.7	−5	−6.68
HPSS-NaPSS	30.3	−3	7.58
HPSS-KPSS	−45.0	2	−11.3
HPSS-CsPSS	−147	20	−36.7
HPSS-TMAPSS	−215	38	−53.8
TMAPSS-LiPSS	−291	−43	−72.8
TMAPSS-NaPSS	−80	4	−20.0
TMAPSS-KPSS	3.7	5	0.92
TMAPSS-CsPSS	7.1	0.7	1.78

[a] Polymer concentration: 0.0600 monoM; t = 25 °C. Results in cal/monomol.

b reported in Table I are obtained. Included are the calculated values of ΔH_m at $X_A = 0.5$ which are $a/4$. The curves drawn in Figures 1 and 2 are the best representatives of the measurements, calculated by using the reported values of a and b. Although the physical meaning of these two constants is questionable in the case of polyelectrolytes, it is remarkable that all of the curves do conform reasonable well to the same quadratic relationship as found for simple electrolytes.

For the system HPSS-NaPSS a few measurements have also been performed at an approximately fivefold higher concentration. The results indicate that the heat of mixing slightly increases with increasing concentration; the value of ΔH_m at $X_A = 0.5$ is 7.6 cal/monomol in 0.0600 monoM solution, and 8.5 cal/monomol in 0.280 monoM solution. By contrast, the heat of mixing of charge symmetrical simple electrolytes has been found experimentally[11] and also predicted theoretically[9] to increase approximately with the square of the ionic strength. For the present, in view of the fact that experimental results for polyelectrolytes are still very scarce, this seems to be also the main difference between heats of mixing of solutions of simple electrolytes and polyelectrolytes containing a common ion.

In the first paper of this series[2] the heat of mixing of polystyrenesulfonic acid with its magnesium salt has been reported. The experimental results have been interpreted with the computations[12,13] based on the cylindrical cell model[14,15] of polyelectrolyte solutions. The experiment and theory have agreed on the sign and magnitude as well as on the concentration dependence of ΔH_m. Theoretical approaches based on the cell model, together with Manning's limiting laws,[16] have been thus far applied with considerable success in the interpretation of thermodynamic properties of polyelectrolyte solutions, as reviewed recently by several authors.[17-19] Consequently, it was quite natural to employ the same model also in the present problem.

The heat of mixing, defined by eq 1, may be formally split into two terms

$$\Delta H_m = \Delta H_m^\circ + \Delta H_{m,e} \qquad (3)$$

where ΔH° is the nonelectrostatic and ΔH_e the electrostatic contribution. In interpretation of various thermodynamic properties of solutions of simple electrolytes and polyelectrolytes the nonelectrostatic terms has usually been assumed to be less significant, and only the electrostatic term has been considered. In the cylindrical cell model, which is a purely electrostatic model, the individuality of counterions can only be considered through the ionic radius. In a recent article[20] from this laboratory the model has been extended to polyelectrolyte solutions containing two kinds of monovalent counterions, differing in size, and expressions which relate the electrostatic potential, ψ, to the distance from the cell axis, r, have been obtained. From the gradient $(d\psi/dr)$ the electrostatic internal energy of the solution can be calculated,[12] and this can be related to the enthalpy of mixing[2] if the nonelectrostatic term ΔH_m° is neglected. Computations show that applying the assumption $\Delta H_m^\circ = 0$, we cannot explain the experimental results of this paper. Employing arbitrary values for the radii of both counterions, the calculated values of ΔH_m are always positive.[21] Thus, the exothermic heats of mixing, which are more typical for the present studies, are not foreseen by the simple cell model. Moreover, also the concentration dependence of ΔH_m is incorrectly predicted. According to the theory ΔH_m should increase with decreasing concentration, a prediction which is just reverse of the experimental findings.

The reason for the failure of the theory in the present case has to be sought in the simplification made in eq 3, i.e., in the neglect of the nonelectrostatic terms, ΔH_m°, which seems to be the essential factor determining the value of ΔH_m. It is beyond doubt that the success of the cell theory in interpretation of various thermodynamic properties of polyelectrolyte solutions, heretofore reported several times,[1-4,12,13,17,18] may be attributed to the fact that in those instances the long-range Coulomb interactions, which are common to all such solutions, and which can be estimated by the theory, have prevailed over the more specific short-range interactions, which are characterized by changes in the solvation shells of the participating species, and which seem to be reflected in the present results. It is our belief, therefore, that also the non-Coulombic interactions between ions will have to be considered by a future, more general theory of polyelectrolyte solutions.

Acknowledgment. We wish to express our thanks to Professor D. Dolar for reading and commenting on the manuscript. The partial financial support by the Boris Kidrič Fund is gratefully acknowledged.

References and Notes

(1) G. E. Boyd, D. P. Wilson, and G. S. Manning, *J. Phys. Chem.*, **80**, 808 (1976).
(2) J. Škerjanc, *J. Phys. Chem.*, **79**, 2185 (1975).
(3) J. Škerjanc, D. Dolar, and D. Leskovšek, *Z. Phys. Chem. (Frankfurt am Main)*, **56**, 208 (1967); **70**, 31 (1970).
(4) J. Škerjanc, S. Hočevar, and D. Dolar, *Z. Phys. Chem. (Frankfurt am Main)*, **86**, 311 (1973).
(5) I. Wadsö, *Acta Chem. Scand.*, **22**, 927 (1968).
(6) D. Kozak, J. Kristan, and D. Dolar, *Z. Phys. Chem. (Frankfurt am Main)*, **76**, 85 (1971).
(7) Y. C. Wu, M. B. Smith, and T. F. Young, *J. Phys. Chem.*, **69**, 1868 (1965).
(8) R. H. Wood and H. L. Anderson, *J. Phys. Chem.*, **71**, 1871 (1967).
(9) H. L. Friedman, *J. Chem. Phys.*, **32**, 1134, 1351 (1960).
(10) J. E. Mayer, *J. Chem. Phys.*, **18**, 1426 (1950).
(11) R. H. Wood and R. W. Smith, *J. Phys. Chem.*, **69**, 2974 (1965).
(12) D. Dolar and J. Škerjanc, *J. Chem. Phys.*, **61**, 4106 (1974).
(13) J. Škerjanc and D. Dolar, *J. Chem. Phys.*, **63**, 515 (1975).
(14) (a) R. M. Fuoss, A. Katchalsky, and S. Lifson, *Proc. Natl. Acad. Sci. U.S.A.*, **37**, 579 (1951); (b) T. Alfrey, Jr., P. W. Berg, and H. Morawetz, *J. Polym. Sci.*, **7**, 543 (1951).
(15) S. Lifson and A. Katchalsky, *J. Polym. Sci.*, **13**, 43 (1954).
(16) G. S. Manning, *J. Chem. Phys.*, **51**, 924 (1969).
(17) A. Katchalsky, *Pure Appl. Chem.*, **26**, 327 (1971).
(18) D. Dolar in "Polyelectrolytes", E. Sélégny, M. Mandel, and U. P. Strauss, Ed., Reidel Publishing Co., Dordrecht, Holland, 1974, p 97.
(19) G. S. Manning, *Annu. Rev. Phys. Chem.*, **23**, 117 (1972).
(20) D. Dolar and J. Škerjanc, *J. Polym. Sci., Polym. Phys. Ed.*, **14**, 1005 (1976).
(21) D. Dolar and J. Škerjanc, manuscript in preparation.

Thermochemical Investigations of Nearly Ideal Binary Solvents. 3. Solubility in Systems of Nonspecific Interactions

William E. Acree, Jr., and Gary L. Bertrand*

Department of Chemistry, University of Missouri—Rolla, Rolla, Missouri 65401 *(Received September 20, 1976; Revised Manuscript Received April 4, 1977)*

Publication costs assisted by the University of Missouri—Rolla

The simple model which has previously led to successful predictive equations for the partial molar excess enthalpy of a solute in nearly ideal binary solvents has been slightly modified for application to the partial molar excess Gibbs free energy (excess chemical potential) of the solute in these systems. Three predictive equations are derived and tested for their ability to predict solubility in mixed solvents from measurements in the pure solvents. The most successful equation involves volumetrically weighted interaction parameters for the excess Gibbs free energy relative to the Flory–Huggins entropy of mixing, and predicts solubility in 22 systems containing naphthalene, iodine, and stannic iodide as solutes with an average deviation of 1.5% and a maximum deviation of 4%, using no adjustable parameters.

Introduction

Recent developments in the investigation of weak association complexes in solution[1,2] have shown a need for improved approximations for the thermochemical properties of a solute or solutes in a binary solvent system, to allow compensation for the effects of solution nonideality, or, from a slightly different viewpoint, to separate "chemical" and "physical" effects on the properties of the complexes. In order to provide a firm thermodynamic basis for these approximations, much simpler systems must be studied, establishing the qualitative and if possible the quantitative trends of behavior of solutes in binary solvent systems of nonspecific (or physical) interactions.

This work is a continuation of our search for mixing models and equations which will provide reasonable predictions for the thermochemical properties of a solute at high dilution in a binary solvent. Earlier studies[3,4] have been primarily concerned with the partial molar excess enthalpy of the solute. In this work, we extend our previous consideration of the chemical potential or partial molar Gibbs free energy of the solute[4] through studies of solubility in binary solvents. Three specific forms of the general predictive equation are compared. It should be noted that these equations are identical in concept and only slightly different in application from equations developed and tested by Heric and co-workers.[5,6] Similar equations have been developed by O'Connell and Prausnitz[7,8] and by Nitta and Katayama.[9] However, we feel that the greater flexibility of our model, and the need to establish the coherence of our model for free energy with our earlier model for the enthalpy of the solute merit this reconsideration of the fundamental equations. Because of the intended application of these approximations to the case of a solute in a complexing solvent, and to the properties of the complex (a second solute), we are particularly concerned with the effects of the relative sizes of the solvent and solute molecules.

We show the development and application of a zero-parameter equation which predicts the solubility of the fairly soluble solute naphthalene in mixtures of small solvents (benzene, carbon tetrachloride, etc.) and those containing a much larger solvent (hexadecane), and of the much smaller and less soluble solute iodine over a similar range of solvent sizes, with a maximum error of 4% in the 22 systems considered. The application to iodine as solute in these systems of nonspecific interactions is particularly important because of the ability of iodine to form a variety of complexes.

Solubility data for naphthalene in a number of solvent mixtures covering a broad range of molar volumes are available in the literature. The solubility of iodine in several noncomplexing solvent mixtures is also available, but since none of the solvent mixtures contain very large molecules, we have measured the solubility of iodine in two mixtures of *n*-hexadecane with smaller molecules. To provide data for a larger solute molecule, we have also measured the solubility of stannic iodide in cyclohexane + carbon tetrachloride.

Experimental Section

Fisher Spectroanalyzed carbon tetrachloride, cyclohexane, *n*-heptane, and isooctane were stored over molecular sieves and distilled shortly before use. Eastman Practical Grade *n*-hexadecane was passed through a silica gel column and distilled. Solvent mixtures were prepared by weight, so that mole fractions could be calculated to 0.0001.

Iodine was Matheson Coleman and Bell Certified ACS Reagent Grade. Stannic iodide was prepared by refluxing metallic tin powder with iodine in chloroform as suggested by Wheatland.[10] The product was recrystallized three times from hot chloroform, giving a melting point of 144 ± 1 °C (lit. mp 144.5 °C).

Saturated solutions of stannic iodide in brown glass bottles, protected from light with aluminum foil, were allowed to equilibrate in a constant temperature bath at 25.00 ± 0.01 °C for several days. The attainment of equilibrium was verified by repetitive measurements after several additional days. The solubility was measured by transferring an aliquot of solution through a coarse filter into a tared container for analysis by the gravimetric procedure used by Dorfman and Hildebrand.[11] Iodine solutions were equilibrated in a similar fashion, transferring a weighed aliquot to a flask containing a known excess of aqueous arsenic trioxide, then back-titrated with a freshly standardized iodine solution to the starch endpoint. Solubilities were reproducible to within 1%. Results are reported in Table I. In the pure solvents our results were in good agreement with previously reported values, as presented in Table II.

TABLE I: Observed and Calculated Values of the Solubility of Iodine and Stannic Iodide in Some Binary Solvents at 25 °C

Solute/solvent (1) + solvent (2)	X_1^0	X^{sat}_{solute}	% deviations of calcd values[a] (XX)	(XV)	(VV)
I_2/n-$C_{16}H_{34}$ + n-C_7H_{16}	0.0815	0.00762	−4.6	+1.0	−0.6
	0.1429	0.00809	−6.4	+2.1	−0.5
	0.1668	0.00816	−5.8	+3.8	+1.0
	0.3267	0.00958	−11.2	+2.5	−1.1
	0.6164	0.01174	−10.7	+1.9	−1.5
I_2/n-$C_{16}H_{34}$ + i-C_8H_{18}	0.1015	0.00681	−4.3	+1.5	−0.6
	0.1563	0.00735	−7.6	+0.4	−1.7
	0.2169	0.00778	−7.9	+2.0	−0.5
	0.3554	0.00896	−9.9	+2.3	−0.7
	0.5800	0.01086	−9.3	+2.1	−0.6
SnI_4/CCl_4 + c-C_6H_{12}	0.1491	0.00823	−1.3	−1.8	−1.7
	0.3617	0.00962	−0.6	−1.3	−1.2
	0.6183	0.01155	−0.6	−1.2	−1.1
	0.8676	0.01357	−0.5	−0.7	−0.6

[a] % deviation = 100 ln $(X^{sat}_{calcd}/X^{sat}_{obsd})$.

TABLE II: Comparison with Literature Values of the Solubilities of Iodine and Stannic Iodide in Pure Solvents at 25 °C

Solute	Solvent	(Mole fraction solubility) × 10^3 Exptl	Lit.
Iodine	Isooctane	5.923	5.92[a]
Iodine	n-Heptane	6.912	6.916,[b] 6.79[c]
Iodine	n-Hexadecane	14.28	14.50[d]
Stannic iodide	CCl_4	14.63	14.59,[e] 14.4[f]
Stannic iodide	Cyclohexane	7.216	7.273[g]

[a] G. R. Negishi, L. H. Donnally, and J. H. Hildebrand, *J. Am. Chem. Soc.*, 55, 4793 (1933). [b] G. Kortüm and V. M. Vogel, *Z. Elektrochem.*, 59, 16 (1955). [c] J. H. Hildebrand and C. A. Jenks, *J. Am. Chem. Soc.*, 42, 2180 (1920). [d] K. Shinoda and J. H. Hildebrand, *J. Phys. Chem.*, 69, 605 (1965). [e] See ref 11. [f] B. E. Smith and J. Walkley, *Trans. Faraday Soc.*, 56, 220 (1969). [g] See ref 14.

Discussion

Burchfield and Bertrand[4] developed general equations for the partial molar excess properties of a solute at high dilution in a binary solvent for a simple model system obeying a ternary mixing equation

$$\Delta Z^{ex}_{123} = (n_1\Gamma_1 + n_2\Gamma_2 + n_3\Gamma_3)^{-1}(n_1\Gamma_1 n_2\Gamma_2 A_{12} + n_1\Gamma_1 n_3\Gamma_3 A_{13} + n_2\Gamma_2 n_3\Gamma_3 A_{23}) \quad (1)$$

in which Z represents any extensive thermodynamic property described in terms of interaction parameters (A_{ij}) and weighting factors (Γ_i). The partial molar excess properties of the solute at infinite dilution in mixtures $[(\Delta\bar{Z}_3^{ex})^*]$ are shown to depend on a weighted average of the properties in the pure solvents $[(\Delta\bar{Z}_3^{ex})^*_{X_1^0=1}, (\Delta\bar{Z}_3^{ex})^*_{X_2^0=1}]$ and a contribution due to the "unmixing" of the solvent pair by the presence of the solute:

$$(\Delta\bar{Z}_3^{ex})^* = f_1^0(\Delta\bar{Z}_3^{ex})^*_{X_1^0=1} + f_2^0(\Delta\bar{Z}_3^{ex})^*_{X_2^0=1} - \Gamma_3(X_1^0\Gamma_1 + X_2^0\Gamma_2)^{-1}(\Delta\bar{Z}_{12}^{ex}) \quad (2)$$

$$f_1^0 = (1 - f_2^0) = n_1\Gamma_1/(n_1\Gamma_1 + n_2\Gamma_2)$$
$$X_1^0 = (1 - X_2^0) = n_1/(n_1 + n_2) \quad (3)$$

Burchfield and Bertrand considered various approximations for weighting factors and concluded that the most accurate predictions for heats of solution could be obtained with weighting factors based on the mixing properties of the binary systems of solvents and solute, but the use of molar volumes for weighting factors provided reasonably accurate predictions. The superiority of the use of molar volumes over the simpler approximation of equating all three weighting factors appeared to derive from the effect of weighting factors on the "unmixing" term of eq 2 rather than from the effect on the weighted average of the properties of the solute in the pure solvents. Enhancement of the unmixing term by a large solute molecule can lead to predictions of maxima or minima of the properties of the solute in simple mixtures. It should be noted that precise applicability of eq 2 to a thermochemical property and its temperature and pressure derivatives (G and H or S, G and V, H and C_P) requires that weighting factors be independent of temperature and pressure. Therefore, molar volumes and other experimentally determined weighting factors must be regarded as approximations to these "true" weighting factors, and for application to conditions of varying temperature and pressure, they should be referred to a specified condition, such as 25 °C and 1 atm, or to an extrapolated state such as a "close-packed" volume.

Interaction parameters and weighting factors are rather straightforward in the case of directly observed excess properties such as enthalpy and volume. In the case of Gibbs free energy, however, the total free energy of mixing is observed and the excess is calculated as the difference between the observed value and the value for an ideal solution of the same composition

$$\Delta G^{mixing} = RT\sum_{i=1}^{N} n_i \ln X_i + \Delta G^{ex} \quad (4)$$

For mixtures of molecules with considerably different molar volumes, excess mixing equations of the form of eq 1 more accurately describe the difference between the observed free energy of mixing and that predicted by the Flory–Huggins equation

$$\Delta G^{mixing} = RT\sum_{i=1}^{N} n_i \ln \Phi_i + \Delta G^{fh} \quad (5)$$

in which ϕ_i represents a weighted mole fraction based on weighting factors which are similar to molar volumes, but which do not vary with temperature or pressure; and ΔG^{fh} has the same form as eq 1 but with specific weighting factors Γ_i^{fh} and interaction parameters A_{ij}^{fh}.[12] Treatment of these mixing equations in the manner of Burchfield and Bertrand[4] leads to two general equations for approximating the partial molar excess Gibbs free energy of a solute at high dilution in a binary solvent:

$$\Delta\bar{G}_3^{ex} = (1 - f_3)^2[f_1^0(\Delta\bar{G}_3^{ex})^*_{X_1^0=1} + f_2^0(\Delta\bar{G}_3^{ex})^*_{X_2^0=1} - \Gamma_3(X_1^0\Gamma_1 + X_2^0\Gamma_2)^{-1}(\Delta\bar{G}_{12}^{ex})] \quad (6)$$

TABLE III: Comparison of Predictive Equations for the Solubilities of Naphthalene, Iodine, and Stannic Iodide in Various Binary Systems

Solute	Solvent	Ref	RMS deviations[u] (%) for the predictive eq (XX)	(XV)	(VV)	ΔG_{12}^{ex} Ref
Naphthalene	Benzene + cyclohexane	*a*	−1.4	−1.2	−1.1	*i*
Naphthalene	Benzene + CCl_4	*a*	+1.5	+1.7	+1.9	*i*
Naphthalene	Benzene + hexane	*a*	+2.3	1.4	1.4	*d*
Naphthalene	Cyclohexane + hexadecane	*b*	−4.0	+2.9	+1.4	*j*
Naphthalene	Hexane + hexadecane	*b*	−6.8	+1.8	+0.8	*o*
Naphthalene	CCl_4 + cyclohexane	*b*	0.3	−0.5	−0.6	*i*
Naphthalene	CCl_4 + hexadecane	*b*	+8.0	+4.5	+2.4	*p*
Naphthalene	Benzene + hexadecane	*a*	+9.2	+2.4	+0.7	*p*
Naphthalene	CCl_4 + hexane	*b*	+3.2	1.3	0.5	*h*
Naphthalene	Cyclohexane + hexane	*b*	0.8	0.6	0.6	*e*
Naphthalene	Benzene + toluene	*a*	+0.5	+0.5	+0.6	*q*
Naphthalene	CCl_4 + toluene	*c*	−1.5	−1.5	−1.5	*k*
Naphthalene	Cyclohexane + toluene	*c*	−1.8	−0.9	−0.8	*f*
Naphthalene	Ethylbenzene + CCl_4	*c*	0.5	0.7	0.6	*w*
Naphthalene	Ethylbenzene + cyclohexane	*c*	−1.7	0.3	0.3	*w*
Iodine	Cyclohexane + hexane	*m*	+1.7	−1.5	−2.5	*e*
Iodine	CCl_4 + hexane	*m*	+5.0	−1.3	−2.0	*h*
Iodine	Hexadecane + heptane	*v*	−8.2	+2.4	−1.0	*l*
Iodine	Hexadecane + isooctane	*v*	−8.1	+1.8	−0.9	*r*
Iodine	Cyclohexane + heptane	*n*	+2.1	−0.5	−0.8	*f*
SnI_4	Cyclohexane + benzene	*g*	2.2	2.8	3.1	*i*
SnI_4	Cyclohexane + CCl_4	*v*	−0.8	−1.3	−1.2	*i*

Properties used in calculations

Solvent	$\bar{V}^0$, mL/mol	Solvent	$\bar{V}^0$, mL/mol	Solute	a_3^{solid}
Benzene	89.41	Iodine	59.593	Iodine	0.258[s]
CCl_4	97.08	Isooctane	166.09	Naphthalene	0.312[a]
Cyclohexane	108.76	Naphthalene	123.00	Stannic iodide	0.1127[t]
Hexadecane	294.12	Stannic iodide	151.00		
Heptane	147.48	Toluene	106.84		
Hexane	131.59	Ethylbenzene	123.06		

[a] See ref 5a. [b] See ref 5c. [c] See ref 5b. [d] V. C. Smith and R. L. Robinson, Jr., *J. Chem. Eng. Data*, 15, 391 (1970). [e] I. P.-C. Li, B. C.-Y. Lu, and E. C. Chen, *ibid.*, 18, 305 (1973). [f] T. Katayama, E. K. Sung, and E. N. Lightfoot, *AIChE J.*, 11, 294 (1965). [g] See ref 14. [h] D. V. S. Jain, V. K. Gupta, and B. S. Lark, *Can. J. Chem.*, 8, 815 (1970). [i] J. R. Goates, R. J. Sullivan, and J. B. Ott, *J. Phys. Chem.*, 63, 589 (1959). [j] J. D. Gomez-Ibanez and J. J. C. Shieh, *ibid.*, 69, 1660 (1965). [k] R. P. Rastogi, J. Nath, and J. Misra, *ibid.*, 71, 1277 (1967). [l] J. N. Brønsted and J. K. Koefoed, *Dank. Videnskab. Selskab. (Mat. Fys. Medd.)*, 22, 1 (1946). [m] See ref 15b. [n] G. Kortüm and V. M. Vogel, *Z. Elektrochem.*, 59, 16 (1955). [o] M. L. McGlashan and A. G. Williamson, *Trans. Faraday Soc.*, 57, 588 (1961). [p] D. V. S. Jain and B. S. Lark, *J. Chem. Thermodyn.*, 5, 455 (1973). [q] J. S. Rowlinson, "Liquids and Liquid Mixtures", Academic Press, New York, N.Y., 1959, p 150. [r] Footnote *q*, p 159. [s] See ref 8, p 142. [t] S. K. Suri and V. Ramakrishna, *Can. J. Chem.*, 47, 3049 (1969). [u] RMS deviation (%) = $(100/N^{1/2})\{\Sigma[\ln(X_{calcd}^{sat}/X_{expt}^{sat})]^2\}^{1/2}$; an algebraic sign indicates that all deviations were of the same sign. [v] This work. [w] D. V. S. Jain and O. P. Yadav, *Indian J. Chem.*, 12, 718 (1974).

and

$$\Delta\bar{G}_3^{fh} = (1 - f_3)^2[f_1^0(\Delta\bar{G}_3^{fh})^*_{X_1^0=1} + f_2^0(\Delta\bar{G}_3^{fh})^*_{X_2^0=1} - \Gamma_3^{fh}(X_1^0\Gamma_1^{fh} + X_2^0\Gamma_2^{fh})^{-1}(\Delta\bar{G}_{12}^{fh})] \quad (7)$$

In eq 2, 6, and 7, and the following equations, the asterisk indicates an extrapolated value for the infinitely dilute solution ($f_3^* = 0$). We have considered evaluation of weighting factors (Γ_i and Γ_i^{fh}) from experimental data, as was done for predicting heats of solution in binary solvents. However, it is clear that weighting factors derived from free energy data are of less utility in predictive equations than are the simple approximations for weighting factors. In addition, calculated weighting factors for the excess free energy of mixing of binary systems are often found to be strongly dependent on temperature. This condition probably arises from the fact that the interaction parameters for the free-energy functions are usually small differences between much larger interaction parameters for enthalpy and entropy. Small changes in the interaction parameters and weighting factors for entropy and enthalpy can show up as large relative changes in the corresponding parameters for the free energy. Thus, to provide a proper "count" of the relative numbers of interactions of the solute with the individual solvents, we feel that weighting factors based on the excess enthalpy or entropy would be more appropriate than those based on the free energy of mixing. However, we do not feel that the relatively small amount of data presently available can provide a conclusive test of these ideas. Also, our main concern at the present time is to find the simplest equations which require the least amount of experimental data to adequately predict the binary solvent effect on the Gibbs free energy of a solute in simple systems. Since we have found approximations which perform adequately for the data available, the introduction of more complex approximations does not seem to be warranted.

The general equation (eq 6 and 7) for the excess partial molar properties of the solute in the binary solvent can be related to the solubility through the basic thermodynamic relationships

$$(\Delta\bar{G}_3^{ex}) = RT \ln (a_3^{solid}/X_3^{sat}) \quad (8)$$

$$(\Delta\bar{G}_3^{fh}) = RT\{\ln (a_3^{solid}/\Phi_3^{sat}) - [1 - (\bar{V}_3^0/\bar{V})]\} \quad (9)$$

in which a_3^{solid} is the activity of the solid solute. It is defined as the ratio of the fugacity of the solid to the fugacity of the pure supercooled liquid.[8] Application of eq 6 and 8 or eq 7 and 9 to the solubilities of the solute in the pure solvents gives values of $(\Delta\bar{G}_3^{ex})^*_{X_1^0=1}$ and

$(\Delta\bar{G}_3^{ex})^*_{X_2^0=1}$, or $(\Delta\bar{G}_3^{fh})^*_{X_1^0=1}$ and $(\Delta\bar{G}_3^{fh})^*_{X_2^0=1}$, if the appropriate weighting factors are known. We have considered three equations based on different types of weighting factors: (XX) based on eq 6 with all weighting factors equal, (XV) based on eq 6 with molar volumes as weighting factors, and (VV) based on eq 7 with molar volumes as weighting factors. A fourth permutation of these equations (VX) has little theoretical justification and was not considered. The three predictive equations are

$$RT \ln (a_3^{solid}/X_3^{sat}) = (1 - X_3^{sat})^2[X_1^0(\Delta\bar{G}_3^{ex})^*_{X_1^0=1} + X_2^0(\Delta\bar{G}_3^{ex})^*_{X_2^0=1} - (\Delta\bar{G}_{12}^{ex})] \quad (XX)$$

$$RT \ln (a_3^{solid}/X_3^{sat}) = (1 - \Phi_3^{sat})^2[\Phi_1^0(\Delta\bar{G}_3^{ex})^*_{X_1^0=1} + \Phi_2^0(\Delta\bar{G}_3^{ex})^*_{X_2^0=1} - \bar{V}_3^0(X_1^0\bar{V}_1^0 + X_2^0\bar{V}_2^0)^{-1}(\Delta\bar{G}_{12}^{ex})] \quad (XV)$$

$$RT [\ln (a_3^{solid}/\Phi_3^{sat}) - \left(1 - \frac{\bar{V}_3^0}{X_1^0\bar{V}_1^0 + X_2^0\bar{V}_2^0}\right)(1 - \Phi_3^{sat})] = (1 - \Phi_3^{sat})^2[\Phi_1^0(\Delta\bar{G}_3^{fh})^*_{X_1^0=1} + \Phi_2^0(\Delta\bar{G}_3^{fh})^*_{X_2^0=1} - \bar{V}_3^0(X_1^0\bar{V}_1^0 + X_2^0\bar{V}_2^0)^{-1}(\Delta\bar{G}_{12}^{fh})] \quad (VV)$$

With these equations, solubility data measured in pure solvents can be used to calculate the excess partial molar Gibbs free energy (or excess over the Flory–Huggins prediction) of the solute at infinite dilution in these pure solvents, then these values can be combined with the excess free energy of the binary solvent[9] to predict the solubility in mixtures without the use of any adjustable parameters.

The predictive abilities of these equations are compared in Table III for 22 systems for which solubility data and the excess free energy of the solvent pair were available at or near the same temperature. Equation VV, based on molar volumes as weighting factors for the excess free energy over the Flory–Huggins entropy, is seen to be the most generally applicable with an overall average (rms) deviation of 1.5%, and a maximum error for a single data point of 4%. This maximum deviation occurs in a system (SnI_4–benzene + cyclohexane) in which complex formation has been suggested.[13] The primary advantage of eq VV over the other two predictive equations is in its applicability to the hexadecane systems. If these systems are excluded, (XV) is slightly better overall than eq VV, but eq XX is significantly poorer than the other two equations. This behavior is in agreement with the findings of Burchfield and Bertrand,[4] who concluded that volume-based weighting factors gave better predictions for the partial molar excess enthalpy of the solute than did the simple mole fraction parameters. It should be noted that differentation of eq 6 and 7 with respect to temperature leads to identical forms of the equation for excess enthalpy.

The success of eq VV in predicting the binary solvent effect on solubilities as large as 0.35 volume fraction in solvents with molar volumes covering a threefold range and for solutes with molar volumes ranging from 60 to 150 mL/mol indicates that this equation will form an adequate base for approximations of the "physical" interactions in a system containing "chemical" interactions such as those between a solute and a complexing solvent. Three treatments of solubility in complexing systems have been reported. Purkayastha and Walkley[14] treated the solubility of iodine in binary solvents containing benzene in a "physical" manner, using a modified form of the solubility parameter approach. Sytilin[15] has treated the solubility of iodine in all solvent mixtures, including those of purely "inert" solvents such as *n*-hexane + cyclohexane, in terms of solvational complexes. The true situation must lie intermediate between these two extremes. Nitta and Katayama[9d] used a combination of "physical" and "chemical" effects to correlate the solubility of iodine in mixtures of benzene + cyclohexane and benzene + carbon tetrachloride. However, their use of a solvent-independent equilibrium constant and a parameterized form of the excess free energy of the solvent pair necessitated the use of an additional parameter in the form of an equilibrium constant for the benzene–carbon tetrachloride complex. It is hoped that our method of using the measured excess free energy of the solvent pair will avoid the problem of dealing with complexes between the binary solvents, and will allow approximations for dealing with the possible solvent dependence of the equilibrium constant for solute complexes.

References and Notes

(1) G. L. Bertrand, *J. Phys. Chem.*, **79**, 48 (1975).
(2) G. L. Bertrand and T. E. Burchfield, "Analytical Calorimetry", Vol. 3, R. S. Porter and J. F. Johnson, Ed., Plenum Press, New York, N.Y., 1974, p 283.
(3) E. L. Taylor and G. L. Bertrand, *J. Solution Chem.*, **3**, 479 (1974).
(4) T. E. Burchfield and G. L. Bertrand, *J. Solution Chem.*, **4**, 205 (1975).
(5) (a) E. L. Heric and C. D. Posey, *J. Chem. Eng. Data*, **9**, 35 (1964); (b) *ibid.*, **9**, 161 (1964); (c) *ibid.*, **10**, 25 (1965).
(6) E. L. Heric and K. Yeh, *J. Chem. Eng. Data*, **15**, 13 (1970).
(7) J. P. O'Connell and J. M. Prausnitz, *Ind. Eng. Chem., Fundam.*, **3**, 347 (1964).
(8) J. H. Hildebrand, J. M. Prausnitz, and R. L. Scott, "Regular and Related Solutions", Van Nostrand-Reinhold, New York, N.Y., 1970 p 142.
(9) (a) T. Nitta and T. Katayama, *J. Chem. Eng. Jpn.*, **6**, 1 (1973); (b) *ibid.*, **6**, 298 (1973); (c) *ibid.*, **7**, 310 (1974); (d) *ibid.*, **8**, 175 (1975).
(10) D. A. Wheatland, *J. Chem. Ed.*, **50**, 854 (1973).
(11) M. E. Dorfman and J. H. Hildebrand, *J. Am. Chem Soc.*, **49**, 729 (1927).
(12) For a binary solvent mixture, the excess molar Gibbs free energy over the predictions of the Flory–Huggins equation is related to the defined excess free energy by

$$\Delta\bar{G}_{12}^{fh} = \Delta\bar{G}_{12}^{ex} + RT \ln [(X_1^0\bar{V}_1^0 + X_2^0\bar{V}_2^0)/(\bar{V}_1^0)^{X_1^0}(\bar{V}_2^0)^{X_2^0}]$$

(13) J. F. Murphy and D. E. Baker, *Can. J. Chem.*, **43**, 1272 (1965).
(14) A. Purkayastha and J. Walkley, *Can. J. Chem.*, **50**, 834 (1972).
(15) (a) M. S. Sytilin, *Russ. J. Phys. Chem.*, **48**, 1091 (1974); (b) *ibid.*, **48**, 1353 (1974); (c) *ibid.*, **48**, 1500 (1974).

Solvent Sorption Isotherms, Swelling Pressures, and Free Energies of Swelling of Polystyrenesulfonic Acid Type Cation Exchangers in Water and Methanol

Deoki Nandan and A. R. Gupta*

Chemistry Division, Bhabha Atomic Research Center, Bombay 400085, India *(Received July 13, 1976; Revised Manuscript Received January 3, 1977)*

Swelling pressures (π) in H^+, Li^+, Na^+, and K^+ forms of Dowex 50W resins of 2, 4, 8, and 12% DVB content in methanol and water have been determined from their solvent sorption isotherms, treating 1% DVB resins as reference "uncross-linked" exchangers. These swelling pressures have been discussed in terms of ionic solvation and ion pair formation in the resins. The linear relationships between π and the measured equivalent volumes of the various ionic forms have been discussed in terms of properties of solvents particularly dielectric constant and ion–solvent interactions. The total electrostriction of the solvent at zero swelling pressure [$\Delta\bar{V}_{es}(b)$] and at maximum swelling [$\Delta\bar{V}_{es}$] was found to be the same within experimental precision. The electrostriction per mole of solvent is much higher in MeOH than in water indicating stronger binding of methanol to cations in the resin phase. The integral free energies of swelling (ΔG_{sw}) of these resins are negative. The $-\Delta G_{sw}$ values follow the sequence $H^+ > Li^+ > Na^+ > K^+$ and 1% > 2% > 4% > 8% > 12% DVB. The contribution of the resin cross linking (swelling pressure) to the free energy of swelling of cross-linked resins has been computed with reference to 1% DVB resins. This contribution was found to be small and positive. It has been concluded that generation of swelling pressures is at the expense of secondary solvation of ions and osmotic effects.

Introduction

Swelling behavior of polystyrenesulfonic acid (PSS) type cation exchangers in aqueous medium is well understood.[1,2] A number of studies on the water sorption isotherms of such resins and swelling pressures in them are available.[3-7] Such studies have shown that the swelling behavior of the ion-exchange resins is governed by two processes: (i) hydration of the counterions and the ionogenic groups and (ii) osmotic effects. Swelling of the resinate stretches the polymer network and the resulting swelling pressure, then opposes the processes promoting the swelling of the resins. The same considerations would be applicable in a general way to the swelling of ion exchangers in any solvent. The ion–solvent interactions (and indirectly ion–ion interactions) would differ from solvent to solvent.[8]

Lately, there has been an increasing interest in ion-exchange equilibria in mixed (aqueous–nonaqueous) and nonaqueous solvents because of the enhanced selectivity exhibited by ion exchangers in these media.[9,10] The various factors governing the selective behavior of ion exchangers in mixed and nonaqueous media have been identified.[11-13] Thermodynamically, the free energies of swelling of the resinates, ΔG_{sw}, in different solvents make significant contributions to the exchanger selectivity. It has, generally, been observed that ion-exchange resins swell to a lesser extent in nonaqueous media.[8,10,14] However, no systematic investigation of the swelling behavior of ion-exchange resins in nonaqueous media, which covers the solvent sorption isotherms and the swelling pressures, is available. The pressure–volume terms, which are insignificant from the point of view of ion-exchange selectivity, could be of significance in the individual free energies of swelling of the resinates. Besides, a comparative study of the swelling behavior of PSS type resins in nonaqueous and aqueous media would help in a better understanding of the ion–solvent and ion–ion interactions in the resin phase.

In the present communication, the results of studies on solvent sorption isotherms of various cross-linked (1% to 12% DVB content) Dowex 50W resins in different ionic forms (H^+, Li^+, Na^+, or K^+) in methanol and water are being reported. Similar data on 4, 8, and 12% DVB resins have been reported earlier.[8] From these solvent sorption isotherms, swelling pressures in the resinates have now been estimated using 1% DVB resinates as reference, "uncross-linked" resins. An attempt has also been made to assess the separate contributions of ionic solvation and pressure–volume terms to the overall free energies of swelling of the various resins.

Experimental Section

Methanol and water vapor sorption isotherms of the H^+, Li^+, Na^+, and K^+ forms of 1–2% DVB Dowex 50W resins have been obtained isopiestically covering the solvent activity range of 0.085–1.000 (MeOH) and 0.065–1.000 (water). For the lower methanolic activity range, $LiClO_4$ solutions, and for the lower aqueous activity range, H_2SO_4 solutions were used. Solvent activities in these solutions have been reported by Skabichevskii[15] (MeOH) and by Stokes and Robinson[16] (H_2O). Anhydrous $LiClO_4$ was prepared using lithium carbonate. All chemicals used were of AnalaR grade. The details of the isopiestic unit and other experimental details have been reported earlier.[8] Water and methanol sorption isotherms of 4, 8, and 12% DVB resins in the various ionic forms reported earlier have now been extended in the low solvent activity range from 0.175 to 0.085 (MeOH) and from 0.180 to 0.065 (H_2O).

The time required for the attainment of isopiestic equilibrium for 1 and 2% DVB resins was more than that for 4–12% cross linkings. At high solvent activities, a week's time was needed for equilibrium while at low activities, upto 10 days time was required.

The methanol and water vapor sorption isotherms of 1% DVB Dowex 50W resins in H^+, Li^+, Na^+, and K^+ forms are shown in Figure 1. The isotherms for 2% DVB resins in different ionic forms were similar in shape. A typical set of methanol sorption isotherms of the variously cross-linked H^+ resinate is shown in Figure 2.

The equivalent volumes of the vacuum dried 4, 8, and 12% DVB resins in the H^+, Li^+, Na^+, and K^+ forms were estimated from resin densities measured using specific gravity bottles and toluene as the suspension liquid. The equivalent volumes of these resins swollen in pure

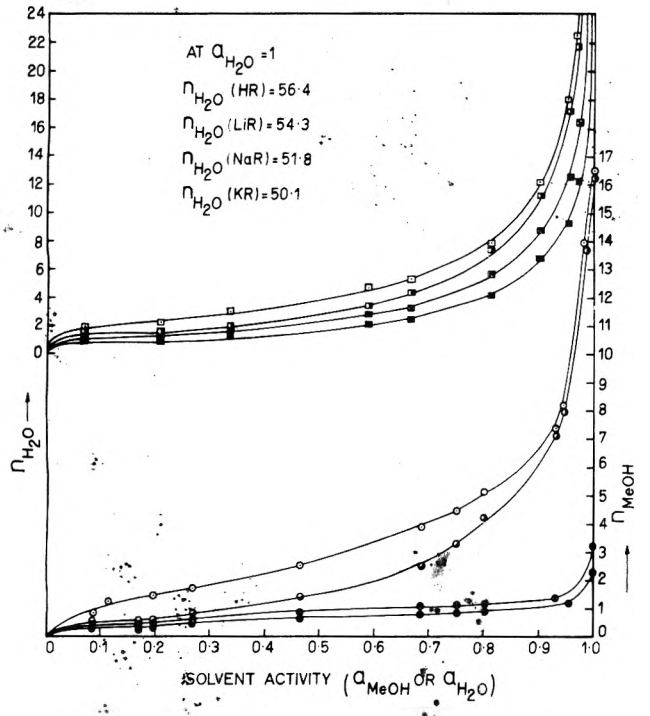

Figure 1. Methanol and water vapor sorption isotherms of Dowex 50WX1 resins at 298 K: (O,□) H^+ form; (◑,◧) Li^+ form; (⊗,⊠) Na^+ form; (●,■) K^+ form.

methanol or water were also determined in a similar way using methanol or water in place of toluene. Surface dried resins were used for these determinations.

Results

A. *Swelling Pressures* (π). The swelling pressure in a resin swollen at a solvent vapor activity a_s is given by

$$\pi = \frac{RT}{\bar{V}_s} \ln \frac{a_s}{\bar{a}_s} \qquad (1)$$

where $\bar{V}_s$ is the partial molal volume of the solvent s (assumed to remain constant throughout the sorption process upto $a_s = 1$), $\bar{a}_s$ is the solvent activity inside the exchanger in equilibrium with outer vapor solvent activity a_s. Generally a very low cross-linked resin (0.5–2% DVB) is treated as an "uncross-linked" reference exchanger.[2] At $a_s = 1$, the solvent activity $\bar{a}_s$ (inside the cross-linked resin under investigation) is given by the external phase activity at which the reference resin has the same molality as the fully swollen cross-linked exchanger.

Swelling pressures have been determined from vapor sorption isotherms employing eq 1. In the present study, 1% DVB resins in the various ionic forms have been treated as the reference uncross-linked resins (Figure 1). Swelling pressures computed for fully swollen resins (a_s = 1) in methanol and water for 2, 4, 8, and 12% DVB resins in the H^+, Li^+, Na^+, and K^+ forms using eq 1 have been summarized in Table I. A comparison of π values in aqueous medium from the present study with those reported by Myres and Boyd[6] using 0.5% DVB reference resins shows a fair agreement except for 12% DVB resins (some differences are expected in resins from different batches). This indicates that the choice of 1% DVB resins is satisfactory. However, for making a comparison of swelling pressures in two different solvents, same resins should preferably be used as has been done in the present study.

The data in Table I show that swelling pressures in MeOH medium are quite high for the H^+ and Li^+ forms

TABLE I: Swelling Pressures[a] (π, atm) and Equivalent Exchanger Volumes ($\bar{V}_e$, mL) of Dowex 50W Resins in Methanol and Water at 298 K

% resin cross linking	Ionic form															
	HR			LiR			NaR			KR						
	$n_{(MeOH)}$	$\bar{V}_e$ (MeOH)	π (H_2O)	$\bar{V}_e$ (H_2O)	π (MeOH)	$\bar{V}_e$ (MeOH)	π (H_2O)	$\bar{V}_e$ (H_2O)	π (MeOH)	$\bar{V}_e$ (MeOH)	π (H_2O)	$\bar{V}_e$ (H_2O)	π (MeOH)	$\bar{V}_e$ (MeOH)	π (H_2O)	$\bar{V}_e$ (H_2O)
2	15		30 (18)		11		27 (17)		8		24 (12)		6		21 (9)	
4	38	434	41 (50)	536	36	432	38 (45)	520	12	216	34 (32)	482	8	206	27 (24)	444
8	125	329	143 (135)	356	119	299	139 (120)	331	18	209	113 (90)	317	12	201	84 (64)	302
12	197	277	213 (290)	312	184	257	205 (245)	296	31	195	158 (190)	280	12	190	121 (135)	265

[a] Values in parentheses are from ref 6.

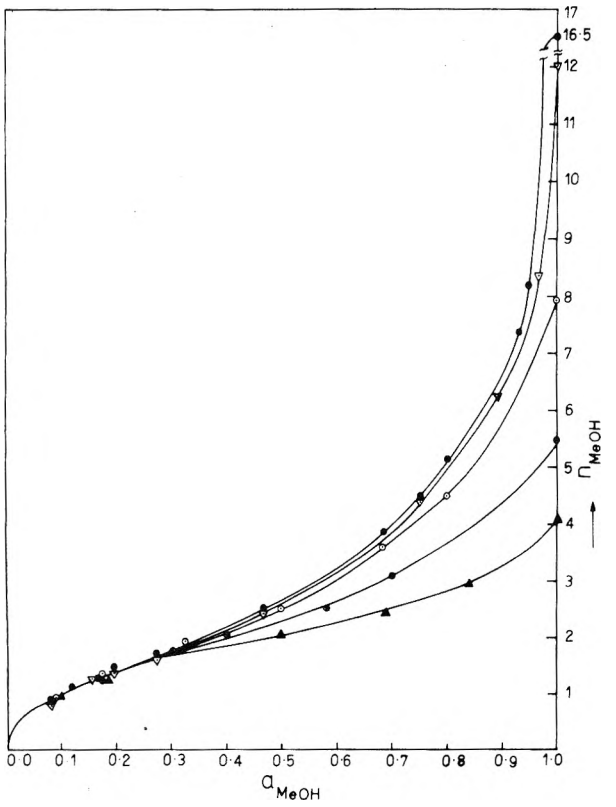

Figure 2. Methanol vapor sorption isotherms of the H^+ form of Dowex 50W resins of 1, 2, 4, 8, and 12% cross linkings at 298 K: 1% (●); 2% (▽); 4% (○); 8% (⊗; 12% DVB (▲).

compared to their values for the Na^+ and K^+ forms. These differences are much more prominent for resins of higher cross-linking. A comparison of these π values with the corresponding values for water swollen resinates shows that H^+ and Li^+ forms show approximately as high values in MeOH as in water for all cross linking. On the other hand, Na^+ and K^+ resins show considerably lower values in MeOH, in particular for the more highly cross-linked resins. The sequence for the swelling pressures in terms of ionic forms of resins in MeOH is thus $\pi_{H^+} > \pi_{Li^+} > \pi_{Na^+} > \pi_{K^+}$.

The equivalent volumes ($\bar{V}_e$) of the various resins at maximum swelling in both solvents have also been given in Table I.

B. *Swelling Free Energies.* The swelling free energy, ΔG_{sw}, of a dry ion exchanger, iR, swollen upto activity a_s is given by[1,2]

$$\Delta G_{sw}(iR) = -RT\int_{a_s=0}^{a_s} n_s \, d \ln a_s + RTn_s \ln a_s$$

or

$$\Delta G_{sw}(iR) = -RT\int_{a_s=0}^{a_s=1} n_s \, d \ln a_s \qquad (\text{at } a_s = 1) \qquad (2)$$

where n_s represents the number of moles of s absorbed at solvent vapor activity a_s. Free energies of swelling of all resinates (H^+–K^+, 1–12% DVB) have been computed from sorption isotherms using eq 2 (for a discussion of the extension of the n_s vs. ln a_s curves to $a_s = 0$, see ref 13) and summarized in Table II. The extension of the reported sorption isotherms of 4, 8, and 12% DVB resins to lower activities as well as $a_s = 1$ has not resulted in any significant changes in ΔG_{sw} values for these resins reported earlier.[13] It should be emphasized here that ΔG_{sw} values as reported in Table II represent the free energy change in the resin system when it goes from a certain reference state (dry ionic form) to its standard state (swollen resin in equilibrium with the pure solvent).

TABLE II: Free Energies of Swelling, ΔG_{sw} (kJ/mol) of Dry H^+, Li^+, Na^+, and K^+ Form Dowex 50W Resinates of 1, 2, 4, 8, and 12% Cross Linkings in MeOH and Water at 298 K

% cross linking	$-\Delta G_{sw}$(MeOH)				$-\Delta G_{sw}$(water)			
	HR	LiR	NaR	KR	HR	LiR	NaR	KR
1	16.9	11.3	6.7	5.6	29.4	22.9	18.0	14.2
2	15.4	9.8	5.9	4.9	27.4	20.1	16.2	13.4
4	14.9	9.0	4.9	4.3	26.8	19.3	15.1	12.6
8	13.5	8.2	4.8	4.1	25.7	18.2	14.1	12.0
12	12.0	6.2	3.9	3.5	24.3	17.3	13.4	11.1

Discussion

Swelling Pressures. The earlier data[13] have indicated ion-pair formation in Na^+ and K^+ forms of resins in methanol and appreciable solvation of the ions in H^+ and Li^+ forms of resins in the same solvent. In the aqueous medium, all the ionic forms show almost full solvation of the ions and no ion-pair formation.[17] This possibility of ion-pair formation in some ionic forms of the resins in nonaqueous media has far reaching consequences for the swelling pressures in these resins. For all ionic forms in aqueous medium and the H^+ and Li^+ forms in methanol, where ionic solvation is very prominent, swelling pressures are high and markedly influenced by resin cross linking (Table I). The effect of the resin cross linking is obviously due to the greater resistance of higher cross-linked resins to osmotic swelling. On the other hand, ion-pair formation in the Na^+ and K^+ forms of resins in methanol results in very small swelling pressures and small variations in them with resin cross linking (Table I). It has been shown from the swelling pressure studies in aqueous medium that a low swelling pressure in a resin indicates greater preference of the resin for the ion.[1] The extremely low swelling pressures in the K^+ form of the present resins in methanol are in conformity with the high selectivity of these resins for K^+ in methanol.[13] The increase in the swelling pressures in higher cross-linked resins should decrease the selectivity. The observed increase in selectivity of higher cross-linked resin is due to a relatively much greater increase in the swelling pressure of the H^+ form, which is used as a reference resin for selectivity studies, with increasing cross linking.

Equivalent Volumes of the Resins and Electrostriction of the Solvent. Boyd and Soldano[3] have observed a linear relationship between swelling pressures (π) and equivalent volumes ($\bar{V}_e$) of the resin Dowex 50X8 in various ionic forms, i.e.

$$\bar{V}_e = a\pi + b \qquad (3)$$

They observed an increase in the constant a, which reflects the elastic properties of the exchanger with the resin cross linking. If the constant a is truly a property of the resin structure and reflects the elasticity of the network, it should be independent of the solvent. The constant b has been interpreted by Boyd and Soldano[3] as the volume occupied by the polymer network when the end-to-end chain distance is the same as in the monomer. Polystyrenesulfonic acid and its salts have highly extended structures in aqueous medium.[18] The end-to-end chain distance in a polymer chain depends upon the interactions between adjacent ionogenic groups and the ionogenic group and the counterion. These interactions would depend upon the nature of the solvent. In a solvent of lower dielectric constant, "site binding" of the counterions would increase and this in turn would reduce the repulsion between adjacent ionogenic groups, leading to a decreased

TABLE III: Electrostriction Values at $\pi = 0$ [$\Delta\bar{V}_{es}(b)$] and for Fully Swollen Dowex 50W Resins [$\Delta\bar{V}_{es}$] of 4 and 8% DVB in H^+, Li^+, Na^+ and K^+ Forms in Methanolic and Aqueous Systems[a]

	4% DVB					8% DVB				
Ionic form	$\bar{V}_e$(dry resin = $\bar{V}_r$)	Aqueous $\Delta\bar{V}_{es}$	Aqueous $\Delta\bar{V}_{es}(b)$	MeOH $\Delta\bar{V}_{es}$	MeOH $\Delta\bar{V}_{es}(b)$	$\bar{V}_e$(dry resin = $\bar{V}_r$)	Aqueous $\Delta\bar{V}_{es}$	Aqueous $\Delta\bar{V}_{es}(b)$	MeOH $\Delta\bar{V}_{es}$	MeOH $\Delta\bar{V}_{es}(b)$
H^+	137	7 (0.31)	10 (2.22)	21 (2.64)	25 (14.7)	144	11 (0.89)	15 (3.41)	35 (6.36)	32 (18.82)
Li^+	140	11 (0.51)	9 (2.09)	12 (1.55)	8 (6.67)	145	17 (1.50)	12 (2.89)	4 (1.01)	5 (5.00)
Na^+	148	13 (0.67)	8 (2.11)	11 (5.58)	8 (8.00)	152	15 (1.50)	12 (3.16)	15 (8.38)	12 (12.00)
K^+	152	14 (0.82)	9 (2.50)	11 (6.75)	8 (8.89)	156	11 (1.26)	7 (2.12)	19 (11.80)	12 (13.33)

[a] Values in parentheses give electrostriction based on per mole of solvent absorbed.

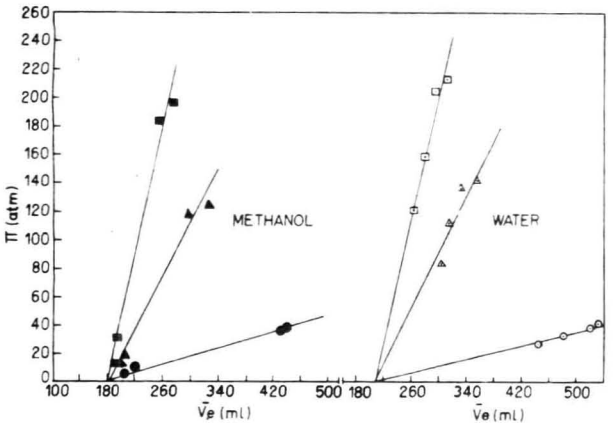

Figure 3. Variation of swelling pressure (π) with equivalent exchanger volume ($\bar{V}_e$) for Dowex 50W resins of 4, 8, and 12% DVB in MeOH and H_2O: (O,●) 4% DVB; (Δ,▲) 8% DVB; (□,■) 12% DVB.

extension of the resin network. This implies that constant b should depend upon the solvent. $\bar{V}_e$ for the variously cross-linked resins in different ionic forms (Table I) have been plotted against π for methanol as well as aqueous systems (Figure 3). Though the points for methanolic systems look scattered, still a linear relationship between $\bar{V}_e$ and π can be seen. The empirical relation, eq 3, is thus applicable to nonaqueous systems. The linear plots (different ionic forms but same cross linking) for different cross linkings in both the solvents converge to a common point at zero swelling pressure. Again due to greater scatter of data in the methanolic systems, the convergence is not as good as in aqueous systems. Still a value of 180 ± 5 mL for constant b can be derived from these plots for methanolic systems and 208 mL for aqueous systems. Boyd and Soldano[3] have also observed a comparable value of 192 mL for b for Dowex 50X8 resin in aqueous medium. The lower value of b in methanol is due to the lower dielectric constant of methanol which influences the end-to-end chain distance in the unstrained form, as discussed above. The constant a is nearly the same for aqueous and methanolic systems for any specific cross linking. Its values (L atm^{-1} mol^{-1}) for different cross linkings are as follows: 4% DVB, 0.14 ± 0.02; 8% DVB, 0.9 ± 0.1; and 12% DVB, 2.1 ± 0.1. These data then confirm the following: (i) constant a is independent of the solvent but depends upon the cross linking and (ii) constant b is independent of cross linking but depends upon the solvent.

From the above analysis, it is clear that resins swell to a volume b ($\bar{V}_b$) before swelling pressures start developing in the network, i.e., upto that point swelling pressures are zero. From the solvent sorption isotherms of the resins, the swelling pressures are zero upto the point where the isotherms for the uncross-linked and cross-linked resins are identical, i.e., at the solvent activity where the cross-linking effects appear in the sorption isotherms. It seems logical to identify $\bar{V}_b$ with the zero swelling pressure point in the sorption isotherms. (This is also implied in the linear relationship between π and the equivalent volumes of partially swollen resinates, observed by Boyd and Soldano.)[3] The volume of the solvent imbibed by different resins in volume $\bar{V}_b$ can then be computed. In this region of low solvent activity, the most important process taking place is the solvation of the ions. It is during this process that the solvent is subjected to the maximum amount of electrostriction. This electrostriction of the solvent in the resin swollen to volume $\bar{V}_b$ is [$\Delta\bar{V}_{es}(b)$] given by

$$\Delta\bar{V}_{es}(b) = n_s' V_s - (\bar{V}_b - \bar{V}_r) \quad (4)$$

where n'_s is the number of moles of solvent absorbed by the cross-linked resin when its sorption isotherm separates out from the reference, uncross-linked resin, V_s the molar volume of the solvent, and $\bar{V}_r$ the equivalent volume of the dry resin. The total electrostriction of the solvent when the resins are fully swollen ($\Delta\bar{V}_{es}$) can be calculated using the relation

$$\Delta\bar{V}_{es} = n_s V_s - (\bar{V}_e - \bar{V}_r) \quad (5)$$

where n_s is the number of moles of solvent in resin when swollen to the maximum. The computed values of $\Delta\bar{V}_{es}(b)$ and $\Delta\bar{V}_{es}$ along with other details for Dowex 50WX4 and Dowex 50WX8 resins in water and methanol are given in Table III. A comparison of $\Delta\bar{V}_{es}$ and $\Delta\bar{V}_{es}(b)$ shows that they do not differ from one another by more than ±3 mL, except in the case of the K^+ form of Dowex 50WX8 in methanol. As these computations involve $\bar{V}_e$, $\bar{V}_r$, n'_s, n_s, and $\bar{V}_b$, the values for $\Delta\bar{V}_{es}$ and $\Delta\bar{V}_{es}(b)$ cannot be better than ±3 mL. On the whole, one can conclude from the data in Table III that there is no further electrostriction of the solvent in the resin after it reaches a volume $\bar{V}_b$. A similar behavior had been observed by the earlier workers also.[3,19-22] They had noted that the partial molal volume of water in the resin becomes the same as the molar volume, after a certain stage of swelling has been reached. That stage in the swelling of the resins has now been shown to be the stage when the swelling pressures in the resin starts increasing from zero. From data given in ref 3, electrostriction of the solvent in the fully and partially swollen Dowex 50X8 (H^+ form) in water has been computed and was found to be the same at all stages of swelling beyond $\pi = 0$. This result when combined with the observed linearity between π and $\bar{V}_e$ (partially swollen resins) suggests the constancy of the electrostriction of the solvent

TABLE IV: A Comparison of ΔG_{sp} (kJ/mol) for Various Ionic Forms and Cross Linkings of Dowex 50W Resins for Methanolic and Aqueous Systems Computed on the Basis of Eq 6 and 7

Ionic form	System	2% DVB		4% DVB		8% DVB		12% DVB	
		Eq 6	Eq 7	Eq 6	Eq 7	Eq 6	Eq 7	Eq 6	Eq 7
H^+	MeOH	0.54	0.46	0.71	0.76	1.08	1.32	1.31	1.32
Li^+	MeOH	0.48	0.38	0.71	0.72	1.00	0.92	1.20	1.20
Na^+	MeOH	0.06	0.02	0.06	0.02	0.06	0.03	0.08	0.04
K^+	MeOH	0.03	0.01	0.03	0.01	0.03	0.01	0.03	0.01
H^+	H_2O	1.08	1.12	1.14	1.12	1.25	1.33	1.31	1.21
Li^+	H_2O	1.02	1.12	1.08	1.12	1.36	1.51	1.59	1.58
Na^+	H_2O	0.63	0.70	0.80	0.75	0.97	0.78	1.14	1.01
K^+	H_2O	0.46	0.60	0.57	0.62	0.74	0.71	0.97	0.82

down to zero swelling pressure. In an earlier discussion of solvent sorption isotherms,[8] it has been suggested that the primary solvation of the ions is essentially complete in the solvent activity region where the solvent sorption isotherms of variously cross-linked resins are identical. The electrostriction data in Table III give further support to this interpretation.

The electrostriction of the solvent generally increases with the electrolyte concentration.[23] This effect can be readily seen if the $\Delta\bar{V}_{es}$ data in Table III are converted to $\Delta\bar{V}_{es}$ per mole of solvent. The latter quantity generally increases with resin cross linking, and for the same cross linking it increases as the overall swelling of the resin decreases. The magnitude of the ion–solvent interactions is reflected in $\Delta\bar{V}_{es}$(b) per mole of solvent. For methanolic systems this is ~11 mL compared to ~2.5 mL in aqueous systems. The stronger binding of methanol to cations is clearly indicated. This is consistent with the free energies of transfer of the single cations from methanol to water.[24]

Free Energies of Swelling of the Resins. Swelling free energies, ΔG_{sw}, would have the largest contribution from the free energies of solvation of the ions and thus would reflect the state of the ionic solvation in the resin phase. The data in Table II show that ΔG_{sw} in the aqueous medium range from ~29 (H^+ form, 1% DVB) to ~11 kJ/mol (K^+ form, 12% DVB), thus showing appreciable solvation of the ions in the resin phase. In comparison ΔG_{sw} for the Na^+ and K^+ forms of resins in methanol are ~5 kJ/mol, indicating much lesser solvation of these ions in this medium.

The free energies of swelling increase as the cross linking increases. The contribution of the cross linking, i.e., of swelling pressure, to these free energies can be estimated by comparing the free energy of swelling of a cross-linked resinate (ΔG_{sw}) with the free energy of swelling of an uncross-linked reference resinate ($\Delta\bar{G}_{sw}$) swollen to the same extent as the cross-linked one, i.e., having the same molality in the resin phase.

Using eq 2 for ΔG_{sw} and $\Delta\bar{G}_{sw}$, we obtain

$$\Delta G_{sw} - \Delta\bar{G}_{sw} = -RT\int_{a_s=0}^{a_s=1} n_s \, d \ln a_s + RT\int_{\bar{a}_s=0}^{\bar{a}_s} n_s \, d \ln \bar{a}_s - RTn_s \ln \bar{a}_s = \Delta G_{sp} \quad (6)$$

These differences between ΔG_{sw} and $\Delta\bar{G}_{sw}$, designated by ΔG_{sp} (sp represents the swelling pressure), have been computed by graphical integration of n_s vs. ln a_s plots between the appropriate limits. The computed values of ΔG_{sp} for the various resinates in methanol and water have been tabulated in Table IV. These are positive quantities, emphasizing that the decrease in the free energy during the swelling of a cross-linked exchanger is less than in an uncross-linked one, swollen to the same extent. This then is the energy used in the extension of the resin network during the swelling process. Another approach to estimate ΔG_{sp}, which uses swelling pressure data and directly gives the contribution of swelling pressures to swelling free energies, is as follows.

Substituting for ln a_s in eq 2 from eq 1, we obtain

$$\Delta G_{sw} = -RT\int_{a_s=0}^{a_s=1} n_s \, d\left[\frac{\pi\bar{V}_s}{RT} + \ln \bar{a}_s\right] + n_s RT\left[\frac{\pi\bar{V}_s}{RT} + \ln \bar{a}_s\right] = -RT\int_{\bar{a}_s=0}^{\bar{a}_s} n_s \, d \ln \bar{a}_s + n_s RT \ln \bar{a}_s - \bar{V}_s\int_{\pi(a_s=0)}^{\pi(a_s=1)} n_s \, d\pi + \bar{V}_s n_s \pi$$

Transferring the first two terms on right-hand side, which are equal to $\Delta\bar{G}_{sw}$, to left-hand side, we obtain

$$\Delta G_{sw} - \Delta\bar{G}_{sw} = \Delta G_{sp} = -\bar{V}_s\int_{\pi(a_s=0)}^{\pi(a_s=1)} n_s \, d\pi + \bar{V}_s n_s \pi \quad (7)$$

The values of ΔG_{sp} from eq 7, computed by graphically integrating π vs. n_s plots between the appropriate limits, are also given in Table IV. The good agreement between these two sets of ΔG_{sp} values supports the above interpretation of swelling free energies of ion exchangers.

As the primary solvation of the ions in the resin is essentially complete before the swelling pressures develop, the processes contributing to free energy changes in the solvent activity region where swelling pressures are positive are secondary solvation of the ions and the osmotic swelling. It is at the expense of these processes which involve comparatively small free energy changes that resin network is stretched. The small values of ΔG_{sp} (~1 kJ/mol) are consistent with this analysis.

The overall picture of the swelling of resins then emerges as follows. The solvation of the ions in the resin phase takes place at low solvent activities. This entails considerable electrostriction of the solvents. The swelling pressure remains zero while this is taking place though the volume of the resin increases. This volume increase, without swelling pressure, is due to the end-to-end chain distance in the polymer network approaching that of the unstrained monomer. The end-to-end polymer chain distance in turn depends upon the nature of the solvent and its interactions with the ions and ionogenic groups. As the polymer network in variously cross-linked resins or different ionic forms is identical, the unstrained fully stretched volume of different resins is also the same. In this region of solvent activity, the free energies of swelling are independent of resin cross-linking. In the region of higher solvent activity, resin network is stretched, swelling pressures develop, and the free energies of swelling are more positive. This loss of free energy, which is the energy spent in stretching the network, is at the expense of secondary solvation and osmotic swelling. There is no electrostriction of the solvent in this region.

Acknowledgment. The authors wish to express their sincere thanks to Dr. M. D. Karkhanavala for his interest

and encouragement during the course of this investigation.

References and Notes

(1) F. Helfferich, "Ion Exchange", McGraw-Hill, New York, N.Y., 1962.
(2) G. V. Samsonov and V. A. Pasechnik, *Russ. Chem. Rev.*, **38**, 547 (1969).
(3) G. E. Boyd and B. A. Soldano, *Z. Elektrochem.*, **57**, 162 (1953).
(4) H. P. Gregor, B. R. Sundheim, K. M. Held, and M. H. Waxman, *J. Colloid Sci.*, **7**, 511 (1952); *J. Phys. Chem.*, **57**, 974 (1953).
(5) E. Glueckauf, *Proc. R. Soc. (London), Ser. A*, **214**, 207 (1952).
(6) G. E. Myers and G. E. Boyd, *J. Phys. Chem.*, **60**, 521 (1956).
(7) O. D. Bonner, V. F. Holland, and L. L. Smith, *J. Phys. Chem.*, **60**, 1102 (1956).
(8) D. Nandan and A. R. Gupta, *Ind. J. Chem.*, **12**, 808 (1974).
(9) G. J. Moody and J. D. R. Thomas, *Analyst*, **93**, 557 (1968).
(10) Y. Marcus, "Ion Exchange and Solvent Extraction", Vol. 4, J. A. Marinsky and Y. Marcus, Ed., Marcel Dekker, New York, N.Y. 1973, pp 1–119.
(11) A. R. Gupta, *J. Phys. Chem.*, **75**, 1152 (1971).
(12) D. Nandan, A. R. Gupta, and J. Shankar, *Ind. J. Chem.*, **10**, 285 (1972); **11**, 655 (1973).
(13) D. Nandan and A. R. Gupta, *J. Phys. Chem.*, **79**, 180 (1975).
(14) D. J. Pietrzyk, *Talanta*, **16**, 169 (1969).
(15) P. A. Skabichevskii, *Russ. J. Phys. Chem.*, **44**, 1162 (1970).
(16) R. H. Stokes and R. A. Robinson, *Ind. Eng. Chem.*, **41**, 2013 (1949).
(17) G. E. Boyd, F. Vaslow, and S. Lindenbaum, *J. Phys. Chem.*, **68**, 590 (1964).
(18) A. Caille and H. Daoust, *J. Polym. Sci., Symp. Ser*, **No. 45**, 153 (1974).
(19) K. W. Pepper, D. Reichenberg, and D. K. Hale, *J. Chem. Soc.*, 3129 (1952).
(20) K. W. Pepper and D. Reichenberg, *Z. Elektrochem.*, **57**, 183 (1953).
(21) H. P. Gregor, F. Guttoff, and J. I. Bregman, *J. Colloid Sci.*, **6**, 245 (1951).
(22) E. Hogfeldt, *Acta Chem. Scand.*, **12**, 182 (1958).
(23) J. Padova, *J. Chem. Phys.*, **40**, 691 (1964).
(24) J. Padova, *J. Chem. Phys.*, **56**, 1606 (1972).

Spectroscopic Characterization and Thermal Stability of Copper(II) Ethylenediamine Complexes on Solid Surfaces. 1. Synthetic Faujasites Types X and Y

Paul Peigneur,† Jack H. Lunsford,*

Texas A & M University, Department of Chemistry, College Station, Texas 77843

Willy De Wilde, and Robert A. Schoonheydt

Katholieke Universiteit Leuven, Centrum voor Oppervlaktescheikunde en Colloïdale Scheikunde, De Croylaan 42, B-3030 Heverlee, Belgium

(Received October 6, 1976)

Publication costs assisted by the National Science Foundation (USA) and Diensten van het Wetenschapsbeleid (Belgium)

Bis(ethylenediamine)copper(II) complexes were ion exchanged from aqueous solution into zeolites X and Y. In Y-type zeolites only the bis complex was observed, but in X-type zeolites mono(ethylenediamine)copper(II) and aquo complexes were also detected in varying amounts, depending on the preparation. Exchange from solutions with an en:Cu ratio of one gives zeolites which contain bis, mono, and aquo complexes. Their relative amounts depend on the preparation conditions, the exchange level, and the type of zeolite. Tris(ethylenediamine)copper(II) complexes were prepared by adsorption of ethylenediamine from the gas phase on dehydrated zeolites with small Cu(II) loadings. The three complexes have apparent axial symmetry. The analysis of the EPR and electronic spectra of the bis complex on the surface shows a small but significant increase of the covalent character of the out-of-plane π orbitals with respect to the complexes in aqueous solution. The replacement of axially coordinated water molecules in solution by surface oxygens in zeolites is thought to be responsible for that effect.

1. Introduction

The preparation, structure, and catalytic properties of copper(II) zeolites have been the subject of numerous investigations involving various experimental techniques.[1-3] Earlier studies dealt with the simple copper(II) ion.[4-6] More recently, attention has been given to complexes which may be synthesized within the zeolite framework.[7-12] These complexes are normally prepared by adsorbing the ligand from the gas phase into dehydrated copper(II) zeolites. Ammonia, monodentate amines, or pyridine have been the most widely studied ligands.

Cremers and co-workers[13,14] have demonstrated that the ion-exchange properties may be drastically altered by complexing an ion before exchange. In an effort to understand this phenomenon we have attempted to characterize, by means of spectroscopic techniques, the copper–ethylenediamine complexes after they have been exchanged into zeolites and certain clay minerals. In this paper data are presented on the mono(ethylenediamine)copper(II) ($Cu(en)^{2+}$), the bis(ethylenediamine)-copper(II) ($Cu(en)_2^{2+}$), and the tris(ethylenediamine)-copper(II) ($Cu(en)_3^{2+}$) complexes in the synthetic faujasites X and Y.

The ethylenediamine (en) molecule is one of the simplest bidentate ligands which is known to form stable complexes with a number of transition metal ions. In aqueous solution the logarithm of the stepwise stability constants for en with copper(II) are 10.73 for the first and 9.31 for the second ligand.[15] Since the log K_3 value is relatively small (log $K_3 \simeq 1$), the tris complex can only be formed in concentrated ethylenediamine solutions.

All three of these complexes have been studied extensively by EPR and optical spectroscopy as well as by x-ray diffraction, both in solution and in crystalline forms.[16-22] The mono, bis, and tris complexes have distinctly different EPR and optical spectra. The EPR and electronic spectra reflect variations in the anion that is associated with each

† On leave of absence from Centrum voor Oppervlaktescheikunde en Colloïdale Scheikunde, De Croylaan 42, B-3030 Heverlee, Belgium.

of the three complexes. Therefore, data taken on solutions and salts provide good references for the present study of the same complexes in zeolites.

2. Experimental Section

Preparation of $Cu(en)_2^{2+}$ and $Cu(en)^{2+}$ in Zeolites X and Y. The commercially available zeolites X and Y in their Na^+ forms were obtained from Union Carbide's Linde Division and exchanged at room temperature with a 1 N NaCl solution, washed, dried, and stored in a desiccator over a saturated NH_4Cl solution. Aqueous solutions of $Cu(en)_2^{2+}$ and $Cu(en)^{2+}$, 0.05 N in Cu^{2+}, were prepared by dissolving the appropriate quantities of $CuCl_2 \cdot 2H_2O$ or $Cu(NO_3)_2 \cdot 3H_2O$ into a 0.05 M en solution. In the case of the bis complex a small excess of en (5×10^{-4} M) was added. The resulting pH values were 10.20 and 6.00 for the bis and mono complexes, respectively. Five grams of zeolite were exchanged with 1 L of these solutions at room temperature for 48 h. With the bis complex the exchange was performed at pH 8.5 and 7.0 or without pH control. Control of the pH was achieved by adding HCl or HNO_3, according to the anion of the cupric salt, to the exchange mixture. When the exchange was performed without pH control, the final pH was 8.75. With the mono complex the exchange was carried out at pH 6.8 or without pH control. In the former case, the addition of the zeolite to the complex solution increased the pH to 6.75. It tended to decrease by 0.2 units during the first part of the exchange reaction (ca. 5 h for Y or 24 h for X), but this was compensated by adding NaOH. In the latter case the final pH values were 6.10 and 6.30 for Y and X zeolites, respectively. In another series of preparations quantities of solution necessary to obtain ca. 10% exchange were diluted to 1 L and the exchange was performed as described above. For the bis complexes this had no effect on the evolution of the pH, but for the mono complexes, the addition of the zeolite to the exchange solution increased the pH to 7.70 both for X and Y. It was adjusted with HCl or HNO_3, according to the anion of the cupric salt, to pH 6.8 for the pH controlled exchange and kept at that value during exchange. When the exchange was performed without pH control, the final pH values were 7.85 for X and 9.25 for Y type zeolites.

The samples were analyzed for their Na^+ and Cu^{2+} contents by atomic absorption spectrometry and for their en content by the Kjeldahl method. The analytical data are shown in Table I together with the pH of exchange. When the pH is not indicated, it was not controlled during exchange. In the symbols used $Cu(en)_2$ or Cu(en) is followed by X or Y to indicate the type of zeolite. The numbers after these symbols increase with increasing copper loading. The samples indicated by a prime in Table I were exchanged as described above, but after exchange the suspensions were allowed to settle down in the reflectance cell without washing and drying.

Optical spectra at room temperature were obtained for the $Cu(en)_2^{2+}$ and $Cu(en)^{2+}$ loaded zeolites in their hydrated forms and after stepwise evacuation under vacuum (10^{-5} Torr) up to 723 K. At each temperature the evacuation time was 48 h. Evacuations at 473 K and higher were followed by a static O_2 treatment at room temperature or at the evacuation temperature with a maximum of 573 K.

For the EPR experiments samples with 0.5 to 1 $Cu(en)_2^{2+}$ per unit cell were prepared. At higher complex exchange levels the unresolved line due to spin–spin exchange dominated the spectrum.[23] Usually 1 g of NaX or NaY and 40 cm^3 of a solution containing the desired quantity of $Cu(en)_2^{2+}$ were used. The anion was NO_3^- and the exchange solution also contained 0.01 N $NaNO_3$. The ion-exchange reaction was carried out at room temperature for 4 days under continuous stirring at a pH of 8.0. It was found that at these low exchange levels the total amount of complex in the solution was exchanged into the solid.[13,14] Therefore, the samples were not washed but immediately centrifuged, the supernatant decanted, and the zeolite dried in air at 293 K. A solution with a Cu:en ratio equal to 1 was prepared and exchanged under identical conditions as the bis complex but without pH control.

TABLE I: Exchangeable Cation Content per Unit Cell and en:Cu Ratios of $Cu(en)_2^{2+}$, $Cu(en)^{2+}$, and Cu^{2+} Exchanged Zeolites X and Y

Symbol	Na^+	Cu^{2+}	en:Cu	pH of exchange
$Cu(en)_2Y$-1	45.7	2.6	2.8	
$Cu(en)_2Y$-1′		2.8		
$Cu(en)_2Y$-2	17.2	13.3	2.4	8.5
$Cu(en)_2Y$-3	14.2	11.1	2.5	7
$Cu(en)_2X$-1	74.4	3.2	2.26	
$Cu(en)_2X$-1′		4.3		
$Cu(en)_2X$-2	42.5	10.7	2.9	8.5
$Cu(en)_2X$-3	34.0	13.4	2.2	7
$Cu(en)_2X$-4	46.4	14.0	2.2	
Cu(en)Y-1	45.6	3.2	1.1	6.75
Cu(en)Y-1′	48.1	2.9	0.89	
Cu(en)Y-2	35.2	12.1	0.62	6.8
Cu(en)Y-3	14.2	21.2	1.0	
Cu(en)X-1	61.8	4.7	1.0	6.75
Cu(en)X-1′	69.8	4.3	0.75	
Cu(en)X-2	26.1	34.2	0.50	6.8
Cu(en)X-3	23.5	30.1	0.57	
CuY-1	53.7	0.6		
CuY-2	54.8	1.3		
CuY-3	52.2	2.6		
CuY-4	21.1	17.5		
CuX-1		<1		
CuX-2	77.5	4.7		
CuX-3	65.4	8.5		
CuX-4	21.9	36.3		

Preparation of $Cu(en)_3^{2+}$ in Zeolites X and Y. Copper(II) zeolites with different loadings were obtained by conventional ion exchange. Their exchangeable cation content is shown in Table I.

For the optical measurements these samples were dehydrated in vacuo up to 723 K and in a static atmosphere of O_2 at 723 K with renewal of the O_2. The reflectance spectra of the dehydrated samples were taken at room temperature in O_2. Oxygen was pumped off and en was allowed to adsorb in a stepwise manner. Each dose was equivalent to ca. 0.5 en/Cu^{2+}. After each step the sample was allowed to equilibrate for 2 days at room temperature or at 353 K prior to recording the spectrum. This procedure was continued up to 3 en/Cu^{2+}. Finally, after the samples were allowed to equilibrate in en vapor the spectra were taken again. For comparison purposes a tris complex was prepared by dissolving Cu(II) in pure en and its spectrum was recorded.

For the EPR experiments only CuY-1 and CuX-1 were used. They were degassed in vacuo with hourly increases of 100 K up to 673 K. Oxygen was adsorbed at that temperature and the sample cooled down. After evacuation of O_2 the sample was equilibrated in en vapor at 373 K for 3 h. The spectra were compared with those obtained after adsorption of en vapor on hydrated zeolites loaded with $Cu(en)_2^{2+}$. These en-saturated samples were also submitted to a desorption process of hourly increases of 50 K until 473 K. The EPR spectra were recorded after each step. A tris-complex solution obtained by dissolving

TABLE II: Band Frequencies and Half-Bandwidths (hbw) of Experimental Spectra and Their Decomposition into Contributions from $Cu(en)_2^{2+}$, $Cu(en)^{2+}$, and $Cu(H_2O)_6^{2+}$

	Experimental			Deconvoluted spectra					
				$Cu(en)_2^{2+}$		$Cu(en)^{2+}$		$Cu(H_2O)_6^{2+}$	
Sample	Wavenumber, cm^{-1}	hbw, cm^{-1}	Drying temp, K	Wavenumber ±100, cm^{-1}	Rel int, %	Wavenumber ±500, cm^{-1}	Rel int, %	Wavenumber ±500, cm^{-1}	Rel int, %
$Cu(en)_2Y$-1	18300	4900	333	18300	100				
$Cu(en)_2Y$-1′	18200	5700	wet + RT	18200	100				
$Cu(en)_2Y$-2	18300	4800	333	18300	100				
$Cu(en)_2Y$-3	18400	5100	333	18400	100				
$Cu(en)_2X$-1	18000	6800	RT	18300	75	15300	10	12500	15
$Cu(en)_2X$-1′	18300	5200	wet + RT	18300	94	15300	6	12500	0
$Cu(en)_2X$-2	17600	6000	333	18300	60	15300	35	12500	5
$Cu(en)_2X$-3	16400	7500	333	18300	51	15300	29	12500	20
$Cu(en)_2X$-4	17300	7200	RT	18300	61	15300	33	12500	6
Cu(en)Y-1	13800	7200	333	18300	4	15300	38	12500	58
Cu(en)Y-1′	14900	7700	RT	18300	21	15300	52	12500	27
			wet	18300	31	15500	47	12500	27
Cu(en)Y-2	15700	7300	333	18300	25	15300	51	12500	24
Cu(en)Y-3	15200	7300	RT	18300	30	15300	45	12500	25
Cu(en)X-1	13200	6900	333	18300	8	15300	14	12500	78
Cu(en)X-1′	14800	7000	RT	18300	16	15300	78	12500	4
			wet	18300	27	15300	58	12500	16
Cu(en)X-2	15300	7000	333	18300	12	15300	35	12500	53
Cu(en)X-3	13900	7100	RT	18300	7	15300	43	12500	45

0.02 M $Cu(NO_3)_2$ in 8 M en was also investigated by EPR after addition of a 100-fold excess $NaNO_3$.

Procedures. All optical spectra were taken on a Cary 17 instrument in the region 1800–360 nm with a type II reflectance unit. The reflectance cell for the optical measurements was similar to that described by Klier.[24] The standard was MgO placed in a matching vacuum cell. The spectra were digitalized and plotted as $F(R_\infty)$ against the wavenumber (cm^{-1}). $F(R_\infty)$ is the Kubelka–Munk function.[25] These optical spectra were compared with those of $Cu(en)_2^{2+}$ and $Cu(en)^{2+}$ solutions.

All EPR measurements were carried out with the samples at 77 K. Spectra were recorded for the air-dried samples after a short evacuation to remove the O_2. In addition all samples were evacuated overnight at room temperature and heated under vacuum in stepwise hourly increases of 50 K to a maximum of 473 K. The EPR spectra were taken after each step. The measurements were carried out using a Varian E-6s spectrometer with a rectangular TE_{102} X-band cavity. The g values were determined relative to a DPPH standard. The spectra were simulated assuming axial symmetry and using a computer program SIM 13 written by Lozos, Hoffman, and Franz of Northwestern University. The parallel parameters could be measured directly from the experimental spectra and the perpendicular parameters were adjusted until a sufficient fit was obtained. The estimated error is ±0.005 for the g values, ±0.0002 cm^{-1} for $A_\parallel$ and ±0.0004 cm^{-1} for $A_\perp$. The experimental EPR spectra were compared with those of the $Cu(en)_2^{2+}$ and $Cu(en)^{2+}$ solutions used to prepare the zeolites, after addition of a 100-fold excess $NaNO_3$ with respect to Cu^{2+}.

3. Results

$Cu(en)_2^{2+}$ Exchanged Zeolites. $Cu(en)_2^{2+}$ loaded zeolites have a characteristic violet color. Typical spectra are shown in Figure 1. All the Y-type zeolites show one band at 18300 cm^{-1} (Figure 1A) with a half-bandwidth of 5000 ± 200 cm^{-1}, in excellent agreement with the aqueous solution spectrum for which the band maximum is at 18200 cm^{-1}. The spectrum of a wet sample ($Cu(en)_2Y$-1′) had the same band position but somewhat larger bandwidth. The band at 7000 cm^{-1} contains the overtones of the hydroxyl

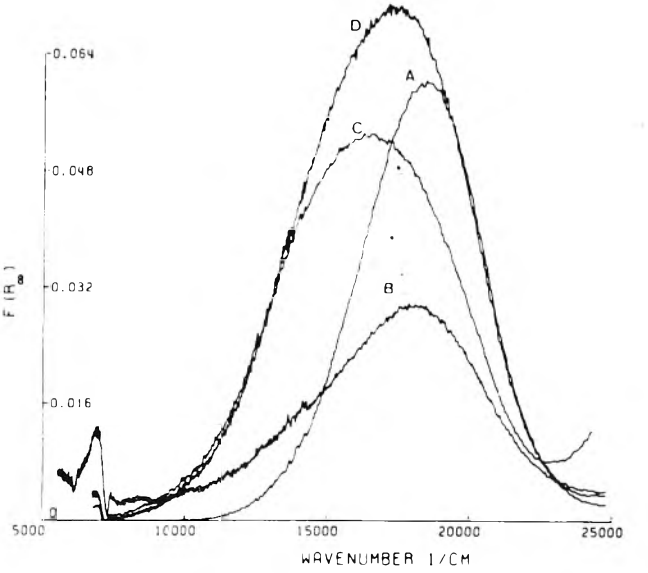

Figure 1. The reflectance spectra of the $Cu(en)_2^{2+}$ loaded zeolites X and Y: A, $Cu(en)_2Y$-3; B, $Cu(en)_2X$-1; C, $Cu(en)_2X$-3; D, $Cu(en)_2X$-4.

stretching vibrations of adsorbed water and lattice hydroxyl groups. Its low frequency tail is the adsorption of the N–H stretching mode of ethylenediamine. Table II summarizes the band frequencies and half-bandwidths.

The spectra of the $Cu(en)_2X$ zeolites show also one band (Figure 1). However, the band position and the half-bandwidth depend on the loading and the preparation conditions of the samples. The spectrum of a suspension after exchange ($Cu(en)_2X$-1′) was identical with those of the Y-type zeolites with a band maximum at 18200 cm^{-1} and a half-bandwidth of 5200 cm^{-1} and did not change after air drying at room temperature. A similar sample ($Cu(en)_2X$-1), air-dried at room temperature before storage, gave a broader band with a maximum around 18000 cm^{-1} (Figure 1B). At higher exchange levels the band maxima shift to lower frequencies and the half-bandwidths increase with respect to those of the $Cu(en)_2^{2+}$ solutions. The pertinent data are summarized in Table II and in Figures 1C and 1D. These low frequency shifts and half-bandwidth increases are indicative of the presence of more than

TABLE III: g Values and Cu^{2+} Hyperfine Splitting Constants for Cu(II)-(Ethylenediamine) Complexes in Zeolites X and Y and in Frozen Solution

Sample	$g_\parallel$	$A_\parallel^{Cu} \times 10^3$ cm^{-1}	$g_\perp$	$A_\perp^{Cu} \times 10^3$ cm^{-1}
$Cu(en)_2Y$	2.194	19.4	2.035	2.8
$Cu(en)_2X$	2.176	20.2	2.034	3.8
$Cu(en)_2$-solution	2.190	20.1	2.041	2.9
Cu(en)X(1) hydrated	2.268	17.5	2.053	1.3
(2) dehydrated	2.239	18.1	2.047	2.2
Cu(en)-solution	2.264	17.9	2.053	1.1
$Cu(en)_3Y$	2.206	17.7	2.043	1.7
$Cu(en)_3X$	2.209	17.3	2.046	2.4
$Cu(en)_3$-solution	2.212	18.3	2.047	1.6

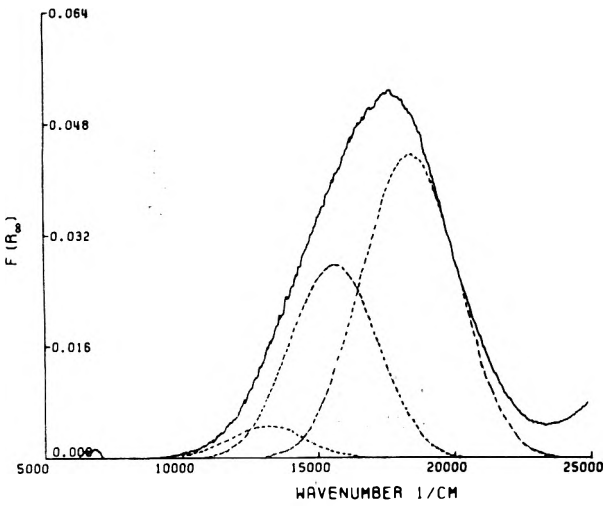

Figure 2. Deconvolution of the reflectance spectrum of $Cu(en)_2X$-2 into its three components at 18 200, 15 300, and 12 500 cm^{-1}.

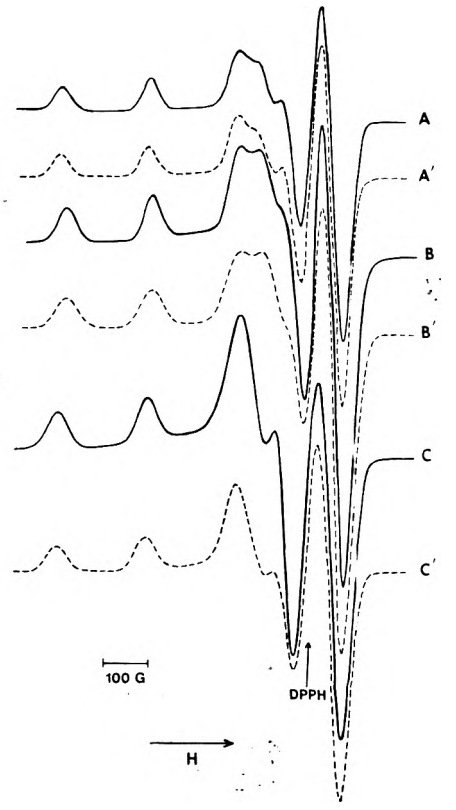

Figure 3. EPR spectra of the $Cu(en)_2^{2+}$ complexes in solution (curve A), in zeolite Y (curve B), and zeolite X (curve C). The simulated spectra are represented by dashed lines.

1 type of complex and are accompanied by color changes from violet to blue.

The nearly Gaussian shape of the bands of $Cu(en)_2^{2+}$ and $Cu(en)^{2+}$ in solution and of the $Cu(en)_2^{2+}$ band in Y-type zeolites (Figure 1A) prompted us to decompose the spectra of the X-type zeolites with a Dupont type 310 curve resolver. An example is given in Figure 2. It shows that three Gaussian shaped bands are necessary to reproduce the experimental spectrum. These are centered around 18 300, 15 300, and 12 500 cm^{-1} and correspond, respectively, to the bands of $Cu(en)_2^{2+}$, $Cu(en)^{2+}$, and $Cu(H_2O)_6^{2+}$ in solution.[26] The relative intensities of the three components (Table II) depend on the preparation conditions of the samples. The results of Table II show that the band shift to lower frequencies, relative to the 18 200-cm^{-1} band, and the band broadening can be observed in the presence of increasing amounts of $Cu(en)^{2+}$ and $Cu(H_2O)_6^{2+}$ on the solid.

The EPR spectra are shown in Figure 3. The spectra of $Cu(en)_2^{2+}$-exchanged zeolite Y (curve B) give evidence for only one type of complex in agreement with the optical spectroscopic data. The spectrum of the air-dried X sample originally showed the presence of two different Cu(II) complexes (not shown in Figure 3): 25% of the total Cu(II) was in the mono complex and the remainder was in the bis complex. Upon heating the sample for 1 h at 323 K under vacuum all the Cu(II) was coordinated in the bis complex. The latter spectrum and that of $Cu(en)_2Y$ compare favorably with that of a frozen $Cu(en)_2^{2+}$ solution, shown in Figure 3A. The 25% mono complex spectrum in X agreed with that of the frozen $Cu(en)^{2+}$ solution (Figure 7A). For each sample the simulated spectrum is represented by the dashed lines in Figure 3 and the values used in the simulation are given in Table III. For all of the copper–ethylenediamine complexes studied here Cu(II) hyperfine splitting was resolved in the perpendicular region, but no N-hyperfine splitting was observed. In an attempt to resolve the N-hyperfine splitting a sample of the Y zeolite was prepared using the ^{63}Cu isotope, deuterated en, and D_2O. No improvement in the resolution was obtained.

The thermal stability of the bis complexes depends on the type of zeolite and the loading. A room temperature treatment in vacuo did not affect the band position of the reflectance spectra of the bis complexes in Y-type zeolites but caused an overall intensity increase (Figure 4B). Heating in vacuo in the range 373–423 K caused a band shift toward 17600–17000 cm^{-1} and the band became assymmetric at its low frequency side. The highest temperature and frequency correspond to the low loadings; the lowest frequency and temperature to the high loadings. Heating the sample under vacuum at 473 K yielded a yellow solid with no spectrum in the visible, but with a strong absorption starting at 20 000 cm^{-1} and extending out of our experimental frequency range (Figure 4C). Oxygen treatment at room temperature after the degassing

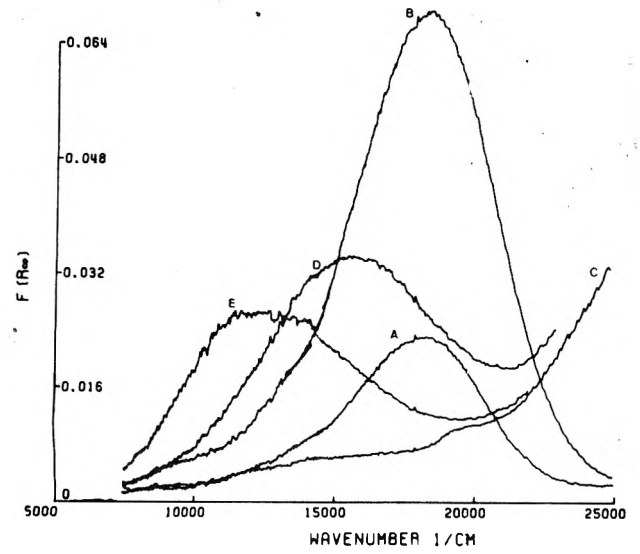

Figure 4. The reflectance spectra of $Cu(en)_2Y$-1′ before (curve A) and after different treatments: B, in vacuo at room temperature; C, in vacuo at 473 K; D, after addition of O_2 at room temperature; E, after addition of O_2 at 453 K.

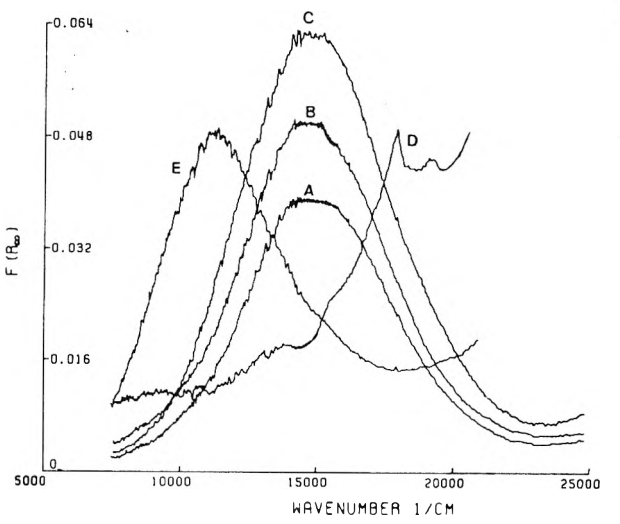

Figure 5. The reflectance spectra of Cu(en)X-1′ before (curve A) and after different treatments: B, in vacuo at room temperature; C, in vacuo at 373 K; D, in vacuo at 471 K; E, after addition of O_2 at 573 K.

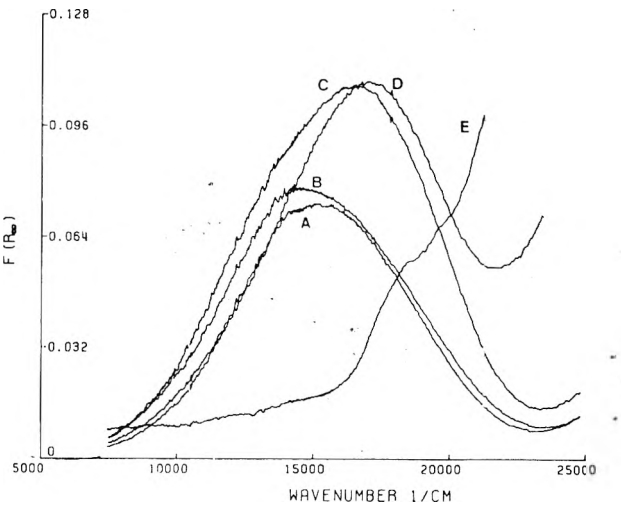

Figure 6. Reflectance spectra of Cu(en)Y-3: A, before thermal treatment; B, after vacuum desorption at room temperature; C, after desorption at 371 K in vacuo; D, after desorption at 423 K in vacuo; E, after desorption at 473 K in vacuo.

at 473 K gave blue samples with complex spectra (Figure 4D). After heating in O_2 to 453–473 K the samples turned green and showed a broad band in the region 12000–14000 cm^{-1} (Figure 4E). When the samples were heated in O_2 above 473 K, typical spectra of dehydrated Cu(II) sieves were obtained with complete removal of the intense 20000-cm^{-1} absorption.[27,28] If O_2 was added after a degassing below 473 K, the samples turned dark brown and could not be converted to the typical green form of the dehydrated sieves. The EPR spectra of the $Cu(en)_2^{2+}$-exchanged Y type zeolite remained unchanged even after heating at 473 K in vacuo, except for an intensity decrease. Addition of O_2 restored the original intensity. When this sample was heated at 473 K in O_2, a new EPR spectrum appeared. The observed g values were $g_{\parallel} = 1.99$ and $g_{\perp} = 2.25$.

The complexes in the X-type zeolites, exchanged from bis(ethylenediamine)copper(II) solutions, were much less stable. Drying at room temperature in air gave a band shift to lower frequency and a band broadening. A vacuum treatment intensified these effects and after degassing at 383 K in vacuo the band maxima were centered around 15500 cm^{-1}.

The EPR data also indicated that the complexes on X-type zeolites were less stable than on Y zeolites. Degassing the X type at 373 K resulted in an EPR spectrum with several new peaks, and addition of O_2 after degassing at 473 K did not restore the original spectrum.

$Cu(en)^{2+}$ Complexes. The mono(ethylenediamine)-copper(II) complexes on zeolites are blue. The reflectance spectra of the hydrated species show one broad band. An example is shown in Figure 5A. The band maxima and half-bandwidths depend on the preparation. Drying at 333 K before storage of the samples lowers the frequency of the band maximum at small loadings with respect to room temperature drying. The opposite behavior is observed at large loadings. The spectra of the wet samples Cu(en)Y-1′ and Cu(en)X-1′ have a somewhat larger bandwidth than those after air-drying but the same position of the band maximum.

All the spectra can be deconvoluted as described for the $Cu(en)_2^{2+}$ zeolites. The pertinent data are summarized in Table II. For comparison purposes the band maximum of $Cu(en)^{2+}$ in an aqueous solution occurs at 15700 cm^{-1}. The relative amounts of each species in X- and Y-type zeolites depend on the exchange conditions, the drying temperature, and the loading. Upon degassing, the X and Y zeolites with small loadings behaved similarly (Figure 5). Degassing in vacuo up to 373 K did not affect the spectra except for an intensity increase (Figure 5A–C). At 473 K in vacuo the solid became yellow with an intense absorption starting at 15000 cm^{-1} and extending out of the experimental frequency range (Figure 5D). Addition of O_2 above 473 K was necessary to convert the spectra to those of the dehydrated Cu(II) zeolites (Figure 5E). The thermal behavior of the samples with high Cu(II) loading was different (Figure 6). Degassing at room temperature did not affect the spectra except for a small intensity increase (Figure 6B). At 373 K in vacuo the band maximum shifted to 16500 cm^{-1} for Y-type zeolites (Figure 6C), but to lower frequencies for the X type (13000 cm^{-1}). After a vacuum treatment at 423 K Cu(en)Y-3 had its band maximum at 17000 cm^{-1} (Figure 6D). Under identical conditions Cu(en)X-3 gave a spectrum similar to that of Figure 5D. Treatments at higher temperatures in vacuo or in O_2 gave spectral changes as described previously for the $Cu(en)_2$ zeolites and Cu(en) zeolites at low loadings.

The EPR spectra of the $Cu(en)^{2+}$ exchanged zeolites are shown in Figure 7. Curve A represents the spectrum of the frozen solution of $Cu(en)^{2+}$, whereas curve B shows the

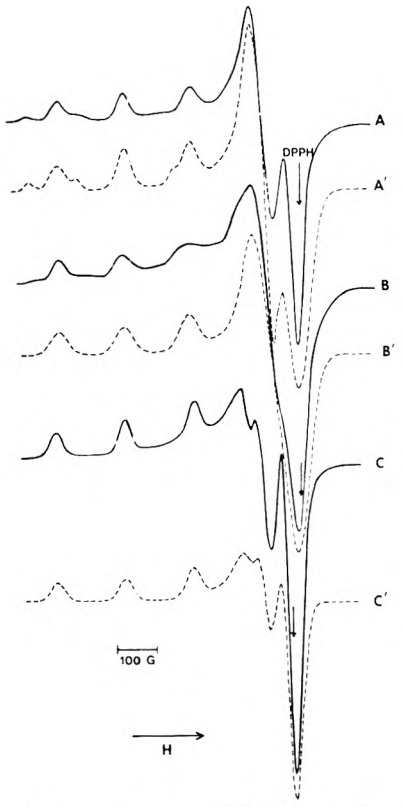

Figure 7. EPR spectra of the $Cu(en)^{2+}$ complexes in solution (curve A) and in zeolite X (curve B hydrated, curve C dehydrated). The simulated spectra are represented by dashed lines.

EPR spectrum of the $Cu(en)^{2+}$-exchanged zeolite X. The resemblance between the EPR parameters for both spectra is evident, although curve A indicates that a small amount of uncomplexed Cu^{2-} ions was present in solution. The g values and hyperfine splitting constants are given in Table III.

Keeping the X sample in vacuo for 15 h at room temperature resulted in a significant change of the EPR spectrum (Figure 7C). Stepwise heating of the complex in vacuo did not alter this new spectrum, except for a partial reduction of the intensity after a 473 K treatment. Addition of 400 Torr of oxygen first for 1 h at room temperature and then for 1 h at 473 K did not restore the intensity of the signal.

At exchange levels less than one complex per unit cell we were unsuccessful in preparing $Cu(en)^{2+}$ in the Y zeolite. A preparation identical with the one for the X zeolite gave an EPR signal which was identical with that of the $Cu(en)_2^{2+}$-exchanged Y-type zeolite. When the exchange was carried out at a pH of 5.8, only the spectrum of the aqueous Cu(II) was observed.

Adsorption of Ethylenediamine. Room temperature adsorption of controlled amounts of en on samples with copper(II) loadings above 16 per unit cell gave bands at 16 800 cm^{-1} (CuX-4) and 17 300 cm^{-1} (CuY-4), assymmetric at their low frequency side, from the very beginning of the adsorption. The intensity increase of these bands was not linear with the amount of en adsorbed but leveled off at higher loading. Heating in excess en at 353 K decreased the band intensity (Figure 8). Adsorption of controlled amounts of en at room temperature or at 353 K on zeolites with small Cu(II) loadings (CuY-2, CuY-3) gave a band around 16 200 cm^{-1}. It increased at the expense of the 10 800-cm^{-1} band of the dehydrated Cu(II) sieve with increasing amounts of en adsorbed (Figure 9). However, a low frequency shoulder could not be eliminated. The same observation was made on CuX-3 and CuX-2, but the

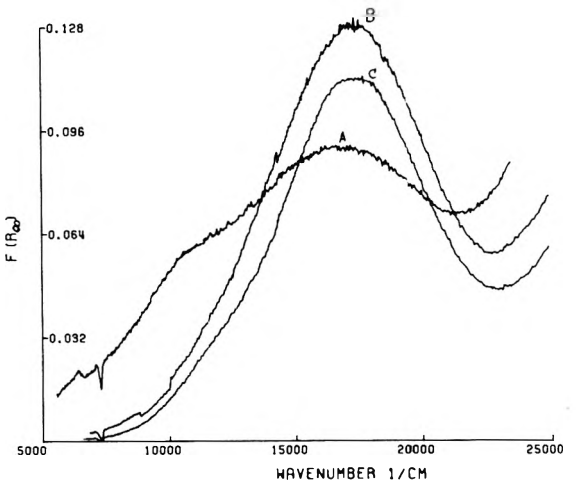

Figure 8. Reflectance spectra of CuY-4 after adsorption of ethylenediamine (en) at room temperature: A, 0.5 en/Cu(II); B, 2 en/Cu(II); C, saturation with en at 353 K.

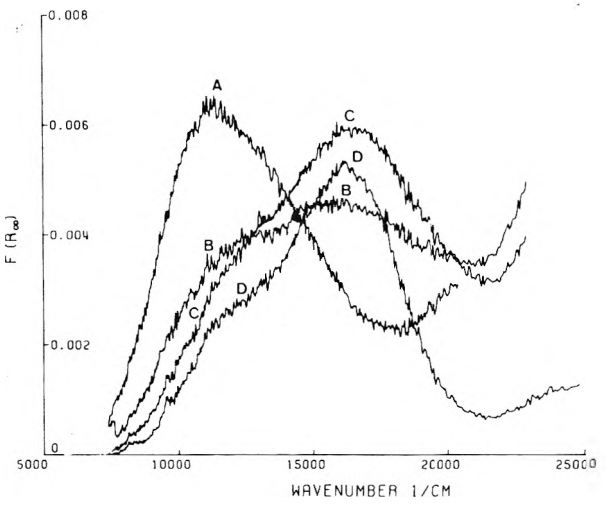

Figure 9. The reflectance spectra of CuY-3 after adsorption of different amounts of ethylenediamine: A, 0.5 en/Cu^{2+}; B, 2.6 en/Cu^{2+}; C, 8.1 en/Cu^{2+}; D, saturation with en at 353 K.

band maximum was at 16 800 cm^{-1}. If after saturation with en at 353 K the samples were exposed to air, the intensity of the bands increased tremendously (up to 4 times the original intensity) and shifted from the region 16 200–16 800 to 17 500 cm^{-1}. The band maximum for $Cu(en)_3^{2+}$ in solution occurs at 16 700 cm^{-1}.

The EPR spectra of CuY-1 and CuX-1 after adsorption of en at 373 K are shown in Figure 10B,C. The EPR spectrum of a frozen $Cu(en)_3^{2+}$ solution is shown as curve A. It is in excellent agreement with those of curves B and C. The same EPR spectrum was also obtained when the violet $Cu(en)_2^{2+}$-exchanged X and Y zeolites were brought in contact with en vapor. The corresponding EPR parameters are shown in Table III. The color of the samples after adsorption of en was blue. The EPR spectra also indicates that these complexes are stable in vacuo up to 473 K in the Y zeolite and 423 K in the X zeolite.

4. Discussion

$Cu(en)_2^{2+}$. The EPR and electronic spectra of $Cu(en)_2^{2+}$ loaded Y-type zeolites and of $Cu(en)_2^{2+}$ in solution are reminiscent of a complex with D_{4h} symmetry and a $^2B_{1g}$ ground state.[29] Bis complexes are also present in wet X-type zeolites, but after drying and at high exchange levels the spectra reflect the presence of increasing amounts $Cu(en)^{2+}$ and aqueous Cu^{2+} ions (Table II). This difference in complex loading between X- and Y-type

TABLE IV: Effective Spin-Orbit Coupling Constant, MO Coefficients, and Energies of the $^2B_{2g} \leftarrow {}^2B_{1g}$ Transitions for $Cu(en)_2^{2+}$ and $Cu(en)_3^{2+}$

		$\lambda_\perp$, cm^{-1} (±45)	$^2B_{2g} \leftarrow {}^2B_{1g}$, cm^{-1} (±2000)	α^2 ±0.01	β^2 ±0.05	β_1^2
$Cu(en)_2^{2+}$	solution	354	15088	0.81	0.63	0.61–0.73
	X	290	13359	0.79	0.54	0.52–0.69
	Y	299	12486	0.79	0.56	0.54–0.76
	Y (dehydrated)	286	12009	0.79	0.54	0.52–0.63
$Cu(en)_3^{2+}$	solution	392	14239	0.78	0.67	0.67–0.78
	X	367	14207	0.75	0.71	0.69–0.80
	Y	330	12947	0.75	0.64	0.62–0.76

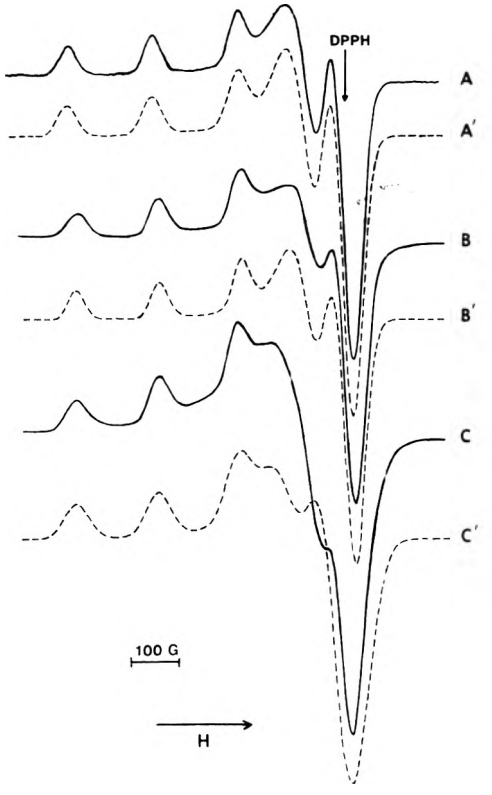

Figure 10. EPR spectra of the $Cu(en)_3^{2+}$ complexes in solution (curve A), in zeolite Y (curve B), and zeolite X (curve C). The simulated spectra are represented by dashed lines.

zeolites for exchange from $Cu(en)_2^{2+}$ solutions in identical conditions suggests the active intervention of the surface. This, and the pH of the exchange solution determine the final product obtained. The analytical data of Table I show that every sample contains some cation deficiency in terms of the number of Na^+ and Cu^{2+} ions. This is compensated partially by the presence of en in protonated form (en:Cu > 2) and partially by proton exchange. The latter is evident by the fact that during the first hours of the exchange reaction the pH tended to increase and this effect was compensated by addition of acid. Nevertheless, the similar wavenumbers for the band maxima suggest that the change in crystal field stabilization energy is small upon exchanging the complex from an aqueous solution into a zeolite. Likewise, the excess stability of the complex in the zeolite is small or even negative with respect to the solution, as determined from the thermodynamics of the ion-exchange reaction.[13,14] This is in contrast to the situation in montmorillonite, discussed in part 2, where the crystal field stabilization energy and the excess stability are approximately 4 kcal mol^{-1}.

The small differences between g values and hyperfine splitting constants for $Cu(en)_2^{2+}$ in solution, in X- or in Y-type zeolites, may reflect the interaction of the complex with the surface. The effect is analogous to the influence of the anion on the g values, hyperfine splitting constants, and electronic band maxima of $Cu(en)_2^{2+}$ in a variety of crystals.[16,18] It is therefore interesting to combine our EPR and electronic parameters into the molecular orbital scheme for copper complexes as described by Kivelson and Neiman.[30]

In D_{4h} symmetry three transitions, $^2E_g \leftarrow {}^2B_{1g}$, $^2B_{2g} \leftarrow {}^2B_{1g}$, and $^2A_{1g} \leftarrow {}^2B_{1g}$, are possible, of which the energies of the transitions $^2E_g \leftarrow {}^2B_{1g}$ and $^2B_{2g} \leftarrow {}^2B_{1g}$ figure in the expressions of the g values and hyperfine splitting constants. In pure D_{4h} symmetry all of the transitions are parity forbidden. However, temporary or static excursions, which lower the symmetry of the complex to C_{4v}, leave the $^2A_1 \leftarrow {}^2B_1$ and $^2B_2 \leftarrow {}^2B_1$ transitions forbidden, while the $^2E \leftarrow {}^2B_1$ transition becomes electric-dipole allowed. Thus, it is likely that the observed band around 18 200 cm^{-1} is the $^2E \leftarrow {}^2B_1$ transition, developed by admixture of odd parity orbitals into the d functions, allowed under C_{4v} symmetry.[31] Polarized spectra on single crystals have confirmed that the transition to the orbitally doubly degenerate level is the most intense.[16,18] If we apply this evidence to our systems it is possible to calculate the effective spin–orbit coupling constant $\lambda_\perp$ from $g_\perp$: $g_\perp - 2.0023 = -2\lambda_\perp / E(^2E_g \leftarrow {}^2B_{1g})$. (One may wish to omit the subscript g in the ^2E_g and $^2B_{1g}$ symbols for the C_{4v} case.) With the assumption $\lambda_\perp = \lambda_\parallel = \lambda$ the transition $^2B_{2g} \leftarrow {}^2B_{1g}$ is calculated from $g_\parallel - 2.0023 = -8\lambda / E(^2B_{2g} \leftarrow {}^2B_{1g})$. These values are summarized in Table IV together with the coefficients of the d orbitals in the MO's of $Cu(en)_2^{2+}$.[30]

Although the absolute values of these coefficients may be questioned, especially the values of the out-of-plane π bonding coefficient β^2 and the in-plane π bond coefficients β_1^2, some physically significant trends emanate from Table IV. Indeed, λ is shown to be systematically smaller for $Cu(en)_2^{2+}$ in the zeolite than in solution. This is translated into a decrease of β^2 for the complex in the supercages with respect to the aqueous solution, while α^2 is nearly constant. The uncertainty on β_1^2 is too large to visualize any trend. We conclude that the change of environment of $Cu(en)_2^{2+}$ from aqueous solution to the supercages of the zeolites induces a small but significant change in the nature of the bonds perpendicular to the plane of the complex, i.e., directed toward the surface. This may be accounted for by the replacement of axially coordinated water molecules by surface oxygens, or at least, a decrease of the interaction between water and the complex in the supercages with respect to aqueous solution. The thermal stability of the complexes also is strongly influenced by the zeolitic environment.

The data of Table II show the influence of the exchange pH and the drying on the complex composition in X-type zeolites. Both these factors influence the surface acidity. The presence of aqueous Cu^{2+} ions and $Cu(en)^{2+}$ is ascribed to a partial decomposition of $Cu(en)_2^{2+}$ on the surface of X-type zeolites under the influence of the surface acidity. Upon dehydration under vacuum the band maximum in X-type zeolites shifts toward 15 000 cm^{-1}, which is near the

band frequency of the mono complex, although the broadness of the band and the complex EPR spectrum indicate the presence of several species.

On Y-type zeolites the bis complex does not decompose below 423 K, but its thermal stability depends on the loading. The EPR spectrum of the bis complex is observed with reduced intensity even after outgassing in vacuo at 473 K, while in the same conditions no electronic spectrum is visible on samples with higher loadings. The latter is also true for all X-type zeolites. Clearly, copper(II) has been reduced, probably to copper(I). Reduction of copper(II) to copper(I) by vacuum dehydration above 650 K has been reported for Y-type zeolites.[28] The fact that this reaction occurs at much lower temperatures with complexed copper(II) ions is analogous to the enhanced reducibility of copper(II) to copper(I) with CO in the presence of NH_3.[32]

If O_2 is adsorbed after degassing below 473 K a complex system of reactions occurs, the zeolite turns yellow-brown, and Cu(II) cannot be regenerated. Addition of O_2 at 473 K after degassing at the same temperature gives a green zeolite with copper(II) in tetrahedral-like symmetry ($g_\perp > g_\parallel$). This is not very clear from the electronic spectra because the spectra obtained in such conditions overlap with those of the dehydrated Cu(II) zeolites. A tetrahedral-like environment has been observed also after partial degassing of an ammonia saturated Cu(II) zeolite.[8,33] The best representation is that of a Cu(II) ion linked to the three oxygens of site II and a residue of an en molecule:

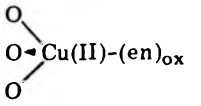

If O_2 is added above 473 K, en is burned off completely and the dehydrated Cu(II) sieve is generated.

Cu(en)$^{2+}$. A solution with en:Cu equal to one contains 71% mono, 14% bis and 14% aquo complexes in the pH range 5.8–6.75. These three species were also found on the Y-type zeolites by deconvolution of the electronic spectra. With the exception of Cu(en)Y-1, dried at 333 K, the band intensity ratios on the zeolite are slightly more in favor of the aquo and bis complexes than in solution. Only the bis complex was found by EPR. It may well be that at the small loadings of the EPR samples only the bis complex is exchanged.

On X-type zeolites the composition of the samples depends on the exchange and drying conditions (Table II), as was the case for the $Cu(en)_2^{2+}$-exchanged samples. At low loadings the mono complex is strongly predominant after air-drying as indicated by the EPR data and the deconvoluted spectra (Cu(en)X-1′). At high loadings the aquo complexes are favored according to the en:Cu ratios of 0.50 and the deconvoluted spectra.

The symmetry of the mono complex is lower than D_{4h}. The complexity of the experimental electronic spectra prevented accurate determinations of band maxima positions. For these reasons we did not extend our calculations to the mono complex on zeolites, although this has been attempted in the past on the basis of an effective D_{4h} symmetry.[29]

The thermal stabilities of these complexes on the zeolites depends on the loading. At small loading (Figure 5) the band maximum remains around 15 000 cm^{-1} up to 373 K in vacuo, indicating predominance of the mono complex. In the highly exchanged X samples the low frequency band shift after degassing at 373 K is due to the formation of lattice-bonded or aqueous Cu^{2+} ions. Indeed, as the initial en:Cu ratio is only 0.5, not enough en is present to convert aqueous Cu^{2+} and $Cu(en)_2^{2+}$ to the mono complex. On Cu(en)Y-3 with an en:Cu ratio of 1.0 the shift to higher frequencies upon drying indicates that the bis complexes are more stable than mono and aquo complexes, or that, upon removal of H_2O, ligand redistribution occurs to give bis complexes and lattice-bound Cu(II).

Ethylenediamine Adsorption on Dehydrated Cu(II)-Exchanged Zeolites. From the optical spectra it can be seen that the type of complex formed depends on the Cu^{2+} exchange level of the zeolite. Thus CuY-4 with 17.5 Cu^{2+} ions per unit cell gives rise to a complex which adsorbs around 17 300 cm^{-1}, independent of the en loading and the temperature of adsorption. This frequency is close to those observed in $Cu(en)_2Y$ sieves after vacuum dehydration at 373 K. No trace of mono complex or tris complex was found. At very high exchange levels (CuX-4) the maximum band intensity is around 16 800 cm^{-1}, but it extends below 10 000 cm^{-1}, indicating that uncomplexed Cu^{2+} and mono complexes are also present. Clearly, the number of Cu^{2+} ions in this sample is too high and the supercage space too small to convert all the Cu^{2+} into the bis complex. We conclude that not more than two bis complexes can be formed in one supercage.

At low exchange levels all the Cu^{2+} ions are located in the small cavities of the dehydrated structure (hexagonal prisms and cubooctahedra).[34] The reflectance spectrum observed for CuY-3 indicates a gradual decrease of uncomplexed Cu^{2+} ion concentration and a gradual increase of a band at 16 200 cm^{-1} with increasing en loadings. Since the latter band remains at the same position even in excess en, and its frequency is close to that of $Cu(en)_3^{2+}$,[20-22] we believe that the tris complex is formed. Additional evidence is found in the similarity between the EPR spectra of en-saturated CuY-1 and the frozen $Cu(en)_3^{2+}$ solution. The direct formation of the tris complex without the formation of intermediates such as the mono and bis complexes indicates that the migration of Cu^{2+} ions from the small cavities toward the supercages is the rate-limiting step in the complexation or that the tris complex is more stable than a bis or mono complexes in the dehydrated zeolite. The intensity decrease (after adsorption at 353 K) indicates a partial reduction of Cu^{2+}. This is evidenced too by the tremendous intensity gain after admission of air. The accompanying band shift to 17 500 cm^{-1} indicates the formation of the bis complex.

The effective spin–orbit coupling constants, MO coefficients, and $^2B_{2g} \leftarrow {}^2B_{1g}$ energies were calculated for the tris complex assuming an effective D_{4h} symmetry. The results are displayed in Table IV. Qualitatively, the same trends were observed as for $Cu(en)_2^{2+}$ but the differences between the various coefficients fall within experimental error.

Acknowledgment. This work was supported by the NSF (U.S.A.) and by the Belgian Government (Diensten van het Wetenschapsbeleid). R. A. Schoonheydt is indebted to the N.F.W.O. (Belgium) for a grant as "Bevoegdverklaard Navorser". W. De Wilde acknowledges a grant from the I.W.O.N.L. (Belgium). The authors are indebted to Professor H. Koch, Department of Zoology, Katholieke Universiteit Leuven, for the use of the curve resolver. The technical assistance of J. Pelgrims is greatly appreciated.

References and Notes

(1) D. R. Flentge, J. H. Lunsford, P. A. Jacobs, and J. B. Uytterhoeven, *J. Phys. Chem.*, **79**, 354 (1975).
(2) I. E. Maxwell and J. J. De Boer, *J. Chem. Soc., Chem. Commun.*, 814 (1974); *J. Phys. Chem.*, **79**, 1874 (1975).
(3) W. B. Williamson, D. R. Flentge, and J. H. Lunsford, *J. Catal.*, **37**, 258 (1975).

(4) I. R. Leith and H. F. Leach, *Proc. R. Soc. London, Ser. A*, **330**, 247 (1972).
(5) J. T. Richardson, *J. Catal.*, **9**, 178 (1967).
(6) J. Turkevich, Y. Ono, and J. Soria, *J. Catal.*, **25**, 44 (1972).
(7) Y. Yamada, *Bull. Chem. Soc. Jpn.*, **45**, 64 (1972).
(8) E. F. Vansant and J. H. Lunsford, *J. Phys. Chem.*, **76**, 2860 (1972).
(9) P. Gallezot, Y. Ben Taarit, and B. Imelik, *J. Catal.*, **26**, 295 (1972).
(10) C. Naccache and Y. Ben Taarit, *Chem. Phys. Lett.*, **11**, 11 (1971).
(11) J. C. Vedrine, E. G. Derouane, and Y. Ben Taarit, *J. Phys. Chem.*, **78**, 531 (1974).
(12) I. D. Mikheikin, G. M. Zhidomirov, and V. B. Kazanskii, *Usp. Khim.*, **41**, 909 (1972).
(13) J. Pleysier and A. Cremers, *J. Chem. Soc., Faraday Trans. 1*, **71**, 256 (1975).
(14) P. Peigneur and A. Cremers, Abstracts, 2nd Meeting of the European Clay Groups, 1974, p 31; Abstracts, 167th National Meeting of the American Chemical Society, Los Angeles, Calif., 1974, Colloid and Surface Chemistry Section, Abstract No. 101.
(15) Sillén and Martell, "Stability Constants of Metal-Ion Complexes", The Chemical Society, London, 1964 and 1971.
(16) D. E. Billing, R. Dudley, B. J. Hathaway, P. Nicholls, and I. M. Procter, *J. Chem. Soc. A*, 312 (1969).
(17) R. Rajan, *Physica*, **29**, 1191 (1963).
(18) I. M. Procter, B. J. Hathaway, and P. Nicholls, *J. Chem. Soc. A*, 1678 (1968).
(19) B. J. Hathaway, D. E. Billing, P. Nicholls, and I. M. Procter, *J. Chem. Soc. A*, 319 (1969).
(20) I. Bertini, D. Gatteschi, and A. Scozzafava, *Inorg. Chim. Acta*, **11** (2), L17-L19 (1974).
(21) R. Barbucci, P. Paoletti, and M. J. M. Campbell, *Inorg. Chim. Acta*, **10**, 69 (1974).
(22) G. Gordon and R. K. Birdwhistell, *J. Am. Chem. Soc.*, **81**, 3567 (1959).
(23) C. C. Chao and J. H. Lunsford, *J. Catal.*, **26**, 440 (1972).
(24) K. Klier, *Catal. Rev.*, **1**, 207 (1967).
(25) G. Kortum, "Reflectance Spectroscopy", Springer-Verlag, Berlin, 1969 (translated by J. E. Lohr).
(26) J. Bjerrum and E. J. Nielsen, *Acta Chem. Scand.*, **2**, 297 (1948).
(27) W. De Wilde, Ph.D., Katholieke Universiteit Leuven, 1976.
(28) P. A. Jacobs, W. De Wilde, R. A. Schoonheydt, and J. B. Uytterhoeven, *J. Chem. Soc. Faraday Trans. 1*, **72**, 1221 (1976).
(29) W. B. Lewis, M. Alei, Jr., and L. O. Morgan, *J. Chem. Phys.*, **45**, 4003 (1966).
(30) D. Kivelson and R. Neiman, *J. Chem. Phys.*, **35**, 149 (1961).
(31) This argument was suggested by one of the referees.
(32) Y. Y. Huang, *J. Catal.*, **30**, 187 (1973).
(33) W. De Wilde, R. A. Schoonheydt, and J. B. Uytterhoeven, submitted to 4th International Conference on Molecular Sieves, Chicago, Ill., April 1977.
(34) R. A. Schoonheydt and F. Velghe, *J. Chem. Soc., Faraday Trans. 1*, **72**, 172 (1976).

Spectroscopic Characterization and Thermal Stability of Copper(II) Ethylenediamine Complexes on Solid Surfaces. 2. Montmorillonite

Firmin Velghe, Robert A. Schoonheydt,* Jan B. Uytterhoeven,

Katholieke Universiteit Leuven, Centrum voor Oppervlaktescheikunde en Colloïdale Scheikunde, De Croylaan 42, B-3030 Heverlee, Belgium

Paul Peigneur,† and Jack H. Lunsford

Texas A & M University, Department of Chemistry, College Station, Texas 77843 *(Received October 6, 1976)*

Publication costs assisted by Diensten van het Wetenschapsbeleid (Belgium) and the National Science Foundation (USA)

Bis(ethylenediamine)copper(II) complexes were exchanged from aqueous solution on Camp Berteau montmorillonite. The complex had effective axial symmetry and its d–d transitions were around 20 000 cm^{-1}. The analysis of the EPR and electronic spectra revealed an increased covalent character of the out-of-plane π orbital with respect to its covalent character in aqueous solution. The crystal field stabilization energy is 3.9–5.5 kcal larger for the bis complex on the clay with respect to the solution. Below 0.70 mequiv g^{-1} the complex is stable up to 493 K in vacuo and located between the clay sheets. At higher loadings the complex fills up external surface sites too, where it is much less stable. The exchange of a Na^+ clay with an aqueous solution of an en:Cu ratio equal to 1 gives a clay with a mixture of bis, mono, and aquo complexes. Their relative concentration depends on the water content of the clay. Tris(ethylenediamine)copper(II) can be prepared by adsorption of gaseous ethylenediamine on a Cu^{2+}-exchanged clay. MO coefficients and crystal field stabilization energies of the tris complex on the clay are not significantly different from those of the tris complex in aqueous solution.

Introduction

The formation of coordination complexes between Cu(II) and alkylamines in the interlamellar space of montmorillonite has been the subject of a number of publications in recent years. In particular, we refer to the elaborate series of papers by Bodenheimer, Heller, Kirson, and Yariv[1-4] who investigated the adsorption of several ligands (mainly amines) in Wyoming bentonite, previously saturated with metal ions capable of forming complexes. Laura and Cloos[5] studied the Cu–ethylenediamine system in more detail, and from x-ray measurements and IR spectroscopic data they concluded that a square–planar chelate complex of composition $Cu(en)_2^{2+}$ was formed when an excess amount of ethylenediamine was adsorbed from aqueous solution onto the homoionic Cu montmorillonite from Camp Berteau.

Several studies have indicated that the stability of complexes on clay surfaces may be different from the ones in solution.[6-8] Peigneur[9] proposed a new method to measure quantitatively the overall stability increase of adsorbed complexes. They found for $Cu(en)_2^{2+}$ that the stability constants in Camp Berteau montmorillonite were $\log K_1 = 11.6$ and $\log K_2 = 11.5$, as compared to 10.7 and 9.3, respectively, in solution; i.e., the overall stability of the complex in the clay exceeds the corresponding value in solution by 3 orders of magnitude. In zeolites, no such stabilization was observed.[9] Nevertheless EPR and electronic spectroscopy revealed a slight increase of the covalent character of the out-of-plane π bonding with respect to the bonding characteristics of the bis complex in aqueous solution.[10]

† On leave of absence from Centrum voor Oppervlaktescheikunde en Colloidale Scheikunde, De Croylaan 42, B-3030 Heverlee, Belgium.

TABLE I: Exchangeable Cation and Ethylenediamine Contents of the Clays and the Wavenumber at the Absorption Maximum of the Complexes

Samples	Na^+, mequiv g^{-1}	Cu^{2+}, mequiv g^{-1}	en, mequiv g^{-1}	en:Cu^{2+}	Wavenumber, cm^{-1}
$Cu(en)_2CB1$	0.59	0.48	1.12	2.33	20200
$Cu(en)_2CB2$	0.34	0.72			19950
$Cu(en)_2CB3$	0.03	1.27	2.58	2.03	19600
Cu(en)CB1	0.36	0.69	0.78	1.13	19000
Cu(en)CB2	0.05	1.24	1.26	1.02	19000
CuCB1		0.86			
CuCB2	0.05	1.32			

To obtain more insight into the stabilization phenomena we extended our EPR and electronic spectroscopy measurements to mono(ethylenediamine)copper(II), bis(ethylenediamine)copper(II), and tris(ethylenediamine)copper(II) on clays. These spectroscopic techniques were supplemented by magnetic susceptibility, x-ray diffraction, and quantitative desorption measurements.

Experimental Section

Samples. The Camp Berteau montmorillonite (from Morocco) which was used in this study had a cation exchange capacity of about 1.05 mequiv g^{-1}. The unit cell formula according to Eeckman and Laudelout[11] was $(Si_4^{4+})^{IV}(Al_{1.46}^{3+}Mg_{0.32}^{2+}Fe_{0.22}^{3+})^{VI}O_{10}(OH)_2$. Following the method described by Cremers and Thomas,[12] the fraction $< 0.5\ \mu m$ was separated, brought into the homoionic Na^+ form, and stored after freeze-drying. For each preparation 2 g of clay was immersed in 150 mL of distilled water and washed salt free. The clay was then placed in dialysis tubings and equilibrated for 24 h at room temperatures with the $Cu(en)_2^{2+}$ or $Cu(en)^{2+}$ solutions. The $Cu(en)_2$ solution contained an amount of en equal to 2 times the $Cu(NO_3)_2$ molarity plus a very small excess. The $Cu(en)^{2+}$ solution was an equimolar solution of $Cu(NO_3)_2$ and en. The Cu contents of these solutions varied in order to obtain clays with different exchange levels. The samples were washed 3 times and freeze-dried. The Na^+ and Cu^{2+} contents of the clays were analyzed by atomic absorption spectrometry and the en content by the Kjelldahl method. The analytical data are shown in Table I together with the sample symbols. In addition, Cu^{2+} montmorillonites with different Cu^{2+} loadings were prepared by exchange of 2 g of freeze-dried, salt-free Na^+ clay with appropriate quantities of $Cu(NO_3)_2$ solutions, in an analogous manner as described above for the complex exchanges. The analytical data are also displayed in Table I.

Tris complexes were prepared by adsorption of en on these Cu^{2+} montmorillonites after room temperature evacuation (Cu CB1) or after evacuation at 413 K (Cu CB2), both for 2 days. En vapor was allowed to adsorb at room temperature in a stepwise manner up to 3 en/Cu^{2+}. Each dose contained an amount equivalent to 0.25 en/Cu^{2+}. The equilibration time at each step was 2 days. Finally, the samples were allowed to equilibrate in excess en vapor for 2 days. After each step optical spectra were recorded as described in the following section.

The $Cu(en)_2^{2+}$ and $Cu(en)^{2+}$ loaded montmorillonites used in the EPR study were prepared separately but in a completely analogous manner except for the fact that after exchange of the complex ion the samples were neither washed nor freeze-dried. Preliminary experiments showed that the powder EPR spectra of the $Cu(en)_2^{2+}$ complex in the montmorillonite were rather poorly resolved, due in part to a spin–spin interaction between the Cu^{2+} ions and the relatively large amount of Fe^{3+} present in the montmorillonite lattice. A sample completely exchanged with $Cu(en)_2^{2+}$ ion had a spectrum consisting of only one very broad asymmetric signal. Lowering the Cu exchange level reduced the broadening effect. Hence, all of the reported EPR spectra of the Camp Berteau were recorded with samples containing about 4 mequiv of $Cu^{2+}/100$ g. EPR spectra were also recorded for the mono, bis, and tris complexes on a hectorite mineral (from Hector, Calif.), which belongs, like montmorillonite, to the smectite group, but contains only small amounts of Fe^{3+} in its lattice structure:[13] $(Si_4^{4+})^{IV}(Mg_{2.71}^{2+}Li_{0.34}^{+}Al_{0.01}^{3+})^{VI}O_{10}(OH)_2$. The preparations of the hectorite samples were in every aspect identical with those described for the montmorillonite samples, but exchange levels of 15 mequiv of $Cu^{2+}/100$ g were used.

Procedures and Techniques. The reflectance cell was similar to that described by Klier.[14] The standard was placed in a matching vacuum cell. Diffuse reflectance spectra were taken at room temperature in the region 360–1800 nm with a Cary 17 instrument equipped with a type II reflectance unit. The standard was MgO or the Na^+ clay. The spectra were digitalized and processed in a computer to obtain plots of the Kubelka–Munk function against wavenumbers. Spectra were recorded of the samples as such and after evacuation at different temperatures up to 423 K. At each temperature the evacuation time was 48 h.

The EPR spectra of the air-dried powder samples were recorded with the sample at 77 K. For the mono and bis complexes spectra also were recorded for frozen suspensions of the clays. In addition, use was made of the fact that clay minerals form highly ordered layers. These samples were prepared by evaporating an aqueous suspension of the clay mineral on a flat polyethylene strip. The evaporation was carried out in air at 298 K and several layers were added to obtain a film of sufficient thickness. The strip was then placed inside an EPR tube. By rotating the tube, and thereby the strip, in the EPR cavity the silicate layers could be oriented with respect to the magnetic field.[15] The EPR measurements were carried out using a Varian E-6S spectrometer with a rectangular TE^{102} X-band cavity. The g values were determined relative to a DPPH standard. The EPR spectra were simulated assuming axial symmetry and using the computer program SIM 13 written by G. Lozos, B. Hoffman, and C. Franz of Northwestern University. The estimated error is ±0.005 for the g values, ±0.0002 cm^{-1} for $A_\parallel$, and ±0.0004 cm^{-1} for $A_\perp$.

The magnetic susceptibility of the Camp Berteau montmorillonite loaded with the bis complex was measured with the Faraday method on a Bruker B-MB7 instrument at 293 K in air and a magnetic field of 13.6 kG. The reference material was $Ni(en)_3S_2O_3$ with a susceptibility per gram $\chi_g = 11.03 \times 10^{-6}$ cgs units. The susceptibilities of our samples were calculated from

$$\chi_g(\text{sample}) = \frac{\Delta w(\text{sample})}{\Delta w(\text{reference})} \times \frac{w(\text{reference})}{w(\text{sample})} \times \chi_g(\text{reference})$$

where Δw is the weight change of reference or sample and

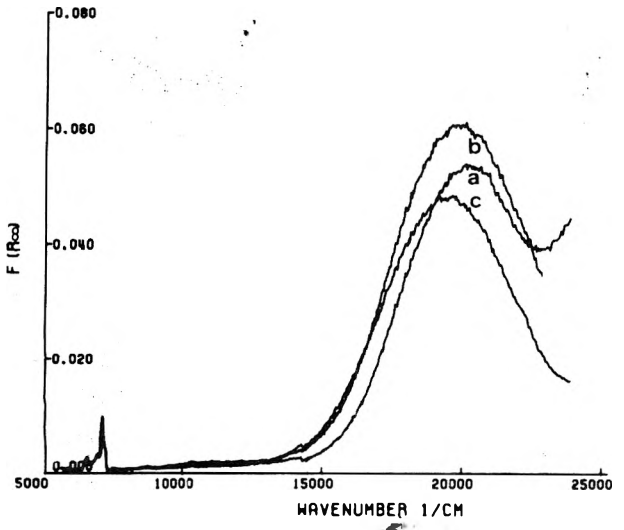

Figure 1. The reflectance spectra of the $Cu(en)_2^{2+}$ samples in the hydrated state: a, $Cu(en)_2CB1$; b, $Cu(en)_2CB2$; c, $Cu(en)_2CB3$.

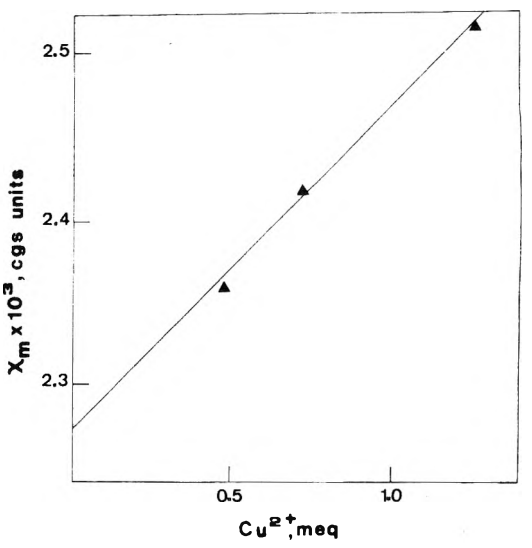

Figure 2. The magnetic susceptibility χ_m in cgs units as a function of the loading in mequiv of Cu^{2+}/gram of clay.

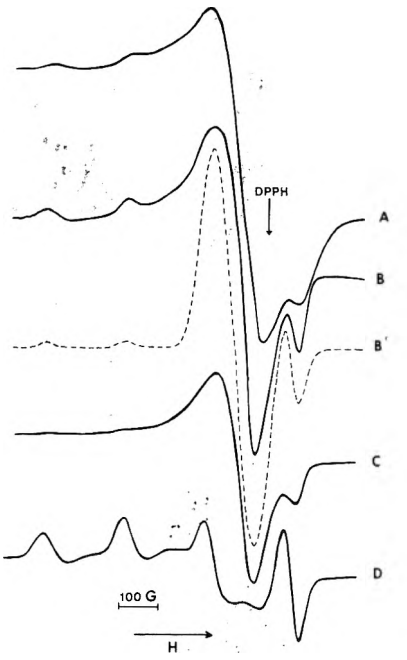

Figure 3. EPR spectra of $Cu(en)_2^{2+}$ complex: A, in montmorillonite; B, in hectorite; B', simulated spectrum; C, in oriented film with silicate layers parallel to the magnetic field; D, in oriented film with silicate layers perpendicular to the magnetic field.

w the weight of sample or reference. About 100 mg of powdered clay was compressed with a glass rod in a polyethylene sample holder (3 mm diameter, 6 mm length), fitted with a cover of the same material, and hung at the sample arm of the balance. After equilibration with the air of a thermostatted room (293 K) the weight of the sample was measured in the absence and presence of the magnetic field. The diamagnetism of the sample holder was measured independently on an empty sample holder. The experimental susceptibilities of the samples were corrected for the diamagnetism of the sample holder and the diamagnetism of the adsorbed water. The latter was calculated from the water content of the clay and the tabulated susceptibility of water.[16] Thus, no correction was made for eventual differences between the susceptibility of the liquid water and adsorbed water.

The samples were also investigated by x-ray diffraction with a Debye–Scherrer camera (ϕ = 114.6 mm) using the Straumanis method.[17] X-ray diffraction spectra were obtained for the clays in their initial state and after stepwise evacuation up to 533 K. The evacuation time at each temperature was 2 days. While under vacuum the clays were brought into a Lindemann capillary (ϕ = 0.5 mm) and the capillary was sealed off for x-ray investigation. The radiation was Cu Kα (λ = 1.5418 Å). The accuracy on the d_{001} spacing was ±0.1 Å.

The quantitative desorption of Camp Berteau montmorillonites loaded with bis and mono complexes was studied in Mac Bain balances. About 100 mg of clay was placed in a sample holder, made of aluminum foil, and connected to the quartz spring. The samples were heated under dynamic vacuum (better than 10^{-5} Torr) in a stepwise manner up to 623 K. After each step the sample was allowed to equilibrate until constant weight. The sensitivity of the springs was 0.5 mg mm^{-1} and the estimated error in the total weight loss was smaller than 5%.

Results

$Cu(en)_2^{2+}$ Montmorillonites. Figure 1 represents the reflectance spectra of Camp Berteau montmorillonite (CB) loaded with $Cu(en)_2^{2+}$ to different extents. The spectra showed a Gaussian-shaped band near 20 000 cm^{-1} with a half-bandwidth of 6000 ± 200 cm^{-1}. With decreasing loadings the band position moved slightly to higher wavenumbers, from 19 600 to 20 200 cm^{-1} (Table I). The band at 7000 cm^{-1} is an overtone of H_2O and lattice hydroxyls vibrations. Its low frequency shoulder is an overtone of the NH_2 stretching mode of en.

The magnetic susceptibilities, expressed in cgs units per gram of dry clay, were linearly dependent on the loading (Figure 2). The straight line in Figure 2 obeyed the equation

$$\chi = 0.1971[Cu^{2+}] + 2.2724 \times 10^{-3}$$

with a regression coefficient k = 0.9943. Here $[Cu^{2+}]$ is the number of mequiv of Cu^{2+} per gram of clay, and 2.2724 × 10^{-3} is the susceptibility due to the clay lattice. The effective magnetic moment of Cu^{2+} in the bis complex, calculated from the slope of the straight line, was 1.6 μ_B.

Curve A of Figure 3 shows the EPR spectrum obtained for the $Cu(en)_2^{2+}$ complex in CB, and curve B shows the $Cu(en)_2^{2+}$ complex in hectorite. Apart from the greater line broadening in CB the two spectra are quite similar. For each mineral the spectra of the frozen suspension and the random powder were identical. Hyperfine splitting due to Cu is resolved in the parallel region but not in the

TABLE II: g Values and Cu^{2+} Hyperfine Splitting Constants (in cm^{-1}) for Cu^{2+}-Ethylenediamine Complexes in Hectorite and in Frozen Solution[a]

	$g_{\parallel}$	$A_{\parallel}$	$g_{\perp}$	$A_{\perp}$
$Cu(en)_2$ hectorite	2.181	0.0204	2.030	0.0019
$Cu(en)_2$ solution	2.190	0.0201	2.041	0.0028
Cu(en) hectorite	2.261	0.0182	2.053	0.0013
Cu(en) solution	2.264	0.0179	2.053	0.0011
$Cu(en)_3$ hectorite	2.204	0.0183	2.048	0.0007
$Cu(en)_3$ solution[a]	2.212	0.0183	2.047	0.0016

[a] The solutions were prepared as described in part 1.[10]

TABLE III: d_{001} Spacings (Å) of CB Loaded with $Cu(en)_2^{2+}$ and $Cu(en)^{2+}$

		Vacuum desorption at			
Samples	Hydrated	Room temp	373 K	446 K	533 K
$Cu(en)_2$CB1	12.56[a]	11.45	10.94	10.98	9.60[a]
$Cu(en)_2$CB2	12.62[a]				9.61[a]
$Cu(en)_2$CB3	12.75[a]	12.70[a]	12.72[a]	12.48[a]	9.60[a]
Cu(en)CB1	12.66[a]	11.45		10.74	9.56[a]
Cu(en)CB2	12.72[a]	12.50[a]		12.54[a]	9.60[a]

[a] Rational series of lines.

perpendicular region. The spectrum of curve B was simulated reasonably well using the parameters listed in Table II, and a rather broad isotropic line which is apparently due to spin-spin interaction between copper ions.[18]

When the silicate layers of the oriented film were parallel to the magnetic field in the cavity, the perpendicular component dominated the EPR spectrum, as depicted in curve C of Figure 3. On the other hand, when the layers were directed perpendicular to the magnetic field the parallel component dominated the spectrum (curve D). The amplitude of the spectrum for the $Cu(en)_2^{2+}$ complex per gram of clay is much greater in the oriented sample than in the random samples; thus, the broad, isotropic line in the polycrystalline spectrum is not a dominant feature in the oriented sample. The high-field minimum in curves A–C is due, in part, to a component of the polycrystalline spectrum; however, an impurity line also appears at this field. The same observations were made with the $Cu(en)_2^{2+}$ montmorillonite sample. This dependence of the EPR spectra upon the orientation in the magnetic field indicates that the symmetry axis of the Cu complex is perpendicular to the layer surface, which can best be understood in terms of a planar complex parallel to the silicate layers.

The d_{001} spacings of CB loaded with $Cu(en)_2^{2+}$ are given in Table III. When a rational series of reflections was found, the d_{001} value was calculated from the first, third, and fourth orders. If no rational series was found, only the first-order reflection is reported. For the hydrated samples the d_{001} spacing increased slightly with the loading from 12.56 to 12.75 Å. Upon vacuum dehydration the d_{001} spacing decreased regularly down to 9.6 Å in the case of $Cu(en)_2$CB1. For $Cu(en)_2$CB3 it remained constant after a vacuum desorption at 373 K, decreased slightly from 12.72 to 12.48 Å at 448 K, and decreased further to 9.60 Å at 533 K. The accompanying weight losses are shown in Figure 4. Only the desorption curves of $Cu(en)_2$CB1 and $Cu(en)_2$CB3 were given explicitly but $Cu(en)_2$CB2 behaved similarly. One notices a large weight loss upon desorption in vacuo at room temperature. Then the weight of the samples remained constant up to approximately 403 K for $Cu(en)_2$CB1 and up to 383 K for $Cu(en)_2$CB3. Between these temperatures and 493 K a second region of weight loss was registered. Finally, the third region was observed above 493 K. Curves 3 and 4 of Figure 4 give the weight loss due to desorption of ethylenediamine. This was calculated from the total weight loss under the assumption that all of the water desorbed below 403 K. These curves show that a considerable amount of en desorbed from $Cu(en)_2$CB3 at room temperature, while for $Cu(en)_2$CB1 en started to desorb only above 423 K. The second and third desorption regions of en are then from 403 to 493 K and above 493 K. The amount of en desorbed in every region is given in Table IV. For $Cu(en)_2$CB1 the amount of en desorbed above 493 K is exactly equal to twice the Cu^{2+} exchange level (Table I). This is not the case for $Cu(en)_2$CB3. The desorption data of Table IV show that the bis complex on $Cu(en)_2$CB3 already starts to decompose by simple room temperature evacuation. In any case, the total amount of en desorbed is equal to the amount determined by Kjelldahl analysis. The optical

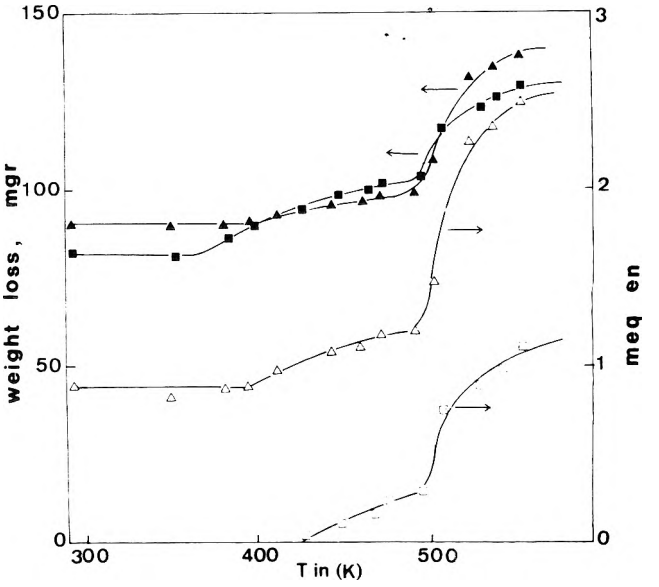

Figure 4. The weight loss of $Cu(en)_2$CB1 (□) and $Cu(en)_2$CB3 (△) as a function of the temperature. The dark symbols represent the total weight loss in mg/g of clay; the open symbols represent the weight loss of en in mequiv/g of clay.

TABLE IV: Experimental Weight Losses due to Desorption of Ethylenediamine as Compared to the Theoretical Weight Losses Calculated from Analytical Data

	Theoretical, mequiv g^{-1}		Experimental, mequiv g^{-1}				
			293-403 K		403-493 K	>493 K	Sum
Samples	H_2O	en	H_2O	en	en	en	en
$Cu(en)_2$CB1	5.31	1.12	5.31		0.26	0.96	1.16
$Cu(en)_2$CB3	3.57	2.58	3.57	0.9	0.30	1.40	2.60
			293-463 K H_2O		463-533 K en		
Cu(en)CB1	4.96	0.78	6		0.71		
Cu(en)CB2	5.36	1.26	4.74		1.31		

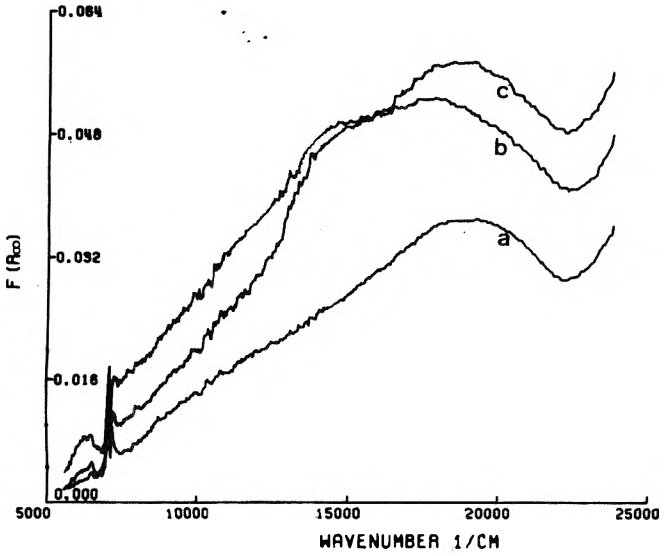

Figure 5. The reflectance spectra of Cu(en)CB1 after different pretreatments: a, hydrated; b, degassed at 298 K; c, degassed at 363 K.

spectra of $Cu(en)_2^{2+}$ on CB did not change after evacuation up to 423 K. After evacuation at higher temperatures the samples turned greyish. The accompanying increase of the background prevented an accurate analysis of the Cu(II) spectrum.

$Cu(en)^{2+}$ Montmorillonite. The diffuse reflectance spectra of the montmorillonites, obtained after exchange with a solution containing the mono complex, are not well resolved as shown in Figure 5 for $Cu(en)^{2+}$CB1. They show a broad band with maximum near 19000 cm^{-1} and asymmetry toward the low frequency side. Degassing at room temperature resulted in a shift of the maximum to 18000 cm^{-1} with the appearance of a distinguishable shoulder at 14500 cm^{-1}. After evacuation of 363 K the band maximum was again at 19000 cm^{-1}. Further heating to 423 K did not affect the spectrum.

The EPR spectrum of a hectorite sample that was exchanged at pH 6.8 with a solution containing the mono complex (Figure 6A) showed the presence of two Cu species: one species was the $Cu(en)_2^{2+}$ complex, and the other had EPR parameters nearly identical with the parameters of a frozen $Cu(en)^{2+}$ solution, as listed in Table II. The simulated spectrum, including the isotropic line, is depicted in curve A′. These parameters are also in good agreement with those found for the mono complex in the synthetic faujasite of type X.[10] An attempt was made to increase the fraction of the mono complex on the clay by lowering the pH of the exchange to 5.75 or 5.35. These samples showed the simultaneous presence of three Cu^{2+} species which were found to be the mono complex, the bis complex, and the aqueous Cu^{2+} ion. A montmorillonite sample prepared under identical conditions as those described for the hectorite sample gave a spectrum which was poorly resolved.

The d_{001} distances of the Cu(en)CB samples after different pretreatments are listed in Table III. Their behavior upon desorption was similar to that of the $Cu(en)_2$CB samples. Thus, at small Cu^{2+} loading (Cu(en)CB1) the initial d_{001} distance of 12.66 Å fell to 11.45 Å after evacuation at room temperature and decreased slowly to 9.6 Å after heating the sample to 533 K. At a high Cu^{2+} loading (Cu(en)CB2) the decrease of the d_{001} distance upon evacuation at room temperature was only from 12.75 to 12.50 Å. The latter value was maintained up to 446 K and it was only after desorption at 533 K that the d_{001} spacing fell to 9.6 Å.

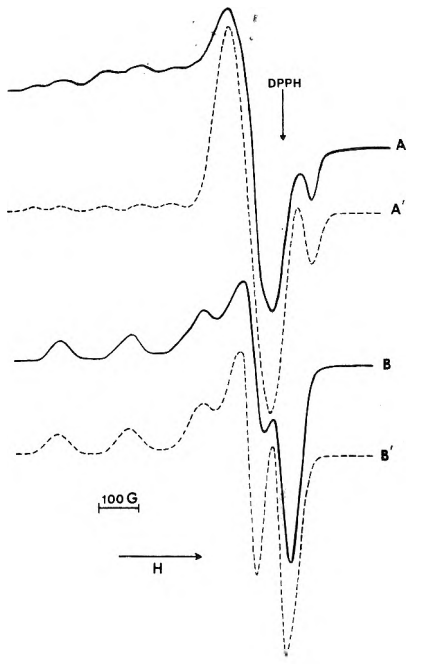

Figure 6. EPR spectra of Cu^{2+} complexes in hectorite: A, after exchange with a solution containing the mono complex; A′, simulated spectrum; B, after adsorption of excess en vapor, forming the tris complex; B′, simulated spectrum of the tris complex.

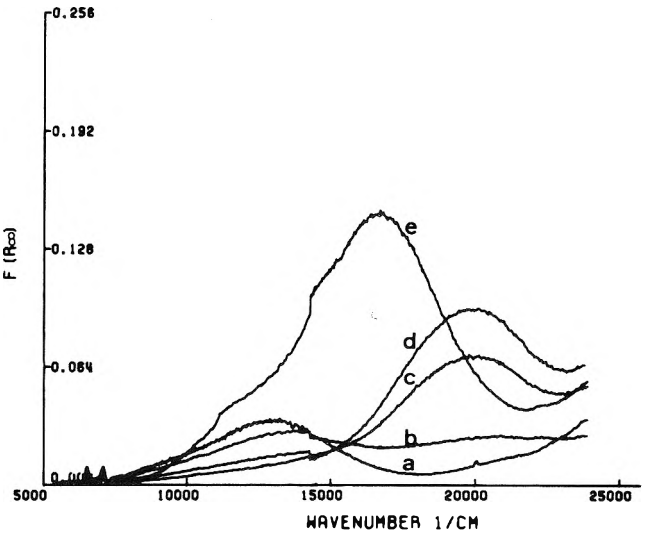

Figure 7. The reflectance spectra of the adsorption of en on CuCB1: a, CuCB1 degassed at room temperature; b, en:Cu = 0.79; c, en:Cu = 1.54; d, en:Cu = 1.94; e, saturated.

The weight losses of the two samples as obtained by desorption in the Mac Bain balances are reported in Table IV. One notices that the weight loss above 463 K is, within experimental accuracy, equal to amount of en on the clay, as determined by Kjelldahl analysis. The weight loss below 403 K is assumed to be due to water desorption and indeed the experimental numbers agree resonably well with the H_2O content determined independently in a muffle furnace.

$Cu(en)_3^{2+}$. Upon adsorption of controlled amounts of en on CuCB1 the reflectance spectra revealed a decrease in the assymmetric band at 13100 cm^{-1}, attributed to the hydrated Cu(II) ion, and a regular growth of a new band near 20000 cm^{-1} (Figure 7). This process continued up to an en:Cu ratio of two. At higher ratios the band maximum shifted to 16600 cm^{-1} and the band became assymmetric on its low frequency side (Figure 7). On CuCB2 adsorption of en gave the same spectral behavior,

TABLE V: Electronic Transitions, Effective Spin-Orbit Constant ($\lambda_\perp$), MO Coefficients, and CFSE for $Cu(en)_2^{2+}$ on Montmorillonite

		$^2E_g \leftarrow {}^2B_{2g}$, cm^{-1}	$^2B_{2g} \leftarrow {}^2B_{1g}$, cm^{-1}	$^2A_{1g} \leftarrow {}^2B_{1g}$, cm^{-1}	$\lambda_\perp$, cm^{-1} (± 45)	α^2 ± 0.01	β^2 ± 0.05	β_1^2	CFSE, kcal mol^{-1}	ΔCFSE
A.	$Cu(en)_2$CB1	20200	12573 ± 2100		280	0.79	0.52	0.54-0.76		
	$Cu(en)_2$CB2	19950	12416 ± 2100		276	0.79	0.52	0.52-0.75		
	$Cu(en)_2$CB3	19600	12214 ± 2100		272	0.79	0.51	0.51-0.74		
	$Cu(en)_2$ solution	18200	15087 ± 2300		352	0.81	0.63	0.64-0.73		
B.	$Cu(en)_2$CB1	20200	17510	15029		0.79	0.52	0.67	51.6	5.5
	$Cu(en)_2$CB2	19950	17437	14956		0.79	0.52	0.67	51.3	5.2
	$Cu(en)_2$CB3	19600	16975	14592		0.79	0.51	0.66	50.0	3.9
	$Cu(en)_2$ solution	18200	15686	13424		0.81	0.63	0.63	46.1	

except for en:Cu < 2. At these lower levels of adsorption the new band appeared around 18700 cm^{-1} and shifted toward 19000 cm^{-1} with increasing en loading. When CuCB2 was first degassed at 398 K, adsorption of en again gave a band at 19000 cm^{-1}. Its shift toward 16600 cm^{-1} started at an en:Cu ratio of 1.02. The shift was completed at an en:Cu ratio of 1.50 and further adsorption did not affect the spectrum. In any case, the samples with a band maximum at 16600 cm^{-1} were blue.

Adsorption of excess en vapor onto an air-dried $Cu(en)_2^{2+}$ hectorite turned the sample from violet to blue within a few minutes. For the latter sample the EPR spectrum shown in Figure 6B was obtained. This spectrum was simulated (curve B′) using the parameters tabulated in Table II. It can be seen from the table that there is good agreement between the magnetic parameters for the blue complex and those of a frozen $Cu(en)_3(NO_3)_2$ solution. Furthermore, an oriented film was made by adsorbing en vapor on an oriented $Cu(en)_2$ clay sample. Rotating the silicate layers in the magnetic field did not change the shape or the intensity of the spectrum appreciably. The spectrum was the same as that of the $Cu(en)_3^{2+}$ powder spectrum.

Using the x-ray diffraction technique the d_{001} distances between the clay layers were measured for hectorite and montmorillonite samples containing approximately 60 and 100% of their total cation exchange capacity in the $Cu(en)_3^{2+}$ form. The 60% exchanged hectorite sample still gave an EPR spectrum sufficiently resolved to conclude that the tris complex was present. Base distances of 13.8 and 14.6 Å were obtained for the 60% exchanged samples and the completely exchanged samples, respectively. These values are nearly the same as those found for corresponding exchange levels with the $Ni(en)_3$ complex in Camp Berteau montmorillonite.[19] These x-ray data together with the observation that the oriented clay sample did not show any appreciable change in the magnetic parameters upon altering the position of the film is consistent with the presence of a (nearly) octahedral complex that has a symmetry axis inclined at an angle of 45° with respect to the silicate layers.

Discussion

$Cu(en)_2^{2+}$ on Montmorillonite. The experimental data gathered on the $Cu(en)_2^{2+}$ CB samples indicate the presence of a square-planar complex between the clay layers. There is not only the Cu:en ratio of two but also the d_{001} distance of 12.75 Å for $Cu(en)_2$CB3. A catalin model of $Cu(en)_2^{2+}$ gives a thickness of 3.4 Å, which, together with the 9.6 Å for the d_{001} of the dehydrated clay pellets, gives 13 Å. The experimental d_{001} is always somewhat lower than the theoretical one due to electrostatic attraction and to keying.[20] At smaller loadings the d_{001} distance decreases (Table III), probably due to segregation. The difference in d_{001} distance is not very large because the hydrated Na^+ clay also has a spacing of 12.5 Å. After degassing the samples the segregation phenomenon becomes clearer.

The resemblance of the g values and hyperfine splitting constants to those of the solution spectra is also in favor of a planar $Cu(en)_2^{2+}$ complex, although slight but significant differences exist (Table II). Within experimental accuracy there is no difference between the EPR parameters obtained on CB montmorillonite and those on hectorite. The latter are better resolved because of the absence of paramagnetic ions in the lattice (Fe^{3+}). The magnetic moment of Cu^{2+} on the clay (1.60 μ_B) also may reflect this interaction with Fe^{3+}; however, the difference with the spin-only value (1.73 μ_B) is too small to attempt a discussion of this interaction.

The spectral frequencies are about 2000 cm^{-1} higher than those of $Cu(en)_2^{2+}$ in aqueous solution or in zeolites.[10] It seems worthwhile, therefore, to analyze these data within the framework of the ligand field theory and the Kivelson and Neiman theory of bonding in axially symmetric Cu^{2+} complexes.[21,22] In a strict D_{4h} symmetry all the d–d transitions are parity forbidden. However, temporary or static excursions which lower the symmetry of the complex to C_{4v} leave the $A_1 \leftarrow B_1$ and $B_2 \leftarrow B_1$ transitions symmetry forbidden while the $E \leftarrow B_1$ transition becomes electric dipole allowed. Thus it is likely that the observed band around 20000 cm^{-1} is the $E \leftarrow B_1$ transition, developed by admixture of odd parity orbitals into the d functions, allowed under C_{4v} symmetry. This was confirmed experimentally by Hathaway and co-workers.[23,24] With this hypothesis it is possible to calculate the effective spin–orbit coupling constant $\lambda_\perp$ and, with the assumption $\lambda_\perp = \lambda_\parallel = \lambda$, the $^2B_{2g} \leftarrow {}^2B_{1g}$ transition energy in D_{4h} symmetry. The latter value is rather inaccurate, due to the uncertainty in $\lambda_\perp$. These parameters are summarized in Table VA together with the MO coefficients.

Our lack of knowledge about the position of the $^2A_{1g}$ level prevented a calculation of the crystal field stabilization energies (CFSE). Therefore we calculated the splitting of the 3d levels in the D_{4h} field with the structure of the bis complex as determined from x-ray studies on single crystals.[25] The energy levels calculated with the methods of Krishnamurthy and Schaap[21] are shown in Figure 8 as a function of the ligand field strength. In Figure 8 ρ_4 is a one-electron radial integral which is proportional to $\langle r^4 \rangle$, the average radial value of the fourth power of the d orbital distance from the metal ion. Again, with the experimental band maximum position equal to the $^2E_g \leftarrow {}^2B_{1g}$ transition energy, the position of the $^2B_{2g}$ and $^2A_{1g}$ levels can be read from the diagram of Figure 8. The corresponding transition energies, MO coefficients, and CFSE's are summarized in Table VB.

In view of the Kivelson and Neiman model used for the calculation of the MO coefficients we do not expect that the absolute values of β_1, the coefficient of the in-plane

TABLE VI: Electronic Transitions, Effective Spin-Orbit Coupling Constant ($\lambda_\perp$), MO Coefficients, and CFSE for $Cu(en)_3^{2+}$ on Montmorillonite

		$^2E_g \leftarrow {}^2B_{1g}$, cm^{-1}	$^2B_{2g} \leftarrow {}^2B_{1g}$, cm^{-1}	$^2A_{1g} \leftarrow {}^2B_{1g}$, cm^{-1}	$\lambda_\perp$, cm^{-1} (± 40)	α^2 ± 0.01	β^2 ± 0.05	β_1^2	CFSE, kcal mol^{-1}
A.	$Cu(en)_3$CB	16600	15102 ± 2000		379	0.77	0.70	0.58-0.73	
	$Cu(en)_3$ solution	16700	14276 ± 2000		373	0.78	0.67	0.53-0.70	
B.	$Cu(en)_3$CB	16600	14154	12160		0.77	0.70	0.65	41.7
	$Cu(en)_3$ solution	16700	14519	12451		0.78	0.67	0.68	42.7

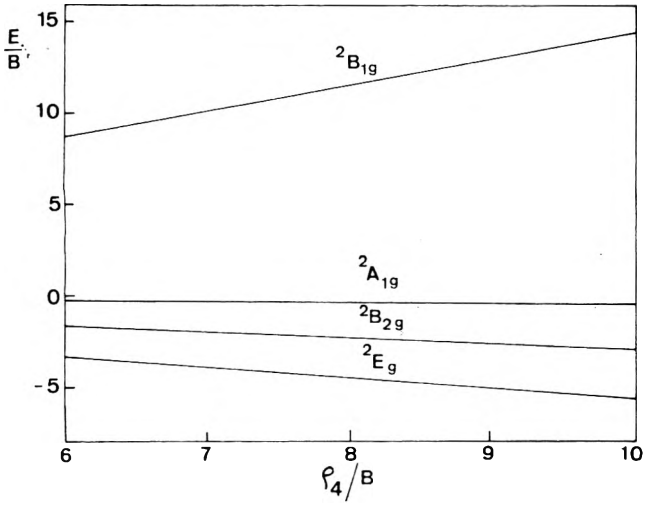

Figure 8. The energies of the $3d^1$ atomic orbitals as a function of the strength of the D_{4h} ligand field.

π bond, and β, the coefficient of the out-of-plane π bond, are very accurate. However, their variation among the different samples may have a physical meaning. It follows from a comparison of the β_1^2 values in parts A and B of Table V that the assumption $\lambda_\perp = \lambda_\parallel = \lambda$ is a rather crude one and that more probably $\lambda_\parallel > \lambda_\perp$. Therefore β_1^2 in Table VA is underestimated.

The following trends can then be extracted from Table V: there is an increase of the CFSE for $Cu(en)_2^{2+}$ on CB montomorillonite with respect to the aqueous solution. It amounts to 3.9–5.5 kcal. These numbers compare favorably with the excess stability of 4 kcal for the complex on the CB clay with respect to the solution, as determined from the thermodynamics of the ion exchange reaction.[9] Such enhanced stability was not observed on zeolites. These differences between zeolites and clay minerals have not only to do with the different geometry of the surface but also with their different surface properties. Secondly β^2, the square of the coefficient of $3d_{xz}$ or $3d_{yz}$ in the ^2E_g MO, is systematically lower for $Cu(en)_2^{2+}$ on the montmorillonite surface than for $Cu(en)_2^{2+}$ in solution. This indicates an increase of the out-of-plane π bonding on the surface. This trend was already observed for the bis complex on zeolitic surfaces,[10] but is now more pronounced. Physically, it may be related to the replacement of axially coordinated water molecules in solution by the clay mineral surface. In the third place, although the bonding coefficients do not depend on the loading, the CFSE increases by about 2 kcal in descending from maximum loading to the lowest exchange levels investigated. It seems then that the clay surface is heterogeneous with respect to the accomodation of $Cu(en)_2^{2+}$.

This heterogeneity is further demonstrated by the desorption experiments (Figure 4 and Table IV). At high loadings desorption of en at room temperature was not accompanied by a significant decrease of the d_{001} distance nor by a change in spectral characteristics. This means that the bis complex between the clay platelets remained intact and that the desorption of en occurred at the external surfaces. Failure to observe en desorption at room temperature from $Cu(en)_2$CB1 indicates that all the bis complex was located between the clay layers. The decrease of the d_{001} distance after degassing of $Cu(en)_2$CB1 at room temperature is due to intercalation. Because of the low loading of this sample not all the platelets are filled with $Cu(en)_2^{2+}$ complexes. Degassing at room temperature removes the water, and the observed d_{001} spacing is an average between 12.8 Å for the loaded platelets and 9.5 Å for the collapsed platelets with Na^+ between the sheets. The weight loss in the region 403–493 K can be accounted for mainly by desorption of en present between the clay layers in a physisorbed or protonated form, although some complex decomposition cannot be ruled out, especially in the case of $Cu(en)_2$CB3. The reason for this explanation is that the amount desorbed above 493 K from $Cu(en)_2$CB1 is exactly twice the Cu^{2+} content and that the en:Cu ratio exceeds 2 in any case (Table I). Thus, the bis complex between the clay layers decomposes mainly above 493 K. Additional evidence is found in the nearly constant d_{001} spacings up to 446 K (Table III). Then, from the desorption data for $Cu(en)_2$CB3 in Table IV 0.70 mequiv of $Cu(en)_2^{2+}$ is strongly held between the clay layers. The sites where this 0.70 mequiv is located are viewed as strong sites.

Finally we remark that the absence of any low temperature desorption of en from $Cu(en)_2$CB1 indicates that $Cu(en)_2^{2+}$ prefers to exchange with Na^+ on these strong sites in the initial stages of the exchange reaction. It is only when these sites are filled that exchange occurs on the external surface sites. This is confirmed by the behavior of the selectivity coefficient of the ion exchange reaction as a function of the loading: it remained constant from 0 to 0.7 mequiv of Cu^{2+}/g of clay and dropped regularly above a loading of 0.7 mequiv.[9]

$Cu(en)^{2+}$ Camp Berteau Montmorillonite. The exchange from an aqueous solution with a en:Cu ratio of one gave a slightly higher en:Cu ratio on the clay, especially at small loadings (Table I). EPR and reflectance spectroscopy indicate the presence of bis, mono, and aquo complexes on the surface. Their relative concentrations depend on the exchange conditions. In any case, the d_{001} spacings (Table III) are indicative of square-planar complexes between the layers: $Cu(H_2O)_4^{2+}$, $Cu(en)(H_2O)_2^{2+}$, and $Cu(en)_2^{2+}$. The reflectance and EPR spectra do not allow a determination of their relative concentrations due to strong band overlap. However, the absorption maximum around 19000 cm^{-1} suggests the predominance of the bis complex. The frequency shifts observed upon degassing (Figure 5) indicate that the relative concentrations of the three species is determined by the presence of water. Indeed, the desorption data of Table IV indicate that water is desorbed below 463 K, while en comes off only above 463 K. We tentatively suggest the following sequence of reactions:

$$nH_2O + Cu(H_2O)_4^{2+} + Cu(en)_2^{2+} \xrightarrow[\text{evacuation}]{\text{room temperature}} 2Cu(en)(H_2O)_2^{2+} + nH_2O \quad (1)$$

$$2Cu(en)(H_2O)_2^{2+} \xrightarrow{393\ K} Cu(en)_2^{2+} + \text{lattice-bonded } Cu^{2+} + 4H_2O \quad (2)$$

$$Cu(en)_2^{2+} \xrightarrow{>463\ K} \text{lattice-bonded } Cu^{2+} + 2en \quad (3)$$

Reaction 1 explains the band shift from 19 000 to 18 000 cm^{-1} and reaction 2 the subsequent shift to 19 000 cm^{-1}. These reactions presumably occur to a limited extent, probably on certain sites. The $Cu(en)_2^{2+}$ formed in reaction 2 must be situated on the strong sites, because all en desorbs only above 463 K. In any case, a square–planar complex remains between the clay layers up to 446 K as indicated by the d_{001} spacing of 12.54 Å after degassing Cu(en)CB2 at 446 K (Table III).

$Cu(en)_3^{2+}$ Camp Berteau Montmorillonite. The adsorption of controlled amounts of en leads immediately to the formation of a band near 20 000 cm^{-1} in the reflectance spectrum. It indicates the formation of the square–planar bis complex. The reaction proceeds quantitatively up to an en:Cu ratio of 2; i.e., all the Cu^{2+} is in the bis complex. The shift toward 16 600 cm^{-1} upon increase of the en level indicates the formation of the tris complex. Indeed, the band maximum is near to that of a tris complex in solution (16 700 cm^{-1}) and also the EPR parameters (Table II) agree with those of the tris complex. Further evidence for the formation of the tris complex is drawn from the d_{001} distance of 13.8 and 14.6 Å for 60% Cu^{2+}-exchanged samples and fully Cu^{2+}-exchanged samples, respectively. This distance is significantly greater than the 12.75 Å observed for the bis complex. The orientation experiments in the EPR spectrometer indicate that the tris complex is inclined by 45° with respect to the *c* direction of the clay layers. This result is identical with that obtained by Mortland et al. for $Cu(H_2O)_6^{2+}$.[15]

When CuCB has been heated under vacuum prior to adsorption of en, the formation of the tris complex starts at much lower en:Cu ratio. Thus, part of the Cu^{2+} has become inaccessible; i.e., the ions have migrated inside the hexagonal holes toward the octahedral layer. This observation confirms a previous one by Mortland and coworkers.[26]

Finally, we conclude this discussion by a MO calculation and ligand field calculation on the tris complex. Its effective axial symmetry allows the application of the model for the bis complex. The results are given in Table VI. In no case is there a significant difference in MO coefficients and CFSE for the tris complex on the montmorillonite surface with respect to the tris complex in solution. We conclude that $Cu(en)_3^{2+}$ does not undergo a significant interaction with the surface except for the electrostatic one between the positive charge of the complex and the negative charge of the lattice.

Acknowledgment. This work was supported by the NSF (U.S.A.) and by the Belgian Government (Diensten van het Wetenschapsbeleid). R.A.S. is indebted to the N.F.W.O. (Belgium) for a grant as "Bevoegdverklaard Navorser". F.V. acknowledges a grant from I.W.O.N.L. (Belgium). The technical assistance of J. Pelgrims in the chemical analysis of the samples is greatly appreciated.

References and Notes

(1) W. Bodenheimer, L. Heller, B. Kirson, and S. Yariv, *Clay Miner. Bull.*, **5**, 145 (1962); *Proc. Int. Clay Conf.*, **2**, 351 (1963); *Isr. J. Chem.*, **1**, 391 (1963).
(2) S. Yariv, W. Bodenheimer, and L. Heller, *Isr. J. Chem.*, **2**, 201 (1964).
(3) W. Bodenheimer, L. Heller, and S. Yariv, *Proc. Int. Clay Conf.*, **1**, 251 (1968).
(4) W. Bodenheimer, B. Kirson, and S. Yariv, *Isr. J. Chem.*, **1**, 69 (1969).
(5) R. Laura and P. Cloos, Proceedings "Reunion HispanoBelga de Minerales de la Arcilla, Madrid", 1970, p 76.
(6) J. Chaussidon, R. Calvet, J. Helsen, and J. J. Fripiat, *Nature (London)*, **196**, 161 (1962).
(7) V. C. Farmer and M. M. Mortland, *J. Phys. Chem.*, **69**, 683 (1965).
(8) P. J. Rupert, *J. Phys. Chem.*, **77**, 6 (1973).
(9) P. Peigneur, Ph.D. Dissertation, Katholieke Universiteit Leuven, 1976.
(10) P. Peigneur, J. H. Lunsford, W. De Wilde, and R.A. Schoonheydt, *J. Phys. Chem.*, preceding paper in this issue.
(11) J. P. Eeckman and H. Laudelout, *Kolloid Z.*, **178**, 99 (1961).
(12) A. Cremers and H. C. Thomas, *J. Phys. Chem.*, **70**, 3229 (1966).
(13) American Petroleum Institute, Research Project 49.
(14) K. Klier, *Catal. Rev.*, **1**, 207 (1967).
(15) D. M. Clementz, T. J. Pinnavaia, and M. M. Mortland, *J. Phys. Chem.*, **77**, 2, 196 (1973).
(16) "Handbook of Physics and Chemistry", R. C. West, Ed., 52nd ed, Chemical Rubber Publishing Co., Cleveland, Ohio, 1971–1972, p E114.
(17) H. S. Peiser, H. P. Rooksby, and A. J. C. Wilson, "X-ray Diffraction by Polycrystalline Materials", J. Wright & Sons, Bristol, 1955.
(18) C. C. Chao and J. H. Lunsford, *J. Chem. Phys.*, **57**, 2890 (1972).
(19) F. Velghe, unpublished results.
(20) B. K. G. Theng, D. J. Greenland, and J. P. Quirk, *Clay Miner.*, **7**, 1 (1967).
(21) R. Krishnamurthy and W. B. Schaap, *J. Chem. Ed.*, **47**, 433 (1970); **46**, 799 (1969).
(22) D. Kivelson and R. Neiman, *J. Chem. Phys.*, **33**, 149 (1961).
(23) I. M. Procter, B. J. Hathaway, and P. Nicholls, *J. Chem. Soc. A*, 1678 (1968).
(24) B. J. Hathaway, D. E. Billing, P. Nicholls, and I. M. Procter, *J. Chem. Soc. A*, 319 (1969).
(25) B. W. Brown and E. D. Singafelsen, *Acta Crystallogr.*, **17**, 254, (1964).
(26) M. B. McBride and M. M. Mortland, *Soil. Sci. Soc. Am. Proc.*, **38**, 408 (1974).

Intersystem Crossing and Internal Conversion Quantum Yields of Acridine in Polar and Nonpolar Solvents

Arlette Kellmann

Laboratoire de Photophysique Moléculaire du CNRS, Université de Paris Sud, 91405 Orsay, France *(Received December 6, 1976)*

Publication costs assisted by CNRS

The present work reports measurements of S ⇝ T intersystem crossing quantum yields of acridine in polar and nonpolar solvents, using the third harmonic of a Nd-glass laser. The intersystem crossing yield was determined by comparing the triplet formation of acridine with that of anthracene in ethanol, used as a reference. The quantum yields of acridine in benzene, *tert*-butyl alcohol, and water were found to be 0.73, 0.61, and 0.39, respectively. These data combined with the fluorescence yields show the existence of internal conversion from the first excited singlet state of acridine in the three solvents. The results indicate a strong solvent effect for the rate constants of the radiationless transitions. No significant deuterium effect was observed on the quantum yields.

Introduction

The radiative and radiationless processes in aromatic molecules have been extensively studied during the last years. The nitrogen-heterocyclic compounds are of particular interest owing to the presence of n,π^* states.[1] Aza and diaza analogues of benzene and naphthalene have been the subject of a number of experimental and theoretical studies.[2-4] However, little quantitative information is available concerning the nonradiative transitions (intersystem crossing and internal conversion) in acridine, the aza analogue of anthracene. In this paper we report an experimental determination by use of a laser of the singlet ⇝ triplet intersystem crossing quantum yields (Φ_{isc}) for acridine in polar and nonpolar solvents (water, *tert*-butyl alcohol, benzene). These systems were chosen for study, as their photochemistry[5-10] and emission properties[16-18] are fairly well known. Acridine (Ac) irradiated in hydrogen-donating solvents abstracts, via an excited state, a hydrogen from the solvent, giving the acridanyl radical (AcH·). This radical leads to acridan (AcH_2), substituted acridan, and to diacridan (Ac_2H_2). The nature of the excited state involved in the photochemical reaction has been discussed,[10-15] and the more recent studies suggest that a n,π^* singlet state is the reactive state.[10,15] In contrast to anthracene, acridine does not show fluorescence in hydrocarbons at room temperature, but fluoresces slightly in alcohols and strongly in water;[16,17] there is no doubt that the fluorescent state is (π,π)* in nature.[18] The solvent dependence of the fluorescence of several polycyclic monoazines has been interpreted as involving the interchange of the lowest n,π^* singlet state in a hydrocarbon solvent to a π,π^* singlet in a hydroxylic solvent, due to hydrogen bonding.[19] The spectroscopic work of Coppens and co-workers on acridine[21] suggests that the n,π^* singlet state is slightly higher than the π,π^* state in polar solvents, in agreement with some other theoretical and experimental studies;[12,13,15,20] however, Whitten and Lee[10] proposed a lower n,π^* state irrespective of the solvent polarity. Indeed, even in the absence of precise information about the relative position of π,π^* and n,π^* singlet states, it can be assumed that these two states, being very close, are strongly mixed by vibronic coupling irrespective of the order of the levels. It has been emphasized[4a] that vibronic coupling may be important in the deactivation via internal conversion of the first excited singlet state of nitrogen-heterocyclic compounds. Indeed our present results on acridine lead to the conclusion of the existence of an internal conversion from the lowest excited singlet state to the ground state.

Experimental Section

Materials. Acridine (Eastman Kodak) was recrystallized three times from an ethanol–water mixture after refluxing with active carbon. Acridine-d_9 (Merck Sharp and Dohme) was purified by vacuum sublimation. Anthracene was an Aldrich Gold Label product. Benzene, ethanol, and *tert*-butyl alcohol (Merck Uvasol) were used without further purification. The aqueous solutions were prepared from twice distilled deionized water. The solutions were made basic using 0.01 M NaOH. Samples for flash and laser photolysis were degassed by several cycles of the freeze–pump–thaw procedure; after each pumping, argon was introduced above the solution.

Apparatus and Method. The conventional flash apparatus used has been previously described in detail.[22] The excitation light source of the laser flash spectroscopy setup is a Nd^{3+} doped glass laser (C.G.E., Model VD 231) emitting at 1058 nm. The third harmonic (353 nm), generated by means of KDP crystals, was used in the present work at energy of a few mJ (1–20 mJ); the pulse half-width was 30 ns.

The laser beam was projected on one side of a 10-mm square silica cell with polished sides containing the sample. A frosted plate of silica was placed close to the cell, to homogenize the laser beam. The analyzing light, a xenon flash (with a maximum remaining constant for more than 20 μs after the laser pulse), crossed the optical cell at 90° to the laser beam, through a 2-mm wide section of the irradiated part of the solution, close to the laser entrance window; the monitoring light was then focused on the slit of a monochromator (Jarrell-Ash f = 0.25 m, band width 2 nm). The transient signal monitored by a photomultiplier tube (Radiotechnique 150 UVP) was displayed on a dual-beam oscilloscope (Fairchild Model 777). Relative values of the laser energy were obtained by measuring a small fraction of the UV laser beam deflected on a calibrated photodiode (ITT 4000 S) and its integrated photocurrent was displayed on the oscilloscope (from these measurements a linear correction of the transient optical densities was applied for variations in the laser energy). The oscillograms were recorded photographically; Figure 1 shows an example of oscilloscope traces of triplets of acridine and anthracene, and of the relative values of the energy laser.

TABLE I: Intersystem Crossing and Internal Conversion Quantum Yields

Molecule	Solvent	ϵ_T, M^{-1} cm^{-1}	Φ_r	Φ_{fl}	Φ_{isc}	Φ_{ic}	k_{isc}/k_{ic}
Acridine	Benzene	27 000	$\leq 10^{-3}$	$<10^{-3}$	0.73 ± 0.07	0.27	2.7
Acridine-d_9	Benzene	26 000		$<10^{-3}$	0.75 ± 0.07	0.25	3.0
Acridine	*tert*-BuOH	26 000	0.01	0.02	0.61 ± 0.06	0.36	1.7
Acridine	Water, 0.01 M NaOH	19 000		0.37[a]	0.39 ± 0.06	0.24	1.6
Anthracene	EtOH	60 000		0.30[b]	0.70[c]		

[a] Reference 17. [b] Reference 34. [c] Reference 24.

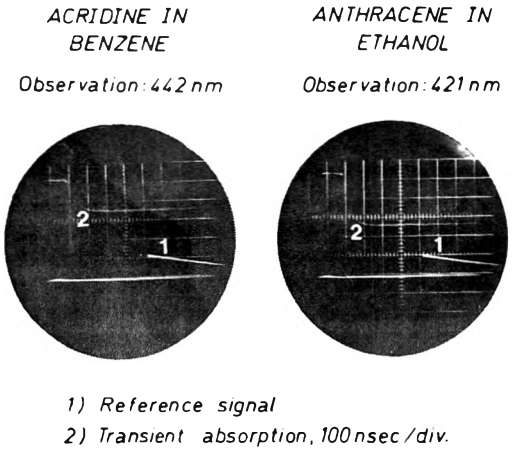

Figure 1. Oscilloscope traces showing the triplet absorption of acridine and anthracene, and the corresponding energy references.

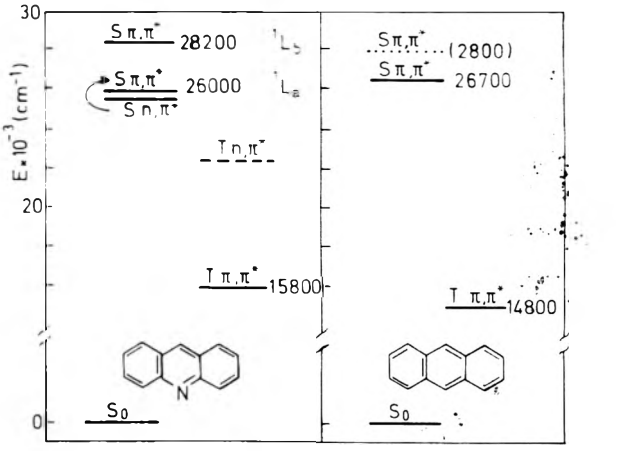

Figure 2. Energy of the lower singlet and triplet states of acridine and anthracene; (——) experimentally observed; (- - -) approximate energy obtained from calculations (ref 20); (····) band of ^1L_b type hidden by ^1L_a band.

In a previous study with a dye laser[23] we determined triplet quantum yields by measuring directly the laser energy. In the present work the energy input was estimated by excitation of a standard solution used as an actinometer. Anthracene was the standard, using solutions of the same absorbance at 353 nm as employed for acridine; optically thin solutions (OD = 0.06 across a 2-mm path) were used to obtain low and relative uniform triplet concentrations over the volume viewed by the analyzing light. The concentrations of anthracene and acridine were respectively 6×10^{-5} and 4×10^{-5} M, giving a conversion to the triplet state of less than 15%. The anthracene actinometry was performed in ethanol and the triplet–triplet absorption monitored at 420 nm. The Φ_{isc} was taken as 0.70,[24] and ϵ_T 60 000 M^{-1} cm^{-1}, obtained as described in the following paragraph.

The triplet–triplet extinction coefficients ϵ_T were measured by a light-saturation technique using a flash-photolysis apparatus: the intensity of the transient absorption increases with increasing flash-light output, reaching an approximately constant level at high light output (1500 to 2500 J discharge energy). The saturation effect was assumed to be due to complete conversion of the ground state to the triplet state. The concentrations used in the flash experiments were 10^{-6} M.

A Cary (Model 14) spectrophotometer and a Hitachi-Perkin-Elmer (MPF 3L) spectrofluorimeter were used for the measurements of the absorption and fluorescence spectra.

Results and Discussion

The first excited electronic states of acridine are shown in Figure 2. The two lowest excited π,π^* singlet states ^1L_a and ^1L_b are located at 25 700 and 28 200 cm^{-1}, respectively, according to the determinations by Zanker[25] and the n,π^* singlet state is assumed to be very close to the ^1L_a state.[10,15,20] The lowest π,π^* triplet state has been experimentally determined[26] and the n,π^* triplet calculated.[20] Anthracene electronic states are given for comparison: the π electronic spectrum of acridine is very similar to that of its isoelectronic hydrocarbon, and both compounds have a strong absorption band at 353 nm.

The quantum yield of the internal conversion from the first excited singlet state is deduced from the relation $\Phi_{ic} = 1 - (\Phi_r + \Phi_{fl} + \Phi_{isc})$, by assuming that the primary photoreduction (Φ_r) (abstraction of a hydrogen from the solvent), fluorescence (Φ_{fl}), and intersystem crossing (Φ_{isc}) are the only deactivating pathways for the acridine molecule in its lowest excited singlet state.

The values of the triplet–triplet extinction coefficients and the quantum yields obtained for acridine in benzene, *tert*-butyl alcohol, and water are given in Table I.

Acridine in Benzene. The triplet–triplet absorption spectrum of acridine (Ac) in benzene has been reported previously[27] (λ_{max} 442 nm, Figure 3). The maximum of the triplet–triplet absorption of the perdeuterated acridine (Ac-d_9) determined in this work is similar to that of Ac-h_9. From our measurements, the fluorescence yields of Ac-h_9 and Ac-d_9 in benzene at room temperature appear to be less than 10^{-3} and the primary photoreduction is negligible ($\Phi_r \leq 10^{-3}$). The value of Φ_{isc} (0.7) is the same for the perhydro and perdeuterio compounds within experimental error, and shows no enhancement relative to that of anthracene in spite of the absence of fluorescence; this result indicates a direct radiationless deactivation of the first excited singlet to the ground state ($\Phi_{ic} \simeq 0.3$). The lack of a deuterium effect suggests that the C–H or C–D vibrations do not play any significant role in the mechanism responsible for the internal conversion quantum yield of acridine. This absence of deuterium effect has already been observed for other heterocyclics such as diazines,[2] whereas a deuterium effect has been demonstrated on the phosphorescence yield of quinoxaline.[4b]

Acridine in tert-Butyl Alcohol. The triplet–triplet absorption maximum was found to be located at 436 nm, with an extinction coefficient of the same value as that in benzene. The photoreduction quantum yield determined in steady-light studies[10,28] is very low ($\Phi_r \simeq 0.01$). Φ_{fl} is of the same order of magnitude as that of acridine in ethanol. The value of Φ_{isc} determined in *tert*-butyl alcohol

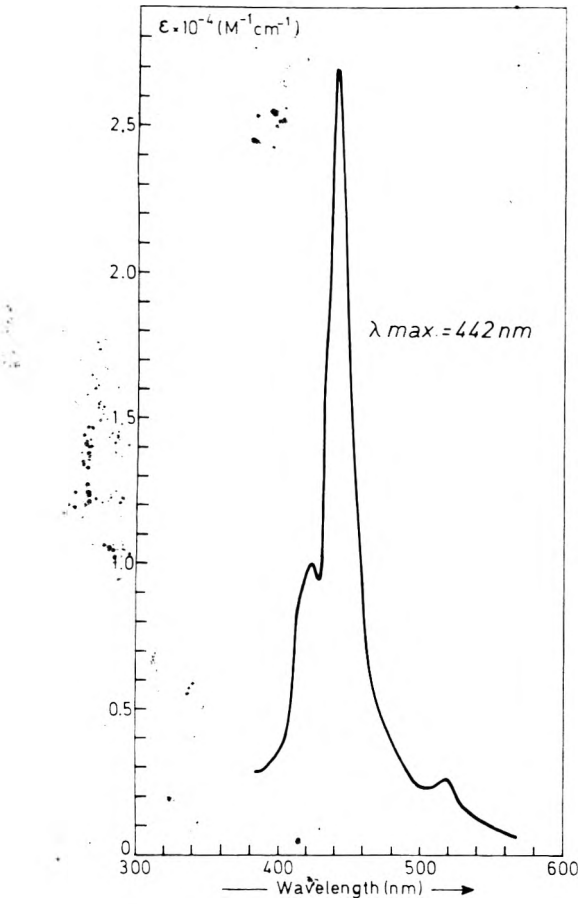

Figure 3. Triplet–triplet absorption spectrum of acridine in benzene.

is a little lower than that in benzene. There are no literature data which can be directly compared with our results in this alcohol. However, the results reported by Koizumi and co-workers on the determination of Φ_{isc} of acridine in different alcohols show no change when going from methanol to propanol.[29,30] Therefore, it seems reasonable to compare our results for acridine in *tert*-butyl alcohol with previously reported determinations of intersystem crossing quantum yields of acridine in ethanol. The latter values vary from 0.7 to 0.4. Values around 0.7 were obtained using either heavy atom quenching of the fluorescence,[31] or triplet energy transfer.[32] The lower value (0.4) was obtained using an absolute method in which the light absorbed by the system is measured by actinometry.[29] Our value of Φ_{isc} in *tert*-butyl alcohol lies between these wide limits. However, a lower value of Φ_{isc} in ethanol may be due to the photoreduction process which takes place with a good hydrogen donor such as ethanol ($\Phi_r = 0.13$[7,28]). Indeed, the value of 0.42 obtained by Koizumi et al.[29] combined with the photoreduction and fluorescence yields leads to a value of $\Phi_{ic} \simeq 0.40$ in good agreement with our value of $\Phi_{ic} = 0.36$ for acridine in *tert*-butyl alcohol.

Our results show that there is no important solvent effect on intersystem crossing quantum yields when going from benzene to a hydroxylic solvent. A similar observation has been made for other heterocyclics, quinoline, isoquinoline, and quinoxaline, studied at low temperature in alcoholic and hydrocarbon solvents.[3,4a]

Acridine in Water. Acridine, weakly or nonfluorescent in organic solvents, shows a strong fluorescence in water ($\Phi_{fl} = 0.37$);[19] the fluorescence yield is not appreciably changed by deuteration ($\Phi_{fl} = 0.40$).[33] The large increase of the fluorescence yield is accompanied by a decrease of the intersystem crossing yield for acridine in water (in comparison with organic solvents), which gives an internal conversion similar to that of acridine in organic solvents. This result stresses the difference between acridine and anthracene; despite a fluorescence yield in water similar to that of anthracene in organic solvents,[34] acridine shows an internal conversion which does not exist in the parent hydrocarbon.

Finally the results in Table I indicate that in water, where the acridine fluorescence quantum yield is enhanced relative to the other solvents, the corresponding intersystem crossing yield is decreased, whereas the internal conversion yield remains nearly constant. In contrast to these results, Li and Lim[4a] reported for isoquinoline that a large increase of the fluorescence yield in alcoholic solvent (relative to hydrocarbon solvent) is accompanied by an important decrease of the internal conversion yield, while the intersystem crossing yield is relatively constant.

Solvent Effect on Radiationless Transitions. It is seem from Table I that the ratios of the rate constants of the radiationless processes k_{isc}/k_{ic} deduced from the quantum yields are little affected by the nature of the solvent. The fluorescence lifetime of acridine in water had been determined by Kokubun[35] as $\tau = 10$ ns; then the rate constants for the radiationless processes as deduced from Φ/τ are $k_{isc} = 4 \times 10^7$ s^{-1} and $k_{ic} = 2.5 \times 10^7$ s^{-1}. Assuming the same radiative lifetime for *tert*-butyl alcohol as for water ($\tau = 3 \times 10^{-8}$ s), a fluorescence lifetime of 0.6 ns is deduced from the fluorescence quantum yield, in good agreement with $\tau = 0.7$ ns in ethanol, obtained by Kokubun. Since the lifetime of acridine in benzene is not available, we used the value of the singlet lifetime of 13 ps determined in isooctane by Hirata and Tanaka[36] (the lowest excited singlet state of acridine is of n–π^* character in isooctane as it is in benzene). Then the rate constants for the radiationless processes k_{isc} and k_{ic} deduced from this lifetime value are in benzene about 1000 times as large are those in water ($k_{isc} \simeq 5 \times 10^{10}$ s^{-1} and $k_{ic} \simeq 2 \times 10^{10}$ s^{-1}). The strong increase of k_{isc} when going from water to benzene observed in the present study is consistent with the theoretical prediction of El-Sayed.[37] This increase is expected from the change in the character of the lowest excited singlet state of acridine from π,π^* in hydroxylic solvents to n,π^* in hydrocarbons ($S_{n,\pi^*} \rightsquigarrow T_{\pi,\pi^*}$). However, the most striking feature in these results is that the enhancement of the internal conversion rate k_{ic} for acridine in benzene (relative to water) is of the same order of magnitude as that of k_{isc}, as is shown from the small variations observed in the k_{isc}/k_{ic} ratios for water, *tert*-butyl alcohol, and benzene.

The existence of internal conversion in the acridine molecule, in contrast with the lack of internal conversion in anthracene, is consistent with the vibronic coupling model developed by Hochstrasser and Marzacco in the case of quasi-degenerate states,[38] and used by Li and Lim for heterocyclics.[4b] The vibronic state obtained by coupling the π,π^* and the nearby n,π^* singlet states through out of plane vibrations increases the Franck–Condon factor corresponding to the radiationless transition toward the ground state.[39] Thus, it is seen that in acridine the internal conversion through vibronic coupling operates in solvents where fluorescence occurs, as well as in the cases where this compound does not fluoresce.

Acknowledgment. I wish to thank Dr. L. Lindqvist for helpful discussions concerning this paper, and I am indebted to Dr. Lhoste for his gift of deuterated acridine.

References and Notes

(1) R. S. Becker, "Theory and Interpretation of Fluorescence and Phosphorescence", Wiley, New York, N.Y., 1969, and references therein.

(2) B. J. Cohen and L. Goodman, *J. Chem. Phys.*, **46**, 713 (1967).
(3) S. G. Hadley, *J. Phys. Chem.*, **75**, 2083 (1971).
(4) (a) Y. H. Li and E. C. Lim, *Chem. Phys. Lett.*, **9**, 279 (1971); (b) R. Li and E. C. Lim, *J. Chem. Phys.*, **57**, 605 (1972).
(5) F. Mader and V. Zanker, *Chem. Ber.*, **97**, 2418 (1964).
(6) A. Kellmann, *J. Chim. Phys. Physicochim. Biol.*, **63**, 936 (1966).
(7) A. Kira, S. Kato, and M. Koizumi, *Bull. Chem. Soc. Jpn.*, **39**, 1221 (1966).
(8) M. Giurgea, G. Mihai, V. Topa, and M. Musa, *J. Chim. Phys. Physicochim. Biol.*, **61**, 619 (1964).
(9) H. Göth, P. Cerutti, and H. Schmid, *Helv. Chim. Acta*, **48**, 1395 (1965).
(10) D. G. Whitten and Y. J. Lee, *J. Am. Chem. Soc.*, **93**, 961 (1971).
(11) A. Kellmann and J. T. Dubois, *J. Chem. Phys.*, **42**, 2518 (1965).
(12) E. Vander Donckt and G. Porter, *J. Chem. Phys.*, **46**, 1173 (1967).
(13) F. Wilkinson and J. T. Dubois, *J. Chem. Phys.*, **48**, 2651 (1968).
(14) M. Koizumi, Y. Ikeda, and H. Yamashita, *Bull. Chem. Soc. Jpn.*, **41**, 1056 (1968).
(15) V. Zanker and G. Prell, *Ber. Bunsenges. Phys. Chem.*, **73**, 791 (1969).
(16) N. Mataga and S. Tsuno, *Bull. Chem. Soc. Jpn.*, **30**, 368 (1957).
(17) E. J. Bowen, N. J. Holder, and G. B. Woodger, *J. Phys. Chem.*, **66**, 2491 (1962).
(18) S. J. Ladner and R. S. Becker, *J. Phys. Chem.*, **67**, 2481 (1963).
(19) (a) J. W. Sidman, *Chem. Rev.*, **58**, 689 (1958); (b) M. A. El-Sayed and M. Kasha, *Spectrochim. Acta*, **15**, 758 (1959).
(20) L. Goodman and R. W. Harrell, *J. Chem. Phys.*, **30**, 1131 (1959).
(21) G. Coppens, C. Gillet, J. Nasielski, and E. Vander Donckt, *Spectrochim. Acta*, **18**, 1441 (1962).
(22) L. Lindqvist, *Rev. Phys. Appl.*, **3**, 15 (1968).
(23) B. Soep, A. Kellmann, M. Martin, and L. Lindqvist, *Chem. Phys. Lett.*, **13**, 241 (1972).
(24) (a) A. R. Horrocks and F. Wilkinson, *Proc. R. Soc. London, Ser. A*, **306**, 257 (1968); (b) D. N. Dempster, T. Morrow, and M. F. Quinn, *J. Photochem.*, **2**, 329 (1973/1974).
(25) V. Zanker, *Z. Phys. Chem. (Frankfurt am Main)*, **2**, 52 (1954).
(26) D. F. Evans, *J. Chem. Soc.*, 1351 (1957).
(27) A. Kellmann and L. Lindqvist, "The Triplet State", A. B. Zahlan, Ed., Cambridge University Press, New York, N.Y., 1967, p 439.
(28) A. Kellmann, *Bull. Soc. Chim. Belg.*, **71**, 811 (1962).
(29) K. Tokumura, K. Kikuchi, and M. Koizumi, *Bull. Chem. Soc. Jpn.*, **46**, 1309 (1973).
(30) These authors reported the values of Φ_{isc} = 0.44, 0.42, and 0.45 for methanol, ethanol, and propanol, respectively, leading to a $\Phi_{ic} \simeq 0.40$ for each alcohol.
(31) Value given in ref 13.
(32) V. L. Pugachev and A. K. Chibisov, *Opt. Spectrosc.*, **34**, 284 (1973).
(33) Similarly, deuteration does not affect the fluorescence of other heterocyclics (monocyclic diazines[2]) and some aromatic hydrocarbons.[4b]
(34) G. Weber and F. W. J. Teale, *Trans. Faraday Soc.*, **53**, 646 (1957).
(35) H. Kokubun, *Bull. Chem. Soc. Jpn.*, **42**, 919 (1969).
(36) Y. Hirata and I. Tanaka, *Chem. Phys. Lett.*, **41**, 336 (1976).
(37) M. A. El-Sayed, *J. Chem. Phys.*, **38**, 2834 (1963).
(38) R. B. Hochstrasser and C. A. Marzzaco, "Molecular Luminescence", E. C. Lim, Ed., W. A. Benjamin, New York, N.Y., 1969, p 631.
(39) J. P. Byrne, E. F. Mc Coy, and I. G. Ross, *Aust. J. Chem.*, **18**, 1589 (1965).

An Electron Spin Resonance Study of Electron Reactions with Amino Acid Anhydrides[1]

Michael D. Sevilla* and R. Failor-Koszykowski

Department of Chemistry, Oakland University, Rochester, Michigan 48063 *(Received January 19, 1977)*

Publication costs assisted by the U.S. Energy Research and Development Administration and the Food Engineering Laboratory of the U.S. Army Natick Development Center

The electron attachment reactions to two amino acid anhydrides (cyclic peptides) in an aqueous glass have been investigated by ESR spectroscopy. Electron attachment to glycine anhydride (GA) at 77 K in 12 M LiCl results in an anion which remains stable to 175 K. At 175 K a second radical is found which is suggested to be the species produced by abstraction of a hydrogen atom from a methylene group in GA. This suggestion is verified by the production of this same species by attack of O^- or ·OD on GA in 8 M $NaClO_4$–D_2O glasses. Electron attachment is alanine anhydride at 77 K results in a stable anion which showed no further reaction on warming. The results found for GA are compared to previous studies of γ-irradiated GA single crystals and a study of γ-irradiated polycrystalline GA reported in this work. A possible mechanism for the production of the second radical from the GA anion is discussed.

Introduction

A number of investigations have established that N-terminal amine groups in peptides are readily deaminated after electron attachment.[2-8] The structures of glycine anhydride (2,5-diketopiperazine) and alanine anhydride (3,6-dimethyl-2,5-diketopiperazine) are therefore of interest to the radiolysis of peptides since they have two peptide bonds and no terminal amine groups; thus the possibility of secondary amine deamination by electron attachment can be investigated.

In this work we have produced the anions of glycine anhydride (GA) and alanine anhydride (AA) in an aqueous glass and studied their subsequent reactions. This work is compared to previous investigations of GA in the solid state and in aqueous solution.

Experimental Section

The same experimental techniques as were employed in our previous investigations of electron reactions with amino acids and peptides were employed in this work.[2] Approximately 50 mM solute is dissolved in 12 M LiCl–D_2O containing 10 mM $K_4Fe(CN)_6$. The glass prepared from this solution is photolyzed with 254-nm light. The photolysis produced electrons from the photooxidation of $K_4Fe(CN)_6$. The electrons generated react with the solute.

In two cases 8 M $NaClO_4$–D_2O glasses were employed to produce specific radicals by O^- (OD·) attack. In this technique the 8 M $NaClO_4$–D_2O glass containing 50 mM solute is either γ-irradiated or photolyzed with 254-nm light (in the presence of $K_4Fe(CN_6)$. Electrons generated in this glass are converted to O^- by the reaction[10]

$$ClO_4^- + e^- \rightarrow ClO_3^- + O^-$$

Fremy's salt (peroxylaminedisulfonate) was employed as a standard for g values and hyperfine splittings (a_N = 13.1 G and g = 2.0056).

Results and Discussion

Glycine Anhydride (GA). Electron attachment to GA in 12 M LiCl–D_2O at 77 K resulted in an ESR spectrum

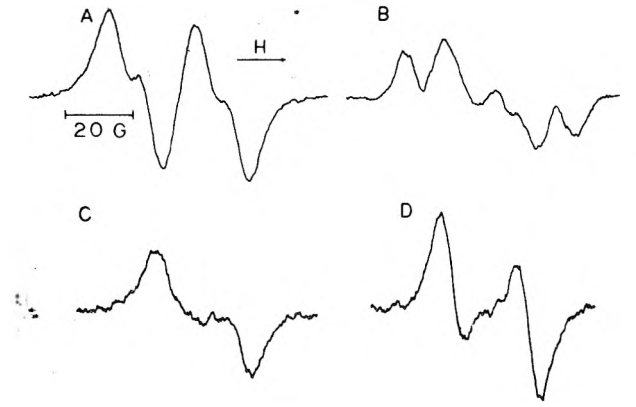

Figure 1. First derivative ESR spectra of amino acid anhydrides in 12 M LiCl–D_2O after electron attachment: (A) the glycine anhydride anion at 128 K; (B) the abstracted species, radical II, at 175 K (this species is formed by warming the glycine anhydride anion to the softening point of the glass); (C) the alanine anhydride anion at 150 K; (D) the alanine anhydride anion at 160 K after warming to 175 K (a second radical was not observed in this case).

consisting of doublet of 26.7 G further split into 8.5-G doublets (g = 2.0030). The spectrum remains unchanged to temperatures near 175 K. The spectrum in Figure 1A shows this species at 128 K. This spectrum is assigned to the anion radical I.

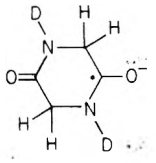

I

The two methylene protons which are next to the position of high unpaired spin are nonequivalent. One has a 26.7-G splitting while the other has a 8.5-G splitting. Such splittings are reasonable only for structures in which the six-membered ring is somewhat nonplanar. The crystal structure shows that the molecule is approximately planar.[9] However, the anion in an aqueous matrix would be likely to have a different conformation from the parent compound in a crystal.

The dependence of β-proton splitting on the dihedral angle (θ) between the C–H bond and the p_z orbital containing the unpaired spin is given by

$$a = B_0\rho^\pi + B_2\rho^\pi \cos^2\theta$$

where B_0 and B_2 are constants and ρ^π is the electron spin density.[11]

The values $B_0\rho^\pi = -3.8$ and $B_2\rho^\pi = 34.6$ were found for the acetamide anion in an alkaline aqueous glass.[12] This species is a model compound for the peptide bond and therefore GA^-. Employing these values we find $\theta_1 = 20°$ (26.7-G splitting) and $\theta_2 = 140°$ (8.5-G splitting). The results are self-consistent in that the difference of 120° is that expected for the difference in *dihedral angle* between the methylene protons. Since θ is expected to be 30° for a planar structure, the angle of 20° suggests only a slight bending of the ring.

Warming the anion to 175 K where the glass softens resulted in the conversion of the spectrum to that found in Figure 1B. The spectrum cannot be interpreted in terms of an anion. The spectrum appears to be due to three protons with splittings of ca. 19 G (1 H) and 12 G (2 H). Resolution of only one of the small central components expected from this interpretation is found. However due to the anisotropic effects expected for the proton with the 19-G splitting, this effect is not surprising. The only

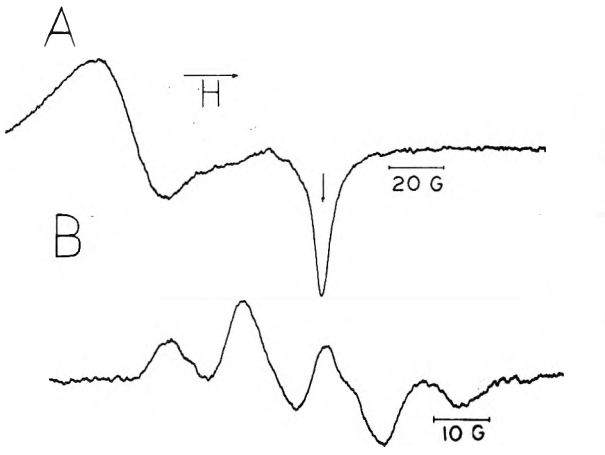

Figure 2. (A) The ESR spectrum of the O^- radical at 110 K in 8 M $NaClO_4$–D_2O. The arrow marks g = 2.002. (B) The ESR spectrum of radical II at 155 K formed by attack of O^-(·OD) on glycine anhydride in 8 M $NaClO_4$–D_2O.

structure consistent with such a spectrum is that of radical II. No couplings to nitrogen are observed.

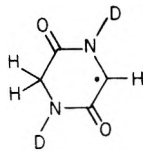

II

Radical II has been observed in single crystal work[9] and the couplings are found to be a_α = 16.6 G and a_{CH_2} = 9 G. No nitrogen couplings were observed. The agreement in splittings is only fair; but considering the broad line width in Figure 2A and the differences in matrices, the results do add some support to our assignment.

To further verify our assignment, radical II was prepared by reaction of ·OD with GA. Pulse radiolysis investigations of GA have shown that ·OH abstracts a hydrogen atom to form radical II.[13] In this work hydroxyl radicals were produced by the reaction of electrons with ClO_4^- in 8 M $NaClO_4$. Electrons are generated by the photolysis of $K_4Fe(CN)_6$. The reaction of e^- and ClO_4^- first produces O^- which likely deuterates as the glass is warmed to produce ·OD. Figure 2A shows O^- radical at 100 K. Figure 2B shows the radical produced by attack of the OH (or O^-) radical on GA. The spectrum consists of a ca. 19.5-G doublet split further by two protons at ca. 13.5 G. The spectrum is thus very similar to that found in 12 M LiCl and is good evidence for the structure of radical II.

The formation of radical II from the GA anion could occur by a number of mechanisms. Considering our previous work with peptides the most likely is the deamination of the anion to produce $ND_2COCH_2NDC\text{-}OCH_2$·. This species could then abstract a hydrogen from the parent molecule to produce radical II. The intermediate suggested by this mechanism was not observed. Since the glass was soft when the reaction occurred it is possible both steps could have occurred rapidly so that the intermediate would not have been observed.

In order to better compare the spectrum found here with that found in crystalline GA, polycrystalline GA was γ-irradiated (50 000 rads) at 77 and at 300 K. To improve resolution the labile N–H protons were exchanged with deuterium. The spectra are shown in Figure 3A and 3B. The spectrum at 77 K shows a 23-G doublet (possibly of an anion radical). Figure 3B is the polycrystalline spectrum of radical II (300 K). This species is that previously identified in single crystals by Lin and McDowell.[9] Our

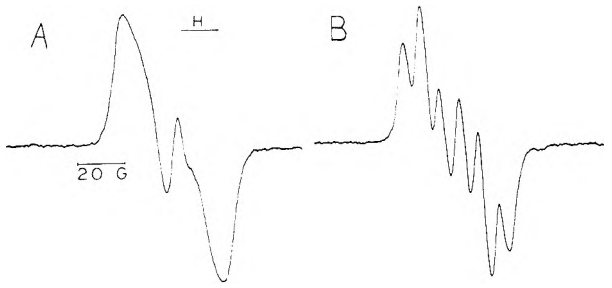

Figure 3. (A) The ESR spectrum of polycrystalline glycine anhydride γ-irradiated and recorded at 77 K. The narrow resonance in the center is a background signal. (B) The ESR spectrum of polycrystalline glycine anhydride γ-irradiated and recorded at 300 K.

spectrum shows an *apparent* 24-G doublet split by two protons at 8.5 G. However, the single crystal work clearly shows a 16.6-G isotropic component of an α-proton splitting with two protons at 9 G. It is usually the case that the anisotropic effects average so as to give close to the isotropic coupling in a powder spectrum. This, however, is not true in this case. Lin and McDowell report the principle values of the α-proton coupling to be 7.4, 15.9, and 26.5 G. Thus the apparent 24-G splitting is close to the maximum value of 26.5 G. This could result if the line width were a function of the orientation so that best resolution occurred at A_{max} and poorer resolution occurred at other orientations. Lin and McDowell show spectra along each of the principal axis. It was found that the resolution is best along A_{max}. Thus, this provides an explanation for the polycrystalline spectrum observed in Figure 3A. The angular dependence of the line width is likely due to unresolved nitrogen splittings. A_{max} corresponds to a direction in the plane of the radical. This corresponds to the $A_{\perp}$ nitrogen splitting which is the minimum value. At directions perpendicular to the radical plane the nitrogen splitting is at its maximum value and would contribute to the line width.

Alanine Anhydride (AA). Electron attachment to AA at 77 K in 12 M LiCl results in an ESR spectrum which consists of a poorly resolved doublet, Figure 1C. Upon warming to 175 K the doublet becomes much more well resolved, Figure 1D. At this temperature the splitting is 23.0 G with $g = 2.0029$. A doublet spectrum arising from the β proton is expected for the anion radical III.

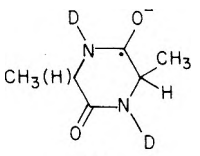

III

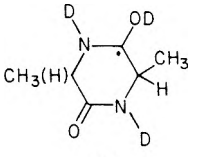

IV

The coupling to the methyl group is expected to be quite small. Using the same values of $B_0\rho^{\pi}$ and $B_2\rho^{\pi}$ employed for GA we find a 23-G splitting corresponds to $\theta = 28°$. This conformation is near that expected for a planar structure ($\theta = 30°$).

The improvement in resolution on warming was not found to be reversible upon cooling. This is likely a result of a permanent change in conformation in the radical. It is known that the protonated anion of the peptide bond has a pK_a of >13.5.[14] Thus, it is possible that upon warming a deuteration reaction takes place to produce structure IV. This structure could then produce the conformation shifts which result in improved resolution. Alternatively the anion could simply be relaxing to a more favored conformation which differs from the parent conformation.

Warming of samples beyond 175 K resulted only in a loss of signal. No second spectrum was observed. Attack of O^- or ·OD on AA in $NaClO_4$ glasses resulted in a spectrum whose splittings (two protons at 22 G and one at 29 G) suggest abstraction from one of the methyl groups. Thus, these results provide no evidence for another radical as was found for GA.

Comparison to Other Work

Hayon and Simic have shown in an pulse radiolysis investigation that the GA and AA anions efficiently transferred their excess electron to acceptor molecules.[13] These authors also found no evidence which suggested a second radical as is found in this work for GA in 12 M LiCl and in GA powder samples. Their results strongly suggest the cyclic peptide anions are relatively stable.

Product analysis of aqueous solutions of AA and GA after radiolysis has shown pyrazine derivatives as products.[15]

A comparison of this work with the cyclic peptides, GA and AA, with our previous work[2] with dipeptides clearly shows a greater stability to the anions of GA and AA than their analogous dipeptides. This is expected since the N-terminal amine group in dipeptides undergoes reductive deamination much more readily than secondary amine groups. However we also find that the AA anion is more stable than the acetylalanine anion.[2] This suggests the ring structure provides some extra measure of stability for this anion.

Acknowledgment. The authors thank Dr. Warren Garrison for helpful discussions, and for the use of his laboratory facilities at Lawrence Berkeley Laboratory; and for kindly supplying the cyclic peptides used in this work.

References and Notes

(1) This research was supported by the U.S. Energy Research and Development Administration and by the Food Engineering Laboratory of the U.S. Army Natick Development Center.
(2) M. D. Sevilla and V. L. Brooks, *J. Phys. Chem.*, **77**, 2954 (1973).
(3) P. Neta and R. W. Fessenden, *J. Phys. Chem.*, **74**, 2263 (1970).
(4) M. Simic and E. Hayon, *Radiat. Res.*, **48**, 244 (1971).
(5) W. M. Garrison, H. A. Sokol, and W. Bennett-Corniea, *Radiat. Res.*, **53**, 376 (1973).
(6) W. M. Garrison, *Radiat. Res. Rev.*, **3**, 285 (1972).
(7) Y. Tal and M. Faraggi, *Radiat. Res.*, **62**, 337 (1975).
(8) M. Faraggi and Y. Tal, *Radiat. Res.*, **62**, 347 (1975).
(9) W. C. Lin and C. A. McDowell, *Can. J. Chem.*, **41**, 9 (1963).
(10) L. Kevan in "Radiation Chemistry of Aqueous Systems", G. Stein, Ed., Wiley-Interscience, New York, N.Y., 1968.
(11) M. D. Sevilla and G. Vincow, *J. Phys. Chem.*, **72**, 3647 (1968).
(12) M. D. Sevilla, *J. Phys. Chem.*, **74**, 669 (1970).
(13) E. Hayon and M. Simic, *J. Am. Chem. Soc.*, **93**, 6781 (1971).
(14) M. Simic and E. Hayon, *J. Phys. Chem.*, **77**, 996 (1973).
(15) M. Kland-English and W. M. Garrison, *Nature (London)*, **189**, 4761 (1961).

Internal Vs. External Referencing in Nuclear Magnetic Resonance Studies of Complex Formation. Acetylene–Anisole Complex Formation

Wayne C. Appleton[†] **and James Tyrrell***

Department of Chemistry and Biochemistry, Southern Illinois University at Carbondale, Carbondale, Illinois 62901 *(Received October 27, 1976)*

Complex formation of benzoylacetylene and phenylacetylene with anisole and a number of methylated anisoles has been investigated using NMR techniques. The results obtained using both internal and external referencing methods are compared and contrasted. Equilibrium constants are given for the various systems studied. Variable temperature studies on the benzoylacetylene–anisole system give a value for the enthalpy of formation of the complex.

Introduction

Solute–solvent complex formation in aromatic solvents has been the subject of considerable investigation.[1,2] One of the principal techniques used in such investigations is nuclear magnetic resonance spectroscopy (NMR) in which the shift of the resonance signal of a hydrogen in the solute molecule is studied as a function of the concentration of the interacting solvent. The aromatic solvent is considered to act as an electron donor through its π orbitals and complex formation has been variously attributed to hydrogen bonding, π–π interactions, and dipole–dipole interactions. While the hydrogen, whose resonance signal is being used as an indicator and measure of the complexation, may be specifically involved, this is not essential since the complex formation may only incidentally place the hydrogen in a position in which its magnetic environment is modified. Though the anisoles contain two possible centers of electron donation, the π orbital system and the oxygen of the methoxy group, the former is considered to be the more likely donor. However, the direction of shift of the solute proton being studied would be quite different if one or other of the two donor sites dominated, i.e., an upfield shift if the π orbitals of the ring were dominant, a downfield shift if the lone pair orbitals of the oxygen were dominant.

Theoretical models of complexation involving one or more types of complex have been studied in some detail.[3] The following treatment is based on a method devised by Landauer and McConnell[4] and contains the assumption that the amount of the donor solvent in the complexed form is always insignificant, under the experimental conditions, relative to the uncomplexed donor. The chemical shift in hertz (Hz) from the reference of the proton resonance signal of the acetylene in pure cyclohexane solvent ("inert") is given as δ_A. The chemical shift in the mixed anisole–cyclohexane solvent is given as δ_1. Then the chemical shift due to complex formation is given by $\delta = \delta_A - \delta_1$. The mole fraction of the donor solvent in cyclohexane is given by X_B, and δ_{AB_n} are the chemical shifts, if complexation were complete (at $X_B = 1$) and of the form AB_n. Here A refers to the acetylene and B to the donor solvent. The acetylene compound was always present at a concentration low enough to prevent self-association. The lack of self-association of the benzoylacetylene at the concentrations used has been previously verified by dilution studies.[5] This allows the elimination from our consideration of all A_nB_m complexes ($n > 1$). The most likely general model for complexation in the systems studied is of the form:

$$A + B \overset{K_1}{\rightleftharpoons} AB$$

$$K_1 = (AB)/(A)X_B$$

$$AB_{n-1} + B \overset{K_n}{\rightleftharpoons} AB_n$$

$$K_n = (AB_n)/K_{n-1}(A)X_B^n$$

Then, if $(A)_0$ represents the total amount of A present:

$$(A)_0 = (A) + \sum_{k=1}^{n} (AB_k)$$

therefore

$$(A)_0 = (A) + \sum_{k=1}^{n} K_k K_{k-1}(A)X_B^k$$

The observed chemical shift can be decomposed as follows:

$$(A)_0\delta = \sum_{k=1}^{n} (AB_k)\delta_{AB_k} = \sum_{k=1}^{n} K_k K_{k-1}(A)X_B^k\delta_{AB_k}$$

therefore

$$\delta = \frac{\sum_{k=1}^{n} K_k K_{k-1} X_B^k \delta_{AB_k}}{1 + \sum_{k=1}^{n} K_k K_{k-1} X_B^k} \qquad (1)$$

where $K_0 = 1$. For the particular case of a 1:1 AB complex or a combination of an AB and AB_2 complex the respective equations are:

$$\delta = \frac{K_1 X_B \delta_{AB}}{1 + K_1 X_B} \qquad (2)$$

and

$$\delta = \frac{K_1 X_B \delta_{AB} + K_2 K_1 X_B^2 \delta_{AB_2}}{1 + K_1 X_B + K_2 K_1 X_B^2} \qquad (3)$$

The unknown K_n's and δ_{ABn}'s can then be evaluated using the experimental δ's and X_B's and nonlinear least-squares analysis.

The vast majority of studies of complex formations using NMR have utilized an internal reference such as chloroform, tetramethylsilane, or cyclohexane. Internal referencing has the advantage of simplicity and also eliminates the need to make corrections for bulk magnetic susceptibility differences. The assumption is of course that the resonance signal of the internal reference does not vary significantly with change in the solvent. Where the shifts, due to complex formation, are very large (of the order of

[†] Present Address: Velsicol Chemical Co., Ann Arbor, Mich.

hundreds of hertz), variation in the position of the internal reference is not critical but where the complex formation shifts are small, as in the systems studied here, this variation in the internal reference position can be significant. Tetramethylsilane, cyclohexane, and chloroform[6,7] have been shown to undergo significant shifts as a function of the composition of the solutions in which they are present. Becker[6] has shown that internal references should be avoided where possible in studying systems containing high concentrations of aromatics. Laszlo[8] and Rummens[9] have also considered problems associated with the use of an internal reference and have suggested methods by which shifts, independent of the internal reference, could be obtained.

When external referencing is employed, in which coaxial tubing is used for both sample and reference, corrections have to be made to the measured chemical shift for differences in magnetic susceptibility between the reference and the sample. This is given by[10]

$$\delta = \delta_0 + \frac{2\pi}{3}(\Delta X) \qquad (4)$$

where $\Delta X = X_r - X_s$ is the difference in bulk magnetic susceptibilities of the reference and the sample. Published values of bulk magnetic susceptibilities are available[11,12] for a large number of solvents and those not so available can be determined either experimentally[13,14] or theoretically.[15,16]

Experimental Section

Benzoylacetylene ($C_6H_5COC{\equiv}CH$) was prepared by the chromic acid oxidation of 1-phenylprop-2-yn-1-ol using a method devised by Bowden et al.[17] giving a product which upon multiple sublimation yielded a white solid mp 48–48.5 °C. The phenylacetylene and all of the anisoles were obtained commercially, dried, and fractionally distilled before use. All of the investigations were carried out at an acetylene concentration of 0.2 M, this concentration being low enough to prevent self-association. The solvent ranged from pure cyclohexane through 0.9 mole fraction anisoles in cyclohexane. NMR spectra were obtained on a Varian HA-100 spectrometer equipped with a variable temperature probe. The ambient temperature runs were carried out at 30 ± 2 °C. The variable temperature runs on the benzoylacetylene–anisole system were carried out at a series of controlled temperatures ranging from 20 to 60 °C. For the internal reference runs cyclohexane was used both as the inert solvent and as the internal reference and the acetylenic proton resonance signal was determined five times for each solution. The external reference experiments were carried out using coaxial tubing with tetramethylsilane being used as the external reference. Here the cyclohexane proton resonance signal is measured relative to that of the external reference and the shifts observed for the acetylene proton resonance signal using the internal referencing technique are adjusted for the observed variation in the cyclohexane signal. The uncertainty in chemical shift measurements was better than ±0.2 Hz.

Results

Tables I and II give the ambient temperature, external reference results for benzoylacetylene and phenylacetylene in anisole and a variety of methylated anisoles. Table III compares the results for benzoylacetylene and phenylacetylene in anisole using internal and external references. Table IV summarizes the values for K for these systems and indicates the uncertainties in the K's and the fit between theory and experiment using the sum of the

TABLE I: Ethynyl Proton Chemical Shifts[a] (Hz) for Benzoylacetylene in Various Anisoles

Active solvent	Mole fraction[b] of active solvent (X_B)																		
	0.05	0.10	0.15	0.20	0.25	0.30	0.35	0.40	0.45	0.50	0.55	0.60	0.65	0.70	0.75	0.80	0.85	0.90
Anisole	6.01	10.69	12.51	15.77	17.55	20.03	20.95	23.20	24.33	25.87	27.02	28.53	29.36	30.55	31.55	32.49	33.14	35.01
2-Methylanisole	8.63	12.50		21.20		27.41	31.13	33.49		36.87		39.89		43.47		45.89	47.30	48.66
3-Methylanisole	3.92	6.96		11.30		14.13	15.61	16.39		18.50		19.28		20.41		21.23		
4-Methylanisole	4.56	8.11	9.14	10.27	12.60	13.20	13.24	14.09	14.96	16.62		17.68		17.89	18.23	18.25	18.54	19.47
2,3-Dimethylanisole	8.84	15.80		24.82		31.75		35.92		39.25		42.49		44.66		47.30		48.60
2,4-Dimethylanisole	2.92	5.72	8.52	11.84	14.50	17.93	20.67	23.42	26.22	28.96	31.82	34.03	36.75	39.60	42.12	44.87	47.25	50.29
2,6-Dimethylanisole	6.39	9.60	11.56	13.40		16.00	18.31	19.08	19.54	20.44	21.89	22.38		24.00	24.88	25.39		26.06
3,4-Dimethylanisole		12.03		16.35		19.95		22.25		24.48		25.59		26.74		27.71		29.28
3,5-Dimethylanisole		7.52		13.09		17.85		19.76		22.62		24.59		25.52		27.52		29.20

[a] Shifts measured relative to TMS as external reference. [b] Inert solvent is cyclohexane.

TABLE II: Ethynyl Proton Chemical Shifts[a] (Hz) for Phenylacetylene in Various Anisoles

Active solvent	Mole fraction[b] of active solvent (X_B)																	
	0.05	0.10	0.15	0.20	0.25	0.30	0.35	0.40	0.45	0.50	0.55	0.60	0.65	0.70	0.75	0.80	0.85	0.90
Anisole	1.60	2.39	2.80	4.05	4.71	5.64	5.90	6.62	7.25	7.80	8.13	8.74	9.09	9.79	10.55	10.82	11.28	11.63
2-Methylanisole	2.05	3.52		6.50		8.77	10.12	11.38		12.91		14.50		16.02		17.43	18.21	18.96
3-Methylanisole	1.27	2.15		3.33		4.16	4.37	4.66		5.02		4.84		4.93		5.07		
4-Methylanisole	1.22	1.88	2.64	2.82	3.27	3.12	3.01	3.21	3.25	3.45	3.00	3.39	3.28	2.97	2.68	3.69	2.67	2.58
2,3-Dimethylanisole	2.84	4.34		7.82		10.99		12.94		14.38		15.81		16.66		18.07		19.13
2,4-Dimethylanisole	2.09	3.25	4.41	6.42	7.61	9.19	10.29	11.43	12.33	13.23	14.24	14.90	15.72	16.53	17.17	17.63	18.29	19.14
2,6-Dimethylanisole	1.79	3.14	4.87	5.36		6.94	8.40	8.78	9.15	9.87	10.57	11.12		11.84	12.09	12.67		12.92
3,4-Dimethylanisole		4.00		6.36		7.60		8.82		9.83		9.61		10.47		11.32		12.00
3,5-Dimethylanisole		2.34		5.27		7.03		8.07		9.43		10.40		10.98		11.71		13.23

[a] Shifts measured relative to TMS as external reference. [b] Inert solvent is cyclohexane.

TABLE III: Chemical Shifts (Hz) of the Ethynyl Proton in Benzoylacetylene and Phenylacetylene in Anisole Using Internal and External References

Mole fraction (X_B)	Internal reference[a]		External reference[b]	
	Benzoyl-acetylene	Phenyl-acetylene	Benzoyl-acetylene	Phenyl-acetylene
0.05	3.66	−0.75	6.01	1.60
0.10	6.40	−1.90	10.69	2.39
0.15	6.79	−2.92	12.51	2.80
0.20	7.82	−3.90	15.77	4.05
0.25	7.83	−5.01	17.55	4.71
0.30	8.46	−5.93	20.03	5.64
0.35	8.06	−7.05	20.95	5.90
0.40	8.36	−8.22	23.20	6.62
0.45	7.64	−9.44	24.33	7.25
0.50	7.34	−10.73	25.87	7.80
0.55	6.86	−12.03	27.02	8.13
0.60	6.39	−13.40	28.53	8.74
0.65	5.52	−14.75	29.36	9.09
0.70	4.50	−16.26	30.55	9.79
0.75	3.93	−18.11	31.55	10.55
0.80	2.23	−19.46	32.49	10.82
0.85	0.75	−21.11	33.14	11.28
0.90	0.44	−22.94	35.01	11.63

[a] Cyclohexane. [b] TMS. Positive shift is an upfield shift, negative shift is a downfield shift.

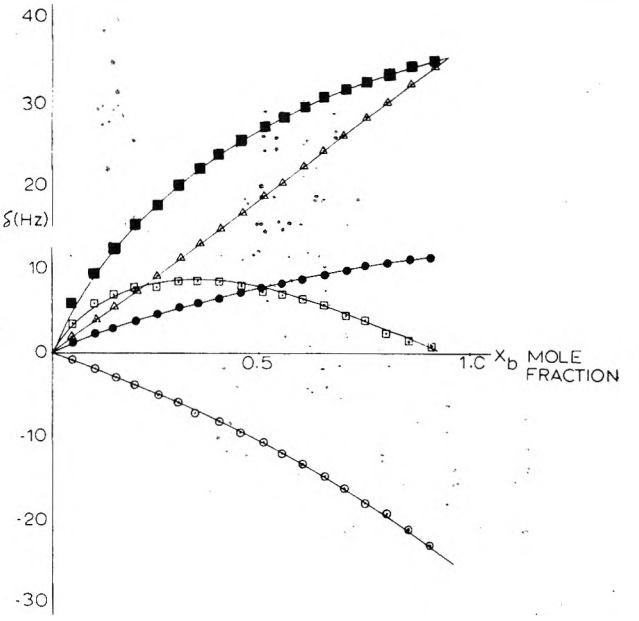

Figure 1. Concentration dependent shifts for benzoylacetylene, phenylacetylene, and cyclohexane in anisole–cyclohexane solutions: (□) benzoylacetylene using internal reference; (○) phenylacetylene using internal reference; (△) cyclohexane relative to TMS as external reference; (■) benzoylacetylene using external reference; (●) phenylacetylene using external reference.

squares of the residuals. Figure 1 shows the variation of the chemical shifts for benzoylacetylene and phenylacetylene relative to both the internal and external reference and the variation of the cyclohexane resonance signal relative to the external reference for a solvent composition ranging from pure cyclohexane to 0.9 mole fraction anisole in cyclohexane. The solid lines associated with the externally referenced data are the theoretical curves. Table V lists the equilibrium constants for the anisole–benzoylacetylene system over the temperature range 20–60 °C, the uncertainties in the K's, and fit between theory and experiment, along with the enthalpy of formation of the complex and Figure 2 illustrates the chemical shifts relative to the external reference and

TABLE IV: Equilibrium Constants[a] and Sum of Squares of Residuals ($\Sigma_i r_i^2$) for Benzoylacetylene and Phenylacetylene in Various Anisoles

Active solvent	Benzoylacetylene		Phenylacetylene	
	K	$\Sigma_i r_i^2$	K	$\Sigma_i r_i^2$
Anisole	1.39 ± 0.01	18.2	0.84 ± 0.04	4.91
2-Methylanisole	1.98 ± 0.05	31.4	0.92 ± 0.02	1.75
3-Methylanisole	3.01 ± 0.43	15.1	*b*	
4-Methylanisole	4.13 ± 0.15	24.3	*b*	
2,3-Dimethylanisole	3.65 ± 0.03	3.08	1.76 ± 0.04	2.92
2,4-Dimethylanisole	2.80 ± 0.05	21.4	0.88 ± 0.02	3.97
2,6-Dimethylanisole	3.60 ± 0.04	7.42	1.74 ± 0.05	3.41
3,4-Dimethylanisole	4.29 ± 0.12	9.65	3.39 ± 0.16	4.41
3,5-Dimethylanisole	2.16 ± 0.06	7.29	1.38 ± 0.08	4.32

[a] (Mole fraction)$^{-1}$. [b] Shifts too small for reliable data.

TABLE V: Equilibrium Constants and Sum of Squares of Residuals ($\Sigma_i r_i^2$) at Various Temperatures for the Benzoylacetylene–Anisole System

Temp, °C	Equilibrium constants (mole fraction)$^{-1}$	$\Sigma_i r_i^2$
20	1.50 ± 0.06	15.8
30	1.39 ± 0.01	18.2
40	1.30 ± 0.04	8.63
50	1.19 ± 0.04	6.45
60	1.13 ± 0.06	9.88

$-\Delta H = 1.4$ kcal/mol

corrected for bulk magnetic susceptibility differences at the different temperatures. Table VI lists the chemical shifts of cyclohexane relative to the external reference for the various anisoles.

Discussion

The results obtained for benzoylacetylene and phenylacetylene using the internal referencing technique could be interpreted, purely qualitatively, as suggesting in the latter case, since the shifts are all downfield, that complex formation exists between the acetylene and the oxygen of the methoxy group and in the former case that perhaps a combination of the two possible donor sites was involved. When an attempt was made to fit the phenylacetylene data using a variety of mathematical models and nonlinear least-squares methods no convergence could be obtained for any of the systems studied. With the benzoylacetylene data, where (Figure 1) the shift is first upfield and then reverses itself, attempts were made to fit the data using a model of the form given in eq 3 with, in some cases, a fair degree of success. For example, in the case of the anisole–benzoylacetylene system, we obtained $K_1 = 1.65 \pm 0.84$, $K_2 = 5.48 \pm 6.42$, and $\sum_i r_i^2 = 73.03$ using the internal reference data in Table III. However, in a number of instances no reasonable fit could be obtained and there was little evidence of consistency within the series of anisoles studied.

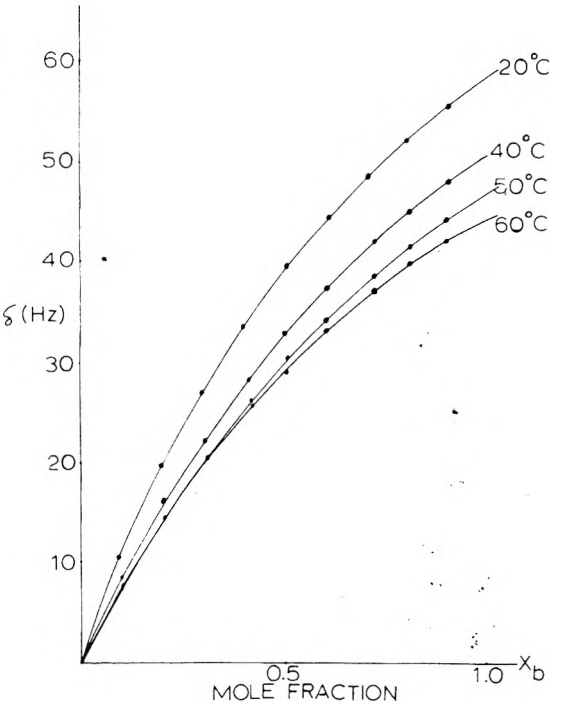

Figure 2. Temperature dependent chemical shifts for the benzoylacetylene–anisole system using an external reference.

When the proton resonance signal of the cyclohexane was studied as a function of changing solvent composition using the external reference it was observed that in all cases the cyclohexane signal shifted upfield (in the order of 30 Hz at 0.9 mole faction donor in cyclohexane). This increasing upfield shift with increasing concentration of aromatic solvent is not reasonably attributable to specific complex formation, there being no donor or acceptor characteristics normally associated with cyclohexane. In fact cyclohexane is generally considered as a suitable "inert" solvent for such complex formation studies. The other more reasonable alternative relates to the changing

TABLE VI: Chemical Shifts of Cyclohexane (Hz) Relative to External Reference in Various Anisoles

Active solvent	Mole fraction of active solvent (X_B)								
	0.1	0.2	0.3	0.4	0.5	0.6	0.7	0.8	0.9
Anisole	4.29	7.95	11.57	14.84	18.53	22.14	26.05	30.26	34.57
2-Methylanisole	3.77	7.39	10.51	14.13	16.76	20.00	23.38	26.75	30.48
3-Methylanisole	3.44	6.16	8.70	11.29	13.79	16.19	18.62	21.24	
4-Methylanisole	3.12	5.93	8.43	10.58	13.10	15.50	17.78	20.49	23.45
2,3-Dimethylanisole	3.52	7.22	10.91	13.76	16.40	19.10	21.67	24.81	27.47
2,4-Dimethylanisole	2.90	6.48	10.05	13.32	16.61	19.67	22.98	26.14	29.37
2,6-Dimethylanisole	4.31	7.90	10.91	14.72	17.77	21.03	23.78	26.93	29.51
3,4-Dimethylanisole	4.80	8.42	11.33	14.51	17.67	20.71	23.20	26.21	29.30
3,5-Dimethylanisole	3.61	7.89	11.23	14.01	17.36	20.39	23.00	25.86	29.58

magnetic anisotropy of the solvent with increasing anisole content. It should be noted that for a particular anisole solvent system the observed shifts in the cyclohexane resonance signals are independent of the acetylenic compound being studied.

When the shift of the cyclohexane resonance signal is taken into account a considerable degree of simplification results for both the benzoylacetylene and phenylacetylene data for all anisole systems studied. Both acetylenes now show a regular upfield shift in their acetylenic proton resonance signal with increasing donor solvent composition, the benzoylacetylene shifts being much larger than the phenylacetylene shifts. It can readily be seen that the reason for the somewhat unusual appearance of the benzoylacetylene curve using the internal referencing technique is that while the variation of the chemical shift of cyclohexane with composition is close to linear the variation in the chemical shift of the acetylenic proton signal (external reference) is initially greater but tends to level off at higher concentrations. On the other hand in all cases the phenylacetylene shift (external reference), while following the same pattern as the benzoylacetylene (external reference) shifts, is significantly smaller than the cyclohexane shifts leading to an increasingly negative shift pattern (downfield) when viewed using the internal reference. All of the data can now be reasonably interpreted in terms of a 1:1 AB type complex using the model given by eq 2. The equilibrium constants obtained using phenylacetylene are, in all cases, less than those obtained for the benzoylacetylene complexes in line with the fact that the ethynyl proton in benzoylacetylene is more "acidic" than in phenylacetylene. The results obtained, particularly for the benzoylacetylene, are in reasonable agreement with what we would expect from a consideration of the steric, inductive, and resonance effects in the various methylated anisoles.[18] Considerable caution needs to be used in interpreting the phenylacetylene data in that, although the data do fit the 1:1 complex model reasonably well, the magnitude of the shifts is less even than those observed for the "inert" solvent cyclohexane. There is, therefore, the possibility that what we are observing in the phenylacetylene systems is not in fact specific complex formation but an effect due to the changing magnetic anisotropy of the solvent.

The results obtained for the variable temperature runs on the benzoylacetylene–anisole system as shown in Table V and Figure 2 would appear to support the belief that complex formation is present in this system. There is a regular change in equilibrium constants over the temperature range 20 to 60 °C and the Van't Hoff plot gives an excellent linear plot giving a value for $-\Delta H$ = 1.4 kcal/mol which indicates a very weak complex. Attempts to obtain similar data for the phenylacetylene systems were abandoned when no regular pattern of behavior with temperature could be obtained.

The results obtained here clearly indicate the need to be careful in the use of an internal reference in complex formation studies. In the situation considered here such a use can lead to misleading interpretations and the use of an external reference becomes imperative.

References and Notes

(1) M. D. Johnston, F. P. Gasparro, and I. D. Kuntz, *J. Am. Chem. Soc.*, **91**, 5715 (1969).
(2) P. Laszlo in "Progress in NMR Spectroscopy", Vol. III, J. W. Emsley, J. Feeney, and L. H. Sutcliffe, Ed., Pergamon Press, London, 1967, Chapter 6.
(3) I. D. Kuntz and M. D. Johnston, *J. Am. Chem. Soc.*, **89**, 6008 (1967).
(4) J. Landauer and H. McConnell, *J. Am. Chem. Soc.*, **84**, 1221 (1952).
(5) J. C. D. Brand, G. Eglinton, and J. Tyrrell, *J. Chem. Soc.*, 5914 (1965).
(6) E. Becker, *J. Phys. Chem.*, **63**, 1370 (1959).
(7) J. R. Zimmerman and M. R. J. Foster, *J. Phys. Chem.*, **61**, 282 (1957).
(8) E. M. Engler and P. Laszlo, *J. Am. Chem. Soc.*, **93**, 1317 (1971).
(9) F. H. A. Rummens and R. H. Krystynak, *J. Am. Chem. Soc.*, **94**, 6914 (1972).
(10) J. W. Emsley, J. Feeney, and L. H. Sutcliffe, "High Resolution Nuclear Magnetic Resonance Spectroscopy", Pergamon Press, Oxford, 1965, p 260.
(11) J. W. Emsley, J. Feeney, and L. H. Sutcliffe, ref. 10, Appendix C.
(12) R. C. Weast, "Handbook of Chemistry and Physics", 52nd ed, The Chemical Rubber Co., Cleveland, Ohio, 1971.
(13) H. J. Bernstein and K. Frei, *J. Chem. Phys.*, **37**, 1891 (1962).
(14) C. J. Lussan, *Chim. Phys.*, **61**, 462 (1964).
(15) H. Suhr, "Anwendungen Der Kernmagnetischen Resonanz in Der Organischen Chemie", Springer-Verlag, Berlin, 1965.
(16) J. Landolt-Bornstein, "Zahlenwerte and Functionen", Springer, Berlin, 1951.
(17) K. Bowden, I. M. Heilbron, and B. C. L. Weedon, *J. Chem. Soc.*, 39 (1946).
(18) K. S. Dhami and J. B. Stothers, *Can. J. Chem.*, **44**, 2855 (1966).

Proton Magnetic Resonance Study of Ion Hydration in Acetone

H. Fukui,* K. Miura, T. Ugai, and M. Abe

Kitami Institute of Technology, 165 Koencho, Kitami 090, Japan

(Received December 6, 1976)

Association constants and hydroxyl proton NMR shifts have been measured for one-to-one complexes in acetone of diamagnetic cations and anions with water. These values indicate that the complex shifts of metal salts are dominated by metal ions and relatively unaffected by anions, whereas the association constants are greatly affected by anions. The relationship between the association constant and the ionic radius, and that for the complex shift, were investigated. Relationships were found for alkali and alkaline earth metal ions, but not for other cations and anions.

Introduction

Water proton magnetic resonance (^{1}H NMR) chemical shifts produced by diamagnetic salts in aqueous solution have been used to study the effects of electrolytes on the structure of water and the nature of solute–solvent interaction.[1-7] In dilute solutions the observed shift was related to the aqueous molal salt shifts.[8] According to Shoolery and Alder,[1] the chemical shift produced by ions in aqueous solution is the sum of at least two factors: (i) polarization of water molecules and (ii) structure breaking of the water hydrogen-bonded network. The interaction between a cation and a water molecule through the oxygen atom produces a shift in electron density away from the protons, leaving them less shielded. Therefore, relative

to pure water, the resonance occurs at a lower field strength. It was also reasoned that the interaction between an anion and a water molecule would produce the same effect due to the attraction of the proton for the anion; the electron density around the hydrogen atom again being shifted toward the oxygen atom owing to repulsion. One must also consider the case in which the water proton might become embedded in the electron cloud of a large anion, thereby becoming more shielded and resonating at a higher field relative to pure water. These effects would constitute the polarization shift by a salt. Ions breaking the water hydrogen-bond structure would produce high-field shifts due to the increased electron density around the protons. The polarization effect and the structure-breaking effect produce generally shifts in the opposite direction, and are of the same order of magnitude.

If we want to investigate the mechanism of the shielding change due to the hydration of ions, it is desirable to separate the above two contributions. Therefore, we have focused attention on the magnitudes of the shifts produced by the polarization effect alone. In order to eliminate the structure-breaking effect, it is necessary to observe the water proton chemical shifts induced by salts in an inert solvent.[9-11] If the structure-breaking effect is negligible, or it can be evaluated, then the direct salt–molecular polarization shift is accessible to experimental observation. If we use solutions of extremely low water content to eliminate water to water hydrogen bonding, the structure-breaking effect would be negligible. Then we have to use time averaging of the water proton signal to observe chemical shift changes. In order to avoid this cumbersome measurement, we may observe the chemical shift at an appropriately low water concentration, and correct the observed polarization shift by adding the dilution shift to the zero concentration shift. Moreover, it is possible to observe a favorable one-to-one complex formation at low water concentrations in an inert solvent.[9,10] The 1:1 complex formation allows us to analyze the chemical shift changes and obtain the polarization shift and equilibrium constant. Stockton and Martin[10] observed and analyzed the 1:1 association of several metal ions with a water molecule in 0.1 M water–acetonitrile solutions at room temperature. They obtained the polarization shifts and hydration constants of Li^+, Na^+, Mg^{2+}, Ca^{2+}, Sr^{2+}, and Ba^{2+} in acetonitrile. Benoit and Lam[11] used similar experimental conditions and estimated the polarization shifts and the water association constants of Cl^-, NO_3^-, Li^+, Na^+, and Ag^+ in several dipolar aprotic solvents.

It is known that the molal salt shift can be written as the sum of the individual cation and anion molal shifts.[1] The salt shifts were divided into individual ion values, assuming some value for one ion to be used as a standard.[8,12-14] However, there have not yet been any studies of the additivity of the polarization salt shift. Stockton and Martin[10] and Benoit and Lam[11] used perchlorate and tetraethylammonium salts to minimize counterion contributions. It is of fundamental importance to know how the extent of hydration is affected by the counterion. In this paper, we will report on the polarization shifts and the hydration constants of various ions, and discuss the additivity of the former. We will also investigate a relationship between the polarization ion shift and the ionic size and the hydration constant.

Stockton and Martin[10] used acetonitrile as an inert solvent. It is available in perdeuterated form, which does not obscure the spectral region of interest. We have used acetone as an inert solvent and it does not overlap the water proton signal. Fratiello et al.[15] indicated that the solvating ability of acetone is comparable to that of acetonitrile. From this fact, it is inferred that acetone is as inert as acetonitrile. The water concentration was kept as low as possible (0.1 M) to minimize water to water hydrogen bonding, and the water proton shielding was observed as a function of salt concentration.

Analysis of the Observed Shift. Our approach to the problem was the measurement of the ^1H NMR chemical shift of water in acetone, relative to some reference, as a function of concentration of added salt. Only one water ^1H NMR peak was observed in these solutions, indicating that exchange of H_2O molecules occurs so rapidly from one state to another that the observed chemical shift is an average of all the states. It is impossible however to know exactly all the states. For simplicity we consider only two states of water: the free and complexed forms. We consider only the reaction

$$IS_n + H_2O \rightleftarrows IS_{n-1}H_2O + S \tag{1}$$

where I and S are an ion and a solvent (acetone in our experiment) molecule, respectively.[16] We assume the following in eq 1: (i) either the cation or the anion contributes to the complex formation with H_2O and (ii) one water molecule exchanges with one solvent molecule. The observed shielding constant σ is given by the equation

$$\sigma = \frac{[F]}{W_0}\sigma_F + \frac{[C]}{W_0}\sigma_C \tag{2}$$

where W_0 is the initial concentration of H_2O (0.1 M in this experiment), [F] and [C] are the equilibrium concentrations of the free and complexed water, respectively, and σ_F and σ_C are the characteristic shielding constants of those forms of water. The concentration of solvent is so large that it is constant in eq 1. The equilibrium constant, K, of reaction 1 is given by

$$K = \frac{[C]}{(I_0 - [C])(W_0 - [C])} \tag{3}$$

where I_0 is the initial concentration of the reactive ion. We define the complex shift, Δ_C, as

$$\Delta_C = \sigma_C - \sigma_F \tag{4}$$

Equations 2 and 4 yield

$$\sigma = \sigma_F + \frac{[C]}{W_0}\Delta_C \tag{5}$$

At the limit of high concentration of the ion, $\sigma - \sigma_F$ is equal to the complex shift, Δ_C. Analyses of the observed shifts were performed using a computer simulation method[17] preferred by one of the authors (H.F.). Analyses of the data yielded sufficiently reliable values of K and Δ_C. The mechanism of the shielding change as pictured here is undoubtedly over-simplified; nevertheless, it provides a tentative working scheme which appears to be in agreement with the facts available.

Experimental Section

Materials. Wako Pure Chemicals acetone was distilled twice from a freshly dehydrated 4 Å molecular sieve. The residual water concentration in the acetone thus obtained was about 0.004 M. Tetramethylsilane (TMS) was added before the sample preparation to serve as a ^1H NMR internal reference.

Water was distilled and passed over cation- and anion-exchange resins.

Calcium and strontium perchlorates were hexahydrates; they were dehydrated by heating at 100 °C under vacuum

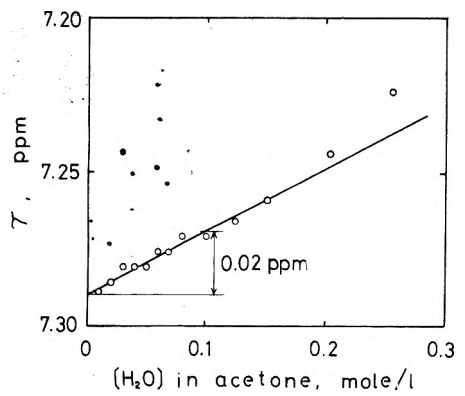

Figure 1. Dilution curve for the water proton chemical shift in acetone.

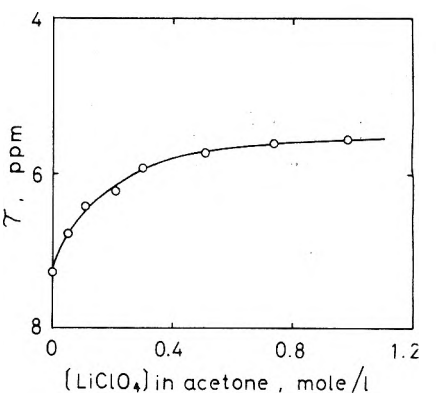

Figure 2. ^{1}H NMR shifts of the water proton in acetone solutions containing 0.1 M water and varying concentrations of $LiClO_4$: solid curve, simulated; circles, observed.

pumping, gradually increasing to 200 °C over several days. Lithium, sodium, magnesium, and barium perchlorates were obtained labeled "anhydrous" and were dried by heating at 200 °C under vacuum pumping.

The lithium and calcium thiocyanates obtained were anhydrous and trihydrate, respectively; they were dehydrated by heating at 100 °C under vacuum for 48 h.

Calcium nitrate was in the tetrahydrate form; it was dehydrated by heating at 125 °C under vacuum for 48 h. Lithium nitrate was obtained labeled anhydrous and was dried by heating.

The lithium iodide obtained was labeled anhydrous, however it contained traces of water. Attempts to dehydrate it by heating under vacuum yielded a sample containing a slight amount of water. Lithium bromide was monohydrate; it was dehydrated by heating at 190 °C under vacuum for 24 h.

The zinc, mercuric, stannous, and antimony chlorides, and cadmium iodide that were obtained were labeled anhydrous and were dried by heating.

The ^{1}H NMR spectrum of the reagent grade tetra-*n*-butylammonium chloride showed a slight impurity signal. The salt was dissolved in a small volume of CCl_4, then precipitated by adding cyclohexane. The salt so obtained was then dried by pumping and found by ^{1}H NMR to be free of impurities. The tetra-*n*-butylammonium bromide, iodide, and perchlorate were used as received, since no ^{1}H NMR impurity signals (dissolved in acetone) were observed.

Solutions of 0.1 M water–acetone, with varying salt concentrations over the range 0 to about 1 M, were prepared. All samples were made up gravimetrically.

^{1}H NMR Spectra. All spectra were obtained on a Hitachi R-20A spectrometer (permanent magnet, 60 MHz). All measurements were made at 34 ± 1 °C. Upfield shifts were taken as positive.

Results and Discussion

(A) *Dilution Shift of Water in Acetone.* The dilution shift of water in acetone from 0.1 M to zero concentration was estimated. Figure 1 shows the concentration dependence of the water proton chemical shift in acetone from 0.01 to 0.25 M. The region below about 0.15 M is very nearly linear. It is evident that extrapolation to infinite dilution gives 0.02 ppm as the dilution shift at 0.1 M water concentration. It is apparent that this value is within the experimental and analytical uncertainty of the complex shift, Δ_C, so we neglected the correction due to the dilution shift. We may assume that the complex shift, Δ_C, obtained in 0.1 M water–acetone solution, is equal to the polarization shift.

(B) *Cation Shifts in Metal Perchlorate Solutions.* The chemical shifts of the water proton signal in the alkali and alkaline earth perchlorate solutions were measured as a function of salt concentration. As an example, the effect of $LiClO_4$ on the water proton signal in acetone is shown in Figure 2, with the simulated curve. Agreement between the observed and calculated shieldings, except for the water–magnesium complex, were so good that the assumption of 1:1 association was confirmed. We assume here that the perchlorate ion is inert and only a metal ion forms a complex with a water molecule. The equilibrium constants, the complex shifts of cations, and the standard deviations between observed and calculated shieldings, obtained by least-squares computer simulation, are listed in Table I with the results reported by Stockton and Martin.[10] The water–magnesium system showed evidence of multiple water–ion association at low salt concentrations, in which a large discrepancy occurred between the observed and simulated shieldings. The equilibrium constant for this system is listed as "large" since it could not be determined from the concentration dependence of the shift.

TABLE I: Equilibrium Constants, K (M^{-1}), and Polarization Shifts, Δ_C (ppm), of Alkali and Alkaline Earth Perchlorates in Acetone at 34 °C, with the Results Reported in Ref 10

Salt	K, M^{-1}		Δ_C, ppm[a]		s,[c] ppm
$LiClO_4$	12	14[b]	−1.85	−1.48[b]	0.024
$NaClO_4$	2.8	2.3[b]	−0.90	−0.89[b]	0.007
$Mg(ClO_4)_2$	Large	Large[b]	−3.36	−2.98[b]	
$Ca(ClO_4)_2$	48	151[b]	−2.33	−2.17[b]	0.076
$Sr(ClO_4)_2$	26	45[b]	−1.67	−1.75[b]	0.039
$Ba(ClO_4)_2$	6.0	16[b]	−1.46	−1.54[b]	0.009

[a] A positive sign indicates increased nuclear shielding. [b] Reported by Stockton and Martin[10] in acetonitrile at 35 °C. [c] The standard deviations between observed and calculated shieldings: $s = (\Sigma_i^n(\sigma_{obsd} - \sigma_{calcd})^2/n)^{1/2}$.

It is evident from Table I that ions of smaller size or larger charge have larger equilibrium constants and complex shifts. This will be discussed later (section E). It is shown that the polarization shifts obtained in acetone are in agreement with those in acetonitrile.[10] Stockton and Martin[10] have asserted that cation-induced shifts should be independent of the solvent. Our experiments support this assertion. However, the equilibrium constants in acetone are smaller than those in acetonitrile which seems to indicate that the solvating ability of acetone is slightly greater than that of acetonitrile.

(C) *Anion Shifts in Tetra-n-butylammonium Salt Solutions.* In order to obtain the values K and Δ_C for anions, the chemical shifts produced by tetra-*n*-butylammonium halides and perchlorate were measured. In this case the tetra-*n*-butylammonium ion should be inert and

TABLE II: Equilibrium Constants and Polarization Shifts of Tetra-*n*-butylammonium Halides and Perchlorate in Acetone at 34 °C

Salt	K, M^{-1}	Δ_C, ppm	s, ppm
$(n\text{-}C_4H_9)_4NCl$	12	−0.75	0.016
$(n\text{-}C_4H_9)_4NBr$	4.1	−0.48	0.005
$(n\text{-}C_4H_9)_4NI$	6.9	−0.06	0.002
$(n\text{-}C_4H_9)_4NClO_4$	8.7	−0.03	0.001

TABLE III: Anion Dependences of the Equilibrium Constants and Polarization Shifts of Lithium and Calcium Salts in Acetone at 34 °C

Cation	Anion	K, M^{-1}	Δ_C, ppm	s, ppm
Li^+	ClO_4^-	12	−1.85	0.024
Li^+	SCN^-	6.2	−1.87	0.032
Li^+	NO_3^-	4.6	−1.92	0.019
Li^+	Br^-	25	−1.86	0.056
Li^+	I^-	27[a]	−1.88[a]	0.050
Ca^{2+}	ClO_4^-	48	−2.33	0.076
Ca^{2+}	SCN^-	27	−2.34	0.060
Ca^{2+}	NO_3^-	11	−2.22	0.010

[a] Lithium iodide contained a slight amount of water.

only an anion will form a complex with H_2O. The equilibrium constants and the complex shifts of anions were determined, and are listed in Table II. The polarization shifts of Cl^- and Br^- are somewhat large, but those of I^- and ClO_4^- are very small. The equilibrium constants show a less regular variation. From the polarization shifts, it is inferred that I^- and ClO_4^- do not associate with water, but Cl^- and Br^- do weakly. It is apparent from Δ_C for $(n\text{-}C_4H_9)_4NClO_4$ that both the perchlorate and tetra-*n*-butylammonium ions are inert.

(D) *Anion Effects on K and Δ_C of Metal Salts.* It is reported that the molar salt shift is the sum of the individual ion values. However, at present no reports are available on the additivity of the polarization shift, so we have attempted to study this additivity. It is desirable to investigate the complex shifts of salts having various anions for a specific cation or vice versa. The kinds of salts studied were limited by the solubilities of salts and the difficulty in obtaining anhydrous salts. We report here on lithium and calcium salts. The results are listed in Table III. In these experiments, both the cation and anion may contribute to complex formation with water. Nevertheless by assumption (i) in the analysis section, it was possible to simulate the observed chemical shifts by assuming only one reaction. This means that either cation or anion is bound to water.

The anion dependences of the equilibrium constants and polarization shifts, given in Table III, are very interesting. The polarization shifts in Table III show little variation with the anion. For a given cation, all the salts have shown the same polarization shift within the uncertainty of the measurement. It seems that the polarization shift of a metal salt is primarily determined by the metal ion and the anion has a negligible effect on it. Notwithstanding the limited data, it is reasonable to suppose that a water molecule forms a complex with a metal ion, but not with an anion. However, the equilibrium constants are greatly affected by the anions which seems to contradict the results for the polarization shifts. We cannot explain exactly the differences in K values. We can only attribute these differences to (i) failure to maintain constant ionic strength and (ii) the interaction between the cation and anion spheres.

(E) *Correlation with Crystal Radius.* The values of the equilibrium constants and polarization shifts in Table I show that they are closely related to the ionic sizes and

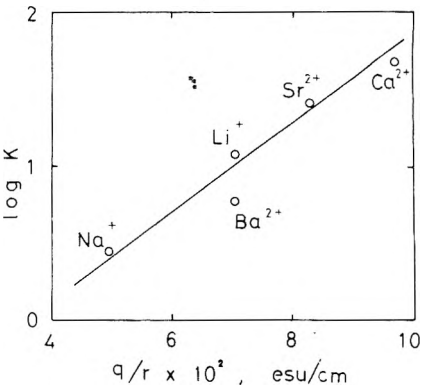

Figure 3. Relationship between the observed cation–water association constant and the electrostatic potential for the alkali and alkaline earth metal ions.

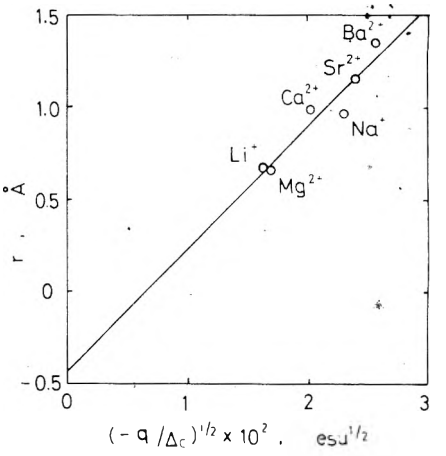

Figure 4. Relationship between the observed cation–water complex shift and the crystal radius for the alkali and alkaline earth metal ions.

ionic charges of the cations. This suggests that K and Δ_C of the alkali and alkaline earth metal ions are determined by the electrostatic interaction between the ion and a water molecule. Figure 3 shows a plot of log K against q/r, in which q is the ionic charge and r is the ionic crystal radius. If, as is usually the case, the entropy changes of reaction 1 are either constant or proportional to the enthalpy changes, then log K should be linear in the electrostatic potential, q/r. Figure 3 indicates that such a relationship does hold.

We have investigated the dependence of the shifts on the electrostatic field of the cations. Assuming, for simplicity, that Δ_C is proportional to the electrostatic field,[18] the shift may be described as follows

$$\Delta_C = -Aq/(r + c)^2 \tag{6}$$

where $r + c$ is the distance from the ion center to the hydroxyl proton, and A is a proportionality factor. Equation 6 yields

$$r = A^{1/2}(-q/\Delta_C)^{1/2} - c \tag{7}$$

If the shifts are proportional to the field, then r, the crystal radius, should be linear in $(-q/\Delta_C)^{1/2}$. Figure 4 shows that such a relationship does hold for Δ_C in Table I. From the slope and intercept of the best straight line, we obtained $A = 0.45 \times 10^{-12}$ cm^2 esu^{-1}, and $c = 0.44$ Å.

In order to examine further the correlation of K and Δ_C with the crystal radius, we measured K and Δ_C of metal ions other than alkali and alkaline earth metal ions. The results shown in Table IV indicate clearly that the linear relations, which were exhibited in Figures 3 and 4, do not hold any longer for cations other than the alkali and al-

TABLE IV: Equilibrium Constants and Polarization Shifts of Various Cations Other Than the Alkali and Alkaline Earth Metal Ions in Acetone at 34 °C

Cation	Salt	K, M^{-1}	Δ_C, ppm	s, ppm
Zn^{2+}	$ZnCl_2$	18	−4.25	0.020
Cd^{2+}	CdI_2	10	−3.44	0.024
Hg^{2+}	$HgCl_2$	0.21	−5.45	0.039
Sn^{2+}	$SnCl_2$	11	−5.28	0.030
Sb^{3+}	$SbCl_3$	0.36	−5.49	0.017

kaline earth metal ions. From similar plots for the anion shifts in Table II, it appears that there are no relationships among r, Δ_C, and K. We conclude that K and Δ_C of the alkali and alkaline earth metal ions can be explained in terms of the electrostatic effect of the ion. However, those of the other cations and anions cannot be explained by the electrostatic model. This reflects the following: (i) the importance of covalent interactions for these ions and (ii) the possibility of ion pairing which is common to ions of small size and large charge.

Acknowledgment. All the simulations in this study were performed on an OKITAC-4500 computer in our college. We wish to thank Mrs. Y. Sugawara for the computer operation. This research was supported in part by the Scientific Research Fund of the Japanese Ministry of Education Grant No. 964076.

References and Notes

(1) J. N. Schoolery and B. J. Alder, *J. Chem. Phys.*, **23**, 805 (1955).
(2) R. C. Axtmann, *J. Chem. Phys.*, **30**, 340 (1959).
(3) H. G. Hertz and W. Spalthoff, *Z. Electrochem.*, **63**, 1096 (1959).
(4) B. P. Fabricand and S. Goldberg, *J. Chem. Phys.*, **34**, 1624 (1961).
(5) M. S. Bergqvist and E. Forslind, *Acta Chem. Scand.*, **16**, 2069 (1962).
(6) J. C. Hindman, *J. Chem. Phys.*, **36**, 1000 (1962).
(7) S. Goto and T. Isemura, *Bull. Chem. Soc. Jpn.*, **37**, 1693 (1964).
(8) J. F. Hinton and E. S. Amis, *Chem. Rev.*, **67**, 367 (1967).
(9) R. D. Green, J. S. Martin, W. B. M. Cassie, and J. B. Hyne, *Can. J. Chem.*, **47**, 1639 (1969).
(10) G. W. Stockton and J. S. Martin, *J. Am. Chem. Soc.*, **94**, 6921 (1972).
(11) R. L. Benoit and S. Y. Lam, *J. Am. Chem. Soc.*, **96**, 7385 (1974).
(12) J. Davies, S. Ormondroyd, and M. C. R. Symons, *Trans. Faraday Soc.*, **67**, 3465 (1971).
(13) J. Davies, S. Ormondroyd, and M. C. R. Symons, *J. Chem. Soc., Faraday Trans. 2*, 686 (1972).
(14) M. C. R. Symons and J. Davies, *J. Chem. Soc., Faraday Trans. 2*, 1037 (1975).
(15) A. Fratiello, R. E. Lee, D. P. Miller, and V. M. Nishida, *Mol. Phys.*, **13**, 349 (1967).
(16) Kraus and co-workers estimated the dissociation constants of various salts in acetone at 25 °C [M. B. Reynolds and C. A. Kraus, *J. Am. Chem. Soc.*, **70**, 1709 (1948); M. J. McDowell and C. A. Kraus, *ibid.*, **73**, 3293 (1951)], and found them to be of the order of 10^{-3}. One of the referees suggested to us that the free ions would be only minor species. However, reaction 1 is not affected directly by the ion-pair reaction, because the distances, d (Å), between centers of charge in the ion pairs are so large that each ion is surrounded on the average by a certain number of solvent molecules (e.g., for KI in acetone, $4.6 \leq d \leq 14$).
(17) S. Shimokawa, H. Fukui, J. Sohma, and K. Hotta, *J. Am. Chem. Soc.*, **95**, 1777 (1973).
(18) A. D. Buckingham, *Can. J. Chem.*, **38**, 300 (1960).

On the Ionization Potential of a Solute and the Ground State Energy of the Excess Electron

D. Grand* and A. Bernas

E.R. CNRS No. 98, Université Paris-Sud, 91 405 Orsay, France *(Received August 4, 1976; Revised Manuscript Received March 11, 1977)*

Publication costs assisted by CNRS

A semiempirical method is used to calculate V_0 the ground state energy of an excess electron in various polar and nonpolar rigid solvents. The following two conclusions are drawn: (1) The previously reported variations of the ionization threshold energy of a solute with some properties of the liquid or solid solvent originate from correlative variations of V_0. (2) V_0 is found to decrease when the polarity (ϵ_{stat}) of the matrix increases. Such a systematic trend describing solvated electrons is not accounted for by present theoretical models which might need revision.

Introduction

Investigating excess, quasi-free electrons in liquid and solid rare gases, Jortner and Raz[1] have expressed the ionization potential (I_{liq} and I_{sol}) of an impurity molecule A in a liquid or solid solution by

$$I_{liq}, I_{sol} = I_g + P_+ + V_0 \quad (1)$$

where I_g is the gas phase ionization potential of A, P_+ the polarization energy of the medium by the positive ion A^+, and V_0 the ground state energy of the excess electron.

Such a linear relationship between I_{liq} and V_0 seems to hold also for a common solute in a series of liquid hydrocarbon solvents,[2] systems for which both quantities were independently determined.

So far, attempts to measure V_0 directly in polar or nonpolar glassy matrices have failed.[3] However, V_0 can be estimated by an indirect method using eq 1, measured values of I_{sol},[4,5] and calculated values of P_+[1,3]. Further, I_{sol} values for various organic matrices have been shown to vary with the polarity,[4] the structure of the solvent molecule,[5] and also with the state of condensation of the system.[5] Consequently it seems interesting to consider the influence of these factors on the P_+ and V_0 terms, respectively. This is the purpose of the present article.

Influence of Solvent Molecular Shape

(a) *Liquid Solutions.* I_{liq} has been measured for the solute TMPD dissolved in various liquid alkanes and it was found that the more globular the solvent molecule (neopentane, tetramethylsilane), the lower is the ionization potential of the solute.[2,6] Such a variation in I_{liq} has been accounted for by differences in the solvent V_0 values, the

TABLE I: I_{sol}, P_+, and V_0 as a Function of the Solvent Molecular Shape for Solid Solutions

Solvent	$I_{sol,77K}$, eV (expt)[a]	$\epsilon_{op,77K}$[b]	I_g = 6.6 eV and r_i = 1.90 Å		I_g = 6.2 eV and r_i = 2.49 Å	
			$-P_+$, eV	V_0, eV	$-P_+$, eV	V_0, eV
MCH	5.60	2.242	2.10	1.10	1.60	1.00
n-Decane	5.65	2.056	1.95	1.0	1.48	0.93
n-Hexane	5.70	2.058	1.95	1.05	1.48	0.98
Isopentane	5.65	2.120	2.00	1.05	1.53	0.98
2,4DMP	5.35	2.116	2.00	0.75	1.52	0.67
2,2DMB	5.30	2.062	1.95	0.65	1.49	0.59
Isooctane	5.25	2.115	2.00	0.64	1.52	0.57
TMSi	5.20	2.00	1.90	0.50	1.44	0.44
Neopentane	5.20	1.853	1.74	0.34	1.33	0.33

[a] Reference 5. [b] Extrapolated.

TABLE II: Influence of the State of Condensation on $V_{0,liq,298K}$ and $V_{0,sol,77K}$

Solvent	$I_{liq,298K}$,[a] eV	$V_{0,liq298K}$,[a] eV	$-P_{+liq}$, eV	$V_{0,sol,77K}$, eV
MCH	4.83	+0.09	1.86	1.00
n-Decane	4.95	+0.22	1.87	0.93
n-Hexane	4.92	+0.14	1.82	0.98
Isooctane	4.63	−0.15	1.82	0.57
2,2DMB	4.60	−0.24	1.76	0.59
Neopentane	4.51	−0.43	1.66	0.34
TMSi	4.29	−0.61	1.70	0.50

[a] From ref 2.

latter being independently measured.[7]

From eq 1, the P_+ term is then obtained by difference. In addition from Born's equation[2]

$$P_+ = \frac{-e^2}{2r_i}\left(1 - \frac{1}{\epsilon_{op}}\right) \qquad (2)$$

the knowledge of the dielectric constant ϵ_{op} permits evaluation of the radius r_i of the positive hole. Taking I_g of TMPD as 6.6[8] or 6.2 eV[9], one finds r_i = 1.93 or 2.49 Å,[10] respectively.

(b) *Solid Solutions.* For solid solutions where V_0 is unknown, one can calculate P_+, as in ref 1 and 3, by assuming $r_{i,TMPD^+}$ to be temperature independent (or rather to be the same for liquid and solid crystalline solutions) and estimating $\epsilon_{op,77K}$ by extrapolation. To that end, n_D being the refractive index, the temperature coefficients dn_D/dT, known within a certain temperature range in the liquid phase, were extrapolated down to the solvent melting point T_M and then considered to be constant from T_M to 77 K.

It should be pointed out that such a procedure neglects the break in n_D and n_D^2 values which may occur at the transition temperature liquid → crystal.

Such a discontinuity in the I values, i.e., in $P_+ + V_0$ has been recently reported.[11]

The V_0 values given in Table I are thus expected to be underestimated. However, even if these values are not accurate, the trend of their variation is indeed expected to be meaningful.

V_0 has thus been derived for the crystalline hydrocarbons for which I_{sol} had been previously determined.[5] I_{sol}, P_+, and V_0 values are gathered in Table I which shows the following: (i) The V_0 values are not very much dependent on the r_i and I_g values chosen (columns 5 and 7) but differ significantly if calculated from the Clausius–Mosotti equation.[12] However, this latter approach, if more precise, requires a knowledge of the crystal density and is thus restricted to a few cases. (ii) The ϵ_{op} values, hence the P_+ terms, are not very much affected by a change in the solvent molecular structure and not in a systematic way. (iii) V_0 is much more affected and *decreases in a regular way when the degree of branching of the hydrocarbon increases.* This trend is consistent with the variation observed for the same liquid hydrocarbons.[2]

Influence of the State of Condensation

It has been found experimentally and emphasized that for the same solute–solvent systems I_{sol} at 77 K was always greater than I_{liq} at 298 K by 0.6 to 0.9 eV; in other words, the following sequence was observed: $I_{gas} > I_{solid} > I_{liquid}$.

Table II summarizes Holroyd's experimental data for I_{liq}[2] and V_0 in liquid hydrocarbons[7] as well as the V_0 values just deduced (Table I) for the same solid compounds. The liquid phase polarization terms $P_{+,liq}$ (Table II, column 4) obtained by difference from eq 1 are seen to differ from the calculated solid phase polarization terms $P_{+,sol}$ (Table I, column 4) by 0.1–0.2 eV, that is P_+ appears to be little affected by a phase change.

On the other hand, the 77 K V_0 values appear significantly greater than the ones measured at 298 K by 0.7–1.0 eV.

Hence, it is clear that the difference $I_{sol} - I_{liq}$ stems essentially from an increase in V_0 going from the liquid at room temperature to the solid phase, and not from a change in the polarization term.

Influence of Solvent Polarity

The experiments where the influence of the solvent polarity was investigated relate to glassy matrices. They have shown that I_{sol} decreases when the matrix dielectric constant increases.

TABLE III: P_+ and V_0 Values for Various Glassy Matrices at 77 K

Solvent	$I_g - I_{sol}$, eV	ρ_{77K}, g cm^{-3}	$\epsilon_{op,77K}$	$-P_+$, eV	$V_{0,77K}$, eV	V_0,[a] eV
MCH	0.86	1.02	2.529	2.29	1.43	1.24
3MP	0.86	0.88	2,312	2.15	1.29	1.20
MTHF	1.06	1.11	2.404	2.21	1.15	0.98
n-BuOH	1.61	0.97	2.225	2.08	0.47	
n-PrOH	1.66	0.96	2.168	2.04	0.38	0.36
EtOH	1.71	1.06	2.186	2.05	0.34	0.24
MeOH	1.86	(1.05)	2.107	1.99	0.13	−0.01
		(0.99)	2.022	1.91	0.05	
H_2O (glass)	(2.0)					−0.36

[a] Reference 3.

TABLE IV

Matrix	V_0 (SC), eV	V_0 (Table III), eV
3MP, MCH	+0.5[a]	1.2-1.4
MTHF	−0.5[b]	1.0-1.15
EtOH	+1[b]	0.25-0.35
MeOH	+0.5[b]	0.0-0.10
Ice	−1[b]	−0.35

[a] Reference 15. [b] Reference 13.

The measured $I_g - I_{sol} = \Delta I$ values[4] are given in Table III, column 2. V_0 terms estimated from dn_D/dT, as indicated above, have recently been published;[3] they are reported in column 7. For these glasses, density values are known.[13] It is thus possible to calculate ϵ_{op} from the Clausius–Mosotti equation

$$\frac{\epsilon_{op} - 1}{\epsilon_{op} + 2}\frac{M}{\rho} = \frac{4\pi}{3}N_0\alpha \qquad (3)$$

(where M is the molecular weight, N_0 Avogadro's number, and α the polarizability) hence to obtain P_+ (column 5) and V_0 (column 6). Examination of columns 6 and 7 shows that the V_0 value deduced by the two methods are very close to each other and that they decrease regularly with increasing matrix polarity.

One may note that for glassy ice the V_0 calculated value[3] is −0.36 eV whereas for liquid water a value of −1.5 eV has been reported.[14] Considering a solute of $r_i \simeq 2$ Å, hence a P_+ term of 1.6 eV, a ΔI value of the order of 3.1 eV might then be expected for liquid aqueous solutions. Smaller ΔI would however characterize biological molecules of larger dimensions, the lower limit for ΔI being precisely the V_0 value.

Conclusion

In conclusion, Tables I, II, and III combine to show that varying the solvent polarity, the solvent molecular shape, or the state of condensation of a given system affects very little the polarization term P_+ whereas the V_0 terms are notably more affected and in a more regular way. Hence, the previously reported variation of I_{sol}[4,5] appears to be correlated essentially with a variation of the ground state energy of the excess electron.

It might also be noted that such a systematic variation of V_0 with some matrix properties does not seem to be accounted for by the theoretical models describing solvated electrons e_s^-.

In particular in the most favored semicontinuum (SC) model, V_0 is treated as a limited (± 1) adjustable parameter. It is so adjusted[13,15] that the calculated values of the energy of the e_s^- absorption band maximum, hc/λ_{max}, fit the experimental determinations. Such a procedure leads to the second column values (Table IV) whereas the present semiempirical approach gives the third column V_0 values. The previously reported[3] or presently determined V_0 are not precise values and their derivation rests on the hypothesis that the positive hole radius is not modified on going from the liquid to the solid solvent. Nevertheless, we suggest that these semiempirical values are to be preferred.

Further, the V_0 data derived from the SC model do not show a systematic variation with matrix polarity as opposed to the semiempirical values. This point seems to deserve more attention and might require that the theoretical model be refined.

References and Notes

(1) B. Raz and J. Jortner, *Chem. Phys. Lett.*, **4**, 155 (1969).
(2) R. A. Holroyd, *J. Chem. Phys.*, **57**, 3007 (1972).
(3) L. Kevan, S. Noda, and K. Fueki, *J. Phys. Chem.*, **79**, 2866 (1975).
(4) A. Bernas, M. Gauthier, D. Grand, and G. Parlant, *Chem. Phys. Lett.*, **17**, 439 (1972).
(5) A. Bernas, J. Blais, M. Gauthier, and D. Grand, *Chem. Phys. Lett.*, **30**, 383 (1975).
(6) S. S. Takeda, N. E. Houser, and R. C. Jarnagin, *J. Chem. Phys.*, **54**, 3195 (1971).
(7) R. A. Holroyd and M. Allen, *J. Chem. Phys.*, **54**, 5014 (1971).
(8) G. Briegleb and J. Czekalla, *Z. Elektrochem.*, **63**, 6 (1959).
(9) Y. Nakato, M. Ozaki, A. Egawa, and H. Tsubomura, *Chem. Phys. Lett.*, **9**, 615 (1971).
(10) R. A. Holroyd and R. L. Russel, *J. Phys. Chem.*, **78**, 2128 (1974).
(11) J. Bullot and M. Gauthier, *Chem. Phys. Lett.*, **40**, 402 (1976).
(12) J. Bullot and M. Gauthier, *Can. J. Chem.*, in press.
(13) L. Kevan, *Adv. Radiat. Chem.*, **4**, 185 (1974).
(14) (a) Ya Zolotovitskii et al. quoted in A. K. Pikaev and A. M. Brodskii, *High Energy Chem.*, **6**, 201 (1972); (b) R. E. Ballard, *Chem. Phys. Lett.*, **16**, 300 (1972).
(15) L. Kevan, D. F. Feng, and H. Yoshida, *J. Chem. Phys.*, **61**, 4440 (1974).

The Integral Representation of the Relaxation Effects in Mixed Strong Electrolytes in the Limiting Law Region

Shoon K. Kim*

Department of Chemistry, Temple University, Philadelphia, Pennsylvania 19122

and Lars Onsager†

Center for Theoretical Studies, University of Miami, Coral Gables, Florida 33124

(Received November 30, 1976)

Publication costs assisted by Temple University

The dissipation matrix due to the relaxation effects for the transport process in mixed electrolytes in the $c^{1/2}$ limiting law region is described by a set of definite integrals over a finite interval which is very convenient for direct numerical calculation of the matrix elements.

The general problem for the relaxation effects in mixed strong electrolytes of s species of ions involves a system of s linear differential equations for the electrostatic potentials of the ionic atmospheres. A $s \times s$ matrix **H** describes the constant coefficients of the differential equations. As shown by us quite some time ago[1] (hereafter this work is refered to as I), the transport processes involved with conduction, diffusion, and viscosity in mixed

† Deceased.

electrolytes are described by the matrix elements, $(\mathbf{H}^{1/2})_{ji}$, with positive square roots of the eigenvalues of $\mathbf{H}$.

We have shown in I two independent methods to calculate the matrix elements $(\mathbf{H}^{1/2})_{ji}$; the one is by the eigenwert problem of the matrix $\mathbf{H}$ and the other is by the integral representation of the matrix elements. The former is complete as it stands. It is the latter which we shall improve in this communication by reducing the infinite integrals involved with the representation into definite integrals by a suitable substitution of the integral variable. Since the matrix element $(\mathbf{H}^{1/2})_{ji}$ directly describes the transport coefficients, the integral representation may give a quicker answer for the numerical values of the transport coefficients in this age of computers.

We shall start with the relation between the matrix elements and the dissipation function F″ due to the relaxation effects in mixed electrolytes. According to eq 4, 3, 15 of I the dissipation function is given by

$$2F'' = \sum_{j=1}^{s}\sum_{i=1}^{s} R''_{ji} J_j J_i \tag{1}$$

where J_i is the flow of the i ions and the coefficients R''_{ji} are given by eq 5, 2, 7 of I

$$R''_{ji} = -\frac{\kappa}{3\lambda^0 DkT}\frac{e_j^2 e_i^2}{t_i}[\mathbf{H}^{1/2} - \mathbf{E}]_{ji} \tag{2}$$

Here, all the notations are the same as before and $\mathbf{E}$ is the unit matrix. The off-diagonal elements ($j \neq i$) are given by eq 5, 3, 5 of I

$$(\mathbf{H}^{1/2})_{ji} = (2\bar{\omega}\omega_j\omega_i t_i/\pi) \times \int_0^\infty \frac{dy}{(y^2 + \omega_j^2)(y^2 + \omega_i^2)\{[d(iy)]^{1/2} + [d(-iy)]^{1/2}\}} \tag{3}$$

where

$$d(\zeta) = \sum_{i=1}^{s} \frac{\bar{\omega} t_i}{\omega_i + \zeta} \tag{4}$$

As shown in I, the singular points of the integrand of eq 3 are all located on the imaginary axis of the complex y plane. According to eq 5, 3, 10 of I, the diagonal elements are expressed by the off-diagonal elements as follows

$$[\mathbf{H}^{1/2} - \mathbf{E}]_{ji} = -\sum_{i \neq j}^{s} \frac{\omega_j}{\omega_i}(\mathbf{H}^{1/2})_{ji} \tag{5}$$

Now, from the definition of $d(\zeta)$ given by eq 4 we obtain

$$(1/\sqrt{2})\{[d(iy)]^{1/2} + [d(-iy)]^{1/2}\} = \left\{\sum_{i=1}^{s}\frac{\bar{\omega}\omega_i t_i}{\omega_i^2 + y^2} + \left[\left(\sum_{i=1}^{s}\frac{\bar{\omega}\omega_i t_i}{\omega_i^2 + y^2}\right)^2 + \left(\sum_{i=1}^{s}\frac{y\bar{\omega} t_i}{\omega_i^2 + y^2}\right)^2\right]^{1/2}\right\}^{1/2} \tag{6}$$

Substitution of the integral variable y in eq 3 by

$$y = \bar{\omega}\sin\varphi/\cos^2\varphi \tag{7}$$

yields

$$(\mathbf{H}^{1/2})_{ji} = (\sqrt{2}\,\bar{\omega}_j\bar{\omega}_i t_i/\pi) \times \int_0^{\pi/2} \frac{(1 + \sin^2\varphi)\cos^4\varphi\, d\varphi}{(\sin^2\varphi + \bar{\omega}_j^2\cos^4\varphi)(\sin^2\varphi + \bar{\omega}_i^2\cos^4\varphi)K(\varphi)} \tag{8}$$

where $\bar{\omega}_j = \omega_j/\bar{\omega}$ and

$$K(\varphi) = [a + (a^2 + b^2)^{1/2}]^{1/2} \tag{9}$$

with

$$a = \sum_{j=1}^{s} \frac{\bar{\omega}_j t_j \cos^2\varphi}{\sin^2\varphi + \bar{\omega}_j^2\cos^4\varphi}$$

$$b = \sum_{j=1}^{s} \frac{t_j \sin\varphi}{\sin^2\varphi + \bar{\omega}_j^2\cos^4\varphi} \tag{10}$$

If we expand the integrand of eq 8 into the partial fractions we obtain the "β-representation" given by eq 5, 3, 8 of I

$$(\mathbf{H}^{1/2})_{ji} = -\omega_j\omega_i t_i \frac{\beta_j^* - \beta_i^*}{\omega_j^2 - \omega_i^2} \tag{11}$$

where β_j^* is now given by

$$\beta_j^* = \frac{\sqrt{2}}{\pi}\int_0^{\pi/2} \frac{(1 + \sin^2\varphi)}{(\sin^2\varphi + \bar{\omega}_j^2\cos^4\varphi)K(\varphi)}\, d\varphi \tag{12}$$

Since the integrands of eq 8 and 12 are periodic and analytic along the path of integration, a simple step-by-step quadrature over φ with end corrections is sufficient to evaluate these integrals.

Finally, it is noted that there exist an alternate approach to the problem by Friedman[2] based on the application of cluster expansion methods to the Kubo formalism for the conductance.

Acknowledgment. This research was supported by NIH Grant GM20284-04 and NSF Grant CHE7-17533.

References and Notes

(1) L. Onsager and S. K. Kim, *J. Phys. Chem.*, **61**, 215 (1957).
(2) H. L. Friedman, *J. Chem. Phys.*, **42**, 462 (1965).

Photopotential and Photocurrent Induced by a Tolusafranine–Ethylenediaminetetraacetic Acid System

Publication costs assisted by The Institute of Physical and Chemical Research

Sir: The photoinduced redox (photoredox) reaction is receiving attention as a photoreaction center in studies of the utilization of solar energy by chemical means.[1,2] For this reason the thionine–ferrous ion system which is known to be a typical photoredox system had been investigated, but the photoinduced potential obtained was only 250 mV.[3] The highest photopotential described in the literatures is 476 mV obtained by the proflavine–ethylenediaminetetraacetic acid (EDTA) system.[4] These values are much lower than the potential difference of ca. 800 mV induced by photosystems I or II involved in the photosynthesis unit in green plants.[5]

The present authors have previously reported an increase of photopotentials by addition of chelating agents to the system dye (phenazine or phenothiazine) and ferrous ion.[6] In this paper it will be shown that a simple system, synthetic dyestuff (tolusafranine (SAF))–EDTA, exhibits a remarkably high photopotential of 844 mV which is comparable to that induced by the photosystem in green plants.

A photochemical cell consisting of light and dark chambers was made and fundamental aspects of the photocurrent induced by SAF–EDTA in the cell was studied as well as the mechanism for photocurrent generation.

Experimental Section. A. *Materials.* Dyestuff (tolusafranine; 2,8-dimethyl-3,7-diamino-5-phenylphenazinium chloride; SAF) was recrystallized in water. Ethylenediaminetetraacetic acid (EDTA) was of the purest grade commercially available.

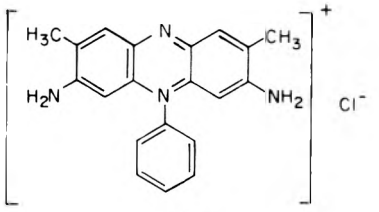

SAF

B. *Apparatus and Measurement.* (a) *Light Source.* The light source was a projector lamp (100 V, 100 W). The band between 400 and 800 nm was selected by passing the light through a UV cutoff filter (Toshiba V-Y 42) and a IR cutoff filter (Toshiba IRQ 80). The distance between the light source and the cell surface was 16 cm; the light intensity at the illuminated cell surface was 30 mW/cm^2, that is about one-third of the average solar energy intensity on earth.

(b) *Photopotential Measurement.* The optical glass cell (1 × 2 × 3 cm) which has a light window of 4 cm^2 was equipped with a needle type calomel electrode (4 M KCl solution; Fuji Kagaku Keisoku Co. Ltd.) and a platinum wire electrode. The distance between the electrodes was 0.6 cm. For potential measurements a potentiometer (Hitachi-Horiba Co. Ltd., Type F-7 DE) was used.

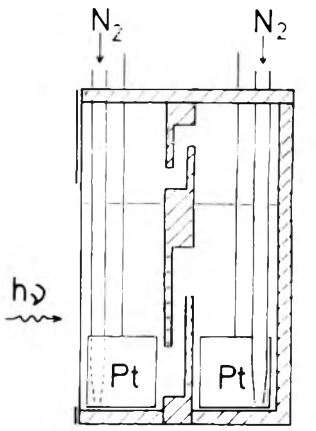

Figure 1. Photochemical cell for photocurrent measurement.

EDTA solution (2 mL) was placed in the cell and deaerated by bubbling with nitrogen gas, and then 2 mL of the SAF solution was added in the dark. The pH of the solution was adjusted by adding HCl or NaOH aqueous solution or by using a buffer solution of pH 6 (KH_2PO_4–NaOH). The potential was first measured in the dark and the potential change under illumination was observed at room temperature.

(c) *Photocurrent Measurement.* The photochemical cell consists of two chambers, light and dark, as illustrated in Figure 1. A light-intercepting black plate placed between the two chambers allows a free flow of the solution. Both chambers are the same size: 1.2 × 1.0 × 4.5 cm. A 1-cm^2 platinum plate electrode was located at the center of each chamber in such a way that it is parallel to the incident light. The photocurrent and its change were measured in a way similar to the measurement of the photopotential.

Results. A. *Photopotential.* The potential of the SAF and EDTA solution in the dark and its change under illumination are shown in Figure 2. The potential decreases rapidly after the start of illumination and reaches an equilibrium value within several minutes. After the illumination is stopped, the potential increases gradually, though it does not recover to the initial value completely. These results suggest that the main reversible photochemical reaction is accompanied by some irreversible reaction. The difference between the initial potential in the dark and the equilibrium potential in the light is defined as the photoinduced potential (photopotential).

SAF has an absorption maximum at 522 nm, while EDTA has no absorption in the visible. A solution of SAF or EDTA alone shows no potential change under illumination. It has been reported that some dyes, e.g., methylene blue, are excited by light and then reduced by EDTA.[7,8] One might conclude that the same reactions, i.e.,

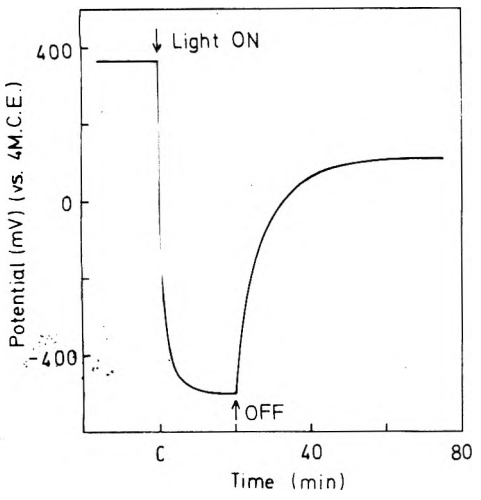

Figure 2. Potential change induced by illumination.

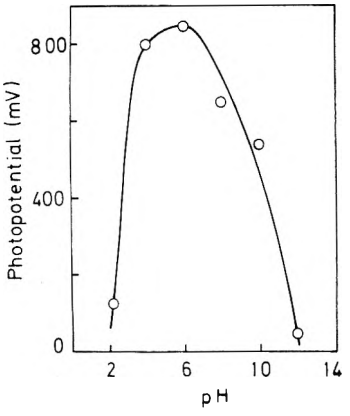

Figure 3. Photopotential vs. pH: SAF 10^{-5} M; EDTA, 5×10^{-3} M, no buffer solution.

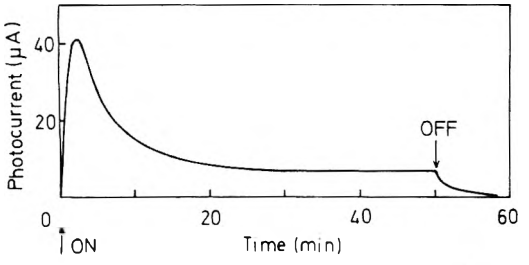

Figure 4. Photocurrent change vs. time: SAF, 2×10^{-4} M; EDTA, 2×10^{-1} M, pH 6 (KH_2PO_4–NaOH buffer), two 1-cm^2 electrodes in each chamber.

light-induced excitation and reduction of SAF by EDTA, occurs in the SAF–EDTA system.

A pH dependence of the photopotential was observed as shown in Figure 3. The maximum value of 844 mV was obtained at pH 6. It would be significant that even a simple synthetic dye as was used in our experiment could produce such a high photopotential of over 800 mV comparable to that induced by photosystems I or II in green plants.[5]

B. *Photocurrent.* In the SAF–EDTA system the electrode in the light chamber is always anodic. A typical pattern of the photocurrent vs. time is given in Figure 4. The photocurrent increases immediately after the beginning of illumination, reaches a maximum value (PC_{max}) within several minutes, and then decreases gradually until it comes to an equilibrium value (PC_{eq}). This photocurrent behavior indicates the presence of a rate-determining step which appears rather late after the initial rapid reaction. More detailed discussions will be given in the next section.

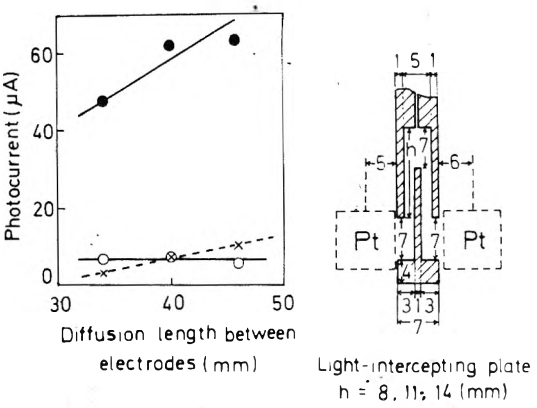

Figure 5. Effect of diffusion length between electrodes on PC_{max} and PC_{eq}: SAF, 5×10^{-4} M; EDTA, 10^{-1} M, pH 6 (KH_2PO_4–NaOH buffer): (●) PC_{max}; (○) PC_{eq}; (×) initial rate of photocurrent generation (μA/min).

Optimum conditions for photocurrent generation are pH 6 and concentrations of SAF and EDTA of 5×10^{-4} and 10^{-1} M, respectively. The quantum yield for PC_{eq} is of the order of 0.1–0.2% based on the absorbed light energy.

Discussion. There exists only insufficient knowledge of the mechanism of the photocurrent in a photochemical cell. In the thionine–ferrous ion system it had been reported that the active species at the electrodes are a semidye and the ferric ion,[2] but the mechanism in the system SAF–EDTA is still unknown. The following is an attempt to elucidate the reaction mechanism occurring in the present experiment.

The redox potential of SAF|leuco-SAF is −0.289 V at pH 7.0,[9] while that of EDTA is unknown. The redox potential of EDTA can be considered to be much higher than that of SAF, because SAF and EDTA do not react in the dark. The following three possible cases are therefore proposed for the electrode active species, i.e., for the chemical species donating an electron to the electrode or accepting one from it:

Case	Electrode active species	
	Light	Dark
I	Leuco- or semi-SAF	SAF
II	Leuco- or semi-SAF	Ox
III	EDTA	Ox

To obtain more knowledge of the mechanism, the following experiment was carried out. The diffusion length of the photoreaction species between two chambers was varied using a different size light-intercepting plate as illustrated in Figure 5, and the photocurrent was observed. The results obtained are also shown in Figure 5. The value of PC_{max} and the initial rate of photocurrent generation were proportional to the diffusion length, while the value of PC_{eq} was independent of the length. These results allow us to identify the true active species. If the oxidized compound of EDTA (Ox) is assumed as the main active species at the dark electrode, PC_{max} and the rate of increase of the photocurrent should be inversely proportional to the diffusion length, because the Ox which is produced only in the light chamber must diffuse into the dark chamber in order to accept an electron from the dark electrode. This is in contradiction to the results shown in Figure 5. Cases II and III must therefore be rejected.

It is, therefore, concluded that the main active species at the dark and light electrodes are the dye itself and the leuco- (or semi-) dye, respectively. The photocurrent generation can then be described as in Figure 6. The reducing agent (EDTA) and its oxidized compound behave as electron carriers, diffusing through the path made by the light-intercepting plate. Considering that a longer path

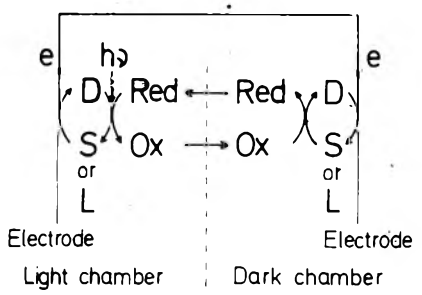

Figure 6. Mechanism for photocurrent generation: D, SAF; S, semi-SAF; L, leuco-SAF; Red, EDTA; Ox, oxidized compound of EDTA.

TABLE I: Results of Changing Electrode Area on PC_{max} and PC_{eq}.[a]

Electrode area, cm^2	PC_{max}, μA	PC_{eq}, μA
1	37	12
2	62	10

[a] SAF, 5×10^{-4} M; EDTA, 10^{-1} M, pH 6 (KH_2PO_4-NaOH buffer).

length produces a higher concentration gradient of dye species, the scheme of Figure 6 can well explain the behaviors of the rate and PC_{max} in Figure 5. The mechanism of the redox system SAF–EDTA is thus different from that of the thionine–ferrous ion system, in which the active species at the dark electrode had been considered to be ferric ion, i.e., an oxidized compound of the reducing agent.[1,2]

We will now consider the reaction concerned with the appearance of PC_{eq} shown in Figures 4 and 5. Since the value of PC_{eq} is much lower than that of PC_{max}, it is concluded that some slow reaction, which determines the value of PC_{eq}, appears after the rapid initial reaction. All of the possible processes taking place in the cell are considered as follows: (1) photoreaction of dye and reducing agent; (2) diffusion of reducing agent and its oxidized compound; (3) adsorption on electrodes, i.e., of semi- or leuco dye on the anode and of dye on cathode; (4) electron transfer between the adsorbed species and the electrodes; (5) desorption from electrodes, i.e., of dye on anode and semi- or leuco dye on the cathode; (6) a recycling reaction of the semi- or leuco dye and the oxidized compound of the reducing agent in the dark chamber. Among them processes 1–4 cannot be rate-determining steps for PC_{eq}, because the photocurrent rises at a high rate having a maximum value and moreover the longer diffusion lengths do not affect PC_{eq} (see Figure 5).

As for process 5, if desorption of the dye species from electrodes is the rate-determining step, PC_{eq} should be proportional to the electrode area. An experiment had therefore been carried out with the electrode area changed. The result is shown in Table I. It shows distinctly that the value of PC_{eq} is not related to the electrode area, and thus process 5 is not a rate-determining step for PC_{eq}. Reaction 6 alone remains as the most probable rate-determining process for PC_{eq}, though no further evidence supporting it could be provided because of the difficulty of isolation of the oxidized compound of EDTA.

The structure of this oxidized compound of EDTA is still unknown. Although the formation of amine oxide has been proposed in the system methylene blue–trimethylamine,[10] it is not certain whether a similar reaction occurs in our system or not.

References and Notes

(1) W. D. K. Clark and J. A. Eckert, *Sol. Energy*, **17**, 147 (1975).
(2) R. Gomer, *Electrochim. Acta*, **20**, 13 (1975).
(3) E. Rabinowitch, *J. Chem. Phys.*, **8**, 551, 560 (1940).
(4) M. Eisenberg and H. P. Silverman, *Electrochim. Acta*, **5**, 1 (1961).
(5) R. Hill and F. Bendall, *Nature (London)*, **186**, 136 (1960).
(6) M. Kaneko and A. Yamada, *Rep. Inst. Phys. Chem. Res.*, **52**, 210 (1976).
(7) W. J. Nickerson and J. R. Merkel, *Biochim. Biophys. Acta*, **14**, 303 (1954).
(8) G. Oster and N. Wotherspoon, *J. Am. Chem. Soc.*, **79**, 4836 (1957).
(9) J. R. Stern, *Tabulae Biol.*, **4**, 1 (1935).
(10) H. Obata and M. Koizumi, *Bull. Chem. Soc. Jpn.*, **30**, 136 (1957).

The Institute of Physical and Chemical Research
Wako-shi, Saitama, 351 Japan

Masao Kaneko*
Akira Yamada

Received December 29, 1976

Evidence for Methyl Radical Intermediates in the Radiolysis of Alcohols. A Spin Trapping Study

Publication costs assisted by Atomic Energy of Canada Limited

Sir: γ radiolysis of aliphatic alcohols produces appreciable yields of alkanes.[1] For example, methane is produced in methanol, ethanol, 2-propanol, and *tert*-butyl alcohol, and ethane is the principal alkane produced in 1-propanol. The alkanes may reasonably be assumed to have alkyl radical precursors; however, there has been no evidence to support this. Electron spin resonance (ESR) spectra of irradiated alcohol glasses at 77 K contained only features from trapped electrons and hydroxyalkyl radicals such as $\dot{C}H_2OH$ in methanol.[2] Similarly, in situ radiolysis of liquid alcohols with 3-MeV electrons directly examined by ESR did not produce any evidence for alkyl radical intermediates.[3] We have successfully applied spin trapping techniques[4,5] to the identification of the principal free-radical intermediates formed in the radiolysis of alcohols,[6] and have measured the yields of alkoxy and hydroxyalkyl radicals in methanol and ethanol.[7] The principle of the method involves the addition of the radical to a nitrone or nitroso compound to produce a stable nitroxide, the ESR spectrum of which is characteristic of the radical trapped. We have primarily used the trapping agent, *t*-BuNO, because it gives ESR spectra which vary greatly with the nature of the radical trapped. This compound reacts with methyl radicals[8] as in

$$CH_3\cdot + t\text{-BuNO} \rightarrow t\text{-BuN(O}\cdot\text{)-CH}_3 \quad (1)$$

I

This prompted us to reexamine our ESR spin trapping spectra, and to perform experiments at high concentrations of *t*-BuNO, to look for evidence for methyl (or other alkyl) radicals in the radiolysis of alcohols. The spectra were examined under conditions of high sensitivity to detect small amounts of I in the presence of very intense ESR peaks from the nitroxides resulting from the trapping of alkoxy and hydroxyalkyl radicals.

Radiolysis of methanolic solutions of *t*-BuNO in the range of 0.01–0.1 mol/dm^3 at temperatures ranging from −40 to −93 °C gave no evidence for methyl radicals. However, radiolysis of *t*-BuNO solutions containing methyl iodide, which produces methyl radicals by reaction of CH_3I with radiation-produced electrons (reaction 2), did give

$$CH_3I + e \rightarrow CH_3\cdot + I^- \quad (2)$$

ESR spectra which contained features of nitroxide I, due to trapped methyl. This demonstrates that, although *t*-BuNO will trap methyl, this radical is not produced in any appreciable yield in γ-irradiated methanol. Alter-

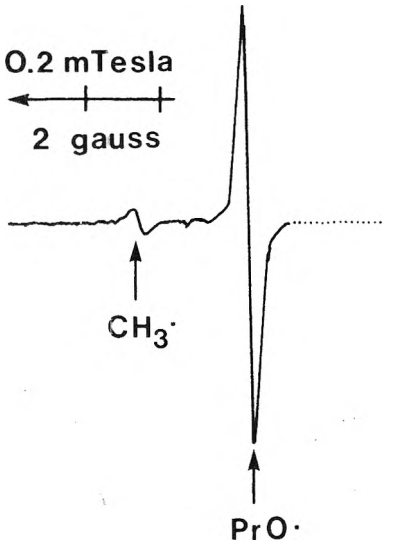

Figure 1. The high field extremity of the ESR spectrum observed during the radiolysis of 2-propanol containing 0.02 mol/dm^3 of *t*-BuNO at +10 °C. The two lines are the outermost peaks of two nitroxides, *t*-BuN(O·)–CH_3 (a_N = 1.63 mT, $a_H^{CH_3}$ = 1.28 mT) and *t*-BuN(O·)–oPr (a_N = 2.9 mT), resulting from the trapping of methyl and isopropoxy radicals, respectively.

natively, if it is formed, it does not behave in the same manner as that produced in reaction 2. Similarly, radiolysis of 1-propanol solutions gave no indication of methyl radicals but the ESR spectra did contain features due to the trapping of a $\dot{C}H_2X$ type radical. The identity of this radical is uncertain but since ethane is a product of the radiolysis, ethyl seems quite probable.

Radiolysis of concentrated solutions of *t*-BuNO in ethanol, 2-propanol, and *tert*-butyl alcohol gave peaks in all their ESR spectra due to I (e.g., Figure 1). The relative intensities of these were such that the methyl radical yields were in the order *tert*-butyl alcohol > 2-propanol > ethanol, which parallels the methane yields in these solvents. Some additional peaks in the spectra suggested the presence of trapped $\dot{C}H_2X$ type radicals but no positive identification was possible.

The production of nitroxide I in the radiolysis of *t*-BuNO solutions of ethanol, 2-propanol, and *tert*-butyl alcohol is positive proof that the methyl radical is an intermediate in the radiolysis of these alcohols. The failure to detect trapped methyl in methanol was surprising and suggests that this radical is not the precursor of the methane yield in this solvent. Alternatively, it is possible that methyl is formed with an excess energy and reacts very rapidly with the solvent rather than with the *t*-BuNO.

References and Notes

(1) (a) G. R. Freeman, *Actions Chim. Biol. Radiat.*, **14**, 73 (1970); (b) R. H. Johnsen and D. A. Becker, *J. Phys. Chem.*, **67**, 831 (1963).
(2) L. Kevan, *Actions Chim. Biol. Radiat.*, **13**, 57 (1969).
(3) F. P. Sargent and E. M. Gardy, *J. Phys. Chem.*, **78**, 1977 (1974).
(4) E. G. Janzen, *Acc. Chem. Res.*, **4**, 31 (1971).
(5) C. Lagercrantz, *J. Phys. Chem.*, **75**, 3466 (1971).
(6) (a) F. P. Sargent, E. M. Gardy, and H. R. Falle, *Chem. Phys. Lett.*, **24**, 120 (1974); (b) F. P. Sargent and E. M. Gardy, *Can. J. Chem.*, **52**, 3645 (1974).
(7) F. P. Sargent and E. M. Gardy, *J. Phys. Chem.*, **80**, 854 (1976).
(8) (a) A. Mackor, Th. A. J. W. Wajer, and Th. J. deBoer, *Tetrahedron Lett.*, 2115 (1966); (b) M. J. Perkins, P. Ward, and A. Horsfield, *J. Chem. Soc. B*, 395 (1970).

Research Chemistry Branch
Atomic Energy of Canada Limited
Whiteshell Nuclear Research Establishment
Pinawa, Manitoba ROE 1L0, Canada

F. P. Sargent*
E. M. Gardy

Received February 14, 1977

ADDITIONS AND CORRECTIONS

1975, Volume 79

Steven M. Schildcrout and Fred A. Fortunato: A Spectrophotometric Study of the Rate of the Aqueous Iodide–Iodate Reaction.

Page 33. The heading of column 8 in Table I should be $10^{-8}k^c$, and the four entries in this column should be respectively 0.80 ± 0.01, 1.08 ± 0.01, 1.46 ± 0.01, and 2.01 ± 0.01. We thank H. A. Liebhafsky for pointing out the inconsistency which led us to discover the error.
—S. M. Schildcrout

New Tape Recordings on ENERGY

☐ FUELS FOR THE NEXT 50 YEARS

A Panel Discussion
Length: 178 minutes
7 Speakers—15 Figures
Price: $18.00

The Panel:

G. R. Hill—Direct Utilization of Coal
L. G. Massey—Gaseous Fuels from Coal and Petroleum
E. Gorin—Liquid Fuels from Coal
R. J. Cameron—Liquid Fuels from Petroleum and Oil Shale
T. J. Joyce—Natural Gas and LNG
D. P. Gregory—Hydrogen, Methanol, and Other Nonconventional Fuels
I. Wender—Fuels from Plant and Waste Materials

Each speaker briefly discusses his subject; the panel then engages in a freewheeling, give-and-take discussion of the energy problem and suggested solutions.

☐ COAL—NATURE'S BLACK DIAMOND

Length: 136 minutes
4 Speakers—61 Figures
Price: $18.00

The Speakers:

R. T. Eddinger—Coal—Nature's Black Diamond
R. F. Moran—Genesis of a Formed-Coke Process
J. F. Jones—Clean Fuels for Power Generation from High-Sulfur Coals
L. Seglin—The COGAS Process for Pipeline Gas

This symposium presents a incisive look at coal as a source for synthetic fuels and includes general economic and process details of the COED and COGAS processes.

☐ LOW SULFUR LIQUID FUELS FROM COAL

Length: 148 minutes
5 Speakers—66 Figures
Price: $18.00

The Speakers:

J. G. Guin—Photomicrographic Studies of Coal Dissolution
H. E. Lebowitz—Deashing of Coal Liquefaction Products via Partial Deasphalting-Hydrogen Donor Extraction Effluents
C. J. Kulik—Deashing of Coal Liquefaction Products via Partial Deasphalting-Hydrogenation and Hydroextraction Effluents
H. P. Malone—Characterization and Upgrading of Coal Liquids to High Value Fuels and Chemicals

Processes for upgrading liquids extracted from coal are described and first details of a new coal liquefaction process from Gulf Oil are revealed.

☐ THE ROLE OF TECHNOLOGY IN THE ENERGY CRISIS

Length: 128 minutes
4 Speakers—60 Figures
Price: $18.00

The Speakers:

H. H. Hasiba—Contribution of Enhanced Recovery Technology to Domestic Crude Oil
R. N. Quade—Process Applications of Nuclear Heat
L. W. Russman—Engineering Perspective of a Hydrogen Economy
A. Decora—Oil Shale Development and its Environmental Considerations

In-depth examination of the gains—and problems—which state-of-the art technology will bring if brought to bear on our energy problems.

☐ UNUSUAL FUELS PRODUCTION

Length: 138 minutes
5 Speakers—91 Figures
Price: $18.00

The Speakers:

D. L. Klass—Long-Range Approach to the Natural Gas Shortage Utilizing Nonfossil Renewable Carbon
R. G. Sheehan—Methanol or Ammonia Production from Solid Waste by the City of Seattle
W. A. Scheller—Production of Ethanol and Vegetable Protein by Grain Fermentation
P. E. Cassady—Use of Methanol as a Motor Fuel
W. A. Scheller—Performance of an Ethanol-Gasoline Blend in Automobiles and Light Trucks

An up-to-date rundown of results achieved in programs to use methanol and ethanol as additives in motor fuel, and details of advanced projects to use solid waste and biomass as sources of fuels.

AVAILABLE ON TAPE CASSETTES ONLY

PRICES: $18.00 per Title (Postpaid)
$45.00 Any THREE Titles (Postpaid)

ORDER FROM:

American Chemical Society
1155 Sixteenth Street, N.W.
Washington, D.C. 20036
Dept. AP

NAME:_____

ADDRESS:_____

City_____ State_____ Zip_____

(Allow 4 to 6 weeks for delivery)